NASA TECHNICAL
MEMORANDUM

NASA TM X-64505

RESEARCH ON ELECTROMAGNETIC CORRELATION TECHNIQUES

Edited by Fritz R. Krause
Aero-Astrodynamics Laboratory

March 17, 1970

NASA

George C. Marshall Space Flight Center
Marshall Space Flight Center, Alabama

MSFC - Form 3190 (September 1968)

TECHNICAL REPORT STANDARD TITLE PAGE

1. REPORT NO.	2. GOVERNMENT ACCESSION NO.	3. RECIPIENT'S CATALOG NO.
NASA TM X-64505		

4. TITLE AND SUBTITLE	5. REPORT DATE
RESEARCH ON ELECTROMAGNETIC CORRELATION TECHNIQUES	March 17, 1970
	6. PERFORMING ORGANIZATION CODE
7. AUTHOR(S) edited by Fritz R. Krause	8. PERFORMING ORGANIZATION REPORT #
9. PERFORMING ORGANIZATION NAME AND ADDRESS Aero-Astrodynamics Laboratory George C. Marshall Space Flight Center Marshall Space Flight Center, Alabama 35812	10. WORK UNIT NO.
	11. CONTRACT OR GRANT NO.
12. SPONSORING AGENCY NAME AND ADDRESS	13. TYPE OF REPORT & PERIOD COVERED Technical Memorandum Nov. 1, 1968 - Nov. 1, 1969
	14. SPONSORING AGENCY CODE

15. SUPPLEMENTARY NOTES

16. ABSTRACT

Advanced data processing and statistical analysis methods have been applied to output signals of active and passive electromagnetic sensors. Single path observations, intersecting beams, and separated lines of sight have been used to study the overall level, spectroscopic structure, and motion of local and remote optical disturbances. The potential of the associated "electromagnetic correlation techniques" is illustrated by model experiments in a jet, in a glow discharge, and in a blow torch. Analytical concepts for remote probing of the earth's atmosphere are illustrated through a discussion of special cross-beam arrangements for ground wind and turbulence detection. Potential applications to the general problems of separating dispersion phenomena from local photochemical processes are introduced through a piecewise accumulation of phase and gain spectra.

17. KEY WORDS	18. DISTRIBUTION STATEMENT
	PUBLIC RELEASE: E. D. Geissler Director, Aero-Astrodynamics Laboratory

19. SECURITY CLASSIF. (of this report)	20. SECURITY CLASSIF. (of this page)	21. NO. OF PAGES	22. PRICE
UNCLASSIFIED	UNCLASSIFIED	221	

MSFC - Form 3292 (May 1969)

PREFACE

Our research on electromagnetic correlation techniques was initiated in 1965 to provide advanced experimental and analytical tools for investigation of turbulent or unstable flows. Tools to provide a level of scientific sophistication not possible in ad hoc engineering studies of launch vehicle configurations were sought. The application of electromagnetic correlation techniques has now been illustrated for the remote probing of sound source intensities in engine exhausts and for the detection of wind shears and turbulence. The above tasks require the coordination of the disciplines of sensor development, electromagnetic wave propagation, fluid mechanics, atmospheric science, physics, statistics, and data processing. Such a combination of disciplines was achieved through organizing cooperative research programs with the Wave Propagation Laboratories of ESSA, the Department of Atmospheric Science of Colorado State University, the Department of Physics of the University of Oklahoma and MSFC's Computation Laboratory. Cooperation in these programs meant a sharing of facilities and resources.

This research review on electromagnetic correlation techniques covers contributions from inhouse engineers and scientists. Most of the papers were contributed by undergraduate and graduate students during their training program at MSFC. This particular combination of cooperative research and cooperative training was initiated in 1966.

It is hoped that this review will be stimulating to organizations which employ electromagnetic sensors for remote probing. Criticism of this review and discussions concerning individual papers with respective authors are invited and will be particularly helpful for the student trainees.

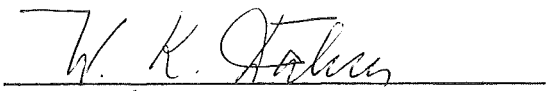

W. K. Dahm
Chief, Aerophysics Division

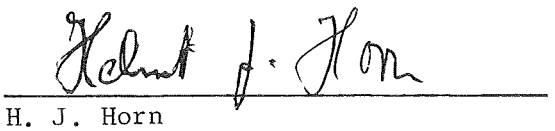

H. J. Horn
Deputy Director,
Aero-Astrodynamics Laboratory

ACKNOWLEDGEMENTS

The authors of these papers wish to thank Mrs. Evelyn Carter for the excellent job she did in making the illustrations for this report, Mrs. Sarah Hightower for her editorial assistance, and Mrs. Irene Dolin for typing the manuscript.

TABLE OF CONTENTS

TABLE OF CONTENTS (Continued)

LIST OF ILLUSTRATIONS

LIST OF ILLUSTRATIONS (Cont'd)

LIST OF ILLUSTRATIONS (Cont'd)

CHAPTER I

INFRARED MEASUREMENTS OF SOUND SOURCE INTENSITIES IN JETS

by

L. N. Wilson
IIT Research Institute, Chicago, Illinois

F. R. Krause and K. A. Kadrmas
NASA - Marshall Space Flight Center, Alabama

SUMMARY

Direct measurements of local sound source intensities in turbulent jets are being attempted using an optical cross-correlation technique. It has been shown that optical cross-beam measurements can be related directly to the volume integral describing the source strength. This paper represents a study of this relationship. The application and limitations of the technique are discussed in detail, with reference to Lighthill's and, in particular, Ribner's mathematical formulations. The latter formulation is particularly suited to cross-beam measurements since it expresses source strengths in terms of volume integrals of mass density fluctuations. Area integrals of density fluctuations are being attempted using a new infrared cross-beam system. Progress to date on subsonic jets with this system shows promise of giving the desired density dependence. Measurements were made using the CO_2 absorption band at 4.3μ. This type of measurement should be applicable to estimations of Mach-wave emission.

NOMENCLATURE

Symbol	Definition
$\vec{x}_f$	position vector $(x_f; y_f; z_f)$
$\vec{x}$	position vector $(x; y; z)$
$\vec{\xi}$	vector in direction of far-field observer $(\xi_1; \xi_2; \xi_3)$

$\vec{\xi}$	vector in direction of flow (ξ, η, ζ)
$\bar{\rho}$	mean density
ρ	fluctuating density
m_f	fluctuating mass fraction
k	absorption
$\bar{P}$	mean pressure
P	fluctuating pressure
$\vec{\bar{u}}$	mean velocity vector $(\bar{u};\ \bar{v};\ \bar{w})$
a_o	ambient speed of sound
a	local speed of sound
i	fluctuating signal
I	mean signal
ℓ	path angle
τ	retarded time
U_c	turbulence convection speed

Subscripts

A, B	radiation beams of the crossed-beam system
a	contribution from absorption
s	contribution from scattering

I-1. INTRODUCTION

The mathematical formulation of the jet noise problem [I-1,-2] has given us considerable insight into scaling laws associated with noise production, but little progress has been made in experimental verification of the predicted sound source strengths. The actual sound source

intensities as predicted by the theory are given in terms of turbulence flow properties which are extremely difficult to measure and even then must be incorporated into a complicated volume integral expression involving retarded time differences between statistical variables. Some attempts [I-3,-4], with a measure of success, have been made in estimating sound source strengths from hot wire measurements in low speed jet flows where the transformation to a moving frame of reference allows retarded times to be ignored to a good degree of approximation. At high speeds, this approximation is invalid; in fact, a singularity occurring at the sonic convection condition results in a prediction of infinite acoustic power radiated. A different type of noise source then dominates, and sound radiates from the jet in a manner analogous to Mach wave propagation [I-5].

An instrumentation technique, called the crossed-beam correlation method, has been recently developed [I-6] which automatically performs an area-integral of pertinent turbulent properties. This technique is similar in form to that required for a direct estimate of sound source intensity [I-7], and thus affords us the opportunity of measuring a part of the sound source volume integral directly. This paper covers the application of the technique to the Mach wave emission expected from supersonic jets and discusses progress on the experimental verification that has been achieved after the last review [I-8].

I-2. ANALYTICAL DEVELOPMENT

A. Sound Source Intensities

Ffowcs-Williams [I-5] has shown that, where turbulent jet convection speeds are in excess of the ambient speed of sound

$$(M_c = \frac{U_c}{a_o} > 1),$$

a pronounced finite sound peak occurs at $\cos \theta = 1/M_c$ where θ is the angle between the line to the observer and the flow direction (see figure I.1). Since this is the direction toward which Mach waves would emanate from supersonic bodies moving at a Mach number M_c, the emission is analogous to the Mach wave emission from supersonically moving eddies, the latter behaving somewhat like solid bodies. The intensity of acoustic radiation is then determined by the "shape" of the bodies (i.e., by the density gradient through the eddy). The sound source in this case is source-like (monopole); whereas, in subsonic flow the sound source is quadrupole in nature. The sound source strength is then determined

(through suitable mathematical manipulation) by density correlations in a fixed frame of reference, thus removing the complication resulting from measurements being required in the moving frame of reference as is the case of quadrupole noise.

The far-field acoustic radiation from the shear layer of a turbulent jet is then predicted to be

$$\langle p^2 \rangle = \frac{1}{16\pi^2} \int \frac{(x_f - x)^2 (y_f - y)^2}{|\vec{x}_f - \vec{x}|^6} \{\partial \bar{u}/\partial y\}^2 \, S(\vec{x}) \, d\vec{x}, \qquad (1)$$

where

$$S(\vec{x}) = \int \left\langle \frac{\partial \rho}{\partial t}\left(\vec{x}, \; t - \frac{|\vec{x}_f - \vec{x}|}{a_o}\right) \frac{\partial \rho}{\partial t}\left(\vec{x} + \vec{\xi}, \; t - \frac{|\vec{x}_f - \vec{x} - \vec{\xi}|}{a_o}\right) \right\rangle d\vec{\xi}. \qquad (2)$$

$S(\vec{x})$ is considered here to be the acoustic source strength per unit volume of turbulence. The other terms in the equations, apart from the mean velocity gradient, are dependent upon the relative position of the observer and the sound source. The velocity gradient can be measured independently of the source integral by other standard measurements. Ffowcs-Williams writes the correlations in terms of the pressure gradients by assuming locally isotropic conditions: $\rho = (1/a^2)P$. This technique requires a knowledge of the local speed of sound in the shear layer. If, however, we can measure density fluctuations directly, this approximation and requirement is not necessary. Ffowcs-Williams also shows that the sound source integral is more properly written in a frame of reference aligned with and perpendicular to the Mach wave direction of propagation.

B. Crossed-Beam Principle

The operation of the crossed-beam technique has been described elsewhere, and will therefore be discussed only briefly here. In principle, two narrow beams of selected wavelength radiation are positioned such that they intersect at a point in the region of interest in the jet. If the beam intensity for each beam is modulated by a process

which is linearly related to the local gas density fluctuations, then the intensities can be expressed by

$$i_A = I_A \int (km_f)\, d\eta = I_A \int \rho d\eta \tag{3}$$

$$i_B = I_B \int (km_f)\, d\zeta = I_B \int \rho d\zeta, \tag{4}$$

where i_A, i_B, I_A and I_B are the fluctuating and mean signals, respectively, for each of the two beams A and B. If the two signals are cross-correlated over a sufficiently long integration time, the product mean value $\langle i_A\, i_B \rangle$ will give information concerning only the fluctuations common to each beam (i.e., in the intersection region). In this way, local information on turbulence has been obtained without the necessity of inserting physical probes into the flow field [I-6]. From a more intuitive viewpoint (see figure I.2), we might consider turbulence as consisting of discrete eddies that are slightly more or less transparent to the beams of radiation than the surroundings. As an eddy passes through a beam of radiation, the light intensity at the detector changes. When the two detector outputs are cross-correlated, only the information concerning eddies passing through the beam intersection point is retained. Signal fluctuations due to source instabilities, detector noise, etc., are normally uncorrelated, although these contributions do affect the overall signal-to-noise ratio of the system [I-9].

Cross-correlation of equations (3) and (4) gives

$$G(\vec{x}) = \frac{\langle i_A i_B \rangle}{\langle I_A \rangle \langle I_B \rangle} = \int\int \langle \rho(x, y+\eta, z, t)\ \rho(x+\xi, y, z, t+\tau) \rangle\, d\eta\, d\xi, \tag{5}$$

where i_A and i_B are correlated with an arbitrary time delay τ between signals and ξ is a displacement of beam B relative to beam A in the direction of U_c. This equation expresses the correlation between two line integrals. If we can write equation (5) as

$$G(\vec{x}) = \int\int \langle \rho(x, y, z, t)\ \rho(x+\xi, y+\eta, z+\zeta, t+\tau) \rangle\, d\eta\, d\zeta \tag{6}$$

or

$$G(\vec{x}) = \underset{\text{point}}{<\rho(x,y,z,t)} \underset{\text{area}}{\int\int <\rho(x+\xi,y+\eta,z+\zeta,t+\tau)\ d\eta\ d\zeta>}, \qquad (7)$$

then, we are dealing with the correlation between the area integral of points in a plane ($x + \xi$ = constant) with an outside point (x,y,z). Such a cross-correlation has been assigned the term "point-area correlation," and is the type occurring in equation (1).

If the turbulent flow is everywhere homogeneous, then the point-area formulation is obviously proper. If departures from homogeneity are pure odd functions of space coordinates about the point (x,y,z), then these departures tend to integrate out and the point-area concept is still valid. In any event, the final proof of the point-area correlation assumption can come only from experiment. Two tests for this proof, discussed in detail in reference I-8, are summarized here.

(1) The spatial resolution of the measurements across streamlines should be limited only by the outside "point" which, in practice, is the optical beam diameter.

(2) Since the cross-correlation of signals i_A and i_B will correspond only to contributions from turbulent fluctuations normal to the beam plane, the energy spectrum should approximate the three-dimensional spectrum of turbulence. This is in contrast to a two-point hot wire measurement of the so-called one-dimensional spectrum which contains contributions due to cross-flow components. As a result, the energy spectrum for crossed-beam data should approach a -11/3 variation in the high frequency portion.

Therefore, assuming the validity of the point-area correlation approximation, equation (7) in abbreviated fashion becomes

$$G(\vec{x}) = \int\int <\rho(\vec{x},t)\ \rho(\vec{x} + \vec{\xi},\ t + \tau)> d\eta\ d\zeta. \qquad (8)$$

C. Application to Sound Source Intensity Measurements

The similarity between equation (1) and equation (8) is striking. It would appear that only one further integration (point-area to point-volume) is required to obtain the sound source intensity. There are, however, two main points to be considered carefully in making the comparison. They are as follows:

(1) The radiation extinction process must be directly gas-density dependent.

(2) Time derivative and not space derivative correlations are required, and the correct retarded time difference must be used.

We will now consider these two points in greater detail.

1. Extinction Process

Several extinction processes have been used in crossed-beam studies in the past. These include scattering from natural and artificial tracers and the use of the absorption of air in the ultra-violet portion of the spectrum (Schumann-Runge bands of oxygen). Each of these has proven to be unacceptable for sound source measurements although they are useful in other turbulence parameter studies. More recently, instrumentation has been developed to measure absorption by naturally occurring CO_2 in air using the near infrared portion of spectrum. The fundamental vibration band of CO_2 near 4.3 microns is the most promising due to the absence of water vapor absorption in this region. Only naturally occurring CO_2 can be used, since only then will the optical fluctuations measured be truly representative of the gas density fluctuations in the jet. The use of the infrared spectrum also reduces the contributions to the signal fluctuations from ever present particle contaminants in the flow.

The extinction process in general can be written as

$$i + I = I_o \exp\left[-\int (\bar{\rho} + \rho) d\ell\right]$$

$$= I_o \exp\left[-\int \bar{\rho}\, d\ell\right] \exp\left[-\int \rho\, d\ell\right]$$

$$= I \exp\left[-\int \rho\, d\ell\right] .$$

Now, for small perturbations

$$\exp\left[-\int \rho \, d\ell\right] \cong 1 - \int \rho \, d\ell.$$

Thus,

$$i = -I \int \rho \, d\ell.$$

This was the form presented in a previous section.

It should be repeated at this point that ρ is analogous to km_f. This means that a comprehensive study must be made using a unique absorption calibration cell to determine the dependence of k on the static and dynamic pressure and static temperature. Therefore, knowing $\partial k/\partial P$ and $\partial k/\partial T$, the experimenter can choose the optimum wavelength and bandpass settings in the absorption band to discriminate against the temperature dependence of k. These experiments can be made only in a controlled environment free of a contribution due to scattering to the observed signal.

In principle then, it is feasible to use infrared absorption by naturally occurring CO_2 for the measurement of gas-density fluctuations. The preliminary results are given in the next section.

2. Time Derivative Requirements and Retarded Time Effects

The point-area correlation in equation (6) must be in terms of the time derivatives of the gas-density fluctuations in order to obtain an experimentally accessible form of equations (1).

For stationary time series, the correlation of time derivatives is identical with the time lag differentiation of the correlation.

$$-\left\langle \frac{\partial \rho(\vec{x},t)}{\partial t} \frac{\partial \rho(\vec{x}+\vec{\xi},\ t+\tau)}{\partial t} \right\rangle = \frac{\partial^2 \langle \rho(\vec{x},t)\ \rho(\vec{x}+\vec{\xi},\ t+\tau)\rangle}{\partial \tau^2} \tag{9}$$

$$\frac{\partial^2 G(\vec{x})}{\partial \tau^2} = \int\int \frac{\partial^2 \langle \rho(\vec{x},t)\ \rho(\vec{x}+\vec{\xi},\ t+\tau)\rangle}{\partial \tau^2} \, d\xi_2 \, d\xi_3 \tag{10}$$

$$S(\vec{x}) = \int \frac{\partial^2 G(\vec{x})}{\partial \tau^2} \, d\xi_1. \tag{11}$$

We can also simplify the retarded times in equation (1) by the approximation

$$|\vec{x}_f - \vec{x}| - |\vec{x}_f - \vec{x} - \vec{\xi}| \simeq \xi_1. \tag{12}$$

The order of time lag differentiation and space integration (equation (11)) may be interchanged in the special coordinate system $\vec{\xi} = (\xi_1; \xi_2; \xi_3)$ where the planes ξ_1 = constant are parallel to the Mach wave fronts that are generated at the source point $\vec{x}$, the reason being that retarded times are constant along such planes within the far-field approximation. This type of crossed-beam orientation is possible, but does not alleviate the problem since θ is not known a priori.

Now, the time delay for the orientation in figure I.2 is

$$\tau = \frac{\xi_1}{a_o} = \frac{\xi}{U_c}.$$

This time delay is also precisely that which allows an eddy to move from the upstream beam to the downstream beam along a streamline in a reference frame oriented in the flow direction $\vec{\xi} = (\xi; \eta; \zeta)$. In other words, the retarded time is correct for the area near the "common" streamline, but away from the streamline τ is a function of the particular points η and ζ. In the first approximation, the contributions should cancel as in the case for cross-flow components. Therefore, we can write equations (10) and (11) as

$$\frac{\partial^2 G(\vec{x})}{\partial \tau^2} = \int\int \frac{\partial^2 \langle \rho(\vec{x}, t) \, \rho(\vec{x}+\vec{\xi}, t+\tau) \rangle}{\partial \tau^2} \, d\eta \, d\zeta \tag{13}$$

$$S(\vec{x}) = \int \frac{\partial^2 G(\vec{x})}{\partial \tau^2} \, d\xi \tag{14}$$

and

$$|\vec{x}_f - \vec{x}| - |\vec{x}_f - \vec{x} - \vec{\xi}| \simeq \xi. \tag{15}$$

Now, $S(\vec{x})$, being an experimentally accessible quantity under the above assumptions, sound source intensities can be measured.

I-3. EXPERIMENTAL STUDIES

The first tests* conducted with the infrared crossed-beam system were made in the shear layer at an axial location of X/D = 4 of a subsonic jet so that comparisons could be made with more standard measuring techniques. A photograph of the one-inch diameter subsonic jet facility and infrared crossed-beam system is shown in figure I.3.

The radiation sources currently in use are glowbars operating at a temperature of 1100°K (equivalent blackbody temperature). Cassegrainian optics are used to focus the radiation from the sources into the jet flow field with an image dimension of 2mm in the flow direction and 1 mm in the transverse direction. The radiation is then collected, using similar optics and refocused on the entrance slit of a McPherson Model 218 monochromator. The experimenter can then choose the center wavelength and bandpass settings desired in the 4.3 micron absorption band of CO_2. The bandwidth initially used was typically 0.08 microns. The radiation level is monitored at the exit slit of the monochromator by using LN_2 cooled Indium-Antimonide detectors. The fluctuating signals obtained are amplified and recorded for a detailed analysis. Simultaneously, the signals are reduced on-line using a PAR correlator. A computer program is available to reduce the digitized data tapes to obtain the correlations and spectra.

The cross-correlations (zero beam separation) and mean levels obtained while traversing the spectral region from 4.1 to 4.5 microns are shown in figure I.4. Both the mean level traverse and cross-correlation traverse follow the shape of the CO_2 absorption curve as expected, but cross-correlations were recorded outside the absorption band where the absorption should fall to zero. It is felt that this is due to the contribution from scattering to the total signal since the jet has contamination from oil mist due to the compressors. In this case, the

*The data presented here were kindly supplied by Dr. R. J. Damkevala of IIT Research Institute.

signal is obviously not entirely due to CO_2 absorption, and therefore some method must be devised to treat this type of problem.

If we consider the fluctuating signals of beam A and beam B to be composed of contributions due to absorption and scattering, then

$$i_A(\lambda, \ldots) = i_{A_a}(\lambda, \ldots) + i_{A_s}(\lambda_1, \ldots) \tag{16}$$

and

$$i_B(\lambda, \ldots) = i_{B_a}(\lambda, \ldots) + i_{B_s}(\lambda_1, \ldots),$$

where we have assumed that the scattering contribution is a linear continuum across the absorption band and can thus be approximated at λ_1.

The cross-correlation of the two composite signals yields

$$\begin{aligned} <i_A(\lambda, \ldots)\, i_B(\lambda, \ldots)> &= <i_{A_a}(\lambda, \ldots)\, i_{B_a}(\lambda, \ldots)> \\ &+ <i_{A_a}(\lambda, \ldots)\, i_{B_s}(\lambda_1, \ldots)> + <i_{A_s}(\lambda_1, \ldots)\, i_{B_a}(\lambda, \ldots)> \\ &+ <i_{A_s}(\lambda_1, \ldots)\, i_{B_s}(\lambda_1, \ldots)>. \end{aligned} \tag{17}$$

Therefore, to obtain

$$<i_{A_a}(\lambda, \ldots)\, i_{B_a}(\lambda, \ldots)>,$$

we must know the three remaining terms on the RHS of equation (17).

By definition,

$$Q_{aa}(\lambda,\lambda) = \frac{<i_{A_a}(\lambda, \ldots)\, i_{B_a}(\lambda, \ldots)>}{<I_A><I_B>} \tag{18}$$

and

$$Q_{ss}(\lambda_1,\lambda_1) = \frac{\langle i_{A_s}(\lambda_1, \ldots)\, i_{B_s}(\lambda_1, \ldots)\rangle}{\langle I_A \rangle \langle I_B \rangle} \quad . \tag{19}$$

Also,

$$Q_{as} = (\lambda,\lambda_1) = \frac{\langle i_{A_a}(\lambda, \ldots)\, i_{B_s}(\lambda_1, \ldots)\rangle}{\langle I_A \rangle \langle I_B \rangle}$$

$$= \frac{\langle i_{A_s}(\lambda_1, \ldots)\, i_{B_a}(\lambda, \ldots)\rangle}{\langle I_A \rangle \langle I_B \rangle} \quad , \tag{20}$$

since both processes are governed by the turbulence convection and are thus well correlated. Now, setting beam A at λ_1 and beam B at λ, cross-correlating the two signals, we get

$$\frac{\langle i_A(\lambda_1, \ldots)\, i_B(\lambda, \ldots)\rangle}{\langle I_A \rangle \langle I_B \rangle} = Q_{as}(\lambda,\lambda_1) + Q_{ss}(\lambda_1,\lambda_1) \tag{21}$$

or

$$Q_{as}(\lambda,\lambda_1) = \frac{\langle i_A(\lambda_1, \ldots)\, i_B(\lambda, \ldots)\rangle}{\langle I_A \rangle \langle I_B \rangle} - Q_{ss}(\lambda_1,\lambda_1). \tag{22}$$

Finally, we can write

$$Q_{aa}(\lambda,\lambda) = \frac{\langle i_A(\lambda, \ldots)\, i_B(\lambda, \ldots)\rangle}{\langle I_A \rangle \langle I_B \rangle}$$

$$- 2\,\frac{\langle i_A(\lambda_1, \ldots)\, i_B(\lambda, \ldots)\rangle}{\langle I_A \rangle \langle I_B \rangle}$$

$$+ Q_{ss}(\lambda_1,\lambda_1), \tag{23}$$

which is the contribution due to absorption only (see figure I.4).

Figure I.5 shows a radial profile measured at a center wavelength of $\lambda = 4.24$ microns. The resolution of the crossed-beam system may be assessed by comparing the width of this intensity peak with the shear layer width. The consistent variation of the two-beam product mean value is evidence of resolution capabilities, and supports the earlier contention of the validity of the point-area correlation concept.

Fourier transforms performed on the cross-correlations are presented in figure I.6. Once again the point-area concept appears to be supported by experimental evidence, since the high frequency portion of the spectrum does approximate the -11/3 power law very well.

I-4. CONCLUSIONS AND FUTURE PLANS

The very promising first results presented in this paper have given confidence that the crossed-beam technique will allow measurements of sound source intensities to be made in jet flows. Toward that end, experiments are being initiated to measure two-beam correlations in a heated subsonic jet, and measurements have already begun in a specially designed absorption calibration cell to verify analytical predictions, with regard to understanding pressure and temperature effects. These measurements are to be made by varying the absorber mass, static and dynamic pressure and static temperature independently.

With this information and the already proven ability to obtain remotely point-area correlations that are not accessible to probe instruments, the crossed-beam system will have the potential of locating and measuring, for the first time, the turbulent sound source intensities in jet flows. Such measurements, taken without disturbing the flow, will not only lend support to analytical predictions, but also aid in the design and evaluation of noise suppression devices.

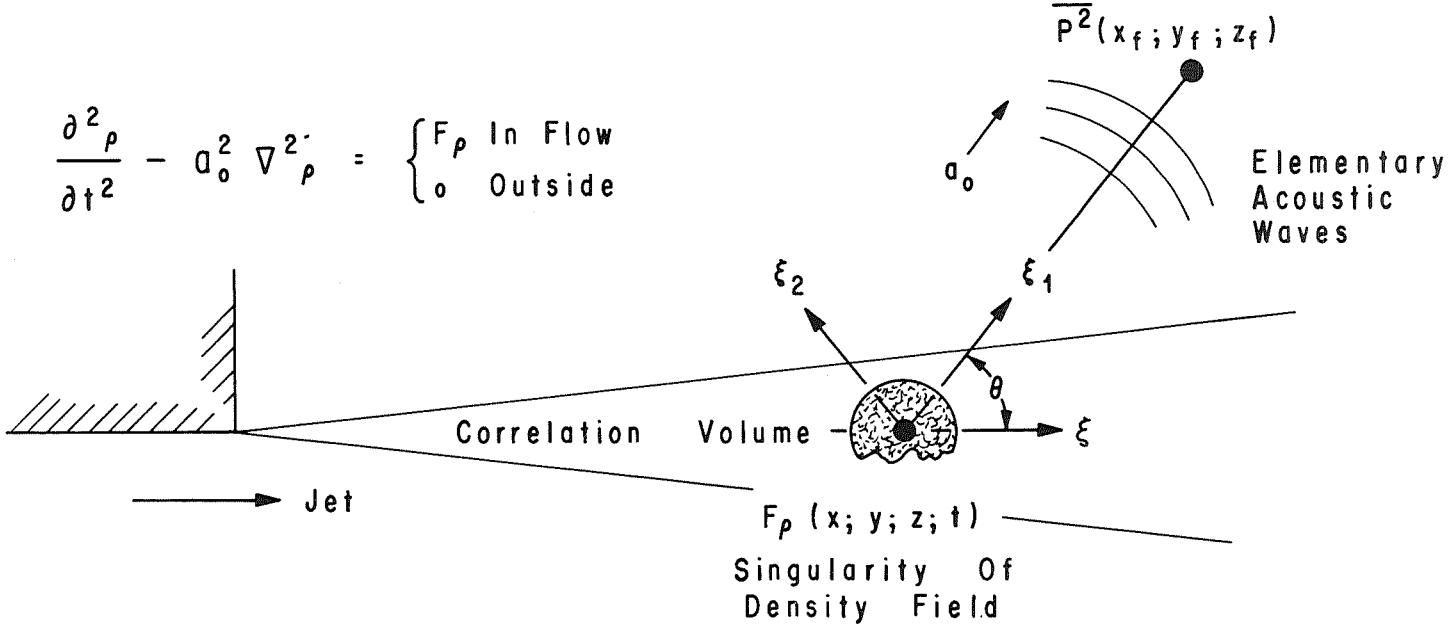

Far Field Sound Source Intensities

$$F(\vec{x}) = \int \langle F_\rho(\vec{x}; t)\, F_\rho(\vec{x} + \vec{\xi}; t - \frac{\xi_1}{a_o}) \rangle \, d\vec{\xi} = \text{Integration Over } \xi_1$$

Of The Time Lag Derivatives Of $\langle \rho(\vec{x}, t) \int \rho(\vec{x} + \vec{\xi}, t - \frac{\xi_1}{a_o})\, d\xi_2\, d\xi_3 \rangle$

Point Area

Product Mean Value Of Gas Density Fluctuations

FIGURE I.1. EXTENSION OF ACOUSTIC WAVES INTO FLOW

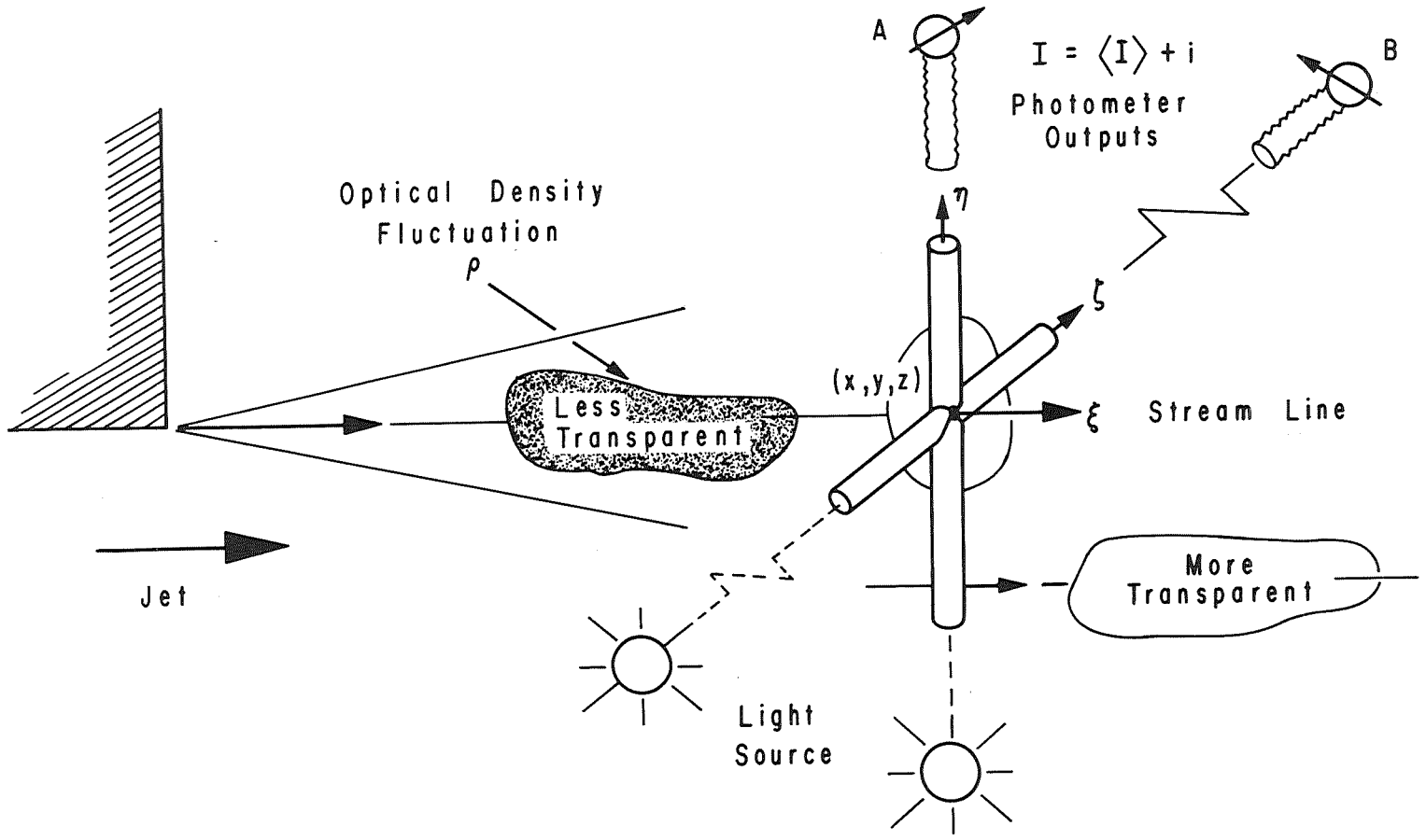

FIGURE I.2. CROSS-BEAM APPROXIMATIONS OF LOCAL SOUND SOURCE INTENSITIES

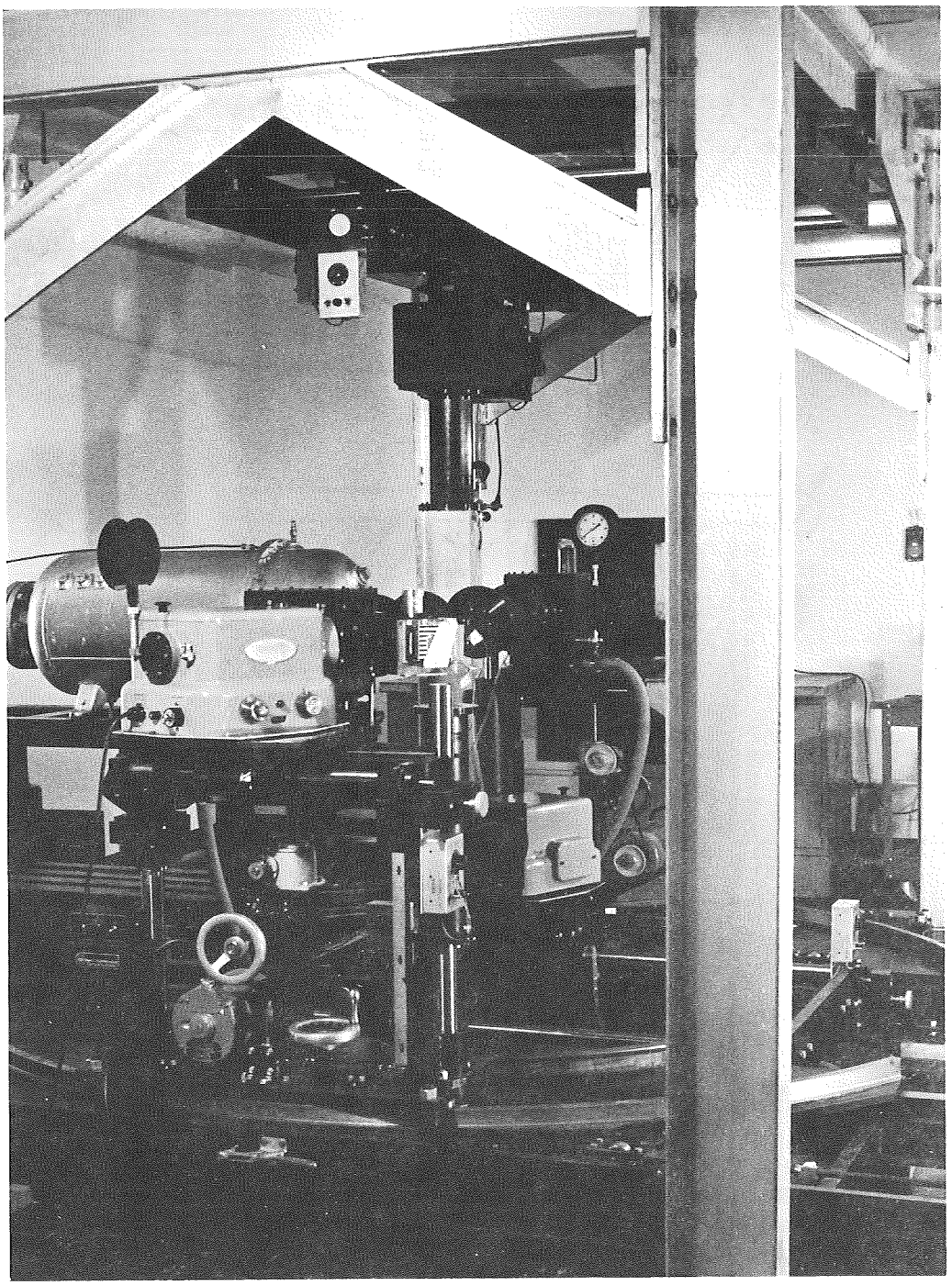

FIGURE I.3. IR X-BEAM FRAME

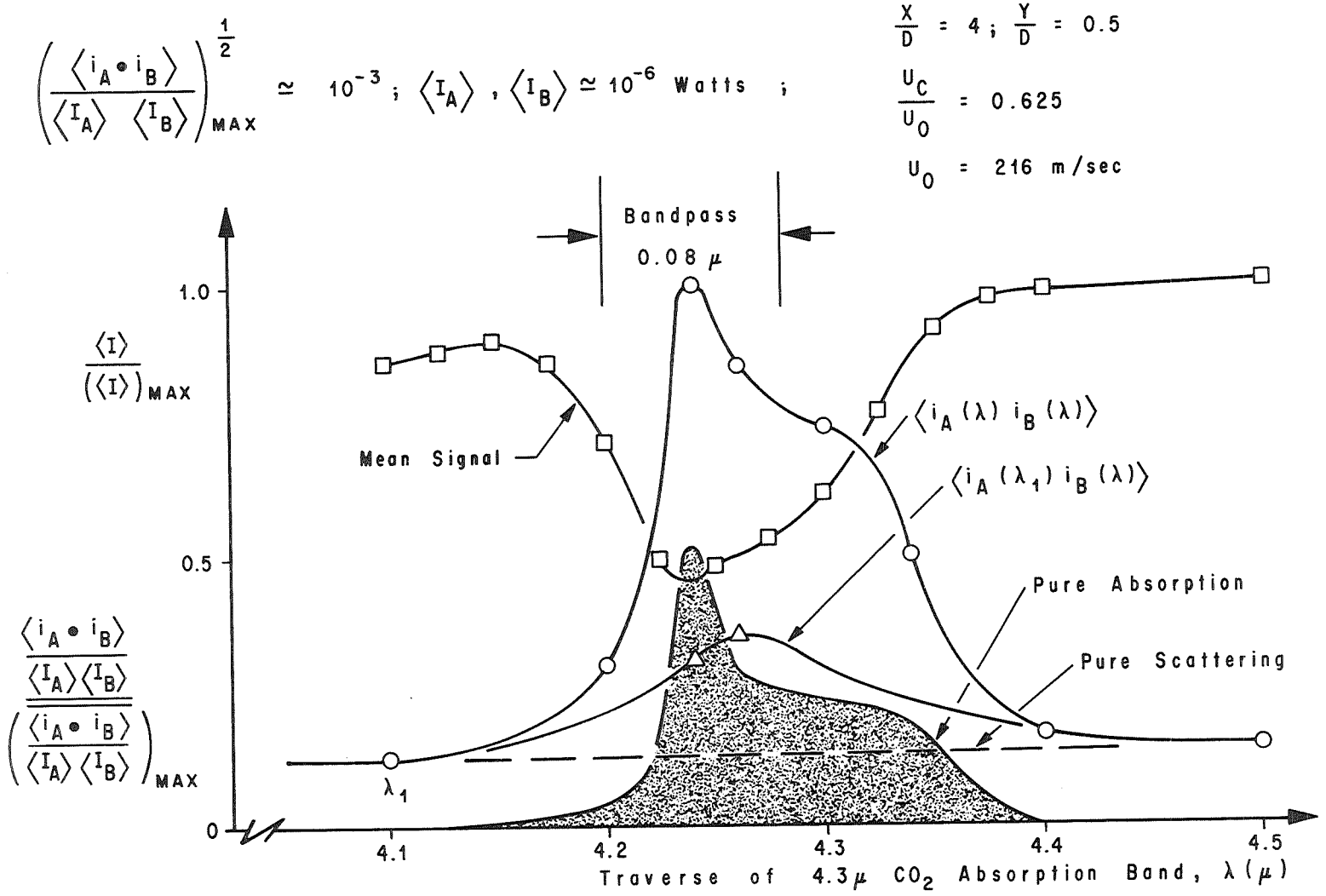

FIGURE I.4. DECOUPLING OF ABSORPTION AND SCATTERING

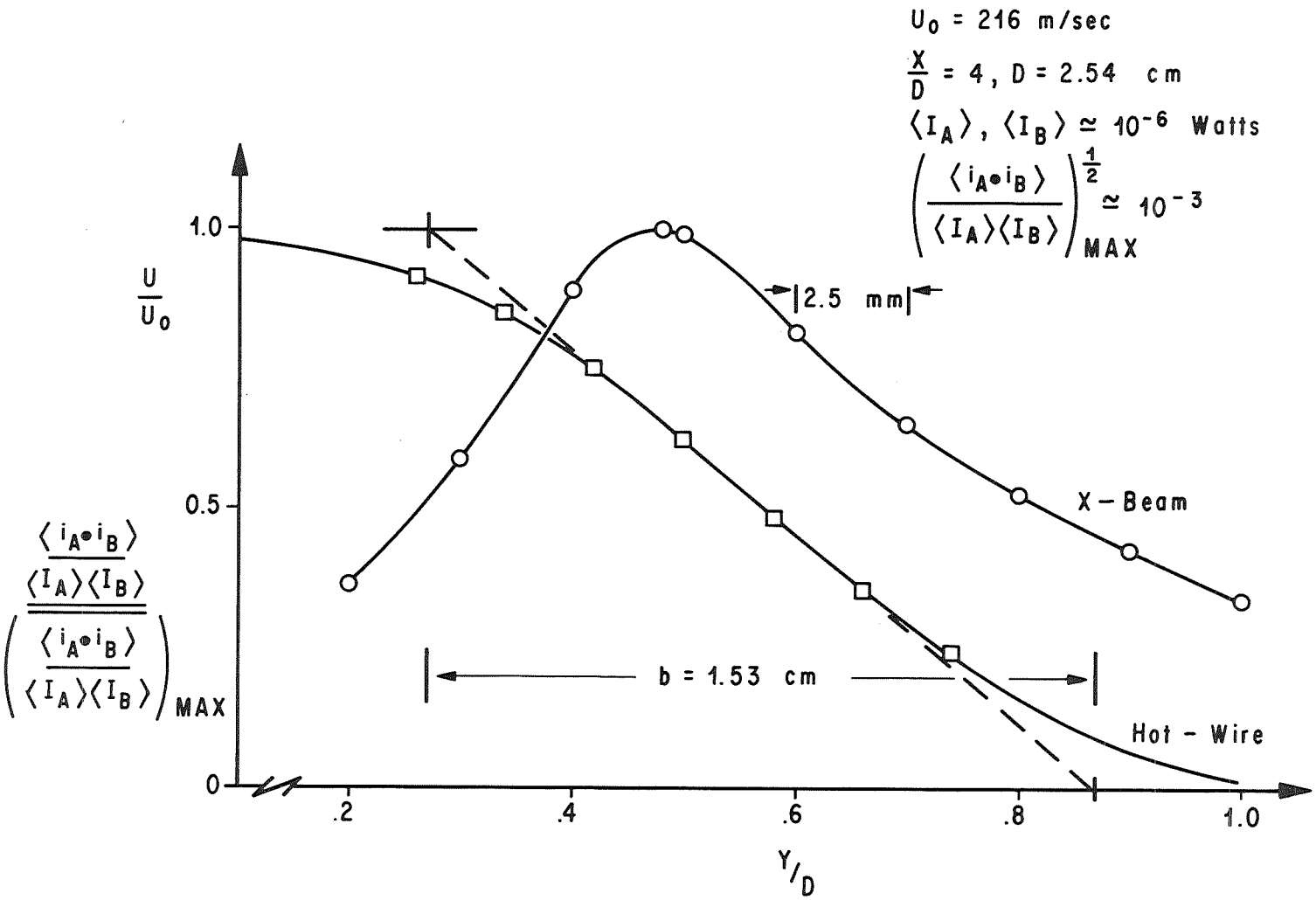

FIGURE I.5. RADIAL PROFILE OF CROSSED BEAM INTENSITY

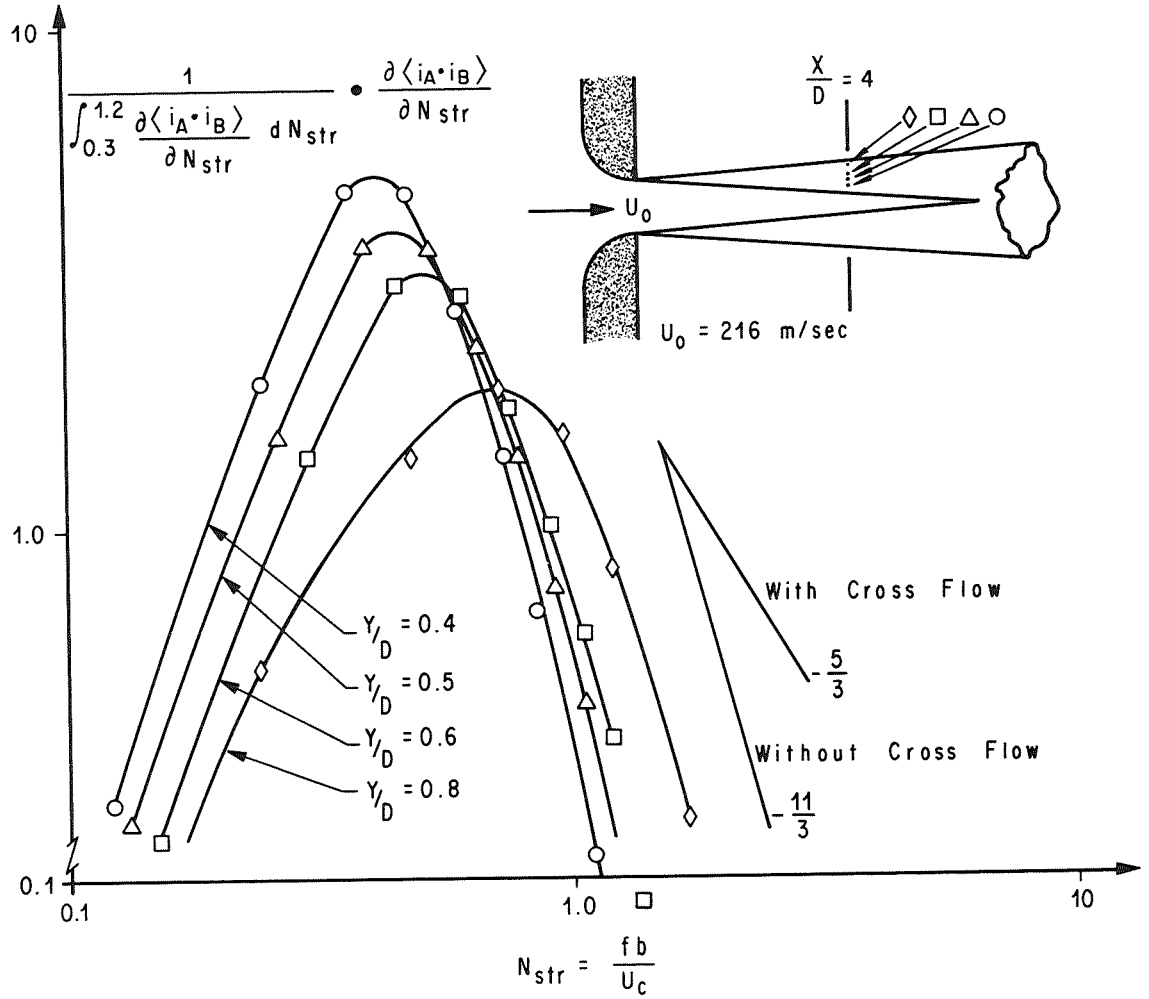

FIGURE I.6. CROSSED BEAM APPROXIMATIONS OF THREE-DIMENSIONAL SPECTRUM FUNCTIONS

REFERENCES

I-1. Lighthill, M. J., "On Sound Generated Aerodynamically, Part I: General Theory," Proc. Roy. Soc. A211, 1107 (1952).

I-2. Lighthill, M. J., "On Sound Generated Aerodynamically, Part II: Turbulence as a Source of Sound," Proc. Roy. Soc. A222, 1148 (1954).

I-3. Chu, W. T., "Turbulence Measurements Relevant to Jet Noise," UTIAS Report No. 119 (1966).

I-4. Jones, I. S. F., "Fluctuating Turbulent Stresses in the Noise Producing Region of a Jet," Journal of Fluid Mechanics, Vol. 36, 3 (1969).

I-5. Ffowcs-Williams, J. E. and G. Maidanik, "The Mach Wave Field Radiated by Supersonic Turbulent Shear Flows," Journal of Fluid Mechanics, Vol. 24, 4 (1965).

I-6. Fisher, M. J. and F. R. Krause, "The Crossed-Beam Correlation Technique," Journal of Fluid Mechanics, Vol. 28, 4 (1967).

7. Krause, F. R. and M. J. Fisher, "Optical Integration over Correlation Areas in Turbulent Flows," Proc. Int. Congr. Acoustics, Paper K65, Liege, Belgium, Oct. 1965 (also published as NASA TM X-53389).

8. Krause, F. R. and L. N. Wilson, "Optical Crossed-Beam Investigation of Local Sound Generation in Jets," Conference on Noise Alleviation of Large Subsonic Jet Aircraft, NASA SP-189 (1968).

9. Fisher, M. J. and R. J. Damkevala, "Fundamental Considerations of the Crossed-Beam Correlation Technique," NASA CR-61252 (1969).

CHAPTER II

OPTICAL DETECTION OF MOVING STRIATIONS WITH THE CROSS-CORRELATION TECHNIQUE

by

J. B. Stephens and J. B. Thomison, Jr.
NASA - Marshall Space Flight Center, Alabama

SUMMARY

Optical observations of emission variations in a plasma generated by a glow discharge have been achieved using the cross-beam correlation technique. Classification of these emission variations at a point into periodic, narrow band, and random processes, is discussed, along with the identification of convection speeds and feedback loops of the system.

II-1. INTRODUCTION

The experiments documented in this paper were designed to develop cross-beam methods for studying local photo-chemical processes in a plasma. Previous investigations of glow discharges by Abria [II-1] and later by others [II-2] indicated that it is composed of moving optical fluctuations. More recent photographic experiments by Garscadden and Lee [II-3] show that these fluctuations can move both toward the cathode and toward the anode. Our tests differ from previous investigations by applying the cross-beam correlation technique which was developed in the wind tunnel by Fisher and Krause [II-4] and in the atmosphere by Stephens *et al.* [II-5] to measure wind speeds. Velocity and frequency information has been obtained by extending the cross-beam technique from extinction processes to emission processes.

II-2. PHOTOGRAPHIC EVALUATION OF GLOW DISCHARGE PHENOMENA

The plasma instabilities that produced the optical fluctuations are defined to be striations in the positive column of the glow discharge (see Fig. II.1). Stationary striations, which are packets of ionized gas separated by dark spots, normally occur at tube pressures below 1 mm Hg (see Fig. II.1b). Figure II.1a is an example of moving striations. Although this picture was taken at 1/100 of a second, fluctuations are not obvious, and the glow appears as a continuum. Figure II.2 shows the test setup as it appeared immediately before a high-speed movie was taken.

If a striation contains an excess of positively ionized gas, it should move toward the cathode. Conversely, if a striation contains an excess of electrons, it should move toward the anode. This is in accord with the current views of plasma physics [II-3]. These two cases are illustrated in Figures II.3 and II.4 taken at 1/400 of a second. In Figure II.3 the smaller striation moves primarily toward the cathode, reverses its direction for a short time, and moves backward toward the anode. In Figure II.4 the movement of the striation tends entirely toward the anode. This is in keeping with the results of Garscadden and Lee [II-3] which show existence for forward- and backward-moving striations.

High-speed movies were taken of this phenomenon, but, unfortunately, movies provide only qualitative descriptions since the photographic film is a logarithmic detector. Therefore, one cannot see a fine structure in the photographs of the large semi-stationary ionization. The present state-of-the-art in photography restricts measurements to those occurring below 1000 Hz. For example, little or no detailed information can be obtained about a glow discharge in argon since its frequency range is from 1000 Hz to at least 10,000 Hz.

II-3. CROSS-BEAM EXPERIMENTS

Both qualitative and quantitative results have been achieved by using two crossed photomultipliers. These photomultipliers are linear over their entire range and have a frequency response better than our electronics.

The experimental setup is shown in Figure II.5. Our measurements, which were restricted to the positive column, were made at an optical wave length of 3100 Å with a bandpass of 50 Å. The focal length of the optics was 11.3 cm with a diameter of the beam at intersection of 1 mm. The work was done in a discharge tube of a diameter of 9 cm and with

stainless steel electrodes 82 cm apart. The major portion of our effort was concentrated in Argon at the pressure range from 1 mm Hg to 25 mm Hg, with some work also being done in CO_2 and air.

The outputs of the optical collectors were then fed into the Princeton Applied Research (PAR) analog correlator to obtain a covariance reading. This on-line analog computer assumes that no D.C. shifts, trends or gain instabilities were introduced by the electronics. Further, the covariance thus obtained will become uncertain as soon as the correlation drops below 10 percent of the mean signal power.

Within the above assumptions, the analog computations of the PAR correlator should form an estimate of the temporal covariance function, which is defined as follows:

$$\overline{\overline{C_{xy}}}\ (\tau) = \frac{1}{TN}\int_{o}^{T} (X(t) - \bar{X})(Y(t-\tau) - \bar{Y})\ dt,$$

where

$x(t)$ = instantaneous fluctuations of intensity from the undelayed channel

$Y(t-\tau)$ = instantaneous fluctuations from the delayed channel

$\bar{X}$ and $\bar{Y}$ = average values of the fluctuations

τ = delay time set during data reduction

t = real time

T = total integration time

N = normalization factor.

This covariance enables one to obtain the best estimate for the amount of time required for the striation to traverse the transit distance of the two beams (see Fig. II.5). The covariance also provides a systematic approach to the classification of narrow- and broad-band processes while systematically treating an entire ensemble.

As shown in Figure II.6 several types of wave form were encountered. The first signal is easy to classify since it is obviously periodic, but the remaining signals require some kind of statistical description. Figure II.7 shows how the top three signals can be classified by use of

an autocorrelation curve. When the maximum amplitude of the peaks does not decay as a function of time delay, then the process is periodic. When the peak decay is a function of time delay the process is either narrow-band or broad-band, depending on the rate of correlation decay. The broad-band process occurs where there is only a fundamental peak and the remaining peaks are washed out. In the narrow band process the higher order peaks decrease in amplitude as the order increases. Physically, these three processes tell you that:

(1) If the signal is periodic, then the signal time history is recurring at exact intervals of time.

(2) If the signal is narrow-band, then the time history will repeat itself for a finite number of periods until it is damped out.

(3) If the signal is broad-band, then the signal time history will not repeat itself.

Thus, the kind of process provides a means of classification of the internal consistency of the structure.

The fourth signal on Figure II.6 affords a more challenging test for the correlation technique as shown in Figure II.8. It was found that by filtering the signal it could be subdivided into a high frequency and a low frequency component. The low frequency component was due to periodic fluctuations and moved in the direction of the cathode. The high frequency component was a narrow-band process and had a velocity in the direction of the anode. This could well be thought of as an ion striation (moving toward the cathode) with a substructure composed of electron waves (moving toward the anode). The direction of flow was determined by starting with intersecting beams and increasing the beam separation. As the separation increased, the transit time increased positively or negatively according to the flow direction.

Another kind of measurement performed was the identification of the feedback loop between the fluctuations of the discharge current and the optical fluctuations in emission. This was done by cross-correlating the optical fluctuations with the current fluctuations. When the beam separation increased, the transit time increased (bottom correlation curve in Figure II.8). Thus, it was possible to close the feedback loop and say that the fluctuations in the current were due to the flow of electrons in the discharge.

When one changes the potential across the discharge, the discharge is unstable until it reaches thermal equilibrium. All of our measurements were made after a short period of time had elapsed, and it was confirmed that all parameters were stable.

II-4. PERIODIC STRIATIONS

The frequencies of the periodic fluctuations ranged from 10 Hz to 50 KHz and the velocities from 0 to 30 km/sec. The results are based on over 200 measurements, which are summarized in Figures II.9, II.10, II.11 and Table II.1.

During the course of our measurements, it was noticed that a periodic waveform would appear out of what had been a random narrow-band process. This periodic waveform was stable for the conditions under which it was observed, but any slight change in conditions resulted in a reversion to the random narrow-band process. The periodic process was observed in Argon over a wide range (1 mm - 20 mm) of pressure, but only certain discharge voltages for each pressure. It was also noticed that the amplitude of the periodic waveform was much larger than that for the associated random narrow-band process.

The wave length of the periodic waveform seemed to fall approximately into two categories (see Fig. II.10):

(1) Wave length equal to length of tube;

(2) Wave length equal to one half of tube length.

The velocity and frequency of the periodic striations are practically independent from the tube pressure within the range between 1 and 20 mm Hg as illustrated in Figures II.9 and II.10. The kind of process, the kind of striation (ion or electron), and the gas composition all have a first order effect on the velocity, frequency, and wave length of moving striations. Even though we could not clearly establish a pattern, there appeared to be times during which only one type of striation was present. Ion and electron striations did not always occur simultaneously.

II-5. STANDING STRIATIONS

The second distinct class of striation that was observed in the glow discharge is a standing striation. We always found that the fluctuations in emission associated with standing striations were broad band. The first zero crossing of the auto-correlation function was taken as an estimate of the time period associated with the center frequency of the broad band process. This period was divided into the measured velocity to obtain a characteristic wave length.

Although the striations appear standing to the observer, the cross correlation tests indicated that they have small velocities about a factor of a hundred less than those associated with the periodic striations. The direction of these small velocities seemed to follow only the electron flux.

II-6. CONCLUSIONS AND RECOMMENDATIONS

Since our results for the velocities and frequencies of moving striations are in keeping with those to be found in the literature, we have confidence in the cross-beam technique to retrieve this information in emission.

This research has demonstrated the feasibility of the cross-beam technique for successful retrieval in emission of (1) phase and group velocities along the main current, (2) separation of periodic and random narrow-band components, (3) classification of optical disturbances using length and time scales in moving frame, (4) classification of flow instabilities through statistical evaluation of changes in surroundings, and (5) correlation between feedback loops and the control system (e.g., correlation of fluctuations in emission and fluctuations in current).

GLOW DISCHARGE

a.

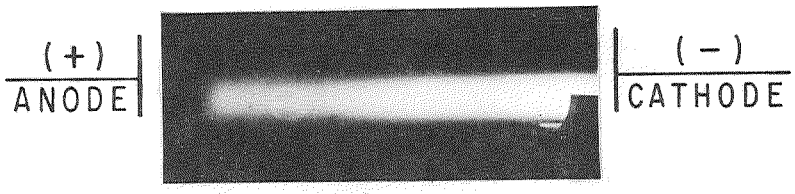

MOVING STRIATIONS IN ARGON

f = 24 KC v = 16 km/sec

p = 2 mm Hg

b.

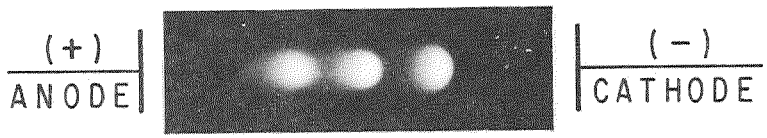

STANDING STRIATIONS IN ARGON

p = 0.02 mm Hg

FIGURE II.1. MOVING AND STANDING STRIATIONS

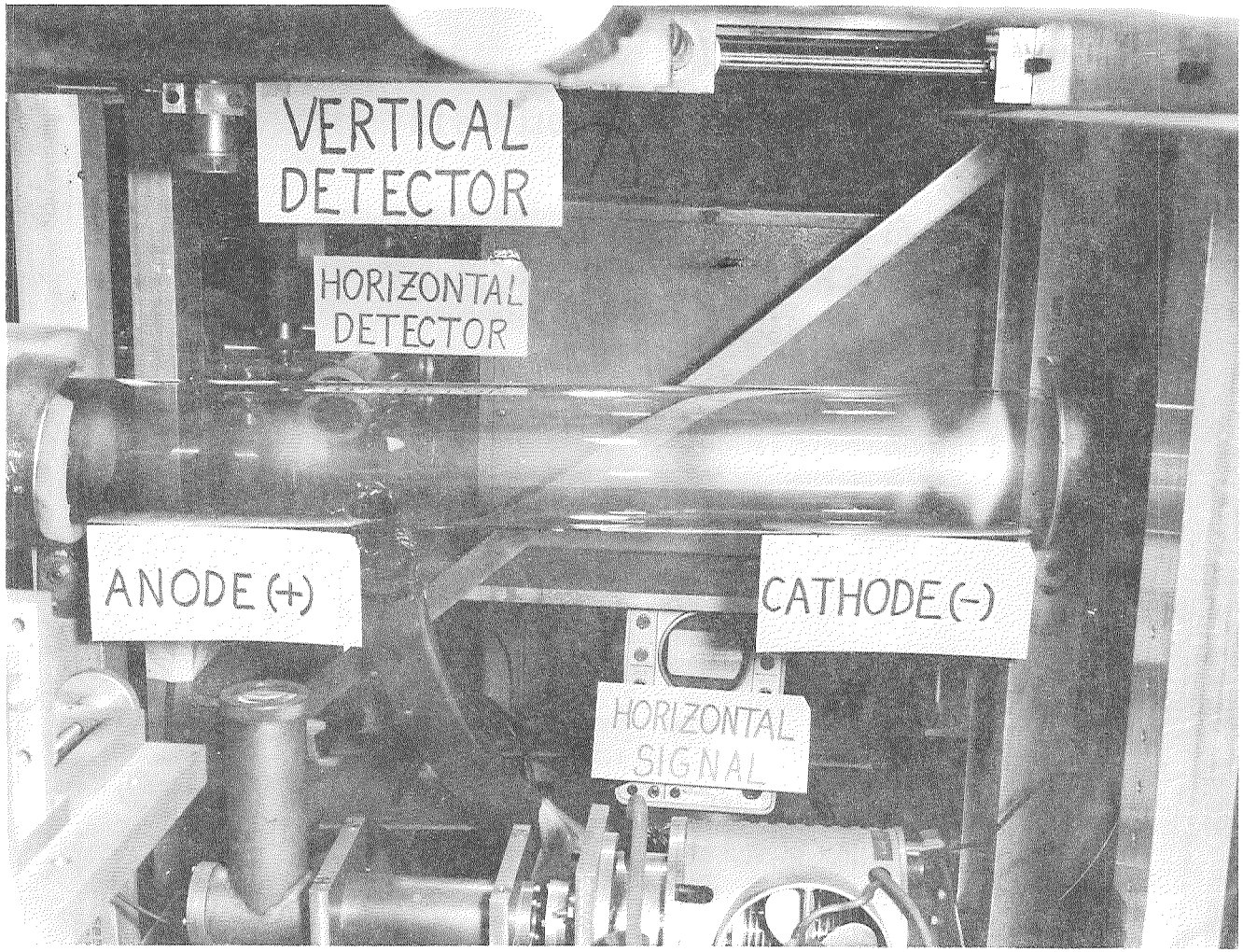

FIGURE II.2. EQUIPMENT SETUP

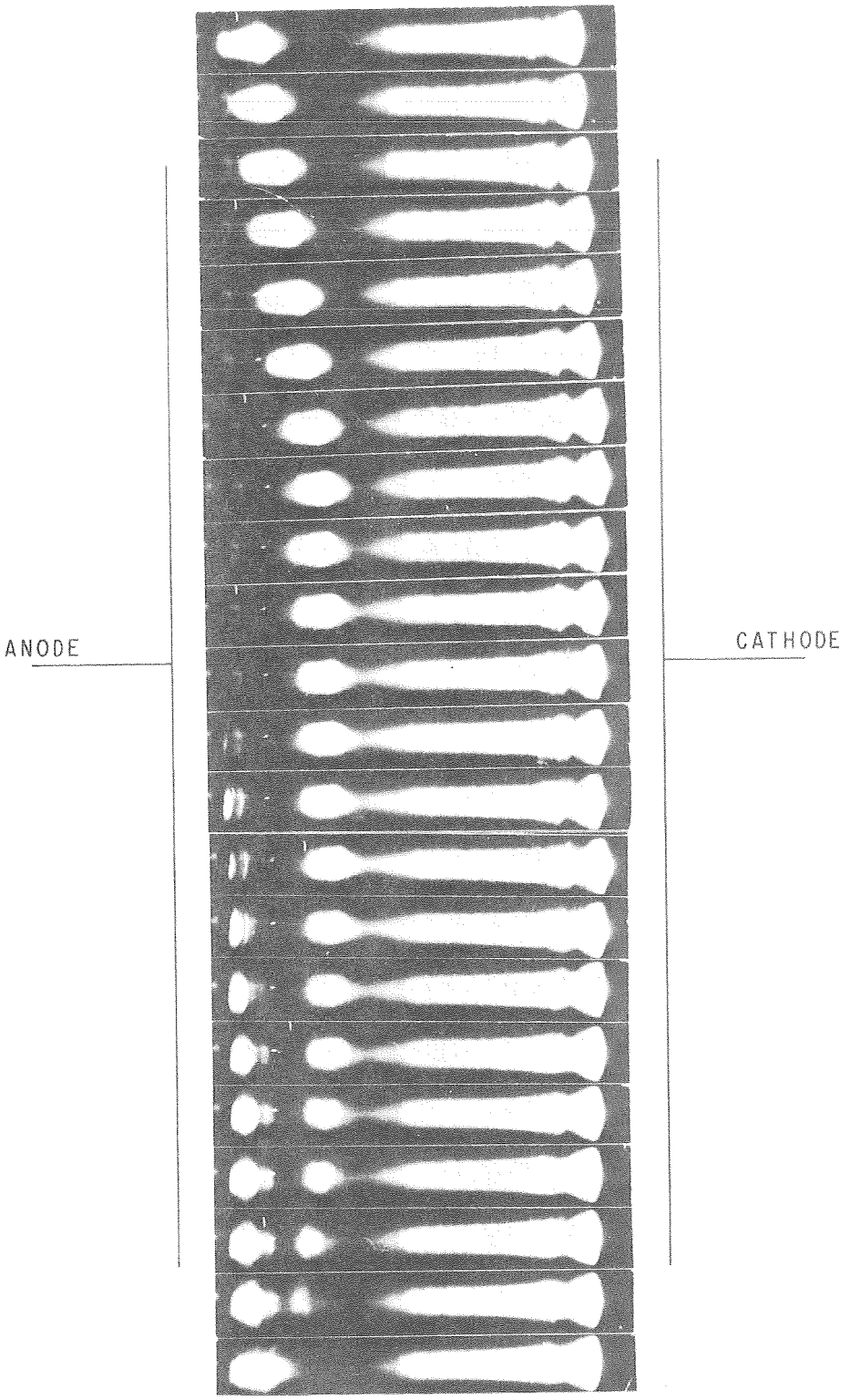

FIGURE II.3. ION STRIATION

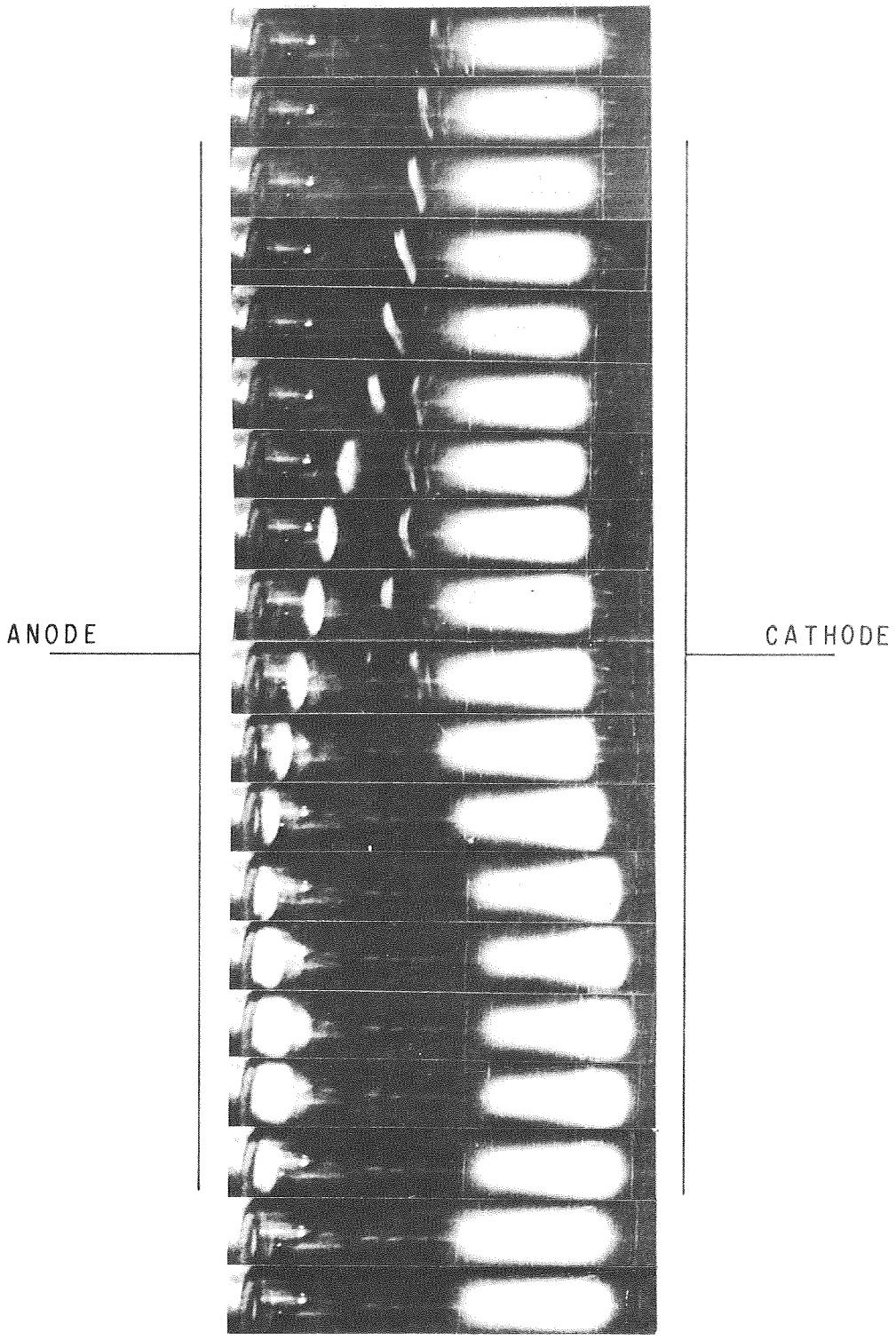

FIGURE II.4. ELECTRON STRIATION

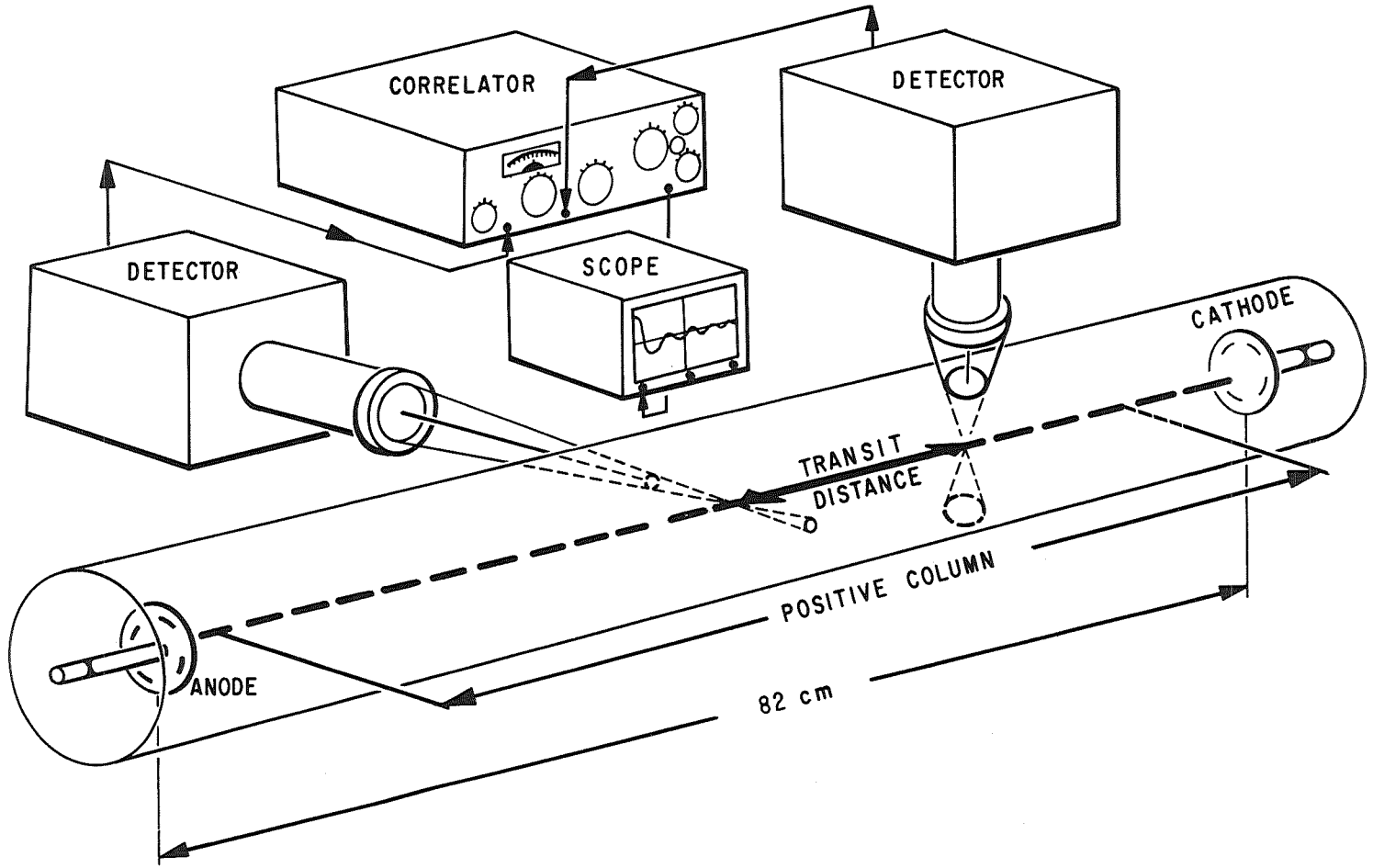

FIGURE II.5. EXPERIMENTAL SETUP FOR GLOW DISCHARGE

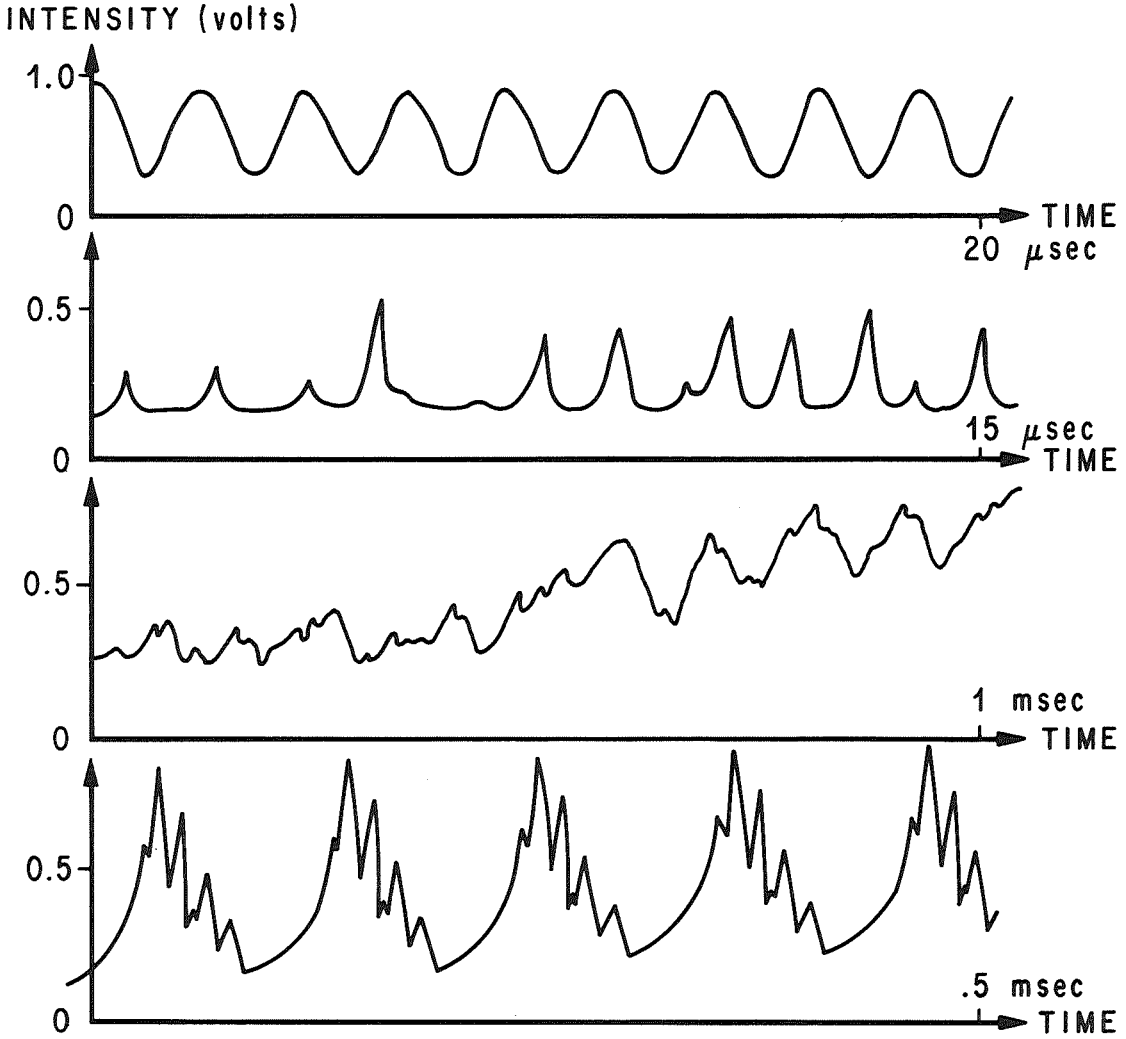

FIGURE II.6. MODES OF FLUCTUATION ENCOUNTERED IN GLOW DISCHARGE PRESSURE RANGE FROM 1 TO 25 MM HG AT 3100 Å AND BANDWIDTH OF 50 Å

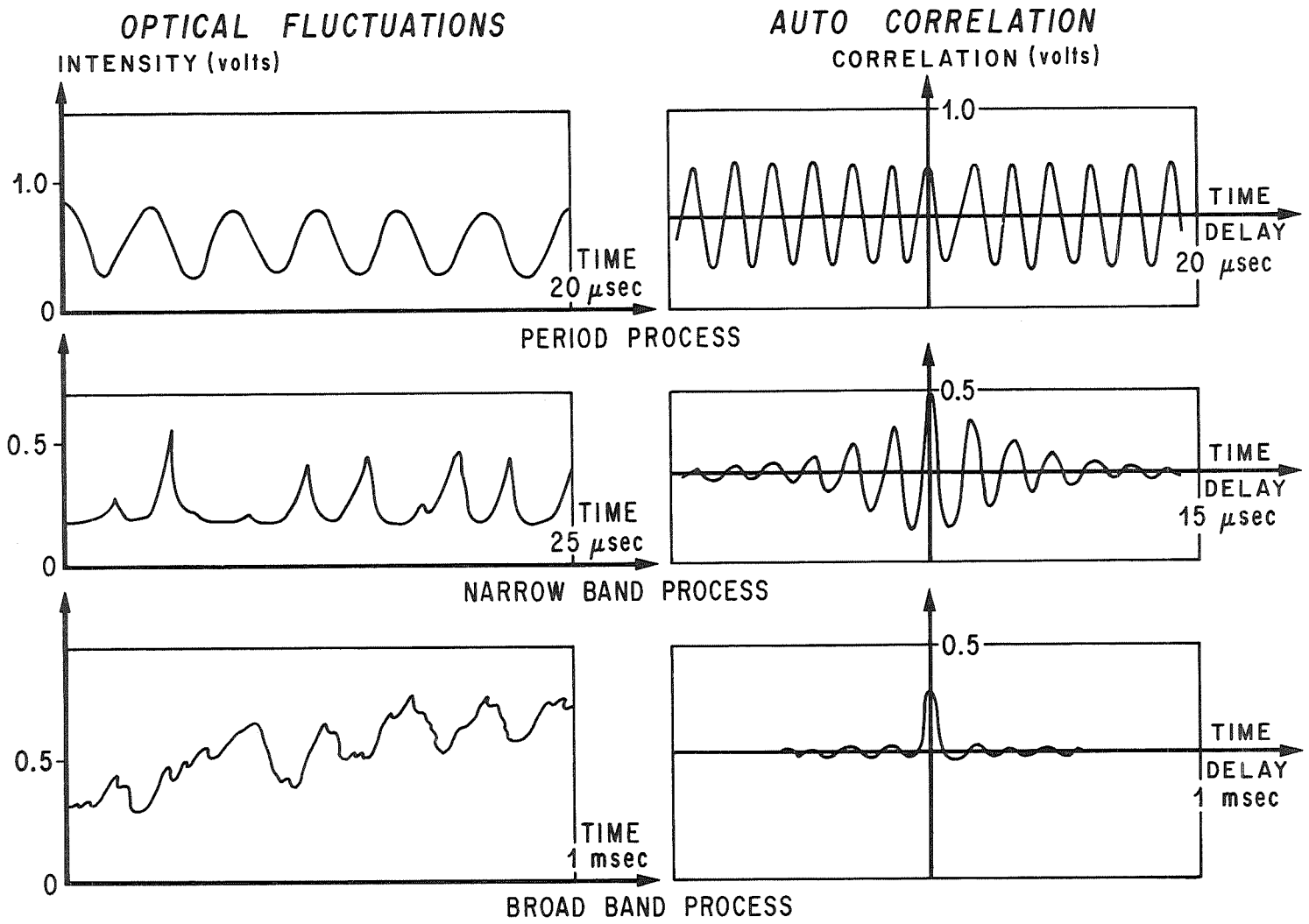

FIGURE II.7. CORRELATION OF SINGLE PHOTOMETER OUTPUTS FOR TYPICAL FLUCTUATIONS

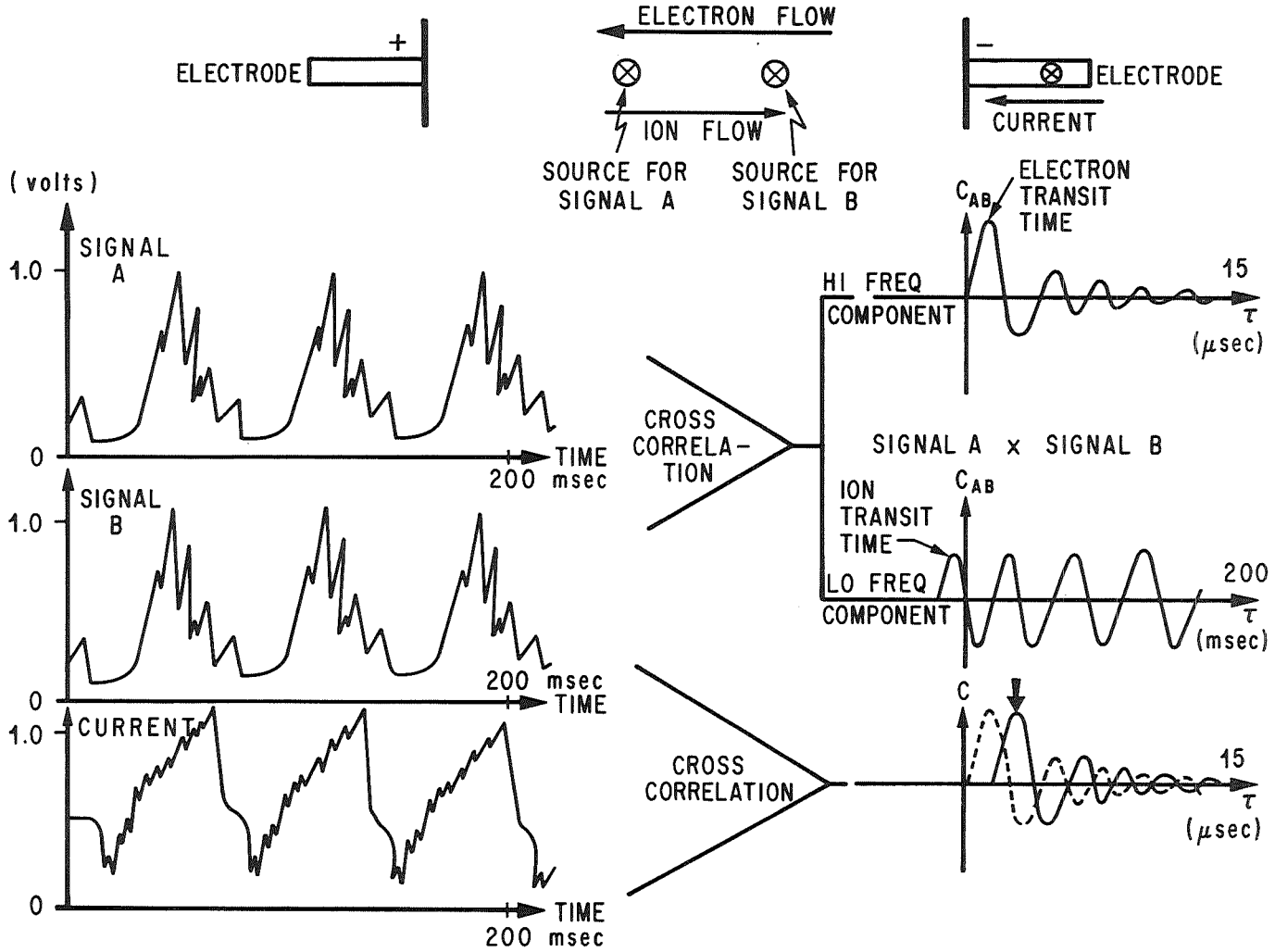

FIGURE II.8. SEPARATION OF ELECTRON AND ION STRIATIONS

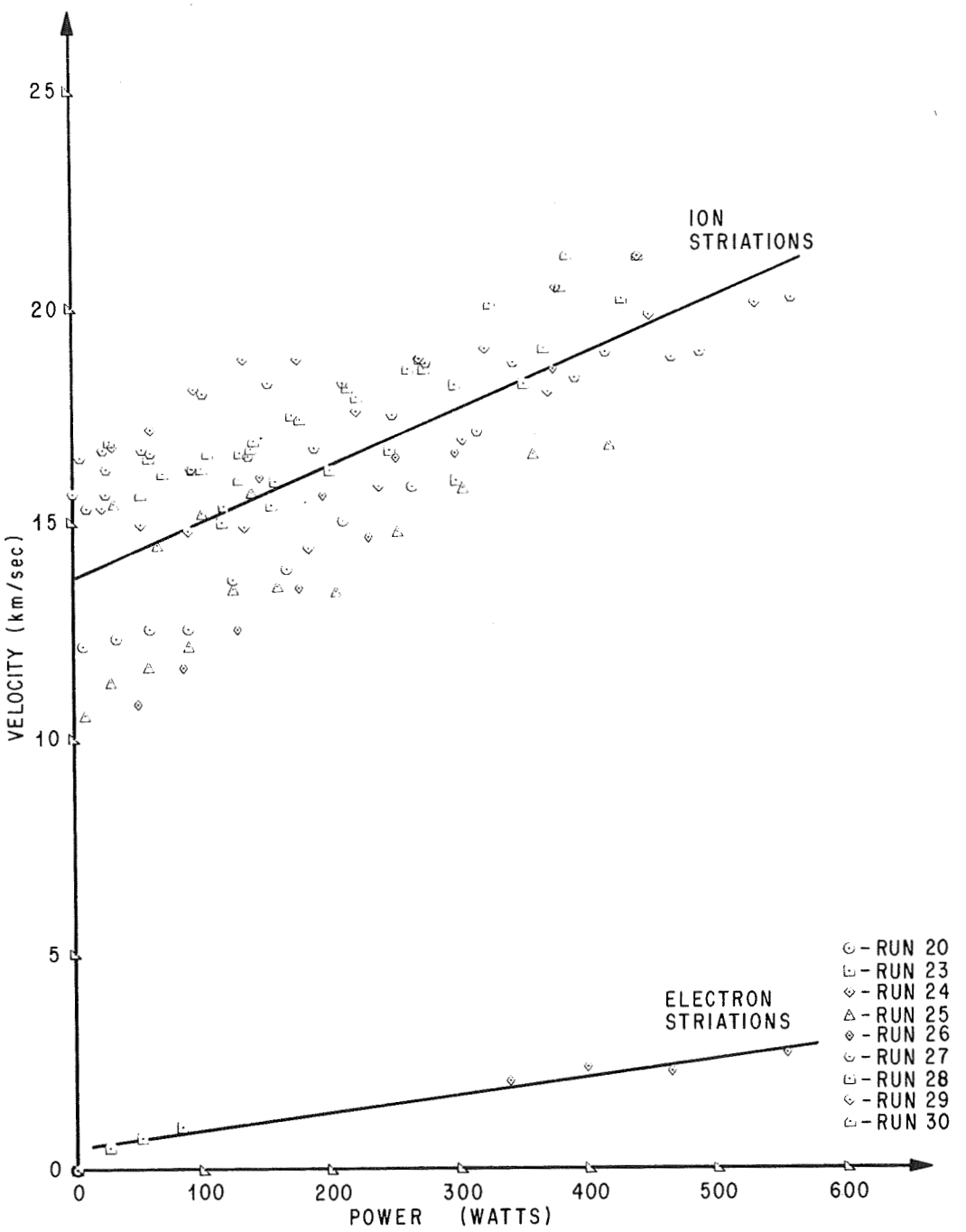

FIGURE II.9. EFFECT OF STRIATION DIRECTION ON ITS VELOCITY

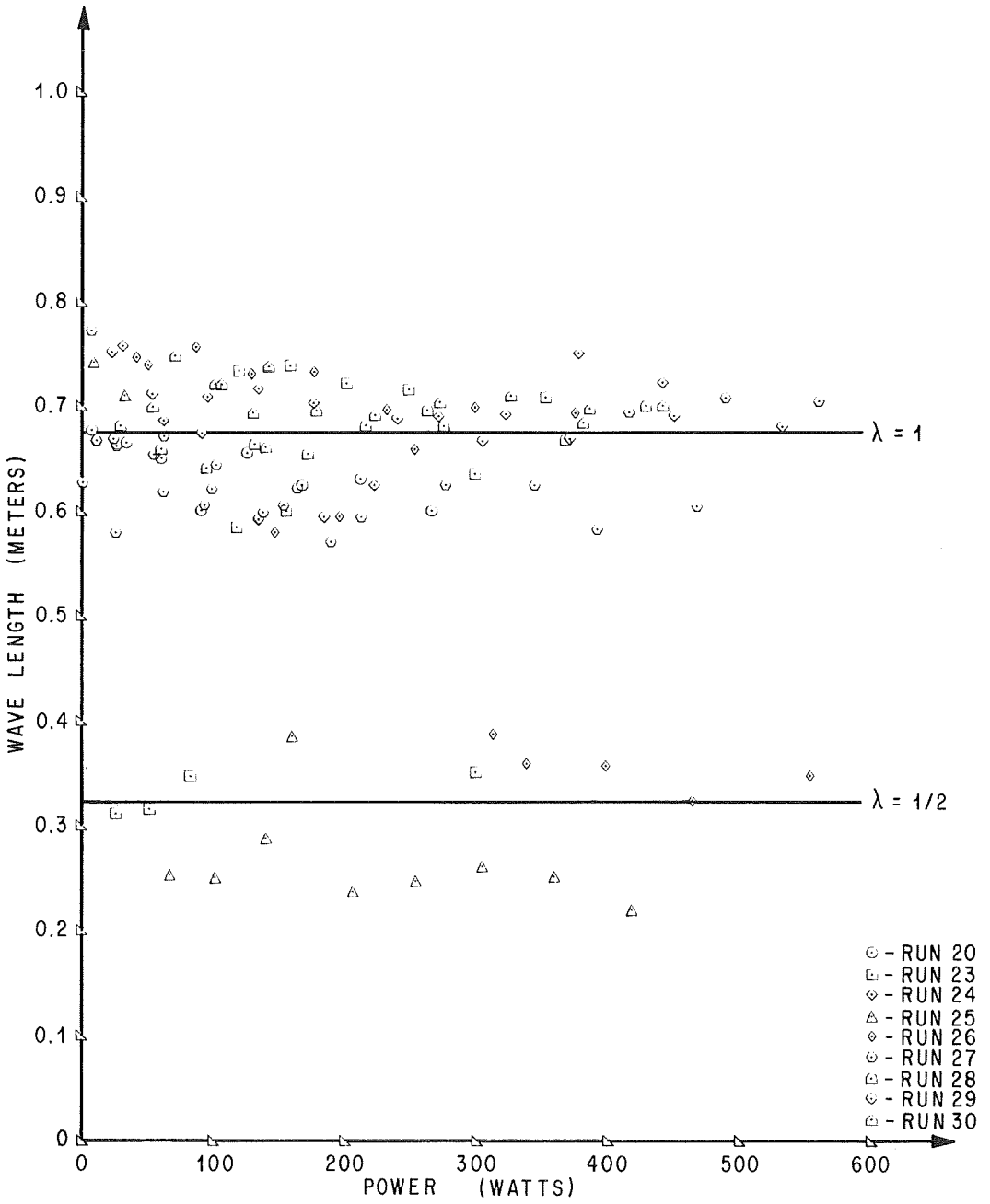

FIGURE II.10. QUANTUM EFFECT OF WAVELENGTH

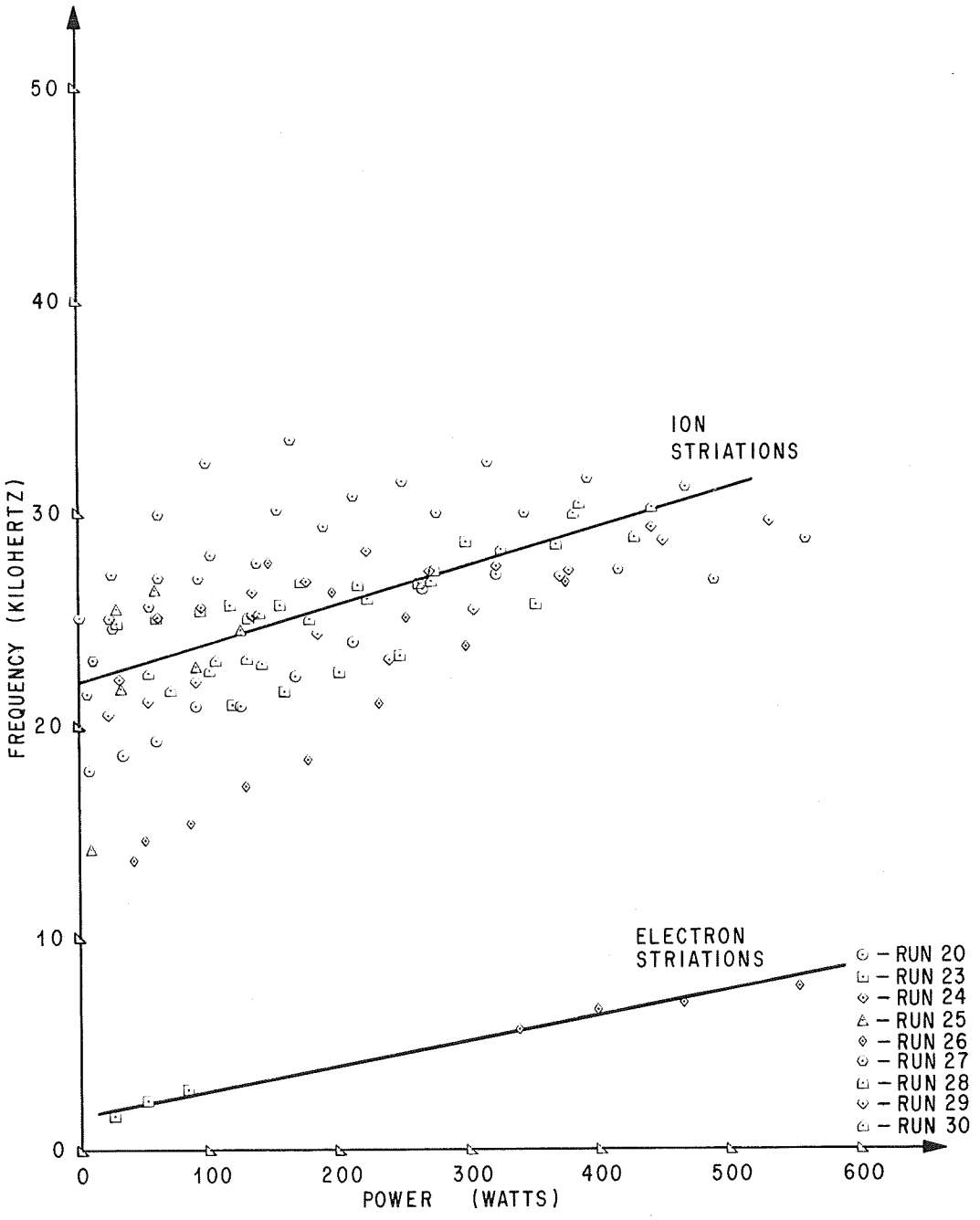

FIGURE II.11. EFFECT OF STRIATION DIRECTION ON ITS FREQUENCY

TABLE II.1. EXPERIMENTAL DATA

GLOW DISCHARGE IN ARGON

RUN NUMBER = 20.0 PRESSURE = 5.0

POWER WATTS	RESIST K OHMS	FREQ KHZ	VEL KM/SEC	WLG METERS	DIS I MA	DIS V VOLTS	PER USEC	TAU USEC
8.100	36.000	17.857	12.097	.677	15.0	540.0	56.0	24.8
33.605	7.954	18.519	12.295	.664	65.0	517.0	54.0	24.4
59.800	4.522	19.231	12.500	.650	115.0	520.0	52.0	24.0
90.255	3.315	20.833	12.500	.600	165.0	547.0	48.0	24.0
125.560	2.716	20.833	13.636	.655	215.0	584.0	48.0	22.0
166.950	2.377	22.222	13.889	.625	265.0	630.0	45.0	21.6
211.050	2.127	23.810	15.000	.630	315.0	670.0	42.0	20.0
264.625	1.986	26.316	15.789	.600	365.0	725.0	38.0	19.0
321.625	1.867	27.027	21.429	.793	415.0	775.0	37.0	14.0

RUN NUMBER = 23.0 PRESSURE = 4.8

POWER WATTS	RESIST K OHMS	FREQ KHZ	VEL KM/SEC	WLG METERS	DIS I MA	DIS V VOLTS	PER USEC	TAU USEC
25.650	10.260	1.600	.498	.311	50.0	513.0	625.0	603.0
51.500	5.150	2.353	.744	.316	100.0	515.0	425.0	403.0
82.500	3.667	2.857	.990	.347	150.0	550.0	350.0	303.0
117.000	2.925	25.641	15.000	.585	200.0	585.0	39.0	20.0
155.000	2.480	25.641	15.385	.600	250.0	620.0	39.0	19.5
297.600	1.860	28.571	18.182	.636	400.0	744.0	35.0	16.5
351.450	1.736	25.641	18.182	.709	450.0	781.0	39.0	16.5
298.000	1.862	45.455	15.957	.351	400.0	745.0	22.0	18.8
247.450	2.020	23.256	16.667	.717	350.0	707.0	43.0	18.0
200.400	2.227	22.472	16.216	.722	300.0	668.0	44.5	18.5
158.000	2.528	21.598	15.957	.739	250.0	632.0	46.3	18.8
118.200	2.955	20.964	15.385	.734	200.0	591.0	47.7	19.5

RUN NUMBER = 24.0 PRESSURE = 4.9

POWER WATTS	RESIST K OHMS	FREQ KHZ	VEL KM/SEC	WLG METERS	DIS I MA	DIS V VOLTS	PER USEC	TAU USEC
30.900	12.360	22.124	16.760	.758	50.0	618.0	45.2	17.9
61.800	6.180	25.000	17.143	.686	100.0	618.0	40.0	17.5
95.550	4.247	25.510	18.072	.708	150.0	637.0	39.2	16.6
134.000	3.350	26.178	18.750	.716	200.0	670.0	38.2	16.0
175.750	2.812	26.667	18.750	.703	250.0	703.0	37.5	16.0
221.700	2.463	28.090	17.544	.625	300.0	739.0	35.6	17.1
269.850	2.203	27.174	18.750	.690	350.0	771.0	36.8	16.0
321.200	2.007	27.397	18.987	.693	400.0	803.0	36.5	15.8
376.650	1.860	27.174	20.408	.751	450.0	837.0	36.8	14.7
440.000	1.760	29.240	21.127	.723	500.0	880.0	34.2	14.2

TABLE II.1. (Continued)

RUN NUMBER = 25.0 PRESSURE = 9.8

POWER WATTS	RESIST K OHMS	FREQ KHZ	VEL KM/SEC	WLG METERS	DIS I MA	DIS V VOLTS	PER USEC	TAU USEC
8.970	39.867	14.184	10.526	.742	15.0	598.0	70.5	28.5
29.500	11.800	25.510	11.321	.444	50.0	590.0	39.2	26.5
59.300	5.930	26.385	11.673	.442	100.0	593.0	37.9	25.7
90.750	4.033	22.779	12.146	.533	150.0	605.0	43.9	24.7
125.600	3.140	24.510	13.453	.549	200.0	628.0	40.8	22.3
160.000	2.560	35.088	13.514	.385	250.0	640.0	28.5	22.2
205.500	2.283	56.497	13.393	.237	300.0	685.0	17.7	22.4
253.050	2.066	59.524	14.778	.248	350.0	723.0	16.8	20.3
303.600	1.897	60.241	15.789	.262	400.0	759.0	16.6	19.0
358.200	1.769	65.789	16.575	.252	450.0	796.0	15.2	18.1
417.500	1.670	76.336	16.760	.220	500.0	835.0	13.1	17.9
139.200	3.480	54.348	15.707	.289	200.0	696.0	18.4	19.1
101.400	4.507	60.606	15.228	.251	150.0	676.0	16.5	19.7
66.500	6.650	57.143	14.493	.254	100.0	665.0	17.5	20.7
32.700	13.080	21.739	15.464	.711	50.0	654.0	46.0	19.4

RUN NUMBER = 28.0 PRESSURE = 5.1

POWER WATTS	RESIST K OHMS	FREQ KHZ	VEL KM/SEC	WLG METERS	DIS I MA	DIS V VOLTS	PER USEC	TAU USEC
30.400	12.160	24.752	16.854	.681	50.0	608.0	40.4	17.8
60.800	6.080	25.000	16.484	.659	100.0	608.0	40.0	18.2
94.800	4.213	25.316	16.216	.641	150.0	632.0	39.5	18.5
131.400	3.285	25.000	16.575	.663	200.0	657.0	40.0	18.1
171.750	2.748	26.667	17.442	.654	250.0	687.0	37.5	17.2
215.400	2.393	26.525	18.072	.681	300.0	718.0	37.7	16.6
262.150	2.140	26.596	18.519	.696	350.0	749.0	37.6	16.2
274.000	1.712	27.174	18.519	.681	400.0	685.0	36.8	16.2
367.650	1.816	28.409	18.987	.668	450.0	817.0	35.2	15.8
428.000	1.712	28.736	20.134	.701	500.0	856.0	34.8	14.9

RUN NUMBER = 29.0 PRESSURE = 2.0

POWER WATTS	RESIST K OHMS	FREQ KHZ	VEL KM/SEC	WLG METERS	DIS I MA	DIS V VOLTS	PER USEC	TAU USEC
23.250	9.300	20.408	15.306	.750	50.0	465.0	49.0	19.6
53.800	5.380	21.008	14.925	.710	100.0	538.0	47.6	20.1
91.050	4.047	21.930	14.778	.674	150.0	607.0	45.6	20.3
134.600	3.365	25.126	14.851	.591	200.0	673.0	39.8	20.2
184.250	2.948	24.213	14.354	.593	250.0	737.0	41.3	20.5
239.400	2.660	22.989	15.789	.687	300.0	798.0	43.5	19.0
303.800	2.480	25.316	16.854	.666	350.0	868.0	39.5	17.8
370.400	2.315	26.882	17.964	.668	400.0	926.0	37.2	16.7
449.550	2.220	28.571	19.737	.691	450.0	999.0	35.0	15.2
531.500	2.126	29.412	20.000	.680	500.0	1063.0	34.0	15.0

RUN NUMBER = 30.0 PRESSURE = 9.8

POWER WATTS	RESIST K OHMS	FREQ KHZ	VEL KM/SEC	WLG METERS	DIS I MA	DIS V VOLTS	PER USEC	TAU USEC
129.584	3.912	23.041	15.957	.693	182.0	712.0	43.4	18.8
141.400	3.535	22.831	16.854	.738	200.0	707.0	43.8	17.8
105.900	4.707	22.989	16.575	.721	150.0	706.0	43.5	18.1
70.900	7.090	21.598	16.129	.747	100.0	709.0	46.3	18.6
54.450	9.680	22.371	15.625	.698	75.0	726.0	44.7	19.2
101.700	4.520	22.523	16.216	.720	150.0	678.0	44.4	18.5
139.600	3.490	25.253	16.667	.660	200.0	698.0	39.6	18.0
178.000	2.848	24.938	17.341	.695	250.0	712.0	40.1	17.3
222.600	2.473	25.840	17.857	.691	300.0	742.0	38.7	16.8
271.250	2.214	26.667	18.750	.703	350.0	775.0	37.5	16.0
325.200	2.032	28.169	20.000	.710	400.0	813.0	35.5	15.0
380.250	1.878	29.851	20.408	.684	450.0	845.0	33.5	14.7
440.500	1.762	30.120	21.127	.701	500.0	881.0	33.2	14.2
385.650	1.904	30.303	21.127	.697	450.0	857.0	33.0	14.2

TABLE II.1. (CONTINUED)

RUN NUMBER = 26.0 PRESSURE = 2.0

POWER WATTS	RESIST K OHMS	FREQ KHZ	VEL KM/SEC	WLG METERS	DIS I MA	DIS V VOLTS	PER USEC	TAU USEC
41.905	5.800	13.605	10.169	.747	85.0	493.0	73.5	29.5
51.100	5.110	14.599	10.791	.739	100.0	511.0	68.5	27.8
86.250	3.833	15.385	11.628	.756	150.0	575.0	65.0	25.8
128.600	3.215	17.094	12.500	.731	200.0	643.0	58.5	24.0
176.250	2.820	18.349	13.453	.733	250.0	705.0	54.5	22.3
231.000	2.567	21.008	14.634	.697	300.0	770.0	47.6	20.5
297.500	2.429	23.697	16.575	.699	350.0	850.0	42.2	18.1
374.000	2.337	26.667	18.519	.694	400.0	935.0	37.5	16.2
463.500	2.289	6.849	2.222	.324	450.0	1030.0	146.0	135.0
553.000	2.212	7.634	2.655	.348	500.0	1106.0	131.0	113.0
397.200	2.482	6.557	2.344	.357	400.0	993.0	152.5	128.0
337.050	2.751	5.650	-2.027	-.359	350.0	963.0	177.0	-148.0
146.000	3.650	27.624	16.043	.581	200.0	730.0	36.2	18.7
195.500	3.128	26.247	15.625	.595	250.0	782.0	38.1	19.2
252.000	2.800	25.000	16.484	.659	300.0	840.0	40.0	18.2
311.500	2.543	15.674	21.739	1.387	350.0	890.0	63.8	13.8

RUN NUMBER = 27.0 PRESSURE = 1.9

POWER WATTS	RESIST K OHMS	FREQ KHZ	VEL KM/SEC	WLG METERS	DIS I MA	DIS V VOLTS	PER USEC	TAU USEC
163.590	3.710	33.333	20.690	.621	210.0	779.0	30.0	14.5
99.000	4.400	32.258	20.000	.620	150.0	660.0	31.0	15.0
62.100	6.210	29.851	20.000	.670	100.0	621.0	33.5	15.0
26.200	10.480	27.027	15.625	.578	50.0	524.0	37.0	19.2
1.207	1.932	25.000	15.625	.625	25.0	48.3	40.0	19.2
25.000	10.000	24.938	16.667	.668	50.0	500.0	40.1	18.0
55.300	5.530	25.510	16.667	.653	100.0	553.0	39.2	18.0
93.150	4.140	26.810	16.216	.605	150.0	621.0	37.3	18.5
137.600	3.440	27.548	16.484	.598	200.0	688.0	36.3	18.2
189.000	3.024	29.240	16.667	.570	250.0	756.0	34.2	18.0
249.600	2.773	31.348	17.442	.556	300.0	832.0	31.9	17.2
315.350	2.574	32.258	17.045	.528	350.0	901.0	31.0	17.6
391.200	2.445	31.447	18.293	.582	400.0	978.0	31.8	16.4
467.100	2.307	31.056	18.750	.604	450.0	1038.0	32.2	16.0
559.000	2.236	28.571	20.134	.705	500.0	1118.0	35.0	14.9
488.700	2.413	26.667	18.868	.708	450.0	1086.0	37.5	15.9
415.200	2.595	27.174	18.868	.694	400.0	1038.0	36.8	15.9
343.000	2.800	29.851	18.634	.624	350.0	980.0	33.5	16.1
275.700	3.063	29.851	18.634	.624	300.0	919.0	33.5	16.1
211.750	3.388	30.675	18.182	.593	250.0	847.0	32.6	16.5
153.000	3.825	30.030	18.182	.605	200.0	765.0	33.3	16.5
102.300	4.547	27.933	17.964	.643	150.0	682.0	35.8	16.7
61.500	6.150	26.882	16.575	.617	100.0	615.0	37.2	18.1
26.650	10.660	24.510	16.216	.662	50.0	533.0	40.8	18.5
12.025	19.240	22.989	15.306	.666	25.0	481.0	43.5	19.6
12.025	19.240	22.989	15.306	.666	25.0	481.0	43.5	19.6
7.095	31.533	21.368	16.484	.771	15.0	473.0	46.8	18.2

REFERENCES

II-1. Thomson, J. J., Bibliography of Early Work, Phil. Mag. 18, 441 (1909).

II-2. Donahue, T. and G. H. Dieke, Phys. Rev. 81, 248 (1951).

II-3. Garscadden, A. and D. A. Lee, "Forward and Backward - Moving Striations in the Constricted Discharge," Int. J. Electronics, 1966, Vol. 20, No. 6, 567-581.

II-4. Fisher, M. J. and F. R. Krause, "The Crossed-Beam Correlation Technique," J. Fld. Mech., No. 28, 1967.

II-5. Stephens, J. B., V. A. Sandborn, and A. J. Montgomery, "Remote Wind Detection with the Cross-Beam Method at Tower Heights," presented at 3rd Nat. Conf. on Aerospace Meteorology, New Orleans, May 1968.

CHAPTER III

FEASIBILITY OF CROSSED-BEAM APPLICATIONS TO COMBUSTIVE FLOWS

by

J. B. Thomison, Jr. and J. B. Stephens
NASA - Marshall Space Flight Center, Alabama

SUMMARY

Group velocities of local areas of combustion in a turbulent flame have been optically measured by employing the crossed-beam correlation technique. Identification of velocity and photo-chemical reactions through correlation of emission fluctuations is discussed.

III-1. INTRODUCTION

The feasibility of applying the cross-beam technique was first developed by Fisher and Krause [III-1] in a subsonic jet. The method was extended to measure atmospheric wind speeds by Stephens, Sandborn and Montgomery [III-2] and later to measure optical fluctuations in a glow discharge described in Chapter II by Stephens and Thomison. The glow discharge measurements studied fluctuations of emission processes rather than extinction processes. Earlier tests depended on fluctuations in the transmission of an independent light source produced by changes in the optical density of a gas. These changes in optical density correspond to like changes in the mass density of the gas. The source for the wind tunnel measurements was artificial light, while that for the atmospheric tests was scattered sunlight. The tests described in this paper use the light emitted from a turbulent flame to study the combustion process of the flame itself. No outside light source is used. These tests demonstrate the feasibility of using the cross-beam technique to successfully retrieve velocity and spectroscopic information from a combustion process.

III-2. PHOTOGRAPHIC EVALUATION OF FLAME PROPAGATION

Optical fluctuations in the body of a turbulent flame are due to turbulent eddies of burned and unburned gases (see Fig. III.1). These turbulent eddies may be defined as blobs of fluid which experience a coherent change of emissivity. In general, these blobs have a random velocity and after traveling a mixing length equal, on the average, to their diameter, they lose their separate identities [III-3].

Before the actual cross-beam flame tests, the flame was photographed with a high-speed movie camera to determine the type of fluctuations present. The best visualizations of the flame motion were obtained at camera speeds in excess of 1000 frames per second. The movies were used primarily to determine the best position along the axis of the flame to observe with cross-beam photo-detectors. Qualitative velocity measurements are illustrated by the consecutive eight frames shown in Figure III.1. The formation and motion of an emitting blob of fluid are observed at the right edge of the figure. The blob is moving to the right with a speed of approximately 5.0 m/sec and its axial scale is approximately 60 mm.

III-3. CROSS-BEAM EXPERIMENTS

Two mutually perpendicular lines of sight were set to select the local point of investigation in the flame. All zero separation measurements refer to the selected position 10.1 cm downstream from the nozzle exit. To achieve separation measurements, the horizontal photo-multiplier beam remained fixed, while the vertical beam was moved downstream as in Figure III.2. The focal length of the optics was 11.3 cm with a beam diameter at an intersection of approximately 2 mm. The measurements were made primarily at 5250 Å.

A flame was achieved by feeding C_2H_2 and O_2 to the nozzle, with an oxygen-to-fuel ratio of 0.92. This ratio was set by adjusting the pressure controls of the feeder lines to 3 psig for C_2H_2 and 1 psig for O_2. The actual oxygen and fuel mass flow ratio, calculated from the pressures assuming sonic speed at the nozzle exit, were 67.2 g/sec and 62.7 g/sec, respectively. The oxygen-to-fuel ratio was insufficient for complete combustion, and most of the burning occurred at the flame boundaries where ambient air was entrained.

The actual experiments were made by feeding the outputs of the photo-multipliers directly into the PAR analog correlator to obtain a covariance reading. This on-line analog computer assumes that no D.C. shifts, trends, or gain instabilities were introduced by the electronics.

Further, the covariance thus obtained will become uncertain as soon as the correlation coefficient (correlation/mean signal power) drops below 10 percent.

Within the above assumptions, the analog computations of the PAR correlator should form an estimate of the temporal covariance function, which is defined as follows.

$$C_{xy}(\tau;\xi;\lambda;\ \ldots) = \langle i_x i_y \rangle$$

$$= \frac{1}{T} \int_0^T i_x(t;\lambda)\ i_y(t-\tau;\lambda)\ dt, \qquad (1)$$

where

$i_x(t)$ - instantaneous fluctuations of intensity from the undelayed channel

$i_y(t-\tau)$ - instantaneous fluctuations from the delayed channel

τ - delay time set during data reduction

t - real time

T - total integration time.

This covariance should be related to the statistics of local emission fluctuations. Let $\ell = \eta$ or $\ell = \zeta$ denote a point on one of the two beams. The emission fluctuations in the beam element $\Delta\ell$ around this point are then described by the emission coefficient fluctuations

$$K'(\ell;\ t;\ \lambda) = \frac{\Delta I'_e(\ell;\lambda;t)}{\Delta\ell\ I(\ell;\lambda;t)}\ , \qquad (2)$$

where

$I(\ell;\ \ldots)$ - radiative power flux through beam cross section at ℓ

$\Delta I'_e$ - emission fluctuation in beam element $\Delta\ell$.

Crossed-beam theory [III-4] now indicates that the normalization of the A.C.-coupled signals with the D.C. mean values should provide a covariance estimate, which is equal to the point-area product mean value of the emission coefficient fluctuations K' around the beam intersection, $\vec{x}$.

$$G(\xi;\tau;\lambda)_{\vec{x}} = \frac{< i_x i_y >}{\bar{I}_x \bar{I}_y} =$$

$$= <K'(\vec{x},t;\lambda) \int\int_{\substack{\text{eddy} \\ \text{correction}}} K'(\vec{x}+\vec{\xi};\ t-\tau;\lambda)\ d\eta d\zeta > , \qquad (3)$$

where

$\bar{I}_x$ = average D.C. intensity from beam x

$\bar{I}_y$ = average D.C. intensity from beam y

ξ = axial separation distance

$\vec{\xi}$ = (ξ,η,ζ) point coordinates in beam fixed frame.

The last equation demonstrates that local emission variations in a flame can be retrieved by crossed-beam correlative techniques. The following pilot experiments were conducted to experimentally check this theoretical claim.

III-4. VELOCITY MEASUREMENTS AND DETERMINATION OF COMBUSTION EFFECTS

To obtain a velocity measurement in the flame, the two photo-multiplier beams were separated along the flame axis, and the peak cross-correlation of these fluctuations revealed the average transit time for a turbulent blob. This transit time yielded the average velocity of the blobs over that distance. The results are illustrated in Figure III.3. They show a decreasing velocity with an increase in the downstream beam separation. The speed of the eddy that was indicated by the noise falls into the speed interval shown in Figure III.3. All photo-multiplier

records taken from single photo-multiplier time histories show a broad band power spectrum (see Chapter II). The signals could easily be resolved out of the photo-multiplier and flow noise, as apparent from the large values of the correlation coefficient for a zero beam separation. The values were at least 20 percent, while some even exceeded 50 percent (see table III.1). Further, the correlation curves were consistent and stable with repeating runs. When the separation was increased to 3.8 cm, the value of the correlation coefficient dropped below 10 percent, and no usable measurements were obtained.

Additional tests were made to separate photo-chemical emission from heat radiation by studying the change of the cross-correlation as a function of optical wave length [III-4]. All these measurements were taken with intersecting beams.

The results of this experiment showed distinct correlation peaks when changing the optical wave length. This would not have been produced by heat radiation. Some of these emission peaks are centered close to optical wave lengths that correspond to known emission bounds for a C_2H_2 - O_2 flame [III-5]. These results are illustrated in Figure III.4. This coincidence of the peak positions in crossed-beam spectra and published mean value emission spectra gives additional confirmation to the claim that local emission variations have been retrieved.

III-5. CONCLUSIONS AND RECOMMENDATIONS

This research has demonstrated the feasibility of the use of the cross-beam correlation technique to successfully retrieve both velocity and spectroscopic information from a combustion. The next logical step would be to attempt similar studies in an actual rocket plume.

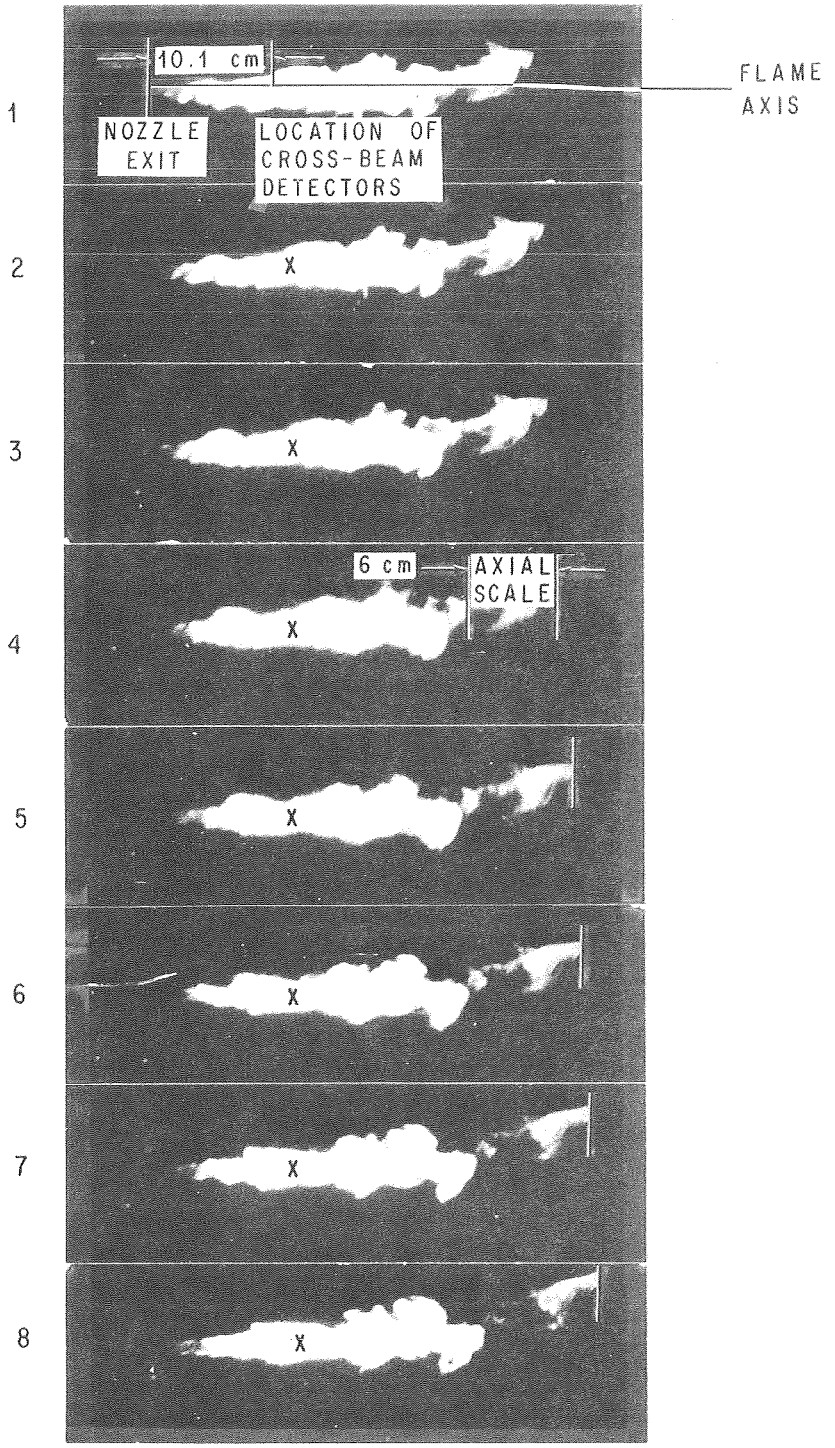

FIGURE III.1. TURBULENT BLOB PROPAGATION IN A C_2H_2 - O_2 FLAME, 500 FRAMES/SEC

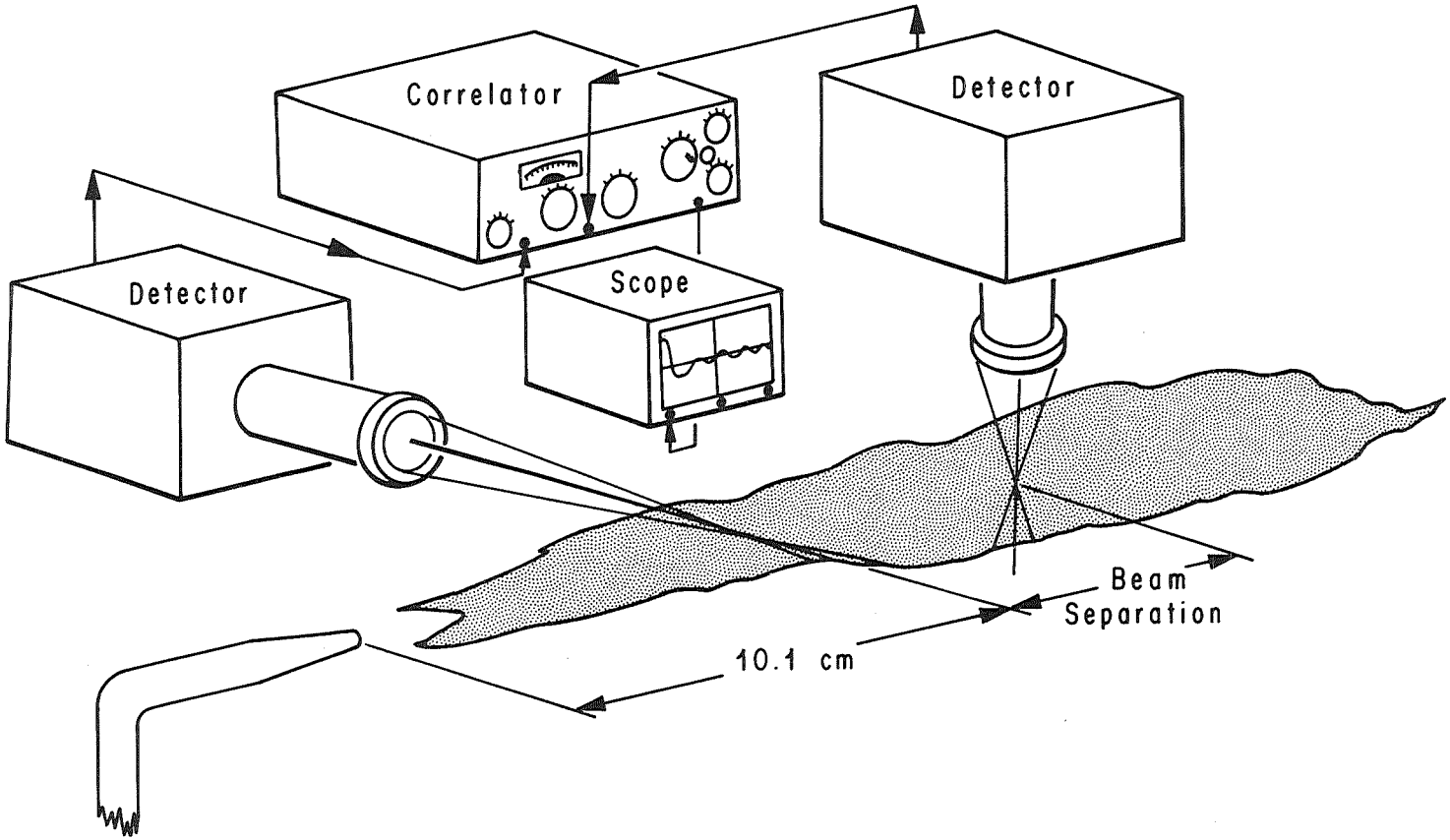

FIGURE III.2. EXPERIMENTAL SETUP

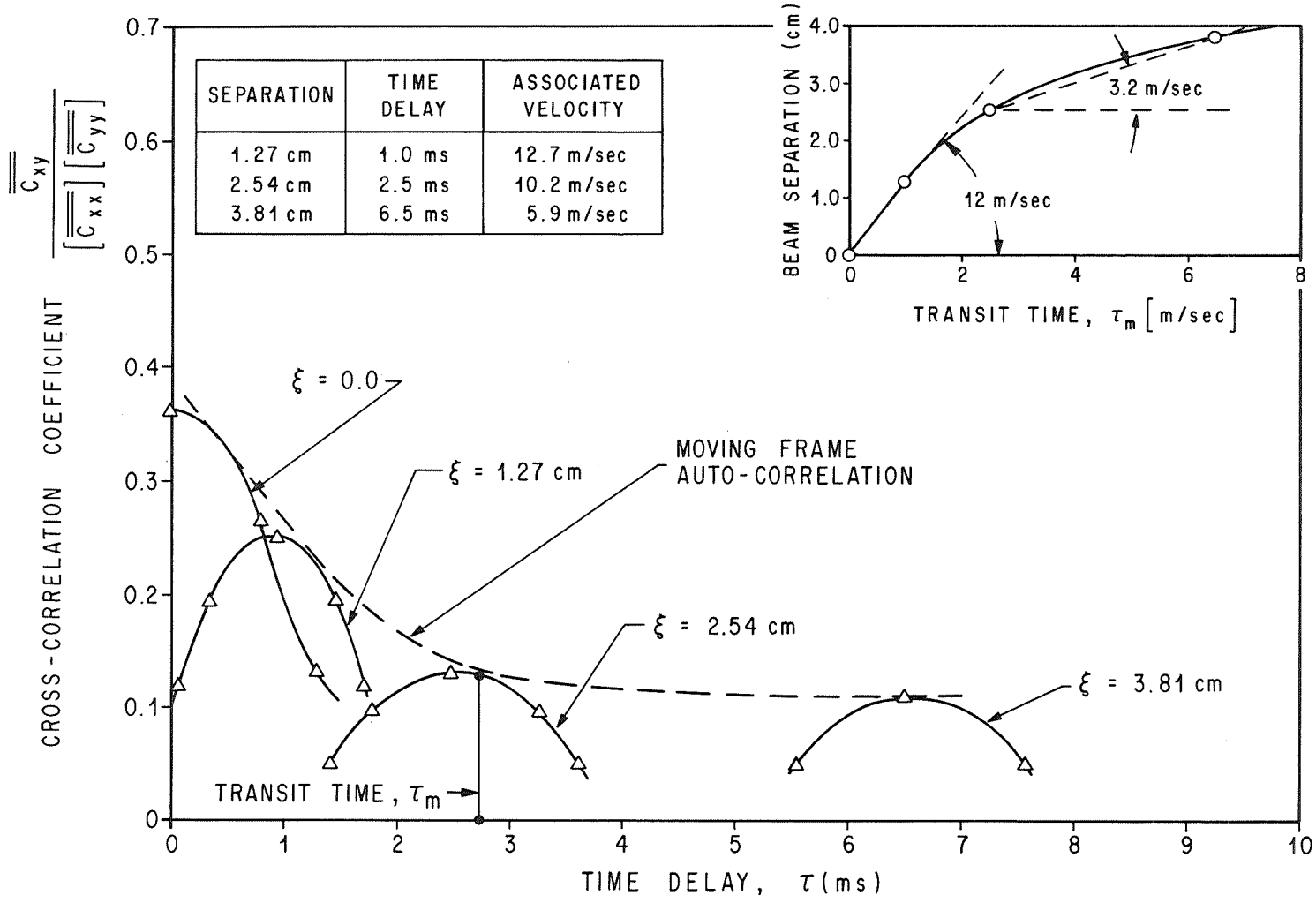

FIGURE III.3. VELOCITY CORRELATIONS

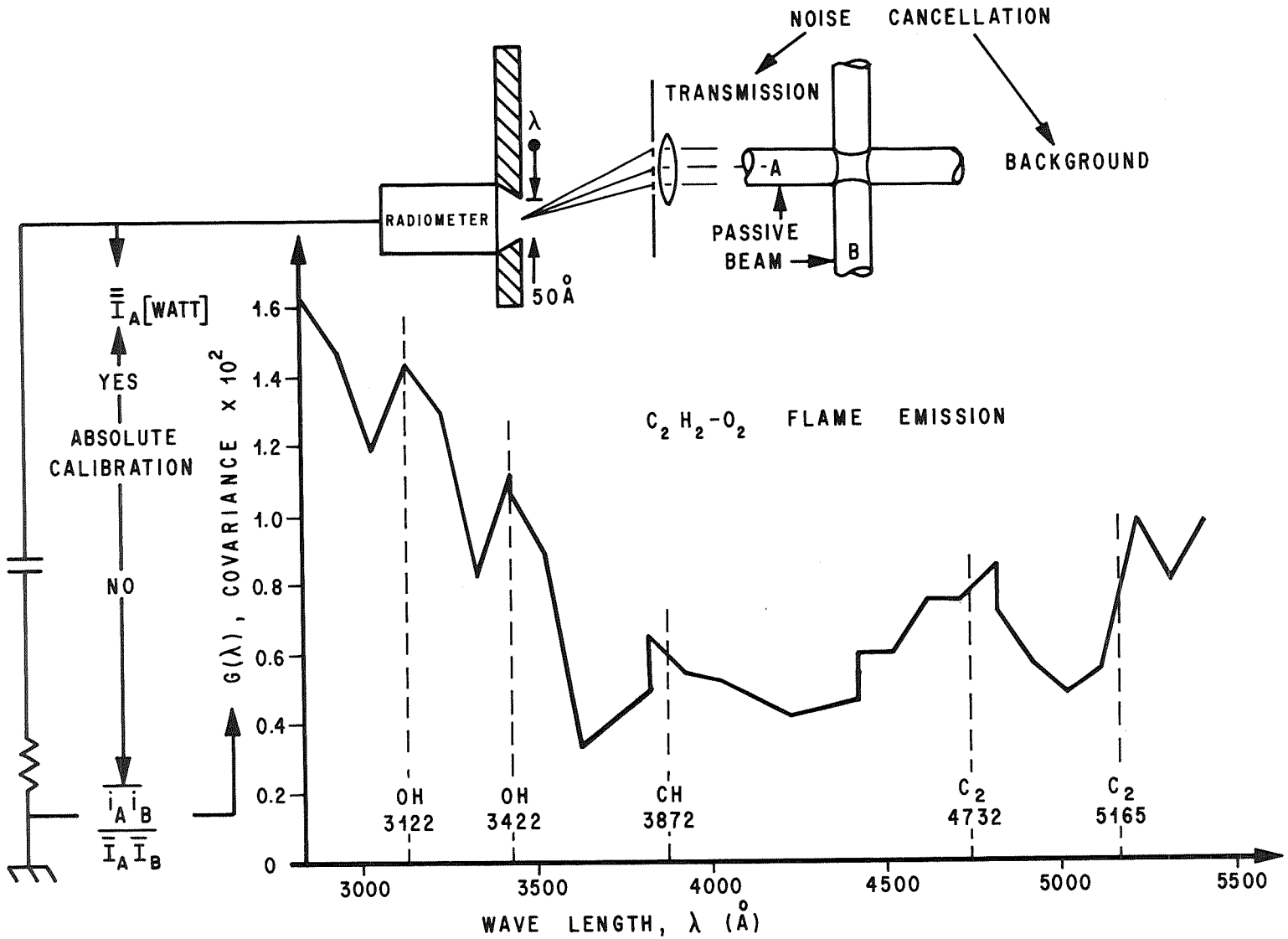

FIGURE III.4. PHOTO-CHEMICAL EMISSION IN A C_2H_2 - O_2 FLAME

TABLE III.1. DATA FOR OBSERVED PHOTO-CHEMICAL EMISSION IN A C_2H_2 - O_2 FLAME

λ WAVE LENGTH ANGSTROMS	$\frac{\overline{C_{xy}(0)}}{\sqrt{\overline{C_{xx}(0)}\ \overline{C_{yy}(0)}}}$ CORRELATION COEFFICIENT	$G(\lambda)_{\xi = \tau = 0}$ EMISSION COEFFICIENT
2850.0	0.238	0.0163
2950.0	0.257	0.0148
3050.0	0.261	0.0119
3150.0	0.262	0.0144
3250.0	0.246	0.0130
3350.0	0.280	0.0082
3450.0	0.335	0.0112
3450.0	0.315	0.0106
3550.0	0.303	0.0089
3650.0	0.191	0.0033
3750.0	0.201	0.0041
3850.0	0.331	0.0065
3850.0	0.344	0.0049
3950.0	0.302	0.0054
4050.0	0.338	0.0052
4150.0	0.322	0.0047
4250.0	0.350	0.0042
4350.0	0.334	0.0044
4450.0	0.350	0.0047
4450.0	0.381	0.0060
4450.0	0.402	0.0060
4650.0	0.442	0.0075
4750.0	0.408	0.0075
4850.0	0.396	0.0085
4850.0	0.387	0.0072
4950.0	0.366	0.0057
5050.0	0.341	0.0048
5150.0	0.391	0.0055
5250.0	0.492	0.0104
5250.0	0.506	0.0080
5350.0	0.331	0.0103
5450.0	0.223	0.0401
5500.0	0.156	0.0670

REFERENCES

III-1. Fisher, M. J. and F. R. Krause, "The Crossed-Beam Correlation Technique," J. Fluid Mechanics, No. 28, 1967.

III-2. Stephens, J. B., V. A. Sandborn, and A. J. Montgomery, "Remote Wind Detection with the Cross-Beam Method at Tower Heights," presented at 3rd Nat. Conf. on Aerospace Meteorology, New Orleans, May 1968.

III-3. Gaydon, A. G. and H. G. Wolf Hard, "Flames, Their Structure, Radiation, and Temperature," Chapman and Hall, Ltd., 1960.

III-4. Krause, F. R., W. O. Davies, and M. W. P. Cann, "Determination of Thermodynamic Properties with Optical Cross-Correlation Methods," AIAA Journal, Vol. , pp. 587-592, 1969.

III-5. Gaydon, A. G., "The Spectroscopy of Flames," Chapman and Hall, London, 1957.

CHAPTER IV

TURBULENCE MEASUREMENTS BY THE CROSSED-BEAM TECHNIQUE

by

M. Y. Su
Northrop - Huntsville, Alabama

and

F. R. Krause
NASA - Marshall Space Flight Center

SUMMARY

An analytical relationship which approximates the probability density of wind component variations through the cross-correlation of the passive photometer outputs of the cross-beam detection system is presented. Specifically, the probability density is shown to be proportional to the cross-correlation of the first time derivatives of the time histories of fluctuating radiation intensities which are monitored by two non-parallel photodetectors. The direction of the measured wind component is normal to both lines-of-sight of the photodetectors. Special data conditioning and handling methods for evaluating the cross-correlation of the signal time derivatives are described, and their effects on the cross-correlation and corresponding spectral densities are discussed. The new analytical relationship and data handling techniques were applied to actual atmospheric crossed-beam field test data. The reduced optically and remotely detected probability density of wind component variations was found to be in reasonable agreement with that obtained by the conventional anemometer readings. Turbulent intensity can be easily evaluated once the probability density is measured. The optical technique can also be applied to other high-temperature, chemically reactive or supersonic turbulent flows such as rocket exhausts, jet plumes, and plasma in nuclear engines. The flow fields associated with these problems still defy accurate measurements by other presently available instrumentation.

NOMENCLATURE

Symbol	Definition
B	bandwidth
$D(\xi)$	factor representing the degree of decay with respect to ξ
$E(\xi)$	function defined by equation (29)
f	frequency
f_c	cutoff frequency in a low-pass filter
f_ℓ	lower frequency in a time history
f_T	terminate frequency in a low-pass filter
f_u	upper frequency in a time history
$G_{AB}(\xi,f)$	gain of $S_{AB}(\xi,f)$
$G_{AB}^{(2)}(\xi,f)$	gain of $S_{AB}^{(2)}(\xi,f)$
$H(f)$	frequency complex frequency response
$h(\tau)$	filter transfer function
$\tilde{H}_\ell(f)$	frequency response of the Martin-Graham type roll-off low-pass filter
$\tilde{h}_\ell(t)$	transfer function of the Martin-Graham type roll-off low-pass filter
$i_A(t)$	fluctuating component of photometer A's output
$i_B(t)$	fluctuating component of photometer B's output
L_τ	integral time scale of atmospheric turbulence
N	total number of digital samples
N_m	total number of digital samples in m^{th} class

Symbol	Definition
$P(\xi, \tau_m)$	probability density of transit times in mth class
$P(U)$	probability density of wind component U
$R_{AB}(\tau)$	cross-correlation of i_A and i_B
$R_m(\xi, \tau_\ell)$	cross-correlation of samples from mth class
$R_{AB}^{(2)}(\xi, \tau_\ell)$	cross-correlation of $\partial i_A/\partial t$ and $\partial i_B/\partial t$
$S_{AB}(\xi, f)$	spectral density of $R_{AB}(\xi, \tau)$
$S_{AB}^{(2)}(\xi, f)$	spectral density of $R_{AB}^{(2)}(\xi, \tau)$
T	total length of photometer output
$\triangle T$	length of each piece of photometer output
t	time
$\triangle t$	sampling interval of digital time history
U	wind component normal to both light beams
$\bar{U}$	mean wind component
U_m	wind component associated with mth class
$\triangle U$	resolution in the wind component U
V	wind speed
X(f)	Fourier transfer of x(t)
x_{m_k}	kth sample of mth class of x(t)
x(t)	common signal in $i_A(t)$
Y(f)	Fourier transform of y(t)
y_{m_ℓ}	ℓth sample of mth class of y(t)
y(t)	common signal in $i_B(t)$

Symbol	Definition
Greek Letters	
$\epsilon(f,N_d)$	measure of error in the frequency response for using N_d samples
θ	angle between the wind vector and the normal to both light beams
ξ	normal separation distance between two beams
ξ^*	normal separation distance between A and the imaginary beam B^*
σ_u	root mean square of the wind component U
τ	time lag between i_A and i_B
Operators	
$\overline{( )}_i$	$\frac{1}{\Delta T}\int_{(i-1)\Delta T}^{i\Delta T} ( )\, dt$ piecewise average of ( )
$\overline{\overline{( )}}_m$	accumulative average over m piecewise averages
$\overline{\overline{( )}}_m$	$\left\{\frac{1}{m(m-1)}\sum_{i=1}^{m}[\overline{( )}_i - \overline{\overline{( )}}_m]^2\right\}^{1/2}$ confidence level of accumulation average
$\overline{\overline{\delta R}}_m$	$\frac{1}{\bar{\bar{\sigma}}_{xm}\,\bar{\bar{\sigma}}_{ym}}\left\{\frac{1}{2\tau_m}\int_{-Jm}^{+Jm}\Delta^2\,\bar{\bar{R}}_m(j)\,dJ\right\}^{1/2}$ relative statistical error of correlation or covariance functions.

IV-1. INTRODUCTION

Remote optical detection techniques are being developed by the Marshall Space Flight Center to provide a means for continuous monitoring of atmospheric wind and turbulence. Successful detection of most probable wind speed at an altitude of about 100 meters by these techniques has been reported [IV-1, -2].

The capability of these techniques has been extended to atmospheric turbulence measurements by optically retrieving the probability density of wind component variations. Direction of the wind component is normal to both lines-of-sight of the photometers employed. The mean, rms, and other higher moments of wind component variations may be easily evaluated from the probability density. Preliminary results on this progress with emphasis on the signal/noise analysis and electro-optical system were reported in reference IV-3.

The optical technique essentially consists of two photodetectors to monitor the optical fluctuations of natural scattered radiations which result from both spatial and temporal variations of atmospheric inhomogeneities. Each photodetector output will thus contain the information of the atmospheric inhomogeneities along its entire field of view. The cross-correlation of these two photometer outputs should reveal the characteristics of the local optical disturbance and atmospheric motion which are common to both fields of view of the two photodetectors. To have an optimum spatial resolution the two lines-of-sight of detectors should be so oriented that they are normal (but separated) to each other. This is the reason for calling this optical technique the crossed-beam technique. Because of the very low signal-to-noise ratio associated with the remotely detected radiation fluctuations, special data conditioning and processing and statistical analyses are needed for evaluating the cross-correlation of the photometer outputs and their time derivatives.

This paper presents the theoretical basis for optical approximations of turbulence levels, together with the necessary additional considerations on data conditioning and processing. In section IV-2, a theoretical relationship between the cross-correlation of the first-time derivatives of the photometer outputs and the probability density of the wind component variations is derived. This wind component is normal to both lines-of-sight of the photometers. Use of the time derivative of the photometer outputs instead of the outputs themselves is one of the essential features which differ from the previous crossed-beam detection of the most probable wind component.

Section IV-3 describes the special data conditioning and processing, and discusses their effect on the cross-correlations and corresponding spectral densities. These considerations are very important for dealing with cross-correlating time derivatives of random time histories.

Section IV-4 presents some experimental and computed results from applying the theoretical relationship and data handling methods to atmospheric crossed-beam field test data. The optically detected probability densities of the wind component variations were then compared with those independently measured by the conventional anemometers mounted on a close-by meteorological tower. The minimum separation of the crossed-beam arrangement was set directly upstream of the anemometer about 60 meters above the ground.

The authors wish to thank the following persons for their contributions to this paper: Professor V. Sandborn, Colorado State University, for carrying out the atmospheric crossed-beam field tests; Messrs. J. Jones and R. Graham, Computation Laboratory, MSFC, for digitization of test tapes, cross-correlation computation and the program for digital filtering; Mr. J. Pooley, Northrop Corporation, for programming an updated version of the error accumulation and spectral decomposition subroutines; and Dr. W. H. Heybey, MSFC, and Dr. L. N. Wilson, IITRI, for their very helpful and constructive critical reviews and comments on the extension of the crossed-beam concept to turbulence measurements.

IV-2. PROBABILITY DENSITY OF WIND COMPONENT VARIATIONS FROM OPTICAL CORRELATION

Wind speeds and directions vary, in general, fairly rapidly. To specify completely the statistics of such wind characteristics, either an infinite series of correlation functions of all orders of wind fluctuations, or an infinite series of all orders of probability densities of wind fluctuations will be needed. However, in usual meteorological applications, only limited quantities are measured, i.e., the first few moments of the wind fluctuations such as the mean wind speed, and the rms wind speed fluctuations.

When the wind direction is constant but unknown, and the speed is varying, it has been shown [IV-4, -5] that both the wind direction and speed can be simultaneously measured by the crossed-beam system. When the wind direction varies, only the wind component normal to the two lines-of-sight of detectors can be measured. The reason is that the crossed-beam measurement gives the transit time of the optical disturbance between two beams only, while the location of the transit path and its length between two beams cannot be determined unless the wind direction remains constant over the period of measurement (see Figure IV.1). Fortunately, the fixed position of two light beams gives a uniquely determined minimum separation between two beams which is in the direction normal to both beams. Thus, the combination of the measured transit time and the shortest beam separation always determine uniquely the wind component normal to both beams. Since, in most meteorological conditions,

the wind direction does vary in the minimum required period of crossed-beam measurements, we shall deal with this wind component throughout this paper.

The first-order probability density of the wind component can be measured by the crossed-beam system to a high degree of approximation. This approximation results from some relatively weak assumptions introduced in order to establish an explicit analytical relationship between the cross-correlation of optical fluctuations and the probability of wind component variations. Also, because of the variation of the wind direction, the resolution of the altitude of the prevailing wind will be questionable from one pair of crossed beams. However, if more than two pairs of crossed beams are used, which are so oriented that mutually perpendicular wind components are to be measured, then the wind direction can be approximately determined also.

The basic geometrical arrangement of the crossed-beam system is shown in Figure IV.1. The various fields of view of two ground-based photometers, A and B, are oriented so that their lines-of-sight differ by 180 degrees in the azimuth angles. Such an orientation will give the wind component both horizontal to the ground and normal to both beams. The wind component will be the one used for this discussion, unless otherwise specified.

Atmospheric inhomogeneities, such as the variations in density of aerosol, various gases and water vapor, will cause both spatial and temporal variations in radiation processes. These radiations include light scattering, absorption, and emission. Thus, the characteristics of local light fluctuations should reflect the characteristics of the atmospheric inhomogeneity (or turbulence). The atmospheric inhomogeneities are transported according to the general rules of fluid dynamics. The lifetime of the atmospheric inhomogeneity, which is a measure of the average time lapse for the inhomogeneity to retain its character (or signature), is finite; so is the lifetime of the optical fluctuation, if the light source can be considered to be relatively constant. The optical detectors A and B thus record the time histories of accumulative radiation outputs within their entire field of view, respectively. Fluctuations of the photometer output, $i_A(t)$ and $i_B(t)$, therefore contain information on the atmospheric motions along the entire line-of-sight. The mean value of the photometer outputs is not of concern here. The fluctuating part is separated from the total recording signal by A.C.-coupling electronic circuitry.

When the two beams actually intersect each other at a certain height (Figure IV.2), the local optical fluctuations radiating from the intersection region will result in some common signals in the outputs of the detectors. The common signals may not be exactly the same, but they are

related, so that the photometer outputs may be expressed as

$$\begin{aligned} i_A(t) &= x(t) + i_{A,n}(t) \\ i_B(t) &= y(t) + i_{B,n}(t). \end{aligned} \tag{1}$$

Here, $x(t)$ and $y(t)$ are the common signals mentioned above, while $i_{A,n}(t)$ and $i_{B,n}(t)$ are light fluctuations outside the intersection region. In contrast to desired common signals, they will be called noises due to transmission, or flow noises. By the nature of the atmospheric inhomogeneities, all the terms in equation (1) are random time histories. The most powerful method available to retrieve such common signals is the correlation technique, which is commonly used in the communication theory and random vibration analysis. A correlation function is computed by adding the products of two time histories, i_A and i_B. That is,

$$R_{AB}(\tau) = \langle i_A(t) i_B(t+\tau) \rangle \equiv \lim_{T\to\infty} \frac{1}{T} \int_o^T i_A(t)\ i_B(t+\tau)\ dt. \tag{2}$$

Substituting equation (1) into (2) yields

$$\begin{aligned} R_{AB}(\tau) = &\langle x(t)y(t+\tau) \rangle + \langle x(t)\ i_{B,n}(t+\tau) \rangle + \langle i_{A,n}(t) y(t+\tau) \rangle \\ &+ \langle i_{A,n}(t)\ i_{B,n}(t+\tau) \rangle . \end{aligned} \tag{3}$$

The first term in the right-hand side of the above equation is the cross-correlation between two common signals. The other three terms are the cross-correlation among statistically unrelated light fluctuations; thus, they will vanish if the integration time T is long enough. That is, the time integration will suppress "noise" components. In actual application, the integration time T is always finite. The uncertainty (or error) due to this finite T will be discussed further in section V. For a sufficiently long integration time, which is also the length of the time histories, equation (3) can be written approximately as

$$R_{AB}(\tau) \cong \langle x(t)y(t+\tau) \rangle. \tag{4}$$

This means that as long as one deals with such product mean values, one can disregard all light modulations that are not common to both fields of view of the two detectors [IV-6].

To measure the wind component the two beams have to be separated. The shortest separation distance is denoted by ξ. The common signals in the two detectors now are caused by the convected atmospheric inhomogeneities which happen to traverse both light beams. The time lapse which an inhomogeneity takes to travel from one beam, say A, to the other beam, B, will be called the "transit time." The distance between the two beams of the traversing path $\overline{CD}$ will be called the "transit distance." Associated with the transit path is the transit height, which is the altitude of the transit path above the ground (see Figure IV.1). When the wind speed, V, and direction, θ, are fixed, the associated transit time can be obtained from the cross-correlation curve (equation (4)). It is the time lag associated with the maximum value (or peak) of $R_{AB}(\tau)$, denoted by τ_{peak}. On the other hand, the transit distance cannot be determined unless the wind direction is known. Without knowing the wind direction, the best one can deduce is the component of the transit distance in the direction normal to both light beams, which is simply the shortest distance ξ. Thus, the relationship between the wind component U and the time lag τ_{peak} from the crossed-beam measurement is

$$U = V \cos \theta = \frac{\overline{CD}}{\tau_{peak}} \cos \theta = \frac{\xi/\cos \theta}{\tau_{peak}} \cos \theta$$

or

$$U = \frac{\xi}{\tau_{peak}} . \qquad (5)$$

Here, the distance ξ is fixed by the crossed-beam arrangement, which is completely known. Hence, equation (5) allows us to measure the wind component through the remote detection of the optical fluctuations and the cross-correlation of these fluctuations if the wind speed and direction remain constant.

The more realistic meteorological situations are those where the wind speed and direction both change with time. Under such situations, the maximum information that can be retrieved from the cross-correlation of the optical fluctuations is the first-order probability density of the wind component variations.

We shall now derive the relationship of the cross-correlation of crossed-beam signals to the probability density of the wind component variations. As discussed above, all the noise components in the two photometer outputs $i_A(t)$ and $i_B(t)$ will be suppressed through cross-correlation. We need only to consider the two time histories of common (desired) signals, x(t) and y(t), without loss of generality. Let the time histories of length T be digitized with a sampling interval, Δt. The total number of digital samples for either time history will be denoted by N:

$$N = \frac{T}{\Delta t} .$$

These digital samples and digital time lags will be denoted as follows:

$$\begin{aligned} x_n &= x(t = n\,\Delta t) \\ y_n &= y(t = n\,\Delta t) \end{aligned} \qquad (6)$$

and

$$\tau_\ell = \ell\,\Delta t,$$

where $n = 1,2, \ldots, N$ and $\ell = 0,1,2, \ldots, L \ll N$.

Since the wind component may vary over the period of measurement, T, the associated transit time may also vary correspondingly. Without loss of generality, we shall assume that the beam A lies in the upstream of beam B. Each digital sample x_n will then have a corresponding digital sample $y_{n+\ell}$. They are attributed to the same atmospheric inhomogeneity which takes the time lag $\tau_\ell = \ell\,\Delta t$ to travel from some point in beam A to another point in beam B. The transit path between these two points is not necessarily straight. It can be of any shape. The corresponding wind component normal to both beams is ξ/τ_ℓ. The cross-correlation (equation (4)) can now be written in the summation form as

$$R_{AB}(\tau_\ell) = \frac{1}{N} \sum_{n=1}^{N} x_n\, y_{n+\ell}. \qquad (7)$$

It should be noted that the value of the summation is invariant under any different ways of grouping the terms $x_n y_{n+\ell}$ in the summation. For

the purpose of retrieving variations of the wind component, the digital samples x_n may be classified with respect to their associated transit times. Let the class interval for transit times be the same as the sampling interval Δt. The mth class of transit times, denoted by τ_m, will be defined as

$$\tau_m: \quad m\,\Delta t \leq \tau_m < (m+1)\,\Delta t, \tag{8}$$

where m = 0,1,2, ..., M. M is any integer that is large enouth to cover all possible transit times of interest. The corresponding mth class of wind components denoted by U_m will be

$$U_m: \quad \frac{\xi}{(m+1)\,\Delta t} < U_m \leq \frac{\xi}{m\,\Delta t}\ . \tag{9}$$

Now group those digital samples x_n according to the classification of equation (8). Further, denote the kth sample in the mth class in the ascending order of time by

$$x_{m_k} = x(t = m_k\,\Delta t) \tag{10}$$

and the total number of digital samples belonging to this class by N_m. Thus,

$$N = \sum_{m=0}^{M} N_m. \tag{11}$$

The probability density of transit times of the mth class over the period T of measurement can be expressed as

$$P(\xi, \tau_m)\,\Delta t \equiv P[\xi,\ m\,\Delta t \leq \tau_m < (m+1)\,\Delta t]\,\Delta t = \frac{N_m}{N}\ . \tag{12}$$

The corresponding probability density of the wind components $P(U_m)$ can be obtained from the above probability density by a transformation of variables from the transit time to the wind component.

$$P(U_m) \equiv P\left[\frac{\xi}{(m+1)\,\Delta t} < U_m \leq \frac{\xi}{m\,\Delta t}\right]$$

$$= P(\xi, \tau_m) \left|\frac{d\tau_m}{dU_m}\right| = \frac{\tau_m^2}{\xi} P(\xi, \tau_m). \tag{13}$$

With the above classification of digital samples and definitions of the probability density, the cross-correlation of the optical fluctuations from the photometers can be expressed as

$$R_{AB}(\tau_\ell) = \frac{1}{N} \sum_{n=0}^{N} x_m \, y_{n+\ell}$$

$$= \frac{1}{N} \sum_{m=0}^{M} \sum_{k=1}^{N_m} x_{m_k} \, y_{m_k+\ell}$$

$$= \sum_{m=0}^{M} \frac{N_m}{N} \left[\frac{1}{N_m} \sum_{k=1}^{N_m} x_{m_k} \, y_{m_k+\ell}\right]. \tag{14}$$

Let us define the term in the parentheses by

$$R_m(\xi, \tau_\ell) = \frac{1}{N_m} \sum_{k=1}^{N_m} x_{m_k} \, y_{m_k+\ell}. \tag{15}$$

By substituting equations (12) and (15), equation (14) can be written as

$$R_{AB}(\xi, \tau_\ell) = \frac{1}{N_m} \sum_{m=0}^{M} P(\xi, \tau_m) \, R_m(\xi, \tau_\ell) \, \Delta\tau_m \quad (\text{with } \Delta\tau_m = \Delta t). \tag{16}$$

Clearly, the function $R_m(\xi, \tau_\ell)$ represents the cross-correlation of the mth class of digital samples. Equation (16) simply states that the total cross-correlation $R_{AB}(\xi, \tau_\ell)$ is equal to the sum of M + 1 cross-correlation of each individual class of samples with the associated probability density of transit times during measurement T as a weighting factor.

In almost all actual applications, both functions $P(\xi, \tau_m)$ and $R_m(\xi, \tau_m)$ can be assumed to be continuous with respect to τ_m; thus, the above summation can be written in the integral form as the increment $\Delta\tau_m$ becomes very small (i.e., $\Delta\tau_m \to 0$).

$$R_{AB}(\xi, \tau_\ell) = \int_0^\infty P(\xi, \tau_m)\, R_m(\xi, \tau_\ell)\, d\tau_m. \tag{17}$$

Strictly speaking, this limiting process $\Delta\tau_m \to 0$ cannot be applied, since this would require the knowledge of the infinitesimal wind component fluctuations. It is known that the highest wind fluctuation measurable by the crossed-beam technique is dictated by the beam separation distance ξ and the maximum prevailing wind component. Specifically, the highest resolution in the wind component is given by

$$\Delta U = \frac{\xi}{\tau_{max}}, \tag{18}$$

where τ_{max} is the maximum time lag used in R_{AB}. This is the lowest possible wind component which can be measured by the crossed-beam system, i.e.,

$$\min(U) = \Delta U = \frac{\xi}{\tau_{max}}. \tag{19}$$

The highest frequency fluctuation of the wind component is given by

$$\max(f_u) = \frac{U_{max}}{2\pi\xi}, \tag{20}$$

where U_{max} is the maximum possible wind component in that particular measurement under consideration. However, we applied the limiting process in the sense of numerical equivalence between equations (16) and (17), which offers a high degree of approximation. Equation (17) is an integral equation for the desired (unknown) probability density of transit times. The simplest possible way to solve for $P(\xi, \tau_m)$ is to uncouple interactions between $P(\xi, \tau_m)$ and $R_m(\xi, \tau_\ell)$ so that the probability density can be expressed in terms of the experimentally accessible cross-correlation. The desired uncoupling is feasible with suitable data conditioning on the photometer outputs under some relatively weak assumptions regarding atmospheric turbulence and wind characteristics. This will now be discussed.

We shall first make an assumption (I) that samples in each class will decay by the same amount in their turbulent characteristics over the same beam separation and that the rate of decay may differ in different classes of samples. According to Bachelor [IV-7], the decay of relative turbulent energy, which is defined as the ratio of the mean square of speed fluctuations to the square of the mean speed, is linearly proportional to the transit distance. The turbulent fluctuation in the photometer outputs is a mixed outcome of fluctuations both in the flow speed and the extinction coefficient of the flow medium. Nevertheless, the assumption would be at least the first order approximation for a transit distance of the order of several integral length scales of atmospheric inhomogeneities. The second assumption (II) is that the number of samples in each class, which is classified at the upstream beam A, is the same if the classification were made at the downstream beam B. This assumption is really a restriction which excludes the consideration of wind component fluctuations with frequency higher than max $[f_u]$ (see equation (20)). By using these two assumptions, the cross-correlation of mth class of samples (equation (18)) can be rewritten as

$$R_m(\xi, \tau_\ell) = D(\xi)\ R(\xi^* \equiv \xi - U_m \tau_\ell,\ 0) \tag{21}$$

or

$$R_m(\xi, \tau_\ell) = D(\xi)\ R(\xi^* = \xi(1 - \frac{\tau_\ell}{\tau_m}),\ 0), \tag{22}$$

where $D(\xi)$ is a factor representing decay of turbulence with respect to the separation distance, while the space-time cross-correlation $R_m(\xi, \tau_\ell)$ is replaced by an equivalent spatial cross-correlation $R(\xi^*, 0)$ with imaginary translation of the downstream beam B closer to the upstream beam A by the amount of $U_m \tau$ for compensating the convective motion of the atmospheric inhomogeneity (see Figure IV.3).

Next, substituting the approximate relationship (equation (22)) into equation (17) yields

$$R_{AB}(\xi,\tau_\ell) = D(\xi) \int_0^\infty P(\xi,\tau_m)\ R(\xi^* = \xi(1-\frac{\tau_\ell}{\tau_m}),\ 0)\ d\tau_m. \tag{23}$$

What has been accomplished in the above equation compared with the equation (17) is that the dependence of the functional form of R_m has been eliminated from the integrand. However, $P(\xi,\tau_m)$ and $R(\xi^*,0)$ is still coupled. It should be noted that the spatial cross-correlation $R(\xi^*,0)$ reaches its maximum value for $\xi^* = 0$, i.e., when the imaginary beam B^* intersects beam A. A certain correlation will persist for $0 < \xi^*$, but will be smaller than the scale of the atmospheric inhomogeneities common to both light beams. In other words, a certain correlation exists if

$$|\tau_m - \tau_\ell| = |\tau_m(1-\frac{\tau_\ell}{\tau_m})|$$

is less than the time lapse for the atmospheric inhomogeneity traversing its own length. This time lapse is usually defined by

$$L_\tau = \frac{1}{R(\xi^*=0,0)} \int_0^\infty R(\xi^*,0)\ d\tau_m, \tag{24}$$

which is normally called the integral time scale of the atmospheric inhomogeneity. For the time being, we shall introduce a third assumption (III) that the integral time scale is much smaller than the half-width of the probability density of the transit time fluctuations (see Figure IV.4). That is,

$$L_\tau << \tau_{rms} = |\tau_2 - \tau_1|, \tag{25}$$

where τ_1 and τ_2 are the two transit times such that

$$P(\xi,\tau_1) = P(\xi,\tau_2) = e^{-1/2} \max(P(\xi,\tau)). \tag{26}$$

The justification of this assumption will be discussed after equation (36). But let us examine first how this assumption will affect equation (23). This assumption essentially implies that the spatial cross-correlation $R(\xi^*)$ behaves like a Dirac delta function. The equation (23) can be approximately written as

$$R_{AB}(\xi,\tau_\ell) \cong D(\xi)\ P(\xi,\tau_\ell) \int_0^\infty R(\xi^* = \xi(1-\frac{\tau_\ell}{\tau_m}),0)\ d\tau_m. \tag{27}$$

Changing the variable in the integration from τ_m to ξ^* yields

$$R_{AB}(\xi,\tau_\ell) \cong D(\xi)\ P(\xi,\tau_\ell) \int_{-\infty}^{\infty} R(\xi^*)\ \frac{d\tau_m}{d\xi^*}\ d\xi^*$$

$$= D(\xi)\ P(\xi,\tau_\ell)\ \frac{\tau_\ell}{\xi} \int_{-\infty}^{\xi} \frac{R(\xi^*)}{(1-\frac{\xi^*}{\xi})^2}\ d\xi^*$$

$$= E(\xi)\tau_\ell\ P(\xi,\tau_\ell), \tag{28}$$

where

$$E(\xi) = \frac{D(\xi)}{\xi} \int_{-\infty}^{\infty} \frac{R(\xi^*)}{(1-\frac{\xi^*}{\xi})^2}\ d\xi^*. \tag{29}$$

Thus, the probability density of transit times can be written as

$$P(\xi,\tau_\ell) = \frac{R_{AB}(\xi,\tau_\ell)}{E(\xi)\ \tau_\ell}\ . \tag{30}$$

The dependence on the factor $E(\xi)$ can be further eliminated by normalization, since it is independent of the transit time. That is,

$$\frac{P(\xi,\tau_\ell)}{\max(P(\xi,\tau_\ell))} = \frac{R_{AB}(\xi,\tau_\ell)/\tau_\ell}{\max(R_{AB}(\xi,\tau_\ell)/\tau_\ell)} \quad . \tag{31}$$

The normalized probability density of transit times can be approximated by the measurable cross-correlation of two photometer outputs. Physically, it will be more useful to have the probability density of wind component variations. This can be accomplished by transforming the variable from the transit time τ_ℓ to the wind component U through the following relationship:

$$U = \frac{\xi}{\tau_\ell}. \tag{32}$$

The normalized probability density of wind components (normal to both light beams) P(U) can be approximated by using equation (30).

$$P(U = \frac{\xi}{\tau_\ell}) = P(\xi,\tau_\ell) \left|\frac{d\tau_\ell}{dU}\right| = \frac{\tau_\ell^2}{\xi} P(\xi,\tau_\ell)$$

$$= \frac{\tau_\ell R_{AB}(\xi,\tau_\ell)}{\xi E(\xi)} \quad . \tag{33}$$

Again, by applying the normalization procedure to the above expression, we obtain

$$\frac{P(U=\frac{\xi}{\tau_\ell})}{\max(P(U))} = \frac{R_{AB}(\xi,\tau_\ell)}{\max[\tau_\ell R_{AB}(\xi,\tau_\ell)]} \quad . \tag{34}$$

Alternatively, one may apply the characteristics of the probability density, i.e.,

$$\int_{-\infty}^{\infty} P(\xi,\tau_\ell)\, d\tau_\ell = 1, \tag{35}$$

to equation (30), and then substitute in equation (33):

$$P(U=\frac{\xi}{\tau_\ell}) = \frac{\tau_\ell \, R_{AB}(\xi,\tau_\ell)}{\xi \int_{-\infty}^{\infty} \frac{1}{\tau'_\ell} R_{AB}(\xi,\tau'_\ell) \, d\tau'_\ell} \quad . \tag{36}$$

This implies that the probability density of wind components normal to both light beams can be approximated by the measurable cross-correlation of photometer outputs. The above optical approximation is valid under the three assumptions made which are summarized as follows:

(I) Samples of common optical fluctuations in each class with the same transit time will decay by the same amount in their turbulent characteristics over the same beam separation.

(II) The number of samples in each class, which is classified at the upstream beam, is the same if the classification were made at the downstream beam.

(III) The temporal integral scale of atmospheric inhomogeneities is much shorter than the half-width of the probability density of the transit times.

The first two assumptions are fairly realistic approximations for atmospheric turbulence, provided the transit distance does not exceed about 200 meters or the transit time does not exceed about 20 seconds. On the other hand, the third assumption is usually not met in the atmosphere. The integral length scale of atmospheric inhomogeneity is between 10 to 100 meters long in the atmosphere [IV-8]. However, a shorter optical disturbance may be expected if we cross-correlate the first time derivatives $\partial x(t)/\partial t$ and $\partial y(t)/\partial t$ of the common signals $x(t)$ and $y(t)$ instead of the common signals themselves. Since we shall employ the cross-correlation technique, these two time derivatives can be simply replaced by the time derivatives of the photometer outputs $\partial i_A(t)/\partial t$ and $\partial i_B(t)/\partial t$. Physically, the integral length scale of the time derivatives is the so-called microscale of optical disturbance [IV-9]. This microscale is usually at least one order shorter than the average integral scale. Mathematically, the time derivative is the time rate of change of optical disturbance; thus, significant values of the derivative may be expected only when a large change in the optical disturbance occurs. Heuristically, if one may simply visualize an atmospheric turbulent eddy as an elongated

body with its major axis along the flow direction, then the time derivative will be directly proportional to the slope of the eddy. Therefore, only when the leading or trailing edge of the eddy passes through the light beam may a significant optical fluctuation occur. Therefore, the unrealistic assumption (III) can now be replaced by the following realistic assumption (III-A), if the time derivatives of the photometer outputs are used to evaluate the cross-correlation.

(III-A) The temporal microscale of atmospheric inhomogeneities is much smaller than the half-width of the probability density of the transit times.

With this consideration, equations (34) and (36) should then assume the following forms:

$$\frac{P(U=\frac{\xi}{\tau_\ell})}{\max(P(U=\frac{\xi}{\tau_\ell}))} = \frac{\tau_\ell \, R_{AB}^{(2)}(\xi,\tau_\ell)}{\max[\tau_\ell \, R_{AB}^{(2)}(\xi,\tau_\ell)]} \tag{37}$$

and

$$P(U=\frac{\xi}{\tau_\ell}) = \frac{\tau_\ell \, R_{AB}^{(2)}(\xi,\tau_\ell)}{\xi \int_{-\infty}^{\infty} \frac{1}{\tau'_\ell} R_{AB}^{(2)}(\xi,\tau'_\ell) \, d\tau'_\ell} \tag{38}$$

where

$$R_{AB}^{(2)}(\xi,\tau_\ell) = \frac{1}{T} \int_0^T \frac{\partial i_A(t)}{\partial t} \frac{\partial i_B(\xi,t+\tau)}{\partial t} dt. \tag{39}$$

For statistical stationary processes, the above expression is equivalent to the negative of the second derivative of the cross-correlation; i.e.,

$$R_{AB}^{(2)}(\xi,\tau_\ell) = -\frac{\partial^2}{\partial \tau_\ell^2} R_{AB}(\xi,\tau_\ell). \tag{40}$$

Once the probability density of the wind component variations is obtained from the cross-correlation of the time derivatives of photometer signals, all the central moments of the wind component variations can be easily calculated. The two most important moments are the mean wind component,

$$\bar{U} = \int_{-\infty}^{\infty} U\ P(U)\ dU,$$

and the mean square value (or variance) of the wind component variations,

$$\sigma_U^2 = \int_{-\infty}^{\infty} (U-\bar{U})^2\ P(U)\ dU.$$

The ratio of the root-mean-square value to the mean wind component ($\sigma_u/\bar{U}$) is a common measure of atmospheric turbulent intensity.

IV-3. DATA CONDITIONING AND PROCESSING METHODS

It was shown in the last section that the time derivatives of photometer outputs are needed for evaluating cross-correlation in order to retrieve remotely the probability density of wind component variations. For stationary atmospheric conditions, this will be equivalent to require evaluating the second derivative of the cross-correlation of the photometer outputs themselves. The atmospheric phenomena are known to be intrinsically nonstationary, but for qualitative understanding of the problems involved in the data conditioning and handling, we would assume for the moment that the time histories of photometer outputs are stationary. Under this assumption, equation (40) holds. Taking the Fourier integral transform of the equation yields

$$S_{AB}^{(2)}(\xi,f) = f^2\ S_{AB}(\xi,f), \tag{41}$$

where

$$S_{AB}^{(2)}(\xi,f) = \int_{-\infty}^{\infty} R_{AB}^{(2)}(\xi,\tau_\ell)\ e^{i2\pi f\tau_\ell} d\tau_\ell \tag{42}$$

and

$$S_{AB}(\xi,f) = \int_{-\infty}^{\infty} R_{AB}(\xi,\tau_\ell)\ e^{i2\pi f\tau_\ell}\ d\tau_\ell. \tag{43}$$

Here, $S_{AB}(\xi,f)$ is the cross-spectral density of the photometer outputs, while $S_{AB}^{(2)}(\xi,f)$ is the cross-spectral density of the first time derivatives of the photometer outputs. These two spectral densities are generally complex functions. For easier discussion, we would rather deal with their gains which are always real and defined by

$$G_{AB}^{(2)}(\xi,f) = [S_{AB}^{(2)}(\xi,f)\ S_{AB}^{(2)*}(\xi,f)]^{1/2} \tag{44}$$

and

$$G_{AB}(\xi,f) = [S_{AB}(\xi,f)\ S_{AB}^{*}(\xi,f)]^{1/2}, \tag{45}$$

where the asterisk indicates the complex conjugate. Hence, equation (41) can be rewritten as

$$G_{AB}^{(2)}(\xi,f) = f^2 G_{AB}(\xi,f). \tag{46}$$

This equation states that the gain from the time derivatives of the photometer outputs is equal to the gain from the outputs themselves multiplied by the frequency square.

In the atmosphere, the gain of the photometer outputs $G_{AB}(\xi,f)$ follows approximately f^{-2} in the range of energy-bearing eddies. This would imply that the gain from the time derivatives would approximate a white noise spectrum. It is also well known that the wider the bandwidth of a white noise spectrum, the narrower the first zero crossing of the corresponding correlation function. Thus, to better approximate the assumption (III-A), we would like to have the bandwidth of the photometer outputs as wide as possible. However, because of the following two factors, the bandwidth of the signals (i.e., the photometer outputs) should be suitably limited. First, the common signal-to-noise ratio of the photometer outputs with natural scattering radiations as light sources is very low. This ratio is usually of the order of 0.4 or less

[IV-3]. It follows that the correlation coefficient of the i_A and i_B, i.e.,

$$\frac{\langle i_A\, i_B\rangle}{\langle i_A^2\rangle^{1/2}\langle i_B^2\rangle^{1/2}}, \tag{47}$$

is of the order of $(0.4)^2 = 0.16$ or less. Such a small correlation coefficient could not be accurately evaluated by commercially available analog correlators. A digital computer is required to achieve a more complete noise cancellation by integrating over very long records without dynamic time placement errors. The f^2 weighting of the high frequency noise which is introduced by differentiating the time series also requires an additional low-pass filter with a sharp roll-off at the high frequency limit of the common signals. Secondly, in using digital computers, the time derivative may be approximated by the finite difference of two consecutive digital time samples. The quantization errors in the individual samples resulting from the analog/digital conversion will further propagate to the time derivatives [IV-11]. The main effects of the above two factors are significant only in the higher frequency portion of the cross-spectral density.

To reduce the quantization errors in the digital time histories, the sample reduction method is employed. In essence, this method consists of two steps: (1) sampling the analog time history at an interval by 2m times smaller than that required by the Nyquist's criterion, i.e., $\Delta t = 1/2(2f_u)$, where f_u is the upper frequency of the time history measured in Hertz and m is any positive integer equal or greater than 1, and (2) averaging every m consecutive digital samples to form a new digital time history with an equally spaced time interval of $1/(4f_u)$. The theory [IV-11] shows that, on the average, about 30 percent reduction in the quantization error may result by reducing five samples to one on a time history having an f^{-2} spectral density. Reductions for other spectrum shapes are also given in reference IV-11.

To determine optimum injection of f^2 weighted high frequency noise components, we have various standard frequency settings for the digital filters. Both center and roll-off frequencies were changed independently of each other. In applying the digital filtering, any desired filter gain and phase functions can easily be accomplished by using a suitable transfer function without worrying about practical limitations in electronics.

Specifically, let us consider an analog time history x(t) and let its Fourier transform be X(f), i.e.,

$$X(f) = \int_{-\infty}^{\infty} x(t)\ e^{-i2\pi ft}\ dt. \tag{48}$$

This function represents the frequency decomposition of the original time history. In a broad sense, the filter is meant to be an operator on X(f) such that X(f) will be weighted according to a desired fashion in a certain range of frequency. Mathematically, this operation can be expressed as

$$Y(f) = H(f)\ X(f). \tag{49}$$

Here, H(f) is the function characterized by the desired operation and is called the (complex) frequency response function of the filter, while Y(f) is the frequency decomposition of the output filtered random time history. The frequency response function can be broken into the real part $H_r(f)$ and imaginary part H(f), i.e.,

$$H(f) = H_r(f) + iH_i(f). \tag{50}$$

The absolute value $|H(f)|$ of H(f) is called the gain of the filter,

$$|H(f)| = [H_r^2(f) + H_i^2(f)]^{1/2}, \tag{51}$$

while the arc-tangent of the ratio $H_i(f)/H_r(f)$ is called the phase function of the filter,

$$\phi(f) = \text{arc tan } \left(\frac{H_i(f)}{H_r(f)}\right). \tag{52}$$

Denote the inverse Fourier transforms of H(f) and Y(f) to the time domain by

$$h(t) = \int_{-\infty}^{\infty} H(f) \exp(i2\pi ft)\, dt \tag{53}$$

and

$$y(t) = \int_{-\infty}^{\infty} Y(f) \exp(i2\pi ft)\, dt. \tag{54}$$

Taking the Fourier transformation of equation (49), and then substituting the above expressions, we obtain

$$y(t) = \int_{-\infty}^{\infty} h(t')\, x(t-t')\, dt'. \tag{55}$$

This equation states that the filtering as defined by equation (49) is equivalent to an integral transform of the original time history x(t) with the weighting function h(t). This weight is called the transfer function of the filter. The output of this transformation y(t) is usually called the filtered time history.

For an ideal low-pass filter with bandwidth $B = f_u$, the frequency response function is simply

$$H(f) = H(-f) = \begin{cases} 1, & |f| \leq B \\ 0, & |f| > B. \end{cases} \tag{56}$$

The corresponding transfer function will be

$$h(t) = B \frac{\sin(2\pi Bt)}{2\pi Bt}. \tag{57}$$

However, because of the Gibb's phenomenon, we cannot use the transfer function of equation (57), directly. This phenomenon essentially states

that oscillations exist in the approximating frequency response function near the discontinuities of the ideal one when one approximates an ideal frequency response function having one or more jump discontinuities with a truncated Fourier series.

To avoid this difficulty, the frequency response function is usually constructed as a continuous function. There are numerous ways to accomplish this. What we shall adopt below, one of the simplest types, is called the Martin-Graham type roll-off filter. Its frequency response function is defined for a low-pass filter [IV-12, -13] as follows:

$$\tilde{H}_{\ell}(f) = \begin{cases} 1, & |f| \leq f_c \\ \frac{1}{2}\,[1 + \cos\,\pi(f-f_c)/\Delta f], & f_c < f < f_T \\ \frac{1}{2}\,[1 + \cos\,\pi(f+f_c)/\Delta f], & f_T < f < -f_c \\ 0, & |f| \geq f_T \end{cases} \tag{58}$$

where f_c and f_T are the cutoff frequency and terminate frequency, respectively, while Δf is the frequency interval between these two frequencies, i.e., $\Delta f = f_T - f_c$. The inverse Fourier transformation of equation (58) yields the transfer function for the Martin-Graham low-pass filter:

$$\tilde{h}_{\ell}(t) = \frac{\sin(2\pi f_c t) + \sin(2\pi f_T t)}{2\pi t[1 - 4(\Delta f)^2\, t^2]} \,. \tag{59}$$

The theory for filtering and the associated equations are formulated in terms of analog time histories. To apply them to discrete digital time histories, all integrations need to be rewritten in summation forms. The frequency contents of the time history should also be known to set a suitable sampling rate for digitization following the Nyquist criterion. In actual application, the limits of integration in equation (55) will be finite.

Obviously one would like to limit the integration limits T as much as possible in order to minimize the required computer time. An explicit relation for the minimum integration time is now derived from the characteristics of both the time histories and the desired filter.

Let us denote the upper frequency in the time histories by f_u, the desired cutoff frequency of the filter by f_c, and terminate frequency by f_T. The upper frequency will determine the minimum sampling interval by Nyquist's or Shannon's criteria as

$$\Delta t = \frac{1}{2f_u} .$$

Then equation (55) can be written in summation form as

$$y_k = \Delta t \sum_{\ell=-N_d}^{N_d} h_\ell x_{k-\ell} , \tag{60}$$

$(k = N_d, N_d + 1, \ldots, (N - N_d),$

where

$$\begin{aligned} y_k &= y(k\Delta t) \\ h_\ell &= h(\ell \Delta t) \\ x_{k-\ell} &= x[(k-\ell)\ \Delta t] \end{aligned} \tag{61}$$

and

$$N = T/\Delta t.$$

The limit of summation $\pm N_d$ is dictated by the tolerance of error in the filter frequency response. Let us define the measure of error [IV-12] as

$$\epsilon(f,N_d) = H(f) - H(f,N_d), \tag{62}$$

where $H(f,N_d)$ is the N_d-term truncation of the infinite series representation of $H(f)$. It has been determined empirically that for the tolerance

$$0.5\% < \epsilon < 1\% \tag{63}$$

the minimum number required is given by

$$\min(N_d) = \frac{5f_u}{4(f_T - f_c)} , \tag{64}$$

with

$$f_u > 2f_T .$$

This shows that the sharper the roll-off rate in the filter, the greater the number of digital samples needed for a fixed accuracy tolerance. Figure IV.5 shows the phase and gain function of the Martin-Graham low-pass filter with f_c = 0.8 Hertz, f_T = 1.0 Hertz and N_d = 39. The figure clearly shows that there is only negligibly small phase distortion and that the gain is almost exactly as desired.

IV-4. EXPERIMENTAL AND COMPUTED RESULTS

To verify the theory that the probability density of wind component variations can be approximated by the crossed-beam technique, and to test the applicability of the data conditioning and handling methods described in the last two chapters, some computer-processed results of actual crossed-beam test data recorded in the lower atmosphere are presented in this chapter.

The field tests were carried out by the Colorado State University at Boulder, Colorado. A schematic crossed-beam test arrangement is illustrated in Figure IV.6. The detailed test site topography, geometry of the photodetectors, and meteorological conditions were reported in references IV-1 and IV-2.

The light source is the natural scattered radiation in the visible spectral range. A block diagram of the crossed-beam detection system is shown in Figure IV.7. Essentially, the incident radiation in the field of view of the telescope (0.5 degree) is focused on a photodetector (silicon diode). The radiation power is converted into voltage in proportion to its power. The fluctuating voltage is electronically separated into the d.c. and a.c. components with a time-constant of 100 seconds. In addition, a low-pass and high-pass filter of 0.01 Hz and 3 Hz, respectively, are set in the recording chain. Both a.c. and d.c. signals, together with the wind speed and direction obtained by anemometers, are recorded on an analog magnetic tape. More details of the optics and electronics, and associated signal/noise analyses were discussed in reference IV-3.

We shall present and discuss two test runs (I and II). The pertinent information is summarized in Table IV-1. The top view of the photometer arrangements and the probabilities of wind directions for these two runs are shown, respectively, in Figures IV.8(A) and (B). It can be seen that the wind direction was fairly constant during the measurements for both runs. For comparisons, anemometers were also mounted on a meteorological tower which was located between two lines of sight of the photometers (Figure IV.6).

The analog time histories of the a.c. signals are first digitized at a rate of 80 samples per second. These digital time histories are then averaged every 10 samples to reduce the sampling rate to 8 samples per second by the sample reduction method discussed in section IV-3. The purpose of the operation is to reduce the quantization errors due to the analog/digital conversion. These reduced digital time histories and their time derivatives are then used to evaluate the cross-correlations. Since the time histories are too long to be stored in their entirety in the computer, this evaluation is performed by a specially devised computer logic for piecewise correlation [IV-14, -15, and -16]. In short, a long time history of length T is to break into m shorter pieces of equal length $\triangle T$; $T = m \triangle T$. Each short piece of data is then processed to obtain a "piecewise" cross-correlation. These "piecewise" cross-correlations are sequentially averaged by a recursion formula to obtain the accumulative cross-correlation which is equal to the cross-correlation evaluated directly from the entire time history. By so doing, the computer needs only to store a time history of length $\triangle T$. In processing the test runs I and II, the piece length $\triangle T$ = 450 seconds, the maximum time lag τ_{max} = 50 seconds and the increment in time lag $\triangle\tau$ = 0.25 second.

Figure IV.9 shows the cross-correlation of the photometer outputs for run I with the lower and upper frequency cut-off, 0.01 Hz and 3.0 Hz, respectively. The extremely erratic curve indicates clearly that the upper frequency of 3 Hz is too high. An examination of the corresponding gain shows that a narrow-band noise component exists at 1.25 Hz. So, to smooth the cross-correlation, the noise component has to be filtered out. Figures IV.10 through IV.12 show three different cases of cross-correlations $R_{xy}(\tau)$ and $R_{xy}^{(2)}(\tau)$ of the outputs and their time derivatives of run I, which are obtained by using three different roll-offs in the digital filtering. All three have the same terminate frequency f_T = 1.0 Hz, while the cut-off frequencies, f_c, equal 0.8, 0.6 and 0.4 Hz, respectively. Also shown in these figures are the 90-percent confidence limits of $R_{xy}(\tau)$ and $R_{xy}^{(2)}(\tau)$ as denoted by $\overline{\overline{R_m(\tau)}}$ and $\overline{\overline{R_m^{(2)}(\tau)}}$, respectively [IV-15]. All three $R_{xy}(\tau)$ curves are much smoother compared to the curve in Figure IV.9, and there is only one peak in $R_{xy}(\tau)$ around τ = 10 seconds, which exceeds the confidence limit at least by two times. This means that only this peak has the sufficient statistical significance, and that the rest of the curve is due to nothing but noises which have not been completely

eliminated. Therefore, only the portion of $R_{xy}^{(2)}(\tau)$ which corresponds to this significant peak should be selected with sufficient statistical confidence. For easy identification, these portions of $R_{xy}^{(2)}(\tau)$ are shaded.

Figure IV.13 presents the statistical errors of $\overline{\overline{\delta R_m}}$ of the cross-correlations $R_{xy}(\tau)$ versus the inverse square root of the integrating time $T = mt$. The statistical error is defined as the average of the confidence limit $\overline{\overline{R_m(\tau)}}$ integrated over the time lag from $-\tau_{max}$ to $+\tau_{max}$ [IV-14]. For statistical stationary processes, the theory shows that these curves should approximate a straight line drawn through the origin of the coordinates, and that the slope of the straight line gives the inverse square root of an equivalent bandwidth B_{eff}, as if the associated spectrum were a white noise spectrum [IV-16]. The figure shows the equivalent bandwidth $B_{eff} = 0.182$ Hz for run I. It is also noted that the statistical error for $f_c = 0.8$ Hz is the smallest, while the error for $f_c = 0.4$ Hz is the largest. This is expected, since the error is proportional to the inverse square root of the bandwidth used.

Figures IV.14 through IV.16 show the gains $G_{xy}(f)$ and $G_{xy}^{(2)}(f)$ corresponding to Figures IV.10 through IV.12. Table IV-2 summarizes the approximate power law for each gain and the corresponding increase in exponent from $G_{xy}(f)$ to $G_{xy}^{(2)}(f)$. For stationary processes, the increase in the exponent of the power from $G_{xy}(f)$ should be 2 (see equation (46)). Table IV-2 indicates that the case with $f_c = 0.4$ Hz and $f_T = 1.0$ Hz gives a power law closest to that for stationary processes. It also implies that the components of the photometer outputs between 0.4 Hz and 1.0 Hz is less stationary than those between 0.01 Hz and 0.4 Hz. To further demonstrate the nonstationarity, $G_{xy}^{(2)}(f)$ and $f^2\, G_{xy}(f)$ for each case are plotted in Figures IV.17 through IV.19. Comparing of these figures also shows that the best agreement between $G_{xy}^{(2)}(f)$ and $f^2\, G_{xy}(f)$ is for the case with $f_c = 0.4$ Hz.

Finally, we come to check our ultimate goal, i.e., to retrieve optically the turbulent wind statistics. Figure IV.20 shows the normalized probability density of wind component variations (normal to both beams) deduced from the optical cross-beam measurements, as well as from the anemometer readings. Clearly, the most probable wind component obtained optically is within 5 percent of that obtained by the direct measurement. The rms of the wind component variations obtained optically is slightly larger than that by the anemometer. The best agreement between them again is offered by using $f_c = 0.4$ Hz and $f_T = 1.0$ Hz. It is also noted that the probability density obtained by the crossed-beam technique is somewhat skewed to higher wind component compared to that by the anemometer. The reason for this skewness is still being investigated. Figure IV.21 shows another comparison of the probability densities obtained both optically and directly for run II with $f_\ell = 0.01$ Hz and

f_u = 0.3 Hz. Once again, the crossed-beam measurement yields very accurately the most probable wind component. The rms of the wind component variations is about 25 percent less than that by the anemometer. The optical probability density also shows a similar skewness to higher wind components.

IV-6. CONCLUSIONS

The crossed-beam technique employing the natural scattered radiations is shown to be capable of remote detection of the wind component variations normal to the two light beams. A theoretical relationship is derived which approximates the probability density of the wind component variations in terms of the measurable cross-correlation of the photometer outputs under three fairly realistic assumptions on the atmospheric turbulence and wind statistics. Specifically, it is shown that the probability density of the wind component is directly proportional to the temporal cross-correlation of the first time derivatives of the light intensity fluctuations multiplied by the time lag introduced between the two time histories. The moments of the wind component variations can be easily evaluated once the probability density is obtained by the optical crossed-beam technique.

Because of the very low signal-to-noise ratio for the time histories intrinsic to this type of remote detection, the digital analysis is far more preferable to analog analysis for higher statistical accuracy. Furthermore, because of the necessity to use the time derivatives of the photometer outputs which are approximated by the finite difference scheme, the sample reduction method is used to reduce the quantization error by about 30 percent. More importantly, a suitable digital filtering should be used to filter out the higher frequency noises which are weighted by a factor of frequency square due to the necessity of using the time derivatives. The digital filtering process is fairly time-consuming even for fast computers, and the computation time required is shorter for slower roll-off in the frequency response function of the low-pass filter. Three different types of roll-offs are studied to see their effects on the evaluations of the cross-correlation and the corresponding spectral densities. These roll-offs have the same terminate frequency of 1.0 Hz, while the cut-off frequencies are 0.8 Hz, 0.6 Hz and 0.4 Hz, respectively.

Actual field tests have been carried out in the atmosphere at Boulder, Colorado. Two lines of sight have been crossed about 61 meters from the ground. The photometer signals were processed by a special piecewise computer program, together with two subroutines for applying the sample reduction method and for the digital filtering. The optically measured probability densities of wind component variations were found

to be in reasonable agreement with those measured directly by the conventional anemometers mounted on a meteorological tower at the same crossing height. The most probable wind components obtained by the crossed-beam technique are within 5 percent of that obtained by the anemometer. The root mean squares of the wind component variations obtained by the former for two different tests are within 5 and 25 percent, respectively, of those measured by the latter. For still-unknown reasons, the probability density curve obtained by the optical means is relatively skewed to higher wind speeds as compared to that from the anemometer. It is also found that the best agreement in the probability density of wind components was obtained by using the slowest roll-off, i.e., f_c = 0.4 Hz and f_T = 1.0 Hz. This strongly suggests that the best frequency range might be between 0.01 Hz to 0.5 Hz for these tests. Theoretical considerations predict that the optimum cut-off frequency f_c will be determined by two factors: (a) the maximum wind component to be expected U_{max} and (b) the smallest atmospheric eddy size L_{min} which will preserve sufficiently its characteristics over the transmission between two light beams. Specifically, $f_c = U_{max}/2\pi L_{min}$. This gives f_c = 0.318 Hz for U_{max} = 20 m/sec (run I) and L_{min} = 10 meters [IV-8], which is close to the experimentally determined value of 0.4 Hz. More experimental results are desirable before we can establish conclusively an optimum frequency range and the shape of frequency response function of the digital filtering with minimum required computation time.

The analytical results and data-processing methods developed for the atmospheric turbulence measurement can be applied to measure turbulence in other fluid flow problems as well. The optical technique is particularly advantageous over the hot-wire and the like in measuring the flow speed and turbulence intensity of high-temperature, chemically reacting or supersonic flow fields associated with rocket engine plume, boiling phenomena in nuclear reactors, plasma, etc. All of these flow fields, at the present time, defy accurate and free-from-interference measurements by conventional direct-sensing instrumentations.

TABLE IV-1. TEST RUN SPECIFICATION

SPECIFICATION	RUN I	RUN II
BEAM SEPARATION	93 meters	117 meters
CROSSING HEIGHT	51 meters	61 meters
ANEMOMETER LEVEL	62 meters	61 meters
BASELINE BETWEEN PHOTOMETERS	220 meters	220 meters
BEAM ELEVATION	45°	45°
BEAM AZIMUTH	4° to N.	14° to N.
MEASURING TIME:		
START	1:43 p.m.	11:01 a.m.
END	2:36 p.m.	12:03 a.m.
SKY CONDITION	clear	clear

TABLE IV-2. APPROXIMATE POWER LAWS OF GAINS OF PHOTOMETER OUTPUTS AND THEIR TIME DERIVATIVES

DIGITAL FILTER SETTING (Hz)		EXPONENT IN THE POWER LAW APPROXIMATION		INCREASE IN THE EXPONENT FROM
f_c	f_T	$G_{xy}(f)$	$G_{xy}^{(2)}(f)$	$G_{xy}(f)$ to $G_{xy}^{(2)}(f)$
0.8	1.0	-1.45	-0.25	1.20
0.6	1.0	-1.58	-0.22	1.36
0.4	1.0	-1.83	0	1.83

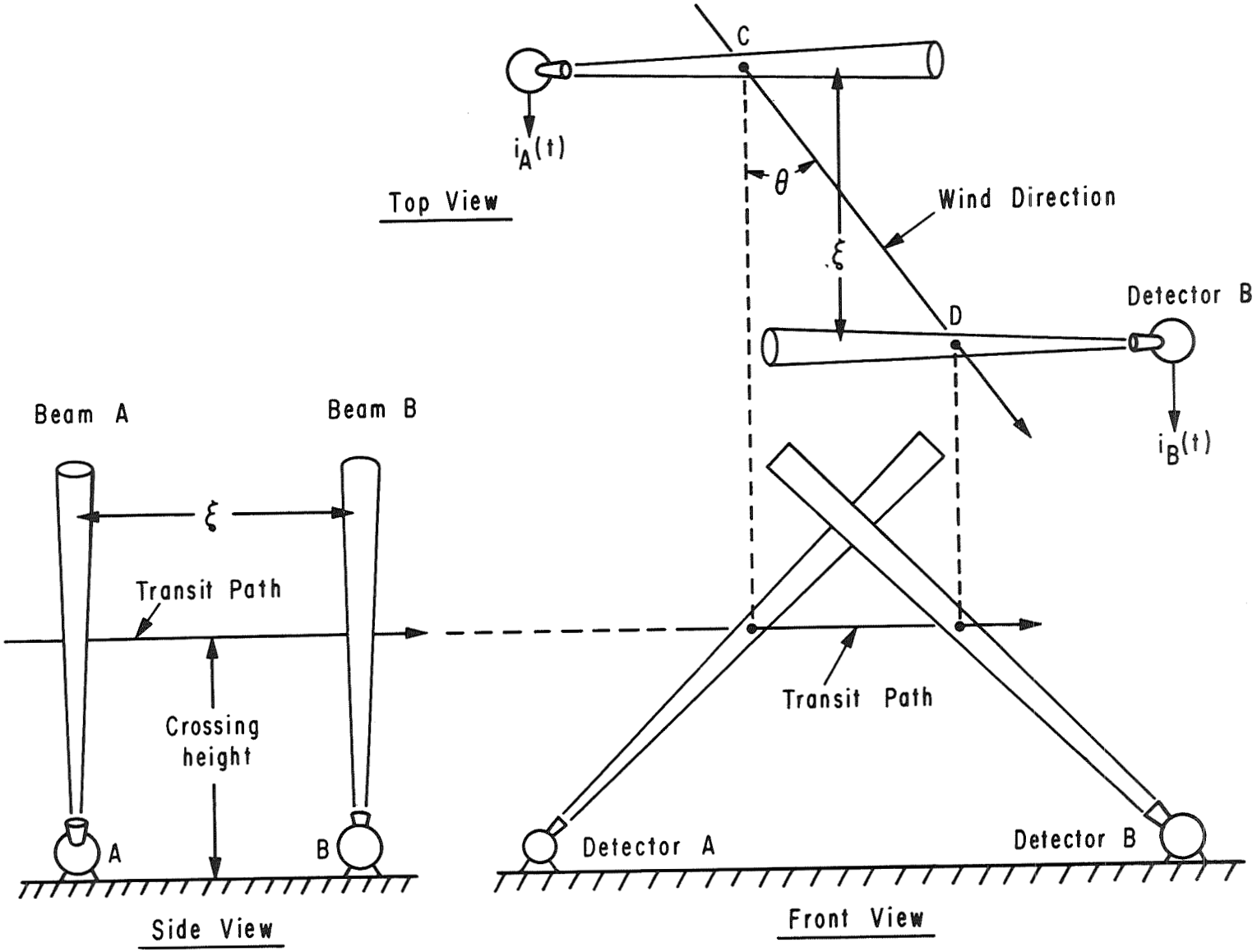

FIGURE IV.1. GROUND-BASED CROSSED-BEAM PHOTOMETER ARRANGEMENT

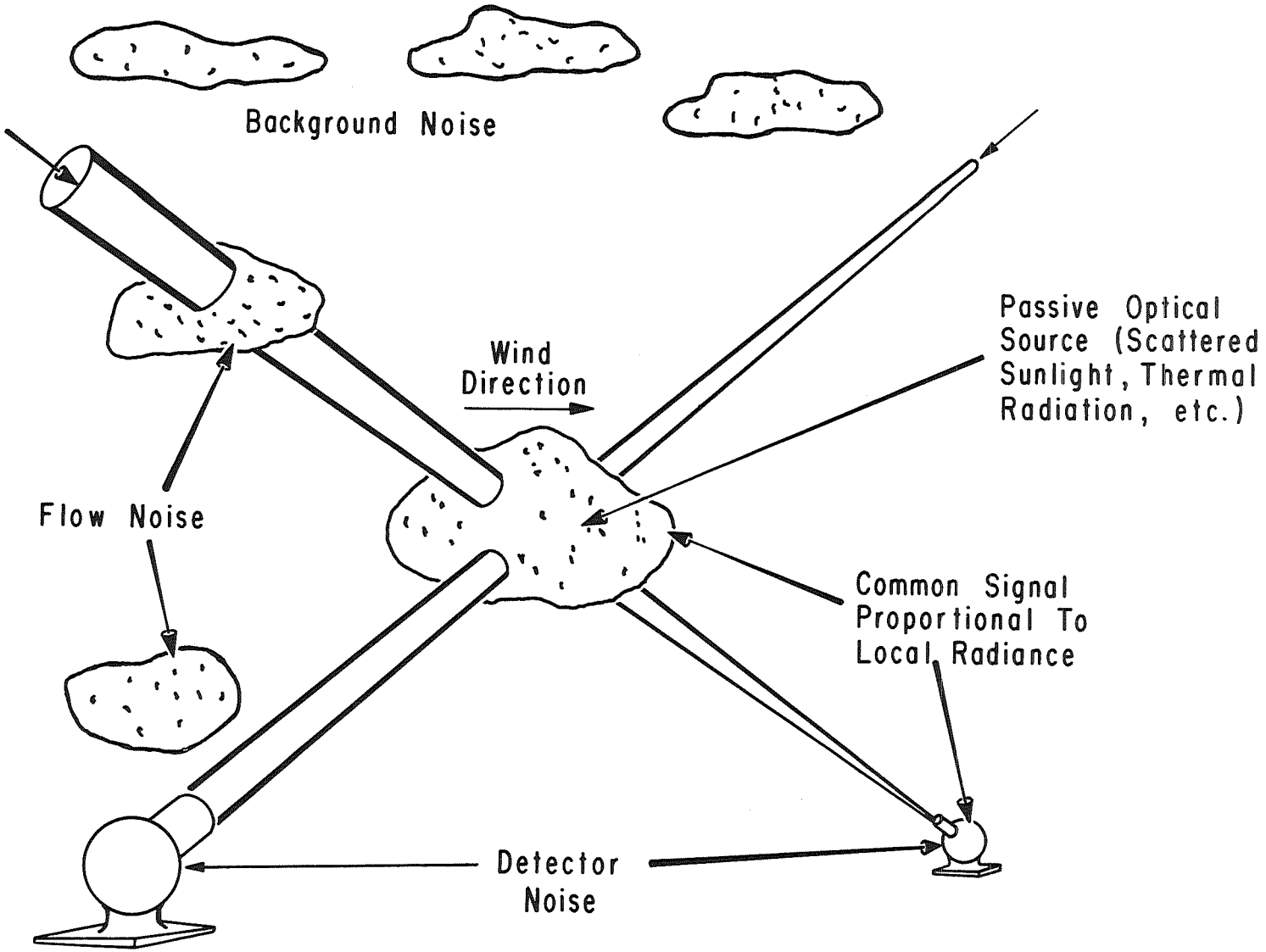

FIGURE IV.2. CROSSED-BEAM SIGNAL AND NOISE SOURCES

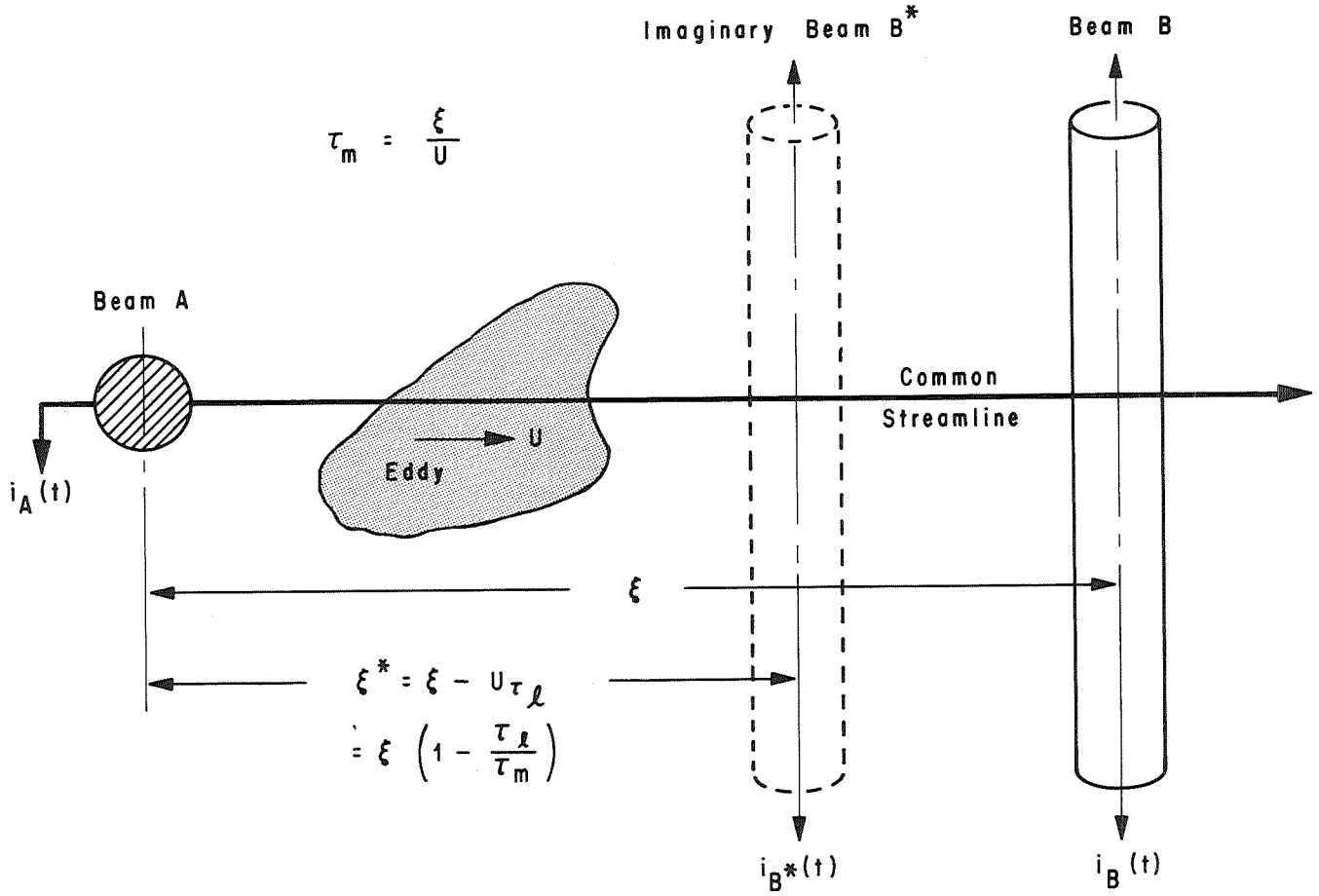

$$\overline{R}(\xi, \tau) \equiv \left\langle i_A(t)\, i_B(t+\tau, \xi) \right\rangle = \left\langle i_A(t)\, i_{B^*}(t, \xi^*) \right\rangle$$

FIGURE IV.3. INTERPRETATION OF IMAGINARY BEAM B*

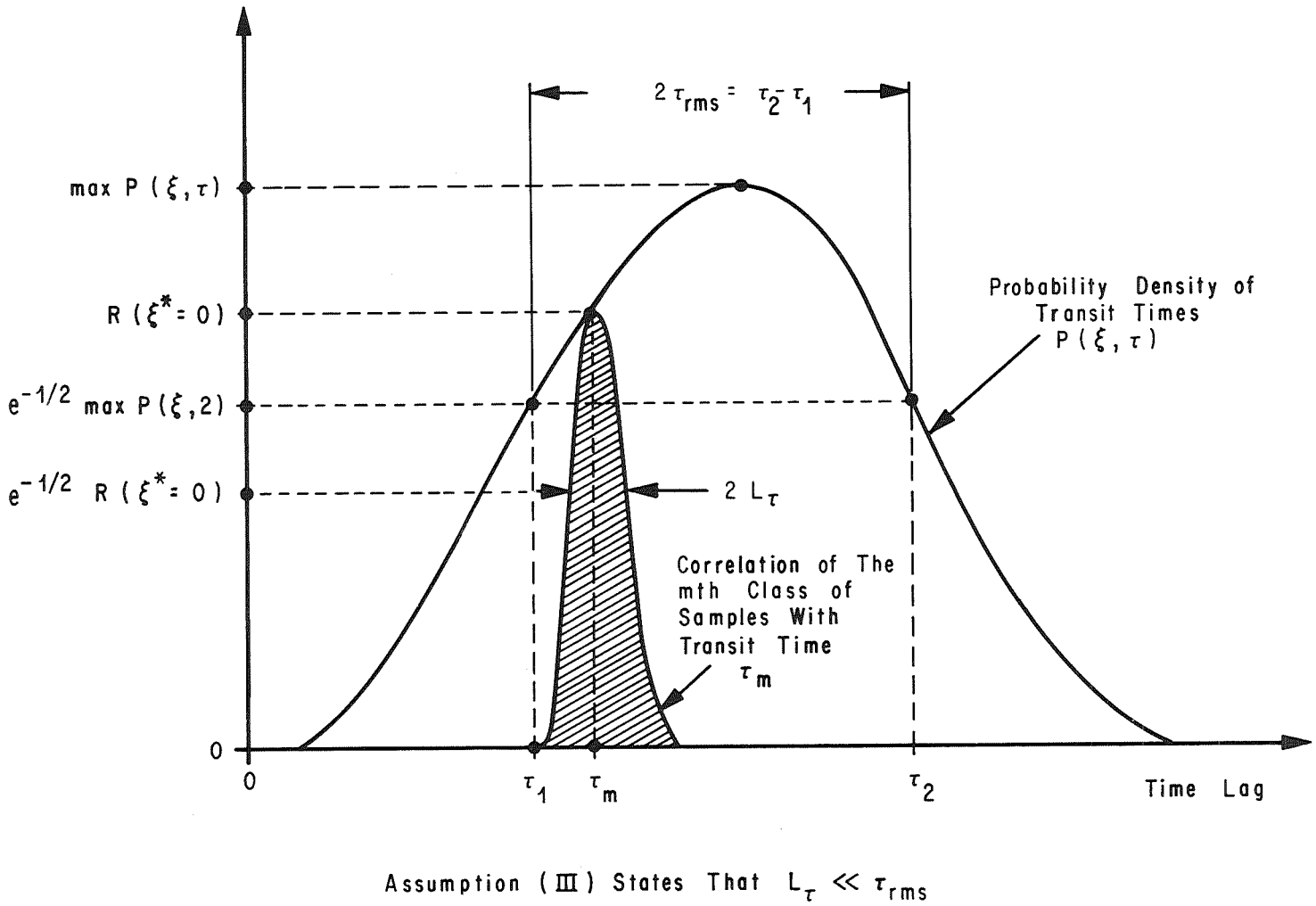

FIGURE IV.4. ILLUSTRATION OF THE ASSUMPTION

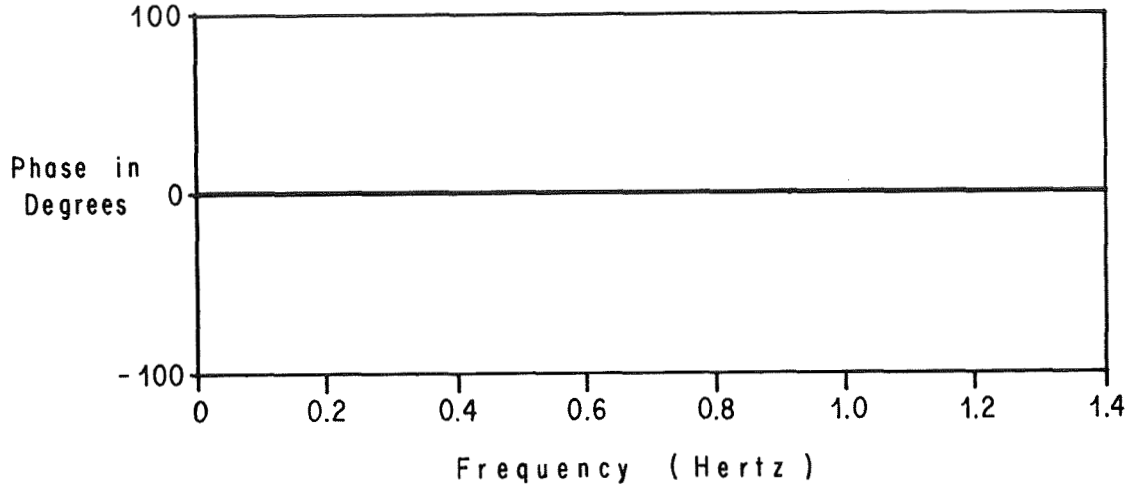

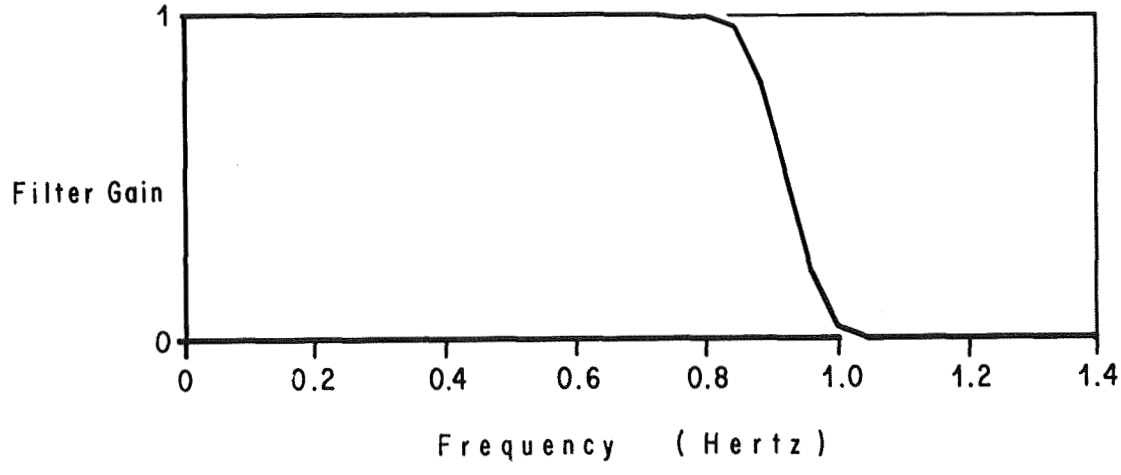

FIGURE IV.5. RESPONSE FUNCTION (PHASE AND GAIN)
OF THE MARTIN-GRAHAM LOW-PASS DIGITAL FILTER

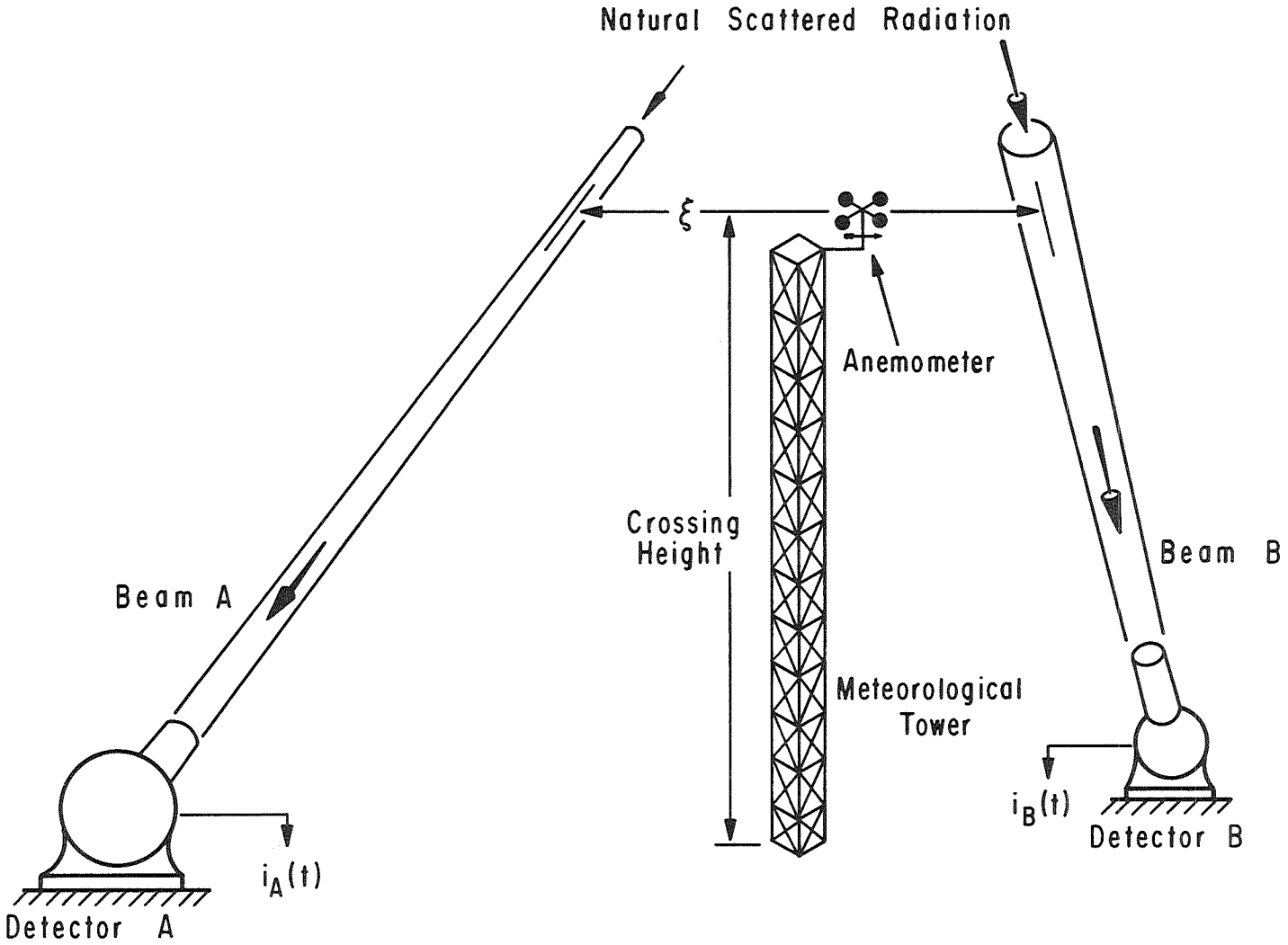

FIGURE IV.6. CROSSED-BEAM TEST ARRANGEMENT

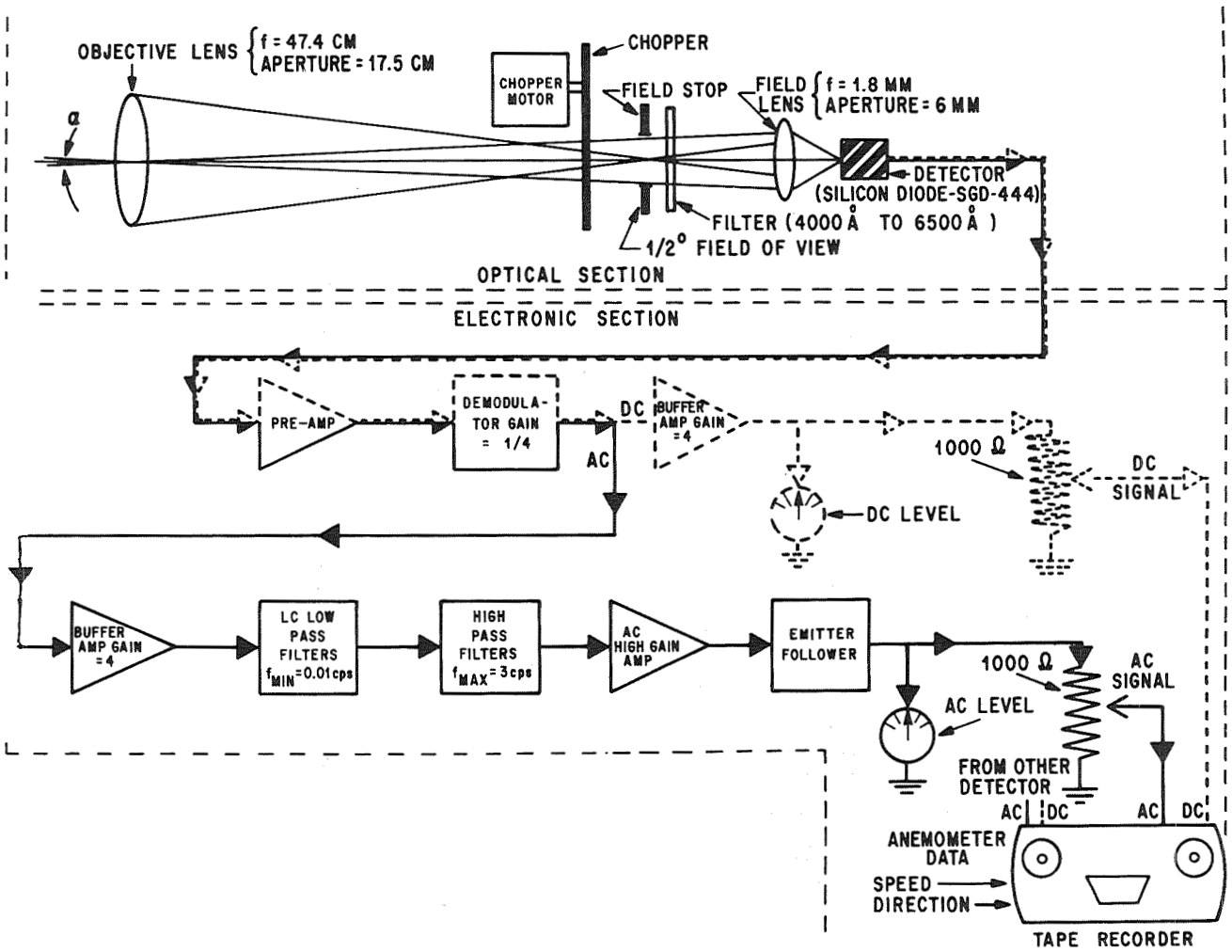

FIGURE IV.7. BLOCK DIAGRAM OF THE DETECTION STAGE

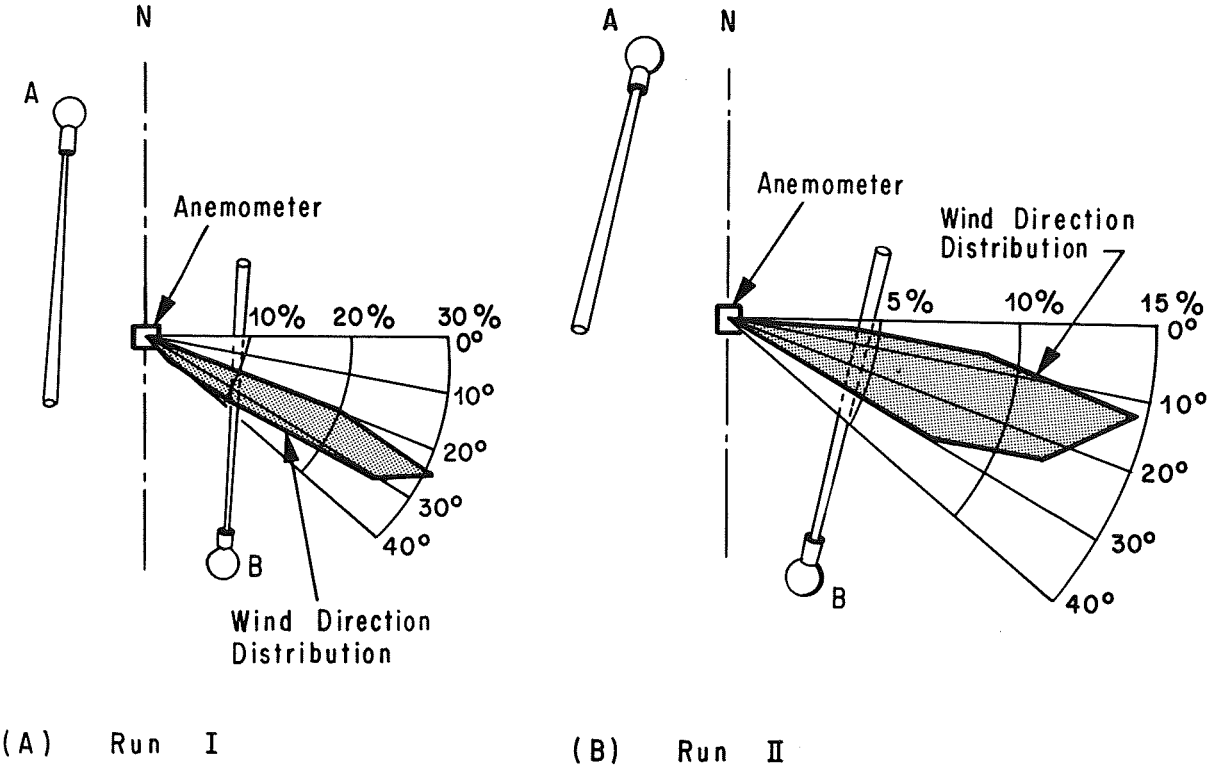

FIGURE IV.8. PROBABILITY OF WIND DIRECTIONS FOR TEST RUNS I AND II

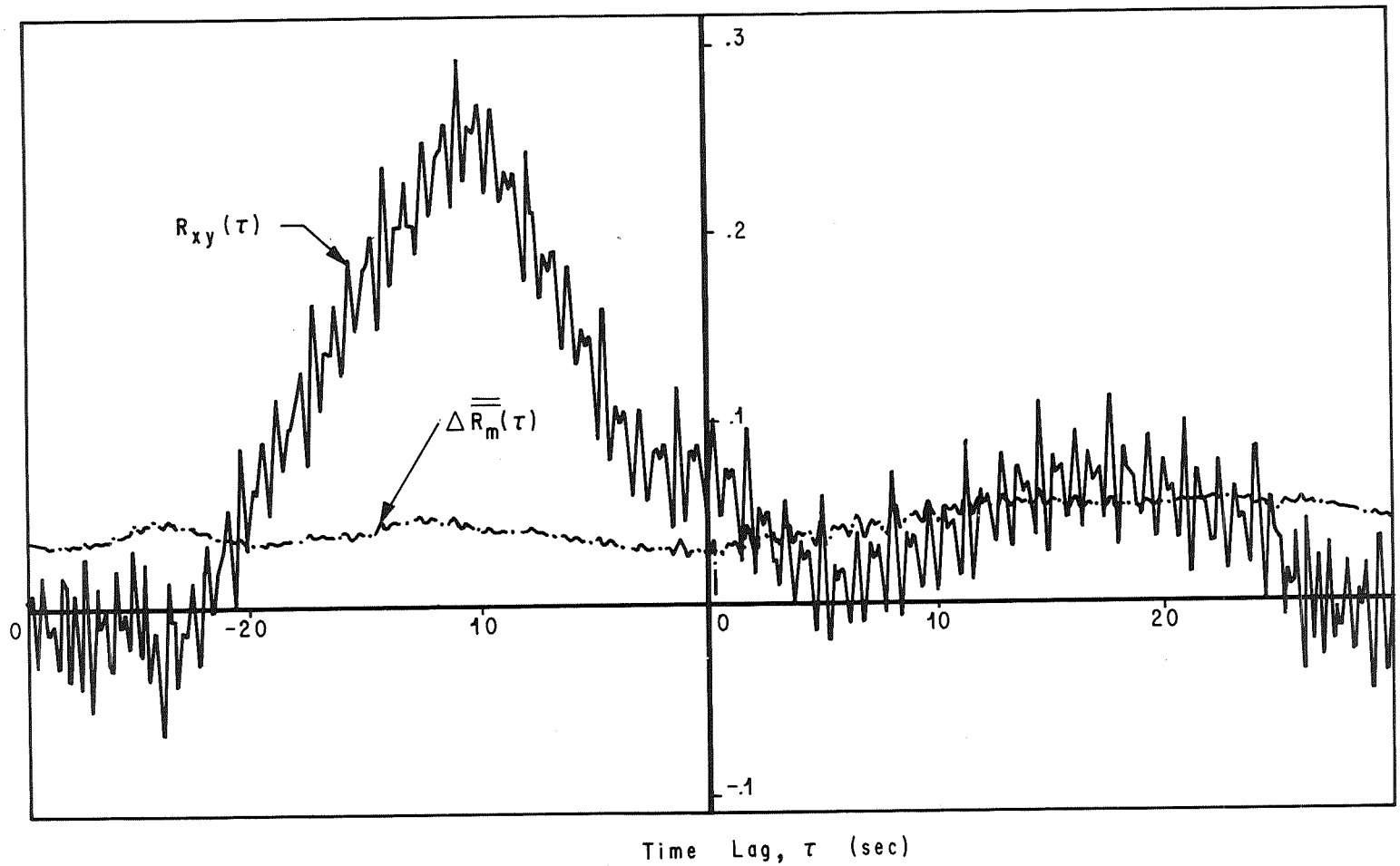

FIGURE IV.9. CROSS-CORRELATION AND CONFIDENCE LIMIT FOR f_l = 0.01 Hz and f_u = 3.0 Hz (RUN I)

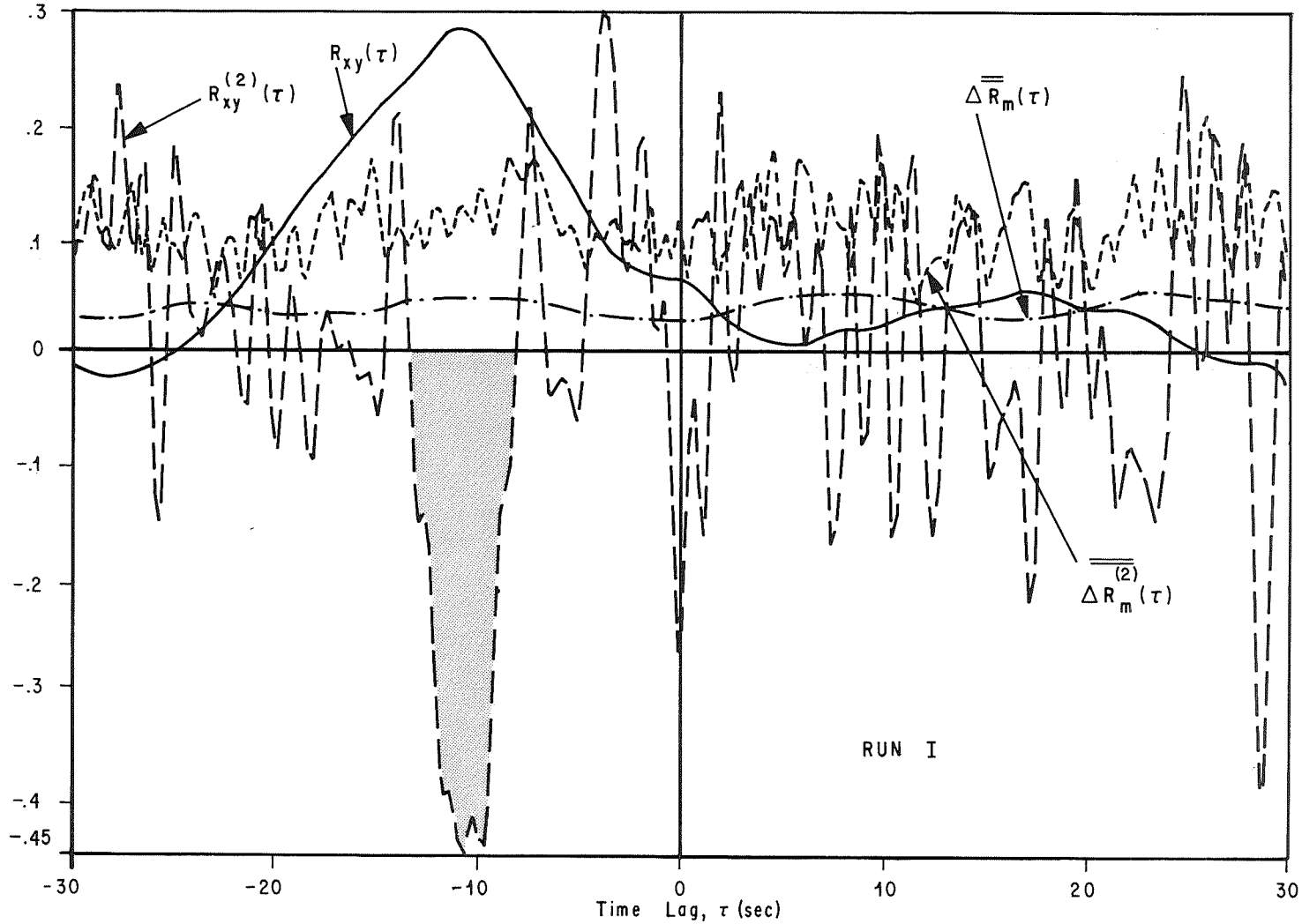

FIGURE IV.10. CROSS-CORRELATIONS AND CONFIDENCE LIMITS FOR f_c = 0.8 Hz and f_T = 1.0 Hz (RUN I)

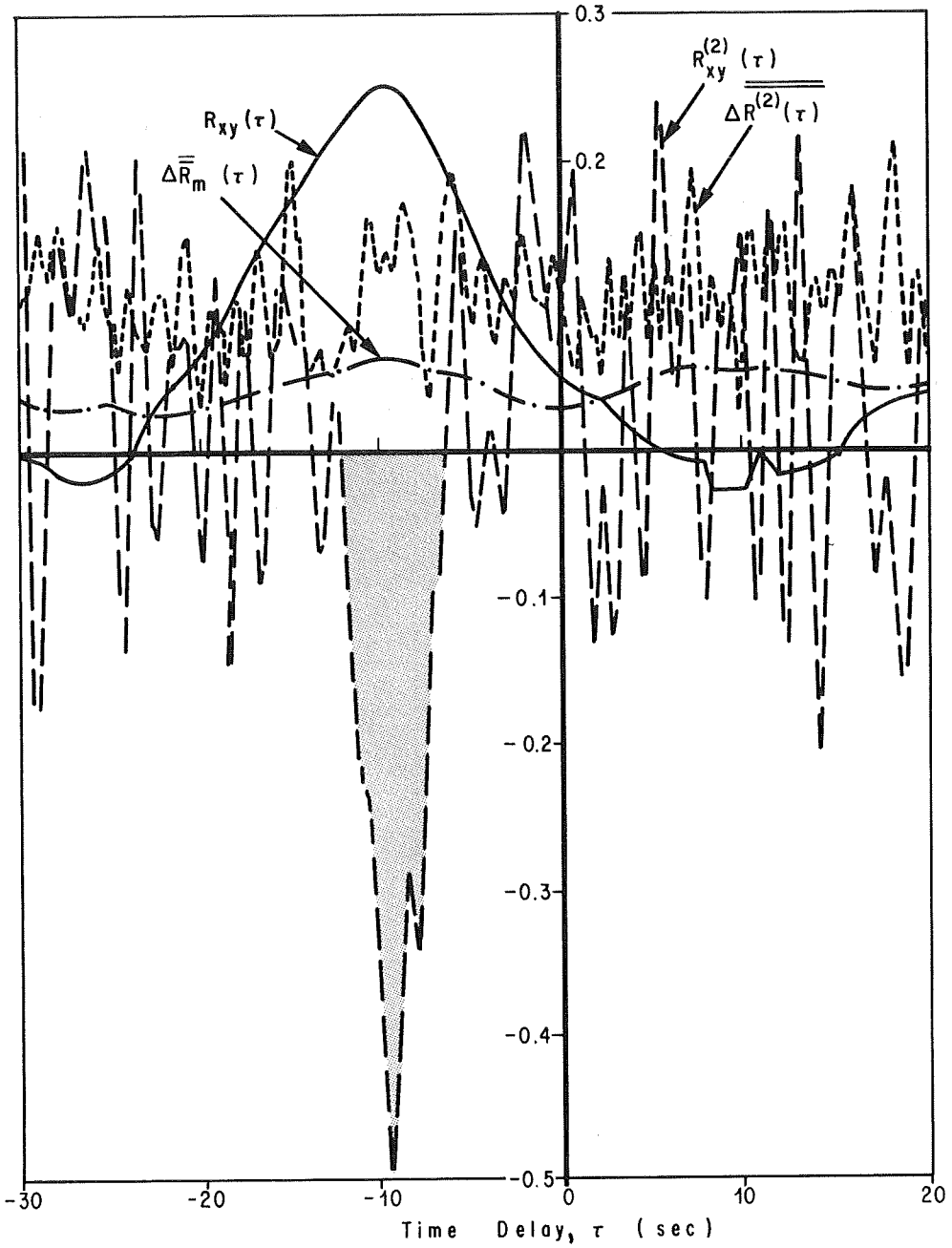

FIGURE IV.11. CROSS-CORRELATION AND CONFIDENCE LIMITS FOR f_c = 0.6 Hz and f_T = 1.0 Hz (RUN I)

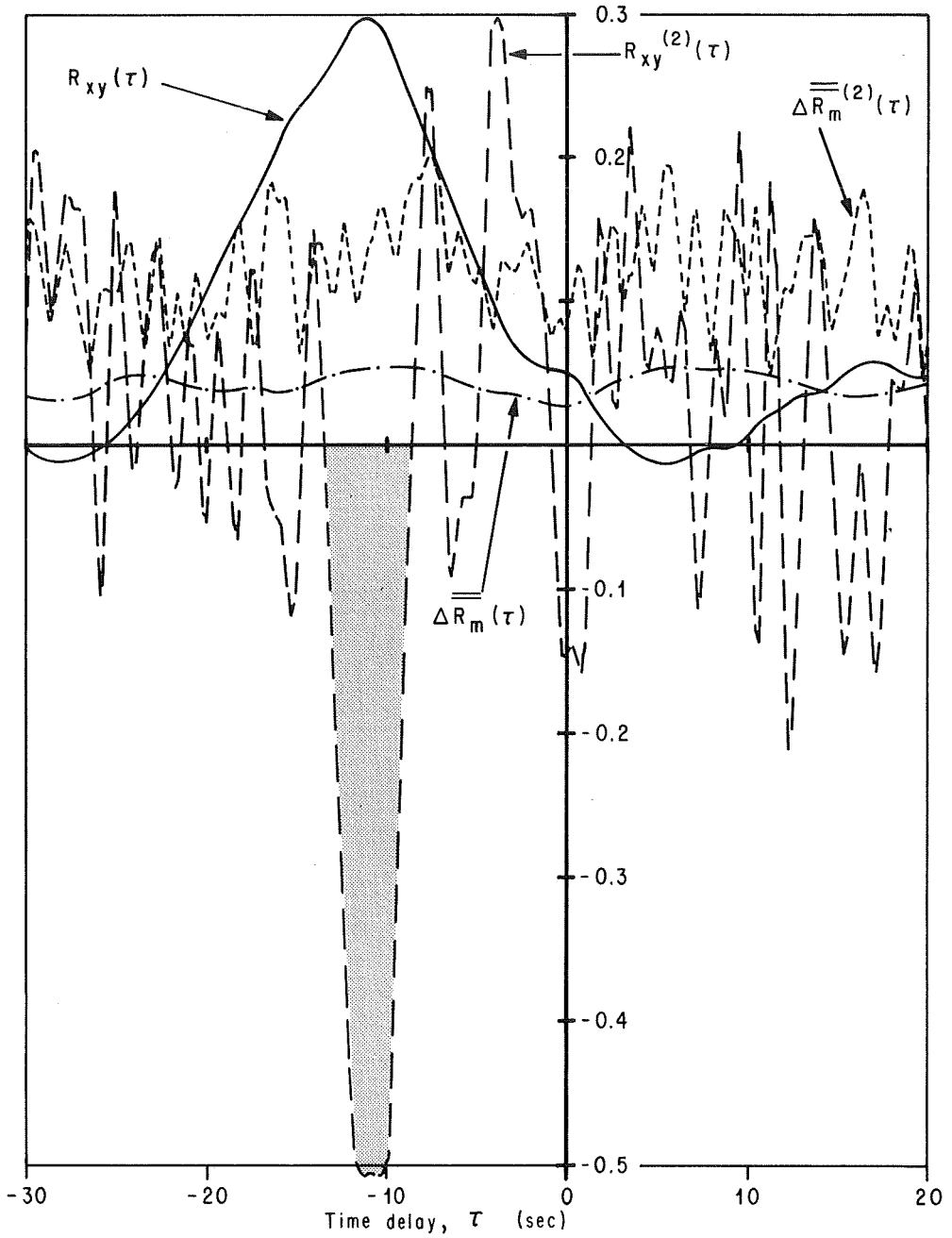

FIGURE IV.12. CROSS-CORRELATIONS AND CONFIDENCE LIMITS FOR f_c = 0.4 Hz AND f_T = 1.0 Hz (RUN I)

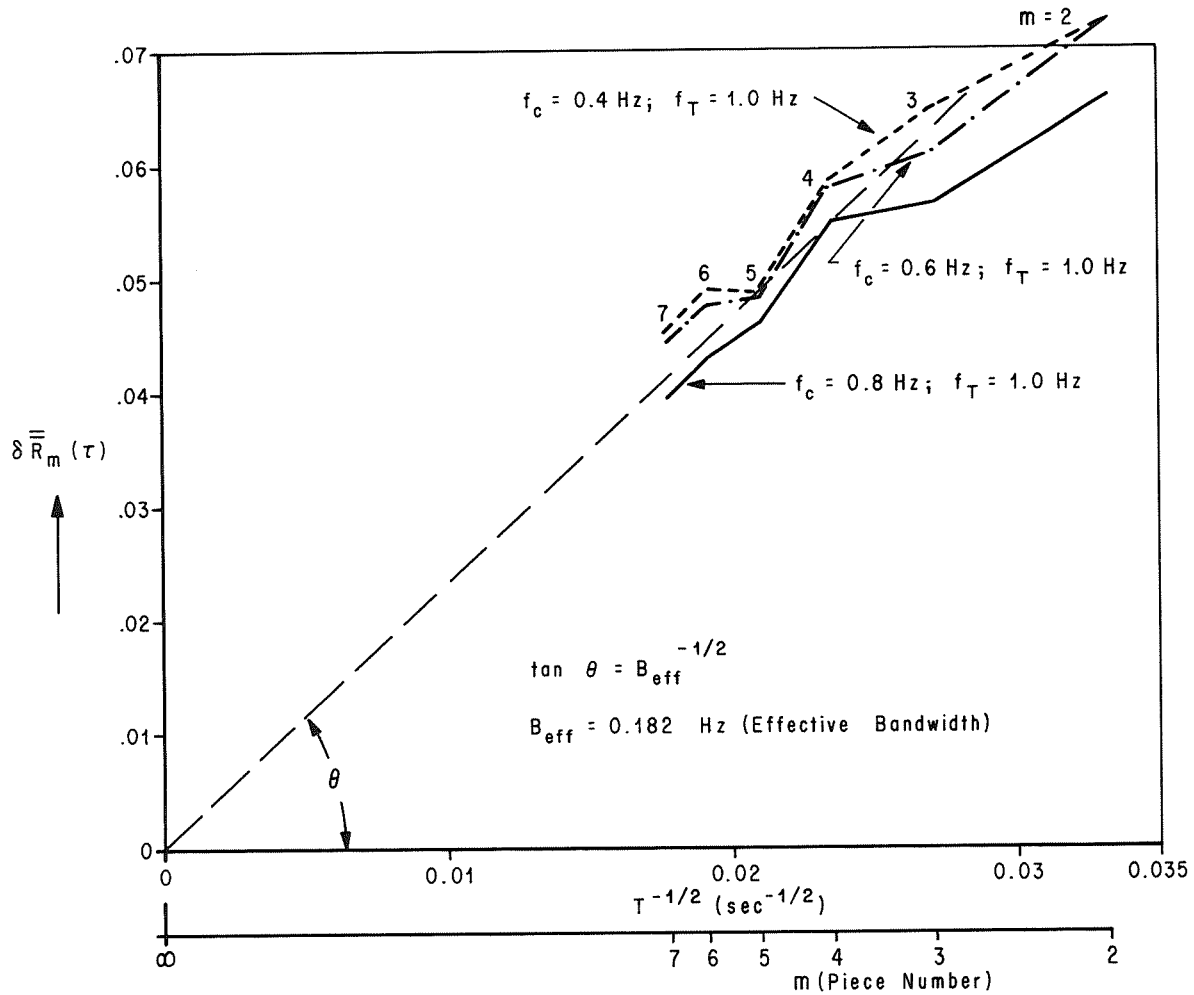

FIGURE IV.13. STATISTICAL ERROR OF CROSS-CORRELATION (RUN I)

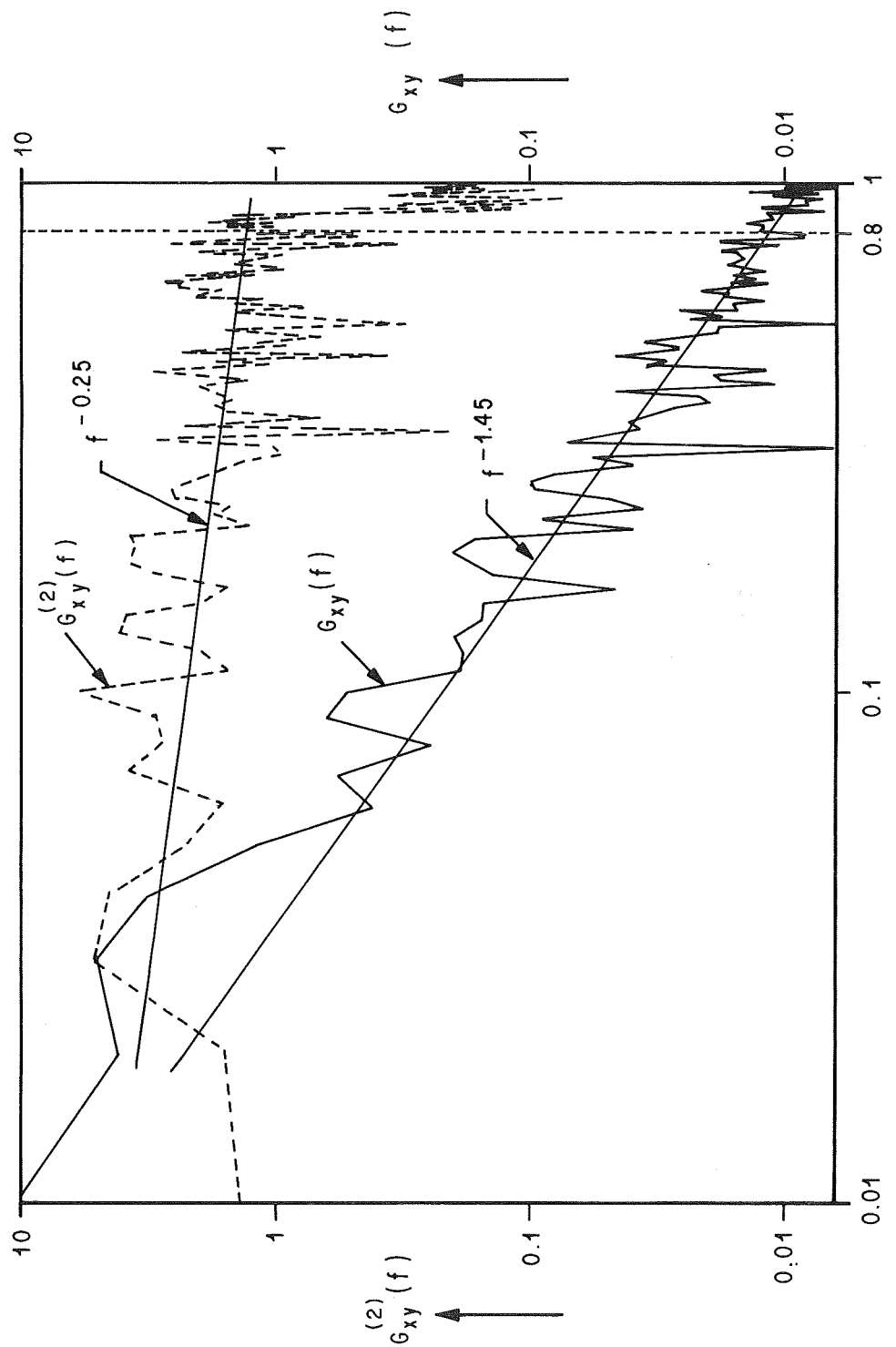

FIGURE IV.14. COMPARISON OF THE GAINS $G_{xy}(f)$ AND $G^{(2)}_{xy}(f)$ FOR f_c = 0.8 Hz and f_T = 1.0 Hz (RUN I)

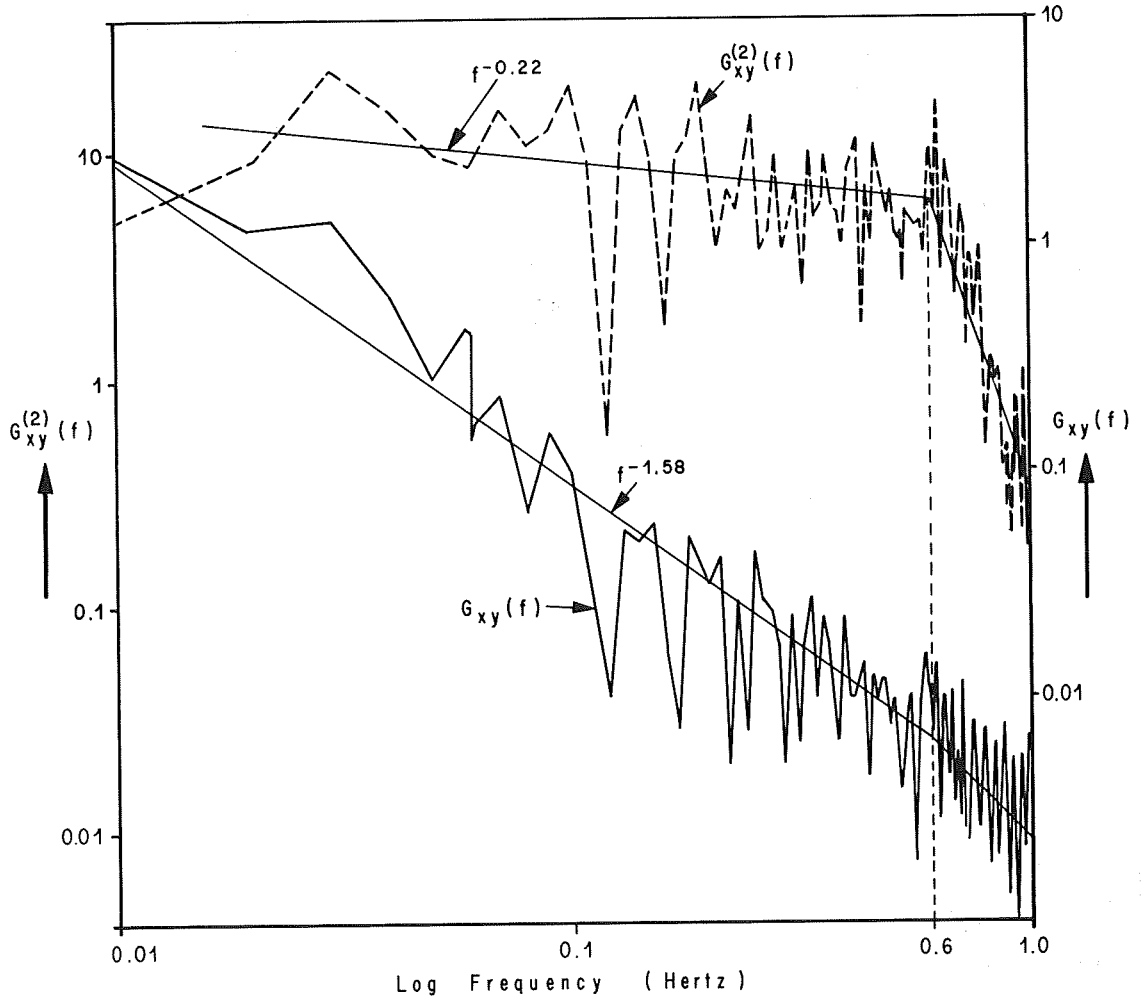

FIGURE IV.15. COMPARISON OF THE GAINS $G_{xy}(f)$ AND $G^{(2)}_{xy}(f)$ FOR f_c = 0.6 Hz and f_T = 1.0 Hz (RUN I)

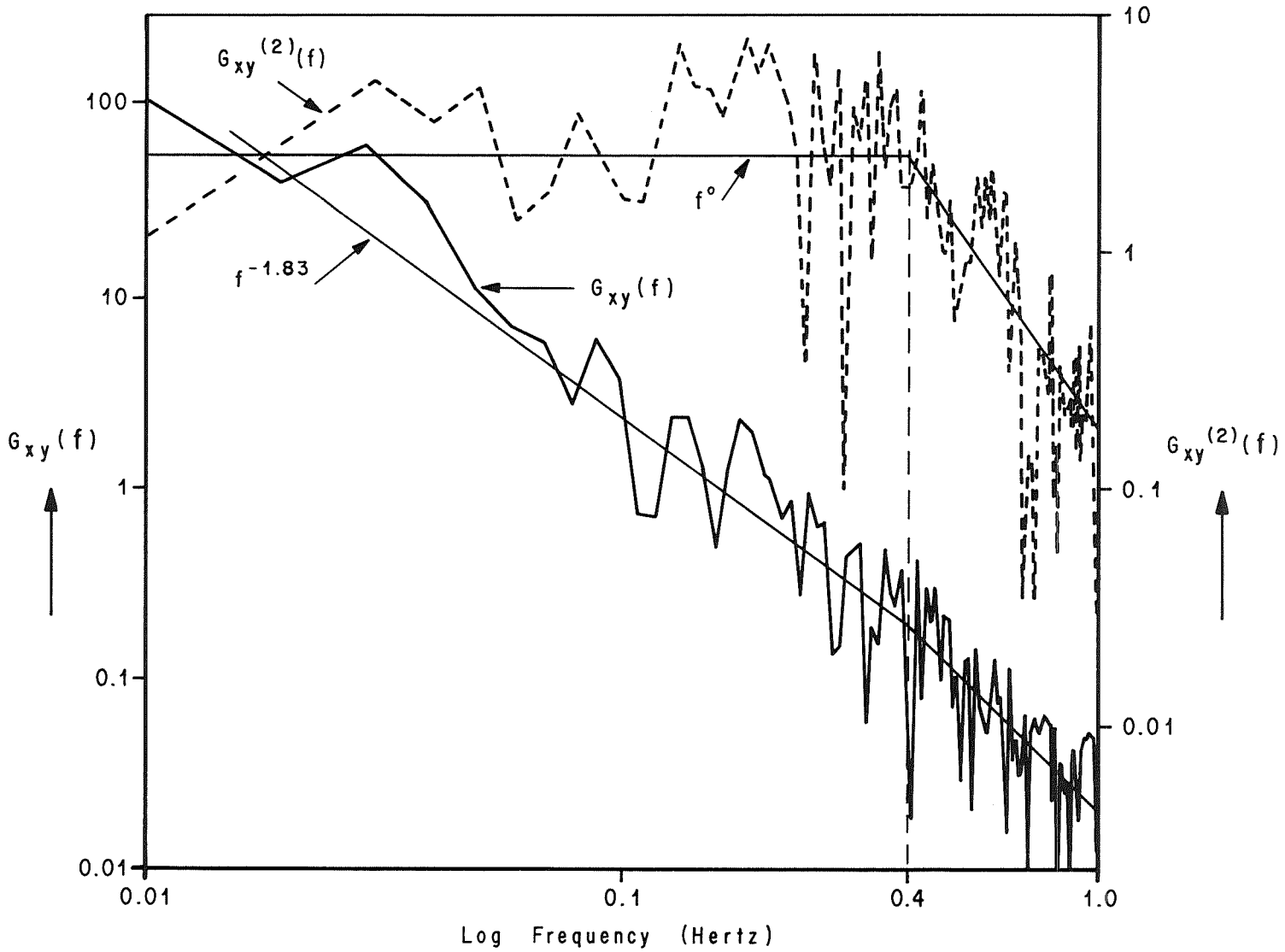

FIGURE IV.16. COMPARISON OF THE GAINS $G_{xy}(f)$ AND $G_{xy}^{(2)}(f)$ FOR f_c = 0.4 Hz AND f_T = 1.0 Hz (RUN I)

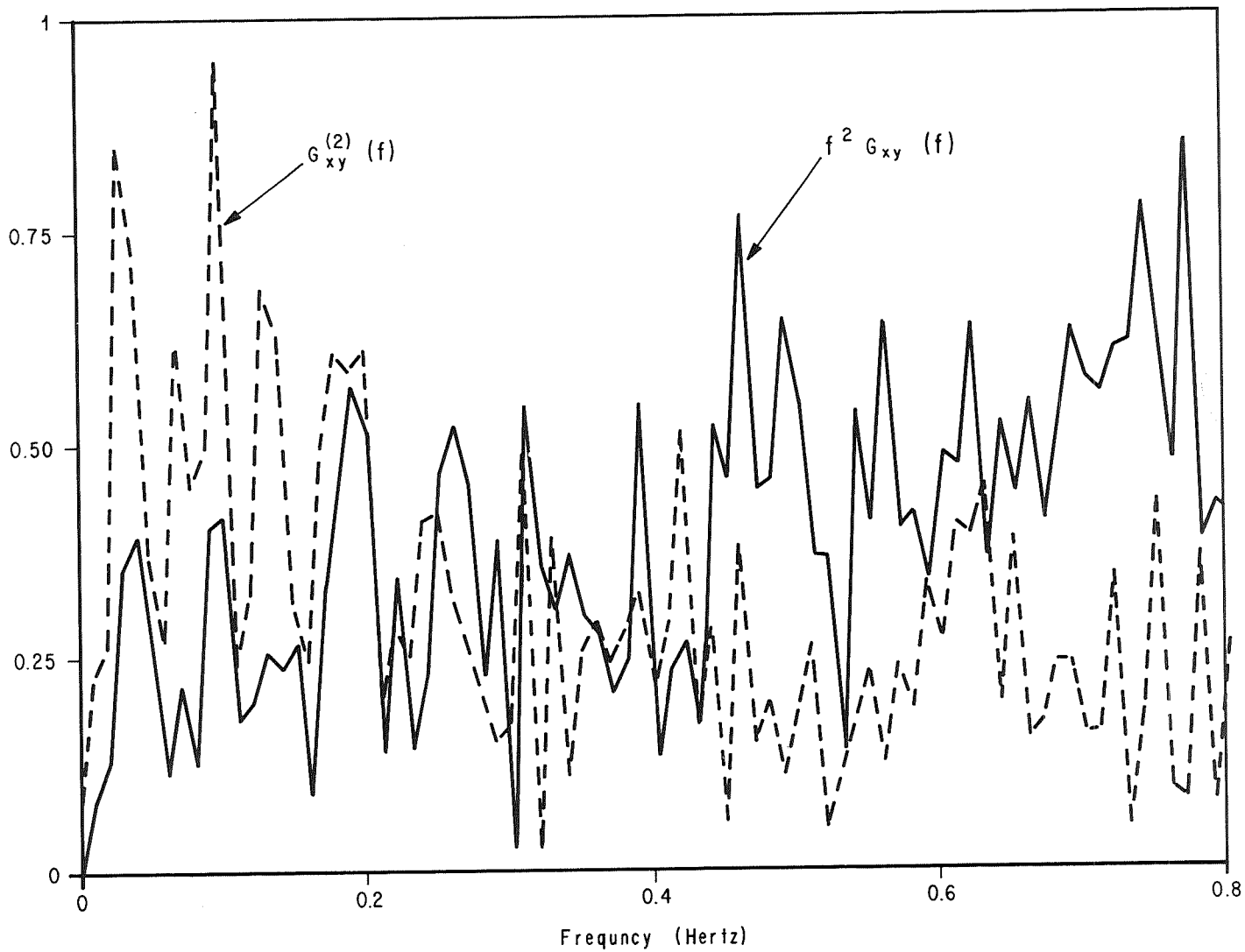

FIGURE IV.17. COMPARISON OF $G_{xy}^{(2)}(f)$ WITH $f^2 G_{xy}(f)$ FOR f_c = 0.6 Hz AND f_T = 1.0 Hz (RUN I)

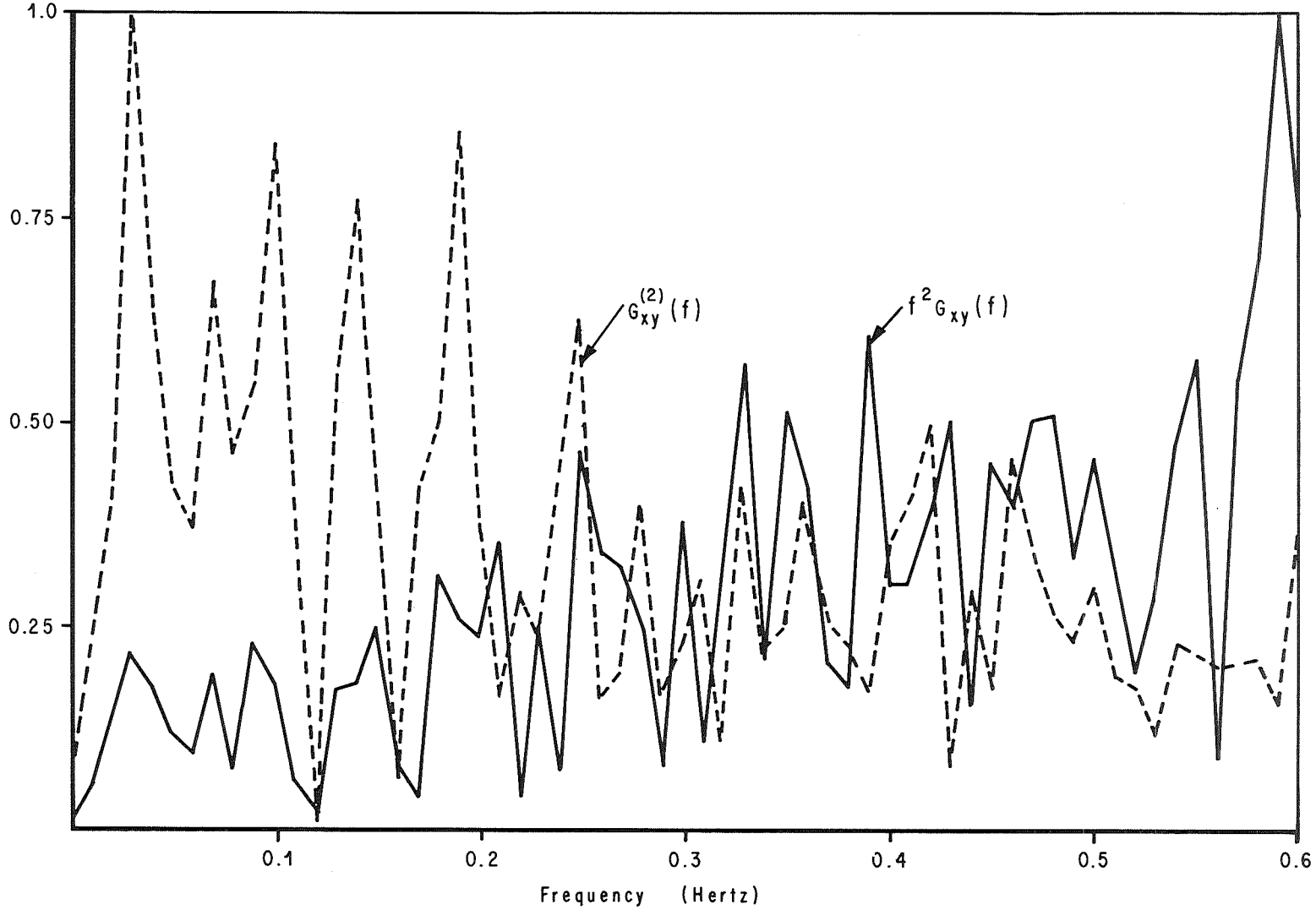

FIGURE IV.18. COMPARISON OF $G_{xy}^{(2)}(f)$ WITH $f^2 G_{xy}(f)$ FOR f_c = 0.6 Hz AND f_T = 1.0 Hz (RUN I)

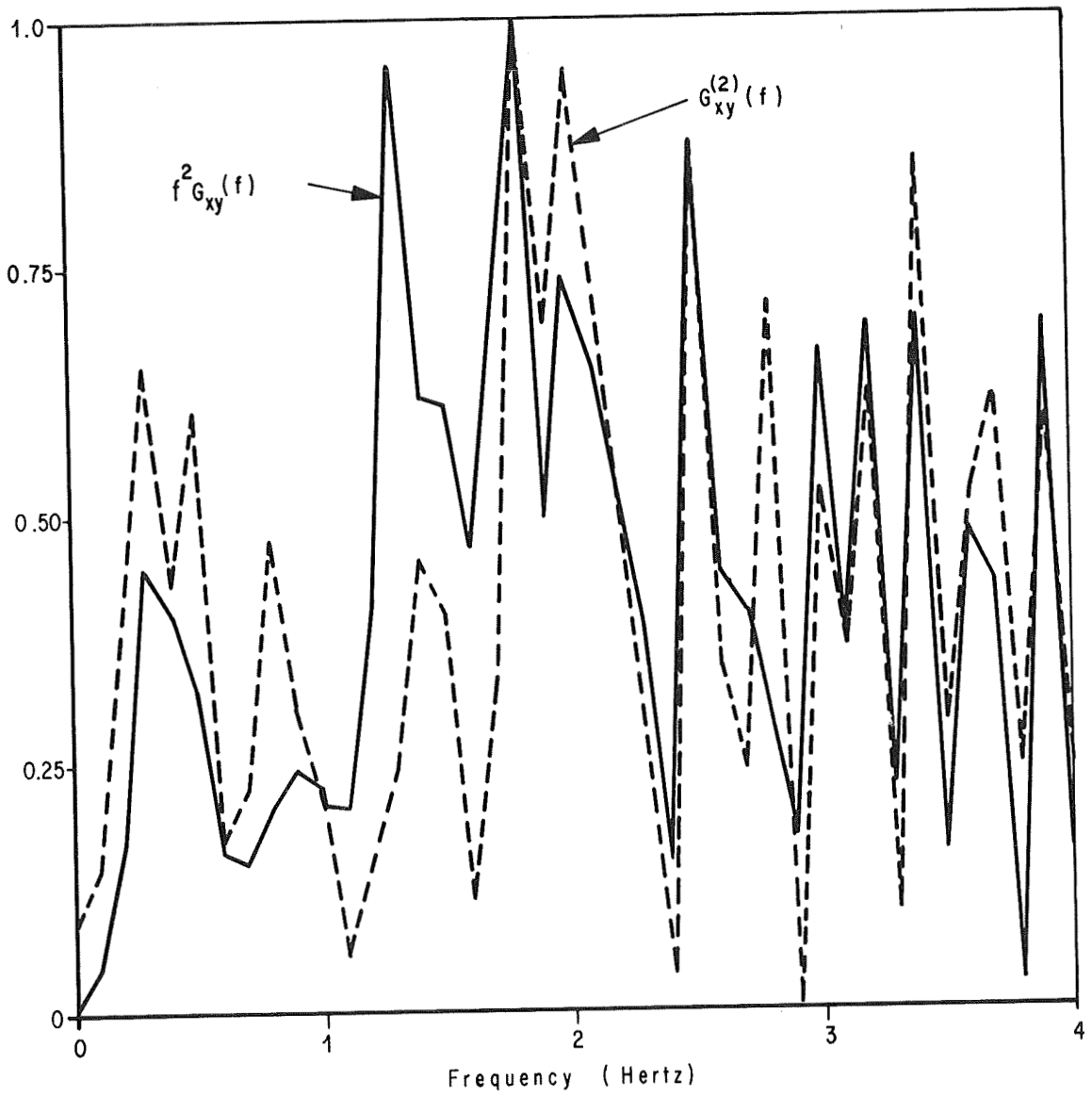

FIGURE IV.19. COMPARISON OF $G_{xy}^{(2)}(f)$ WITH $f^2 G_{xy}(f)$ FOR f_c= 0.4 Hz AND f_T = 1.0 Hz (RUN I)

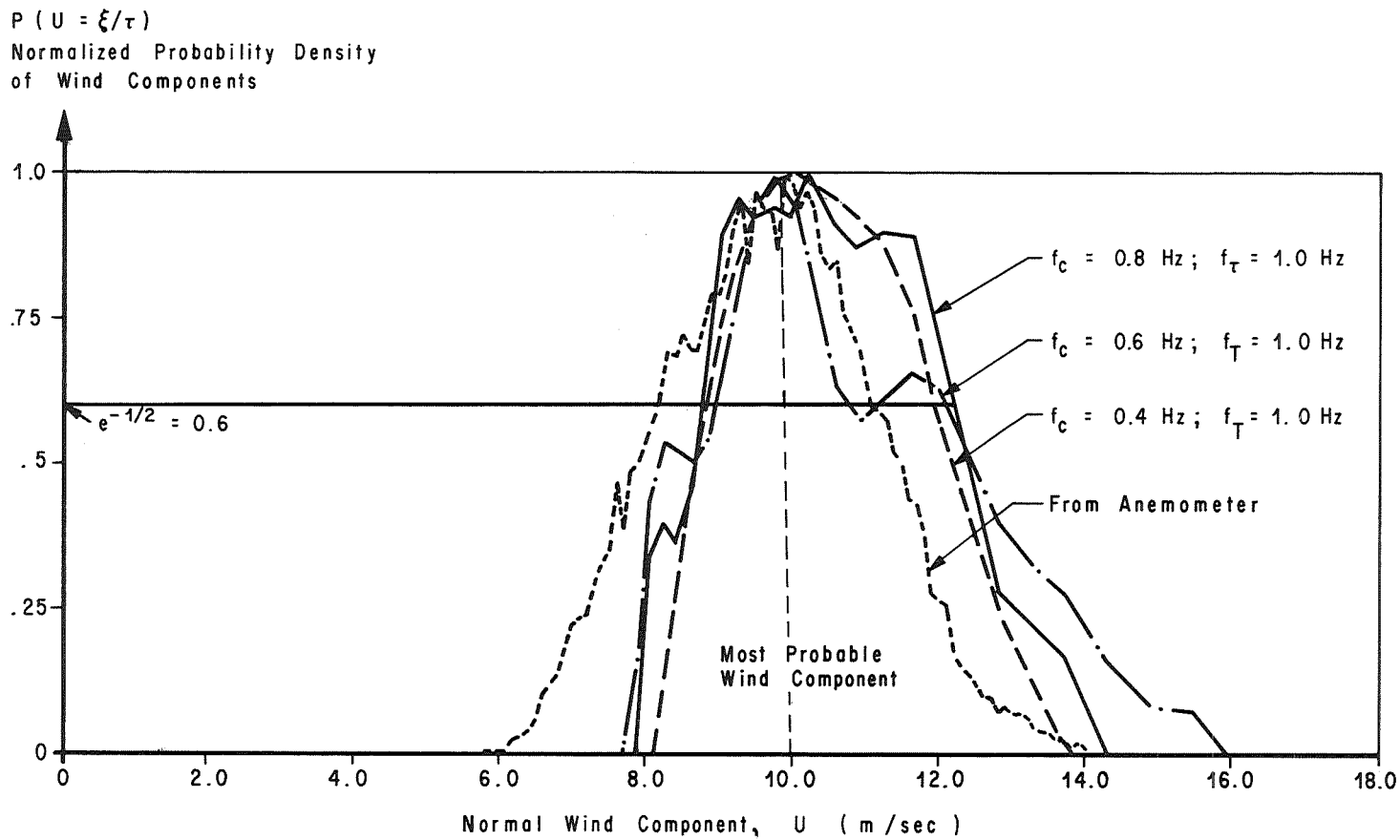

FIGURE IV.20. PROBABILITY DENSITY OF WIND COMPONENT VARIATIONS (RUN I)

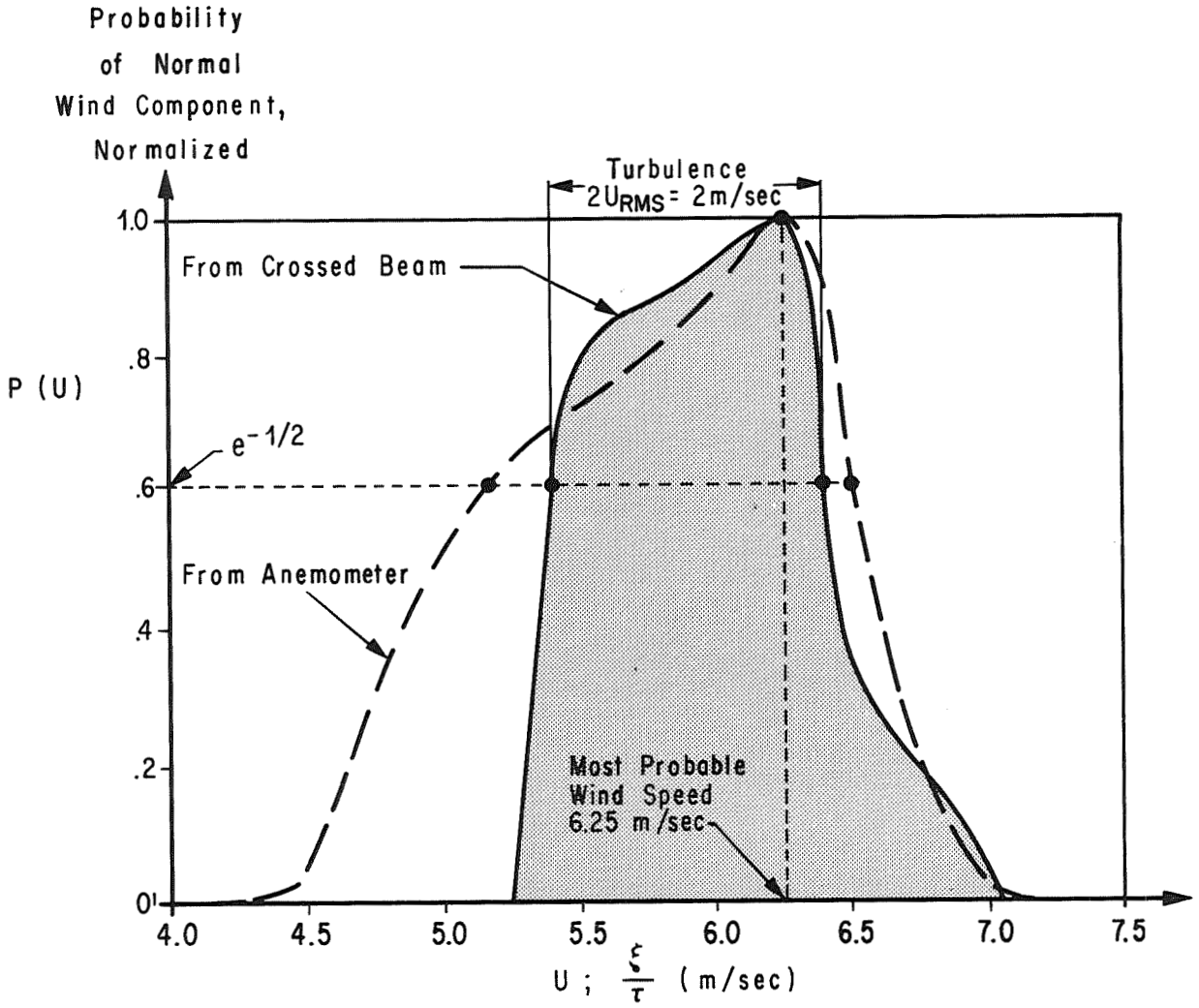

FIGURE IV.21. PROBABILITY DENSITY OF WIND COMPONENT VARIATION (RUN II)

REFERENCES

IV-1. Stephens, J. B., V. A. Sandborn, and A. J. Montgomery: Remote wind detection with the crossed-beam method at tower heights. NASA TM X-53782, October 1968.

IV-2. Sandborn, V. A. and D. J. Pickelner: Measurements of wind speeds with an optical cross-beam system. Ann. Inter. Aeroscience Electronics Symp., Washington, D. C., 1969.

IV-3. Krause, F. R., M. Y. Su, and E. H. Klugman: Passive optical detection of meteorological parameters in launch vehicle environments. To be published in Applied Optics in a special issue on Remote Sensing Techniques.

IV-4. Su, M. Y., J. B. Stephens, and M. Phillips: The theory for the determination of wind velocity and the associated altitude by the crossed-beam method. NASA TM X-53782, October 1968.

IV-5. Heybey, W. H.: The use of a ground-based multiple-beam detector in crossed-beam atmospheric experimentation. NASA TM X-53813, January 1969.

IV-6. Fisher, M. J. and F. R. Krause: The crossed-beam correlation technique. J. Fluid Mech., Vol. 28, 1967.

IV-7. Batchelor, G. K.: The Theory of Homogeneous Turbulence. The University Press, Cambridge, 1956.

IV-8. Lumley, J. L. and H. A. Panofsky: The Structure of Atmospheric Turbulence. Interscience, 1964.

IV-9. Sutton, O. G.: Micrometeorology. McGraw-Hill, 1953.

IV-10. Su, M. Y: Statistical error and required averaging time for evaluating cross-correlation of crossed-beam data. Northrop-Huntsville Tech. Memo M-794-8-362, May 1968. To be published as a NASA-CR.

IV-11. Su, M. Y.: Quantization errors and their reduction for digital time histories. To be published as a NASA Contractor Report.

IV-12. Taylor, J. T.: Digital filters for non-real time data processing. NASA CR-880, 1967.

IV-13. Graham, R. J.: Determination and analysis of numerical smoothing weights. NASA TR R-179, 1963.

IV-14. Krause, F. R., J. A. Jones and M. J. Fisher: Digital analysis of random processes by piecewise estimated covariance functions. To be published as a NASA-TR.

IV-15. Krause, F. R. and B. C. Hablutzel: Noise elimination by piecewise cross-correlation of photometer outputs. NASA TM X-53782, October 1968.

IV-16. Jayroe, R. R., Jr. and M. Y. Su: Optimum averaging times of meteorological data with time dependent means. NASA TM X-53782, October 1968.

CHAPTER V

ON THE TRANSFORMATION BETWEEN TRANSIT DISTANCES AND WIND COMPONENT DISTRIBUTIONS

by

Fritz R. Krause
NASA - Marshall Space Flight Center, Alabama

V-1. INTRODUCTION

The recent conceptual development of the crossed-beam concept indicates that the correlation of A.C.-coupled photometer outputs can be employed to approximate the probability distribution of either transit times or transit distances between spatially and temporally separated lines of sight. Applications of these measurements then require us to relate these transit times or distances to the velocity components associated with the transport of heat, mass, or momentum. The objective of this memorandum is to extend this transformation to the use of transit distances instead of transit times.

Present experiments have been restricted to the use of transit times. These transit times may be uniquely related to wind components, if the direction and length of the transit distance are known. In wind tunnel and jet applications, the transit distance is set by separating two mutually perpendicular beams along the known flow direction [V-1]. Subsequent transformation from transit times to longitudinal velocity variations has successfully matched pitot tube and hot-wire measurements. The early field tests of ground winds at tower heights [V-2] employed an outside wind direction reading with a wind vane to obtain the transit distance. The wind direction at the top of the tower was measured before the test run, and both beams were then rotated normal to this direction. The beam separation at the tower height is then a good estimate of the transit distance provided that the wind direction fluctuations during the run do not exceed ±20 degrees [V-3].

Analytical studies of multibeam geometries were initiated to determine whether suitable test geometries could be found which do not require independent wind direction readings for relating transit times to wind

components. W. H. Heybey [V-4] in his investigation of three ground telescopes showed that the two horizontal wind components could be determined at preselected altitudes, provided that vertical wind components are negligible. A recent extension of his work [V-5] also indicates that the third telescope may be replaced with one additional photodetector in the focal plane of the second telescope. This simple single-beam fan geometry will measure horizontal winds over a restricted range of wind azimuths ($\approx \pm 22°$). Vertical wind measurements are beyond the capability of both the single-beam fan arrangement and the three-telescope arrangement. They would require the use of at least four ground-based telescopes.

The purpose of this paper is to present physical arguments that wind components may be uniquely determined with a simple two-telescope arrangement if a plurality of photodetectors is used in the focal plane of one telescope to monitor transit distances instead of transit times. The use of a third or fourth telescope and the restrictions on wind azimuth are not necessary, if the measurement objectives are to measure one wind component rather than two or three.

V-2. THE MEASUREMENT OF TRANSIT DISTANCES

Consider the test geometry of Figure V.1. One distant radiometer, B, is set to look at almost horizontal lines of sight which are all contained in the same vertical plane. A second radiometer, A, is set normal to this plane such that its horizontal line of sight intersects the lowest beam of the distant telescope, B. The fan angles between the other lines of sight of radiometer B are assumed to be so small that deviations from the horizontal may be neglected in the vicinity of the intersection point. Each line of sight of radiometer B may thus be characterized by its altitude $z = h, h_2, h_3, \ldots$, above the intersection point. Transit distances are measured with the above arrangement by differentiating the output signals $i_A(t)$ and $i_B(t,h)$ of the two radiometers by delaying signal i_A relative to the signals i_B, and by adding the lagged product of these time derivatives. The result of this cross-correlation calculation is then multiplied with the selected time delay and normalized with the resultant peak value as shown in Figure V-2. Plotting this normalized multibeam product mean value against the abscissa h/τ should then directly approximate the probability $P(w = h/\tau)$ that the vertical speed w of optical disturbances has the value h/τ.

The above claim of approximating vertical wind speed variations is based on the same physical model of the common path that was used by Heybey. The common signals, which are retrieved by the correlation calculation, are identified with optical disturbances which intersect beam A at time $t - \tau$ and B at time t. These disturbances therefore

travel along a "common path" that intersects beam A and beam B at the altitude h above beam A. Let us assume that the vertical wind component, w, does not change along the common path. A disturbance can then be "common" to the altitudes z = 0 and z = h only if the vertical transit distance component $w\tau$ is equal to the given altitude h.

$$w = h/\tau. \tag{1}$$

The time history of horizontal wind component, v, will determine the displacement of the common path intersection of beam A relative to the beam intersection point at z = 0. This displacement distance is given by

$$\int_{t-\tau}^{t} v \, dt.$$

Let us now assume for a moment that the turbulence is homogeneous over such distances. The common signals which are generated at this intersection are then statistically equivalent to the disturbances for any path intersection point on beam A. In other words, the displacement of the path intersection along beam A does not change the product mean value calculations. The magnitude of variations of the horizontal wind components v are thus suppressed in the product mean value calculations. Any displacement of a common disturbance along the beam cannot be detected because of the optical integration along the beam. The above arguments may be repeated for the displacement

$$\int_{t-\tau}^{t} u \, d\tau,$$

of the common path intersection along beam A at altitude z = h. As a result, we thus find that any horizontal motion is cancelled by the optical integration along the beams in fields of homogeneous turbulence. These same arguments should hold, in first approximation, for inhomogeneous fields of turbulence, where the linear dependence of point-beam product mean values on translational disturbances

$$\int v \, dt \quad \text{or} \quad \int u \, dt$$

is cancelled by the subsequent integration over all such displacements.

The above arguments are completely general in that they do not depend on the special orientations of the beams B or beam A. The arrangement of horizontal beams that is illustrated in Figure V-1 was chosen to demonstrate that vertical wind components can be obtained with only two telescopes. The same arrangement would also closely simulate the desired airplane instrument-package [V-6]. However, the particular crosscorrelation calculations given in Figure V-2 will indicate transit distance components, h, across the fan regardless of orientation of the fan normal. For example, horizontal wind components would be measured if the beam configuration of Figure V-1 is rotated around their common baseline until the fan beam normal is in a horizontal position. In any case, the crosscorrelation should indicate the probability of normal wind components across the fan of beams B

$$P(w = h/\tau) = \text{const}\ \frac{\tau}{h} < \frac{\partial i_A(t-\tau)}{\partial t}\ \frac{\partial i_B(t,h)}{\partial t} > . \qquad (2)$$

The transformation of these transit distances to wind components is already included in equation (2). This transformation no longer requires an independent measurement, since the transit time is equal to the time delay τ = const., which was set by the computer.

V-3. ACCEPTABLE RANGE OF TIME DELAYS

The above discussions would be incomplete without considering the restriction on the acceptable range of time delays. A lower limit for the time delay, τ_{min}, is given by the condition that the associated transit distance, $\bar{w}\tau$, should exceed the class interval of its probability distribution. This class interval is given by the length scale of the common disturbance, and was reduced to the turbulent microscale, L_h, by correlating the signal derivatives $\partial i/\partial t$, instead of the signals [V-7].

$$L_h = \frac{\bar{w}}{2\pi} \sqrt{\frac{< i_A(t)\ i_B(t;\ h=0) >}{< \frac{\partial i_A(i)}{\partial t}\ \frac{\partial i_B(t,0)}{\partial t} >}} \quad . \qquad (3)$$

The lower limit of transit distances is thus provided by the condition:

$$\frac{L_h}{\bar{w}\tau_{min}} = \frac{1}{\tau_{min}} \sqrt{\frac{< i_A(t)\ i_B(t;\ h=0) >}{< \frac{\partial i_A(t)}{\partial t}\ \frac{\partial i_B(t,0)}{\partial t} >}} \ll 1. \qquad (4)$$

An upper limit of the time delay, τ_{max}, is given by the condition that the transit time should be much smaller than the eddy lifetime, L_τ. A first approximation of this eddy lifetime may be derived from the envelope to the various time correlation curves, as illustrated in Figure V-3.

$$\tau_{max} \leqq L_\tau.$$

Both inequalities together define the range of acceptable time delays:

$$\frac{1}{2\pi} \sqrt{\frac{< i_A(t)\ i_B(t;\ h=0) >}{< \frac{\partial i_A(t)}{\partial t}\ \frac{\partial i_B(t;0)}{\partial t} >}} \ll \tau \ll L_\tau. \qquad (6)$$

Within this acceptable range of transit times, one should expect that the crossed-beam approximation of statistical wind-component distributions, equation (2), is valid. One may thus verify this approximation by repeating the crosscorrelation calculations for various time delays, $\tau = \tau_1; \tau_2; \tau_3 \ldots$, within the acceptable range. The resulting points should all collapse on one curve. The same condition may also be used to obtain a sufficient number of points from comparatively few (≈ 5) beams B. This additional advantage is also illustrated in Figure V-2 for two selected time delays, $\tau = \tau_1$ and $\tau = \tau_2$. The same procedure might be used to develop an on-line wind component display system.

V-4. ACCEPTABLE RANGE OF FAN ANGLES

An arrangement of photodiodes in the focal plane of telescope B will give a fan of narrow conical fields of view. These fields of view replace our hypothetical parallel beams in an actual photodetection system. We

therefore have to consider a finite range of fan angles, B, and field of view, $\Delta\beta$. The previous idealization of parallel beams may be considered as the limiting case, where the fan angles all approach zero.

The effects of a finite fan angle, $\beta > 0$, are illustrated in Figure V.4. Consider the horizontal displacement,

$$\tau \sqrt{\bar{u}^2 + \bar{v}^2},$$

across a single photodiode's field of view. The normal displacement, h, of a common signal will be subject to a geometrical uncertainty,

$$\frac{1}{2} \tau \tan \beta \sqrt{\bar{u}^2 + \bar{v}^2},$$

due to the finite fan angle. This uncertainty should be smaller than the tolerance, L_h, of the normal displacement distance, h. This gives the following geometrical condition for the acceptable range of fan angles, β:

$$\frac{1}{2} \tau \tan \beta \sqrt{\bar{u}^2 + \bar{v}^2} \leq L_h. \tag{7}$$

The effects of a finite viewing angle, $\Delta\beta$, will be to generate a finite beam diameter, $h\Delta\beta/\sin\beta$, which should also be smaller than the tolerance on transit distance. This leads to a geometrical condition for the acceptable field of view.

$$\frac{h \Delta\beta}{\sin \beta} \leq L_h. \tag{8}$$

However, the ratio $n = h/L_h$ gives the number of beams in the fan. Equation (8) may thus be rewritten as

$$\Delta\beta = \frac{1}{n} \sin \beta. \tag{9}$$

Equation (7) becomes

$$\tan \beta \leqq \frac{2L_h}{h} \frac{h}{\tau \sqrt{\bar{u}^2 + \bar{v}^2}} = \frac{2}{n} \frac{\bar{w}}{\sqrt{\bar{u}^2 + \bar{v}^2}} \quad . \tag{10}$$

In case of vertical wind measurements, $\bar{w}/\sqrt{\bar{u}^2 + \bar{v}^2}$ has values of ≈ 0.1 and the largest acceptable fan angle of a five-beam fan would be

$$\tan \beta = \beta \leqq \frac{2}{5} \cdot 0.1 \approx 2°.$$

The associated viewing angle would be

$$\Delta\beta \leqq \frac{2}{5} = 0.4°.$$

Such a system can obviously be achieved by installing a variable-fiber optics block in the already existing detector fan.

V-5. CONCLUSIONS

A plurality of no more than five photodetection elements in the focal plane of a single telescope is proposed to monitor wind components in preselected directions by monitoring transit distances instead of transit times. Physical arguments are presented which lead to the following tentative conclusions.

(1) Any component of the atmospheric motion along one of the beams will not affect the result of crosscorrelation calculations, since a displacement of a common disturbance along a beam cannot be detected.

(2) The crosscorrelation calculations indicate only the components of the transit distances which are normal to both beams.

(3) The measured transit distances can be directly transformed into wind components, since the transit time is known from the time delay, which was set in the computer.

(4) Both horizontal and vertical wind components can be determined using no more than two telescopes.

(5) The above wind component measurements require us to approximate the probability density of wind component variations for various time delay parameters. The range of these parameters may be determined experimentally with crossed-beam systems.

(6) A plurality of photodetectors will always give a finite fan angle and a finite viewing angle; whereas, the analysis was based on the idealized case of a vanishing fan angle. However, because of the finite size of the turbulent microscale, small fan angles and viewing angles, which are within the capability of the already existing detector fan, are tolerable.

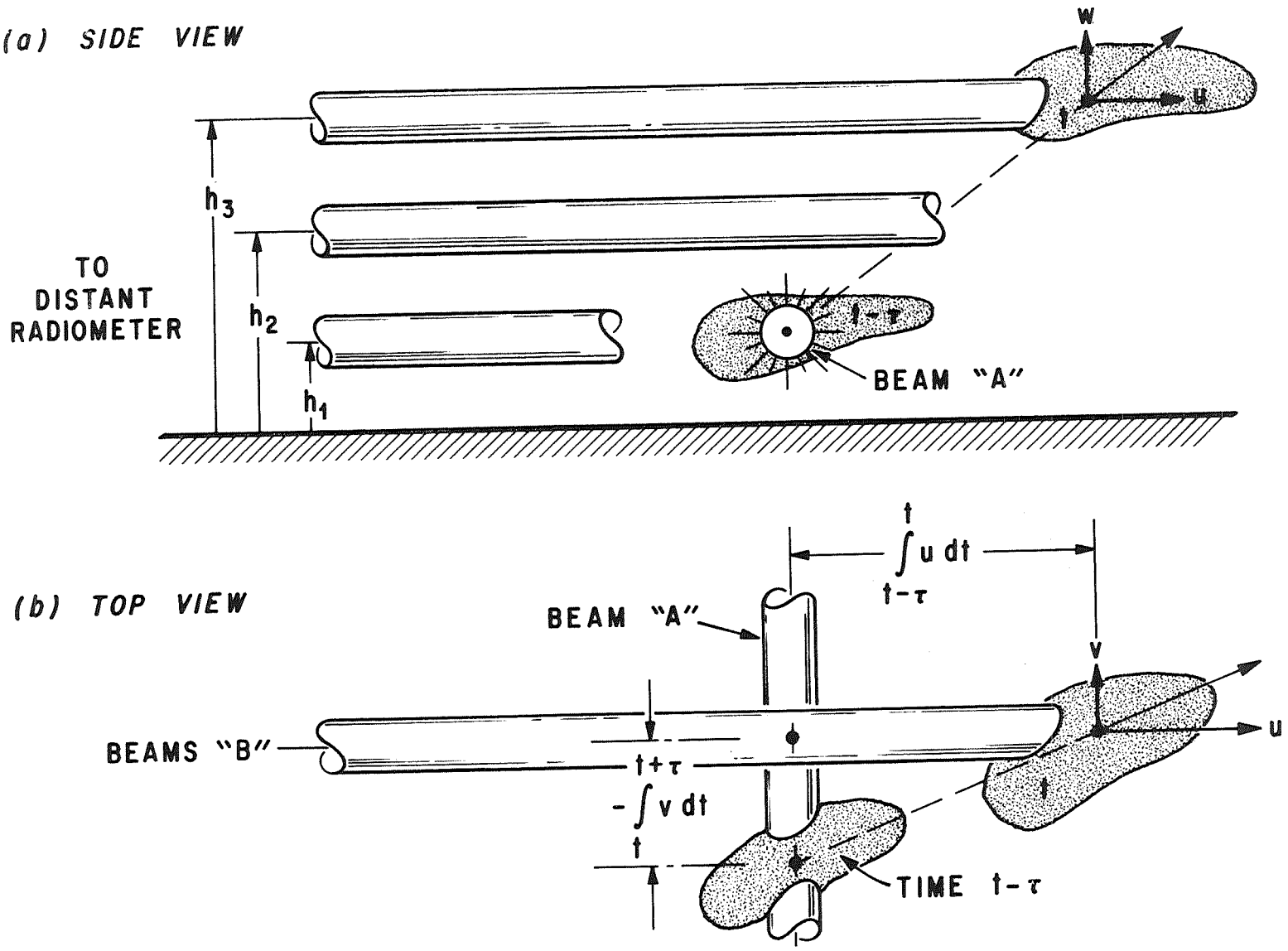

FIGURE V.1. CROSSED BEAM TEST ARRANGEMENT FOR TRANSIT DISTANCE MEASUREMENT

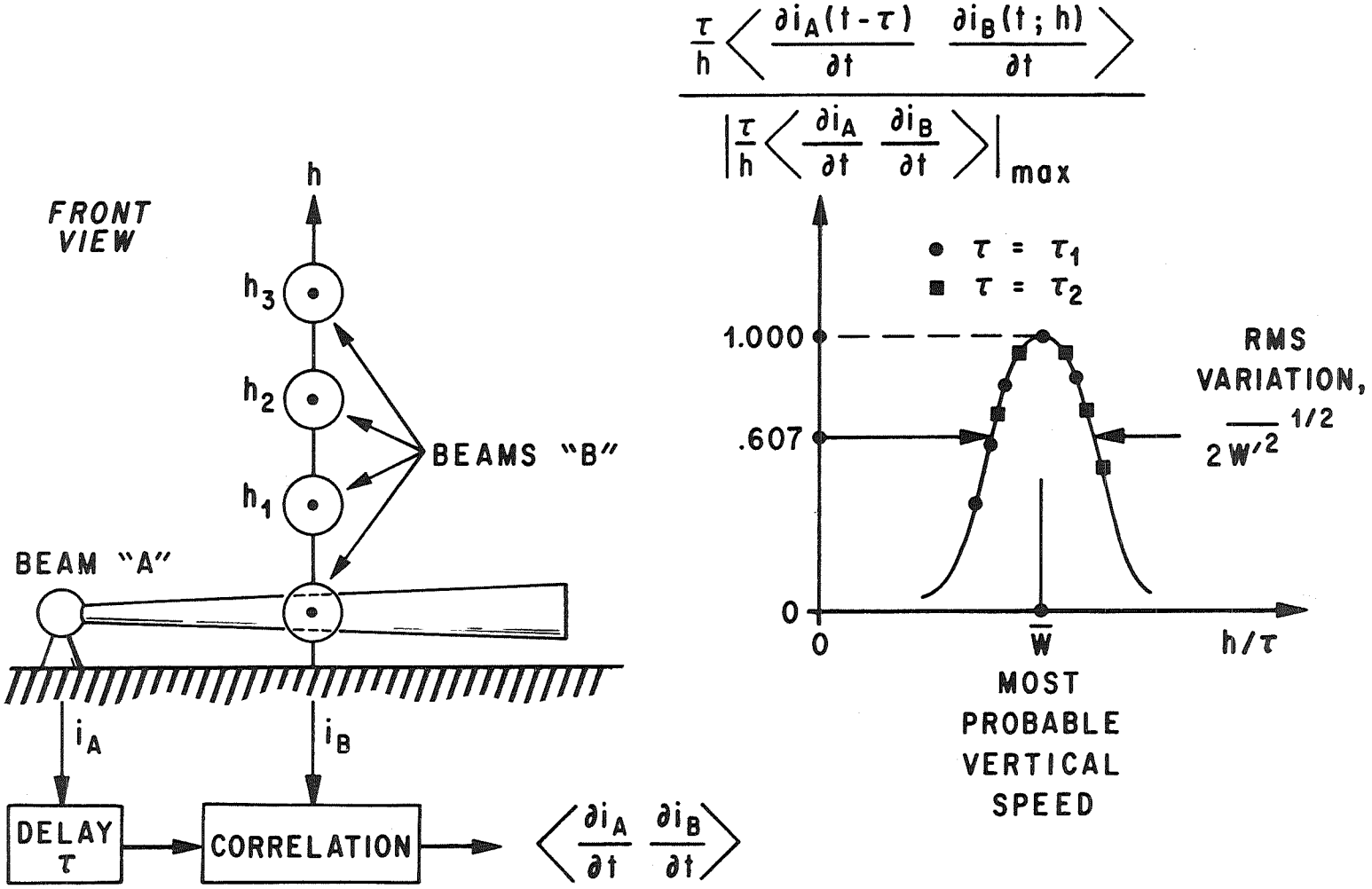

FIGURE V.2. PROBABILITY DENSITY OF WIND COMPONENT VARIATIONS

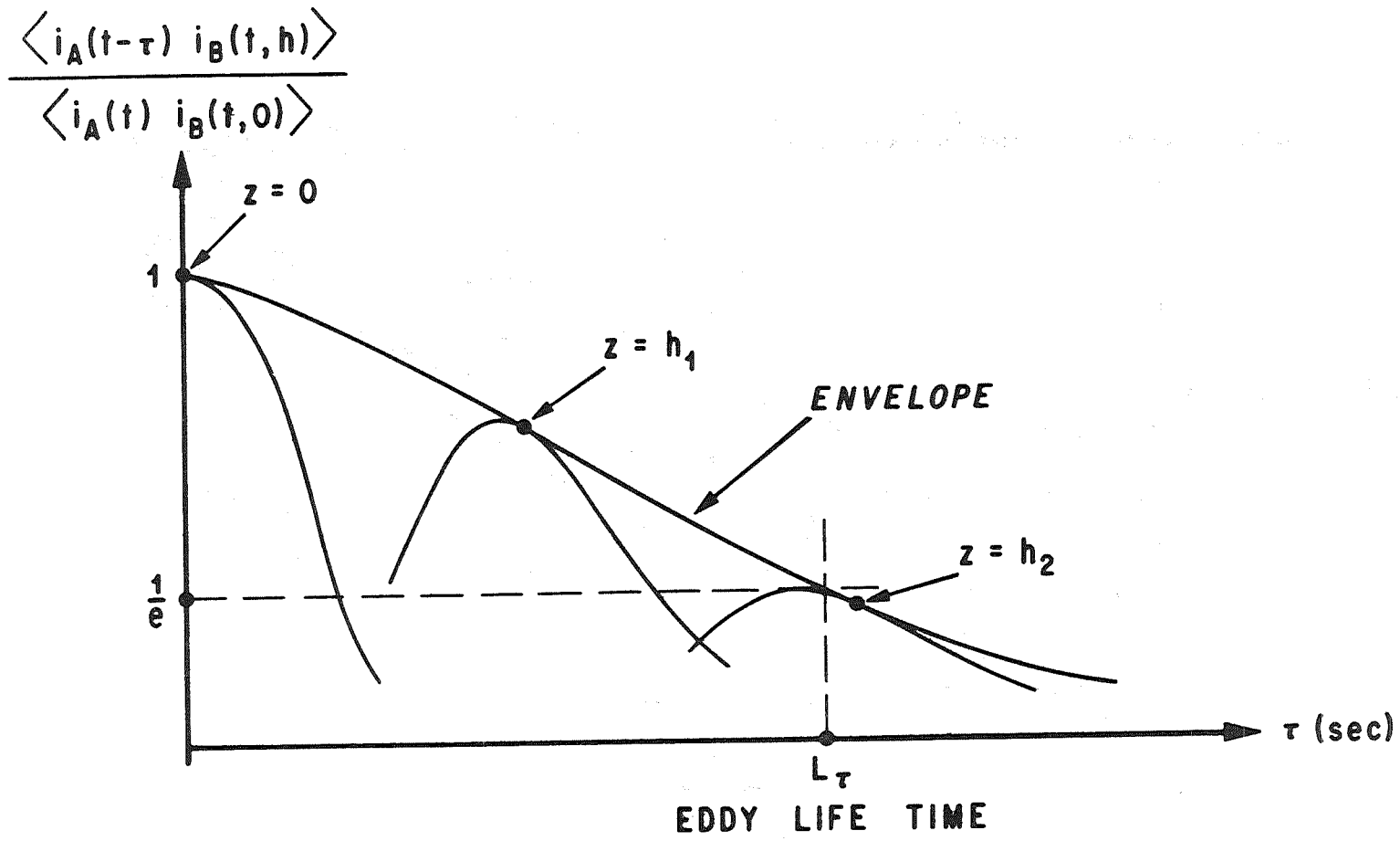

FIGURE V.3. APPROXIMATION OF EDDY LIFETIME

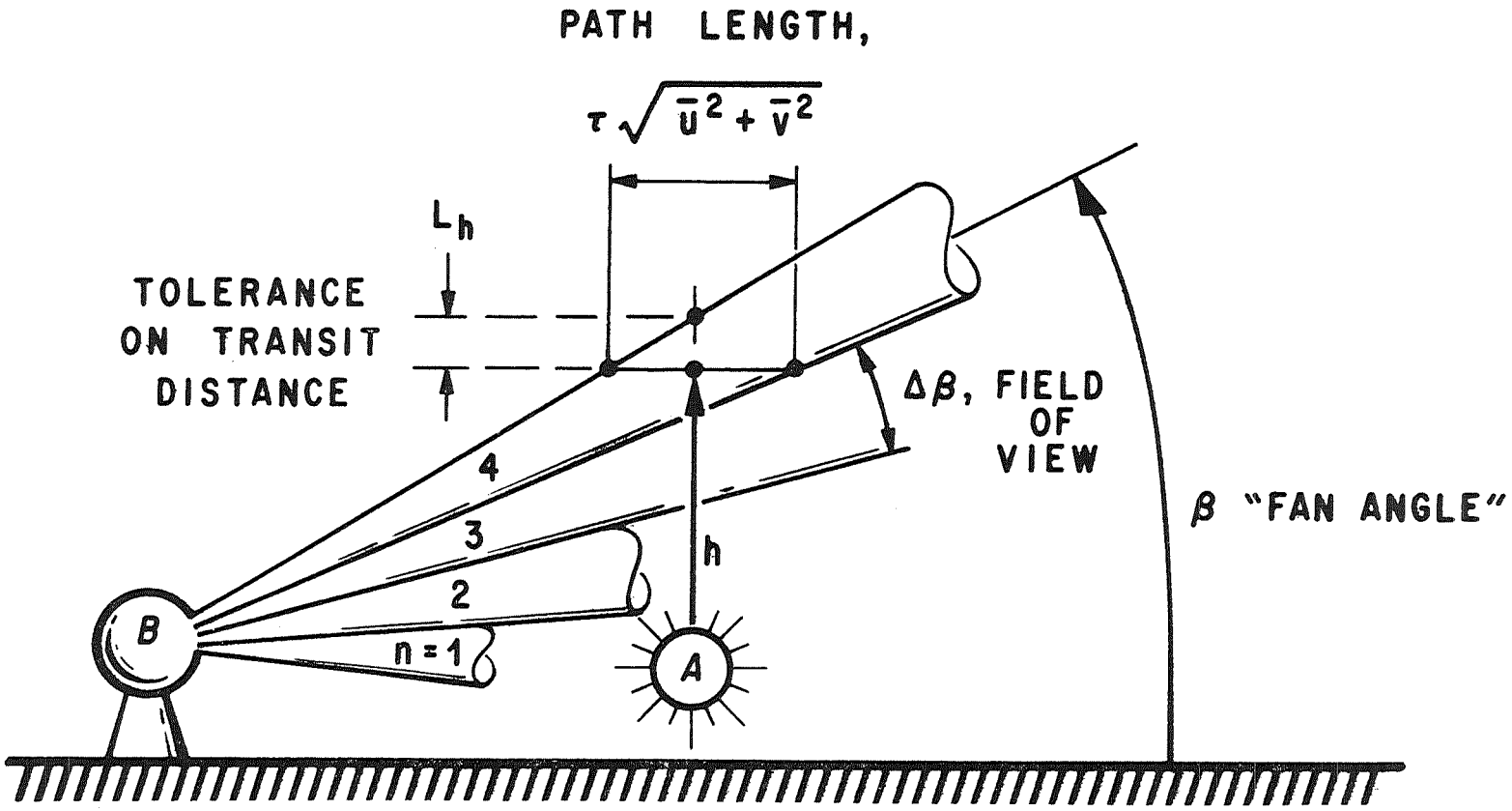

FIGURE V.4. ACCEPTABLE RANGE OF FAN ANGLES

REFERENCES

V-1. Krause, F. R. and L. N. Wilson, "Optical Crossed-Beam Investigations of Local Sound Generation in Jets," NASA SP-189, pp. 335-357, October 8-10, 1968.

V-2. Stephens, J. B., V. A. Sandborn, and A. J. Montgomery, "Remote Wind Detection with the Crossed-Beam Method at Tower Heights," NASA TM X-53782, pp. 88-103, October 15, 1968.

V-3. Su, M. J., J. B. Stephens, and M. Phillips, "The Theory for the Determination of Wind Velocity and the Associated Altitude by the Cross-Beam Method," NASA TM X-53782, pp. 29-88, October 15, 1968.

V-4. Heybey, W. H., "Wind Vector Calculations using Crossed-Beam Detector in Crossed-Beam Data and Detector Arrangement for Measuring Horizontal Winds," NASA TM X-53754, July 11, 1968.

V-5. Heybey, W. H., "The Use of a Ground-Based Multiple Beam Detector in Crossed-Beam Atmospheric Experimentation," NASA TM X-53813, Jan. 30, 1969.

V-6. Krause, F. R., S. S. Hu, and A. J. Montgomery, "On Cross-Beam Monitoring of Atmospheric Winds and Turbulence with Two Orbiting Telescopes," NASA TM X-53538, November 1966.

V-7. Sutton, O. G., Micrometeorology, McGraw Hill, Inc., ed., New York, N. Y., 1953, pp. 95-99.

CHAPTER VI

CROSS-POWER SPECTRAL ANALYSIS FOR ATMOSPHERIC CROSS-BEAM DATA

by

J. Briscoe Stephens and John M. Locklin
NASA - Marshall Space Flight Center, Alabama

and

John C. Pooley
Northrop - Huntsville, Alabama

VI-1. INTRODUCTION

This is the first attempt to physically interpret cross-beam atmospheric results using spectral analysis. The cross-beam program has used just the time domain for the retrieval of wind velocity information [VI-1, -2]. While the spectral formulation applied to this analysis is not new [VI-3], the method of combining is new.

The concept of a piecewise spectrum is introduced, along with the statistical error of the spectrum. This paper analyzes the above concepts and applies them to actual cross-beam data.

Chapter VII will give the details of how these techniques can be applied to retroactive filtering.

VI-2. NOMENCLATURE

INDEPENDENT VARIABLES

Symbol	Definition
t	total observation time
T	total integration time

Symbol	Definition
ΔT	length of time for each piece -- the whole data record is subdivided into pieces for data processing
i	piece number
m	total number of pieces of data integrated over ($m = T/\Delta T$)
f	frequency
τ	time lag between the two signals
τ_m	maximum time lag

DEPENDENT VARIABLES

$x(t)$	signal time history for the sensor
$y(t-\tau)$	delayed time history for the second sensor
$r_i(\tau)$	covariance of the ith piece of data at time lag τ
$\overline{r_i(\tau)}$	accumulative covariance average over the first ith piece of data
$\overline{\overline{r(\tau)}}$	accumulative covariance average over the entire integration time
$\Delta r(\tau)$	statistical error of the covariance
$C(f)$	co-spectra (real part)
$Q(f)$	quad-spectra (imaginary part)
$G(f)$	gain, $G^2 = C^2 + Q^2$
$\langle G(f) \rangle$	mean gain over m pieces of data
$\overline{\overline{G(f)}}$	accumulative gain over m pieces of data
$\langle \Delta G(f) \rangle$	mean statistical error of the gain
$\overline{\overline{\Delta G(f)}}$	accumulative statistical error of the gain

Symbol	Definition
$r_{G,\phi}$	the Fourier transpose of the spectra to the correlation curve will have the subscripts of those spectra components used
$r_{yx}(\tau) = r_{xy}(-\tau)$	this is the cross-covariance (subscript xy indicates positive time lags and yx indicates negative time lags

OPERATORS

$( )$	statistic
$\overline{( )}_i = \frac{1}{\Delta T} \int_{(i-1)\Delta T}^{\Delta} ( )\, dt$	piecewise mean (note: when average done over real time or time lag, the symbol $< >$ is used
$<( )_k> = \frac{1}{k} \sum_{i=1}^{k} ( )_i$	accumulative mean where k is the kth piece of data (when average over pieces)
$\overline{\overline{( )}} = <\overline{( )}_{k=m}>$	total accumulative mean
$<( )_k>^2 = \frac{1}{k-1} \sum_{i=1} (( )_i - \overline{( )}_k)^2$	statistical error
$<( )> = F\ \{<( )>\}$	the symbols used in the time domain will be transferred into the frequency domain showing the origin of the terms

VI-3. FORMULATIONS

A. Spectra

Two types of spectrum routines are used in this analysis: the accumulative spectra and the mean spectra. The accumulative is obtained from a Fourier transformation of the final accumulative correlation curve,

whereas the mean spectra is obtained by averaging the Fourier transformation of each piece correlation curve. The spectrum obtained by these formulations is not the common method of spectral analysis. Analog and most digital methods of spectral analysis use a fast Fourier transform technique. This means that the spectrum is obtained from the raw data (before correlation of the data). Since we are Fourier-transforming the crosscorrelation curves, we have the spectrum from only the common modulations of the two signals. Therefore, for large noise, the advantage is that most of the noise is cancelled out before the spectrum is taken.

The formulation used to obtain the accumulative cospectra $\overline{\overline{C(f)}}$ is

$$\overline{\overline{C(f)}} = \int_0^{\tau_m} [\overline{\overline{r_{xy}(\tau)}} + \overline{\overline{r_{yx}(\tau)}}] \cos 2\pi f\tau \, d\tau, \tag{1}$$

where τ is the delay, $\overline{\overline{r(\tau)}}$ is the accumulative covariance, and f is the frequency. The accumulative quad-spectrum $\overline{\overline{Q(f)}}$ is

$$\overline{\overline{Q(f)}} = \int_0^{\tau_m} [\overline{\overline{r_{xy}(\tau)}} - \overline{\overline{r_{yx}(\tau)}}] \sin 2\pi f\tau \, d\tau. \tag{2}$$

It then follows that the modulus of the accumulative gain $\overline{\overline{G(f)}}$ is

$$\overline{\overline{G(f)}} = \sqrt{\overline{\overline{C(f)}}^2 + \overline{\overline{Q(f)}}^2} \tag{3}$$

and the accumulative phase $\overline{\overline{\phi(f)}}$ is

$$\overline{\overline{\phi(f)}} = \arctan \frac{\overline{\overline{Q(f)}}}{\overline{\overline{C(f)}}} . \tag{4}$$

These values given by the last four equations are calculated in the computer program given in the appendix.

The values for the piecewise gain $\bar{G}_i$, co-spectra $\bar{C}_i$, and quad-spectra $\bar{Q}_i$ are calculated in exactly the same manner as their accumulative counterparts except that the covariance curve used is now the piecewise covariance curve. With these terms, the mean gain can be defined as

$$\overline{\overline{\langle G_i(f) \rangle}} = \frac{1}{m} \sum \overline{\overline{G_i(f)}}. \tag{5}$$

The mean gain is a unique term not normally found in the literature. There are reasons to believe that the mean gain is free from small oscillations in time delay.

After the error criteria are considered, these two gains will be tested on actual data.

B. Statistical Spectra Error

One of the key problems in spectral analysis is the lack of a good error routine. If one deals with either the co-spectra or the quad-spectra, then the standard error routines give unique results. However, this is not true for either the gain or the phase, since these errors depend on (a) which average (accumulative or mean) is used, and (b) the differences in error propagation with changes in integration time and summation.

The statistical error of the accumulative gain $\overline{\overline{\Delta G(f)}}$ is defined as

$$\overline{\overline{\Delta G(f)}} = \sqrt{\frac{1}{m-1} \sum_{i=1}^{m} [\overline{G_i(f)} - \overline{\overline{G(f)}}]^2}, \tag{6}$$

and it follows then that the statistical error of the mean gain $\langle \overline{\Delta G(f)} \rangle$ is defined as

$$\langle \overline{\Delta G(f)} \rangle = \sqrt{\frac{1}{m-1} \sum_{i=1}^{m} [\overline{G_i(f)} - \langle \overline{G(f)} \rangle]^2}. \tag{7}$$

These error calculations were performed using the computer program given in the appendix.

C. Inverse Transform of Spectra

The next question is, what happens when the spectrum is transposed back into the time domain? This, in effect, does provide a check on the work done in the frequency domain.

Two types of inverse transforms exist: a transpose of the co-spectra and quad-spectra, and a transpose of the gain and the phase. The component transpose is given by

$$r_{\underset{CQ}{==}}(\tau) = \int_{f_{min}}^{f_{max}} [\overline{\overline{C(f)}} \cos (2\pi f\tau) - \overline{\overline{Q(f)}} \sin (2\pi f\tau)] \, dt, \qquad (8)$$

and the gain transpose is given by

$$r_{\underset{<\bar{G}>\emptyset}{\bar{=}}}(\tau) = \int_{f_{min}}^{f_{max}} \overline{<G(f)>} \cos [2\pi f\tau + \overline{\overline{\emptyset(f)}}] \, df. \qquad (9)$$

The subscripts indicate the source of the terms used in the transpose. The computer program for the above calculations is given in the appendix.

VI-4. RESULTS

The formulations discussed in the preceding section will be tested on actual atmospheric data from a separated cross-beam run with high statistical accuracy to perhaps gain a reasonable empirical understanding of the spectra.

The first formulation calculated was the accumulative gain (equation (3)) and its associated error (equation (6)). The results are shown in the top graph of Figure VI.1. These results show that the accumulative gain is not statistically significant over the range of frequencies from 0.01 cps to 1.0 cps. We have required only about a 65 percent level of probability in the test of significance. Since this run contains a peak in the correlation curve with a statistical probability of better than 99 percent, the spectra from other curves are going to be even less significant. To check for errors, the spectrum was transposed back to the time domain by equation (8). These results are shown in Figure VI.2. One observes that the transpose of this spectrum gives the initial correlation curve; therefore, the accumulative spectrum must have the same information in it that was contained in the original curve.

Before drawing any conclusions we tried another spectral routine. Rather than using the accumulative spectrum, we used the mean spectra (equation (5)) with its associated error (equation (7)). The results are shown in the lower portion of Figure VI.1. That the mean gain is statistically significant suggests that perhaps we are on the right track. To verify these results, the mean gain and the mean phase were transposed back to the time domain by equation (9). These results, shown in Figure VI.3, appear to be bad, but the mean gain is approximately the same as the accumulative gain, according to Figure VI.1. Thus, this result seemed to be only an effect of the variations in phase. This theory was tested by transposing both the mean gain and accumulative phase, and the accumulative gain and mean phase (see Figures VI.4 and VI.5). The correlation curve obtained from the mean gain and the accumulative phase (Figure VI.4) gives the best correlation curve thus far obtained, and the accumulative gain and the mean phase (Figure VI.5) give about the same results as were obtained for the mean gain and the mean phase (Figure VI.3).

VI-5. CONCLUSIONS

Thus far, the spectral results obtained have been analyzed only for the most statistically significant atmospheric data we have. Based on the empirical results just given, the following tentative conclusions are reached.

The computation of covariance functions from an inverse Fourier transform of piecewise-estimated phase and gain spectra may deviate from the direct product integration, if the phase spectrum is taken from an accumulation of piecewise averages. A reasonable explanation for this observation is that the mean gain cancels the effects of nonstationarities in transit times that are normally reflected in changes in the phase. Thus, evaluating the piecewise correlation curve in the frequency domain, where shifts in the peak can be neglected, and then transposing the final mean result back into time domain may prove to be a better technique for dealing with nonstationarities than just normalizing each piecewise correlation curve.

Another tentative conclusion is that error criteria can be established only after plotting the error curves for both accumulative and mean gain and phase, and comparing the absolute error with the relative error. The present error curves should allow the separation of environmental variations of gain and phase.

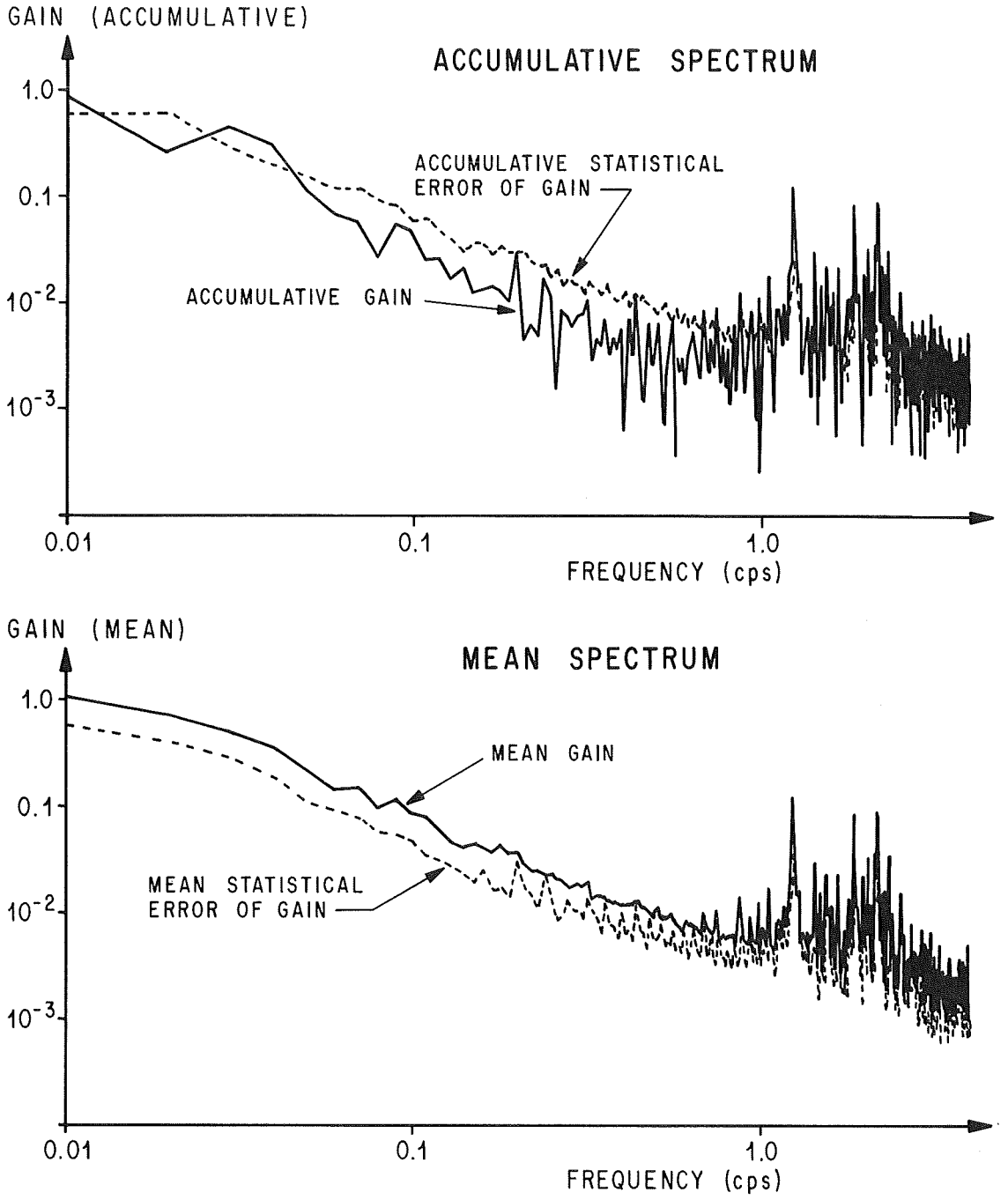

FIGURE VI.1. EXCHANGED ORDER OF ACCUMULATION AND SPECTRUM CALCULATIONS

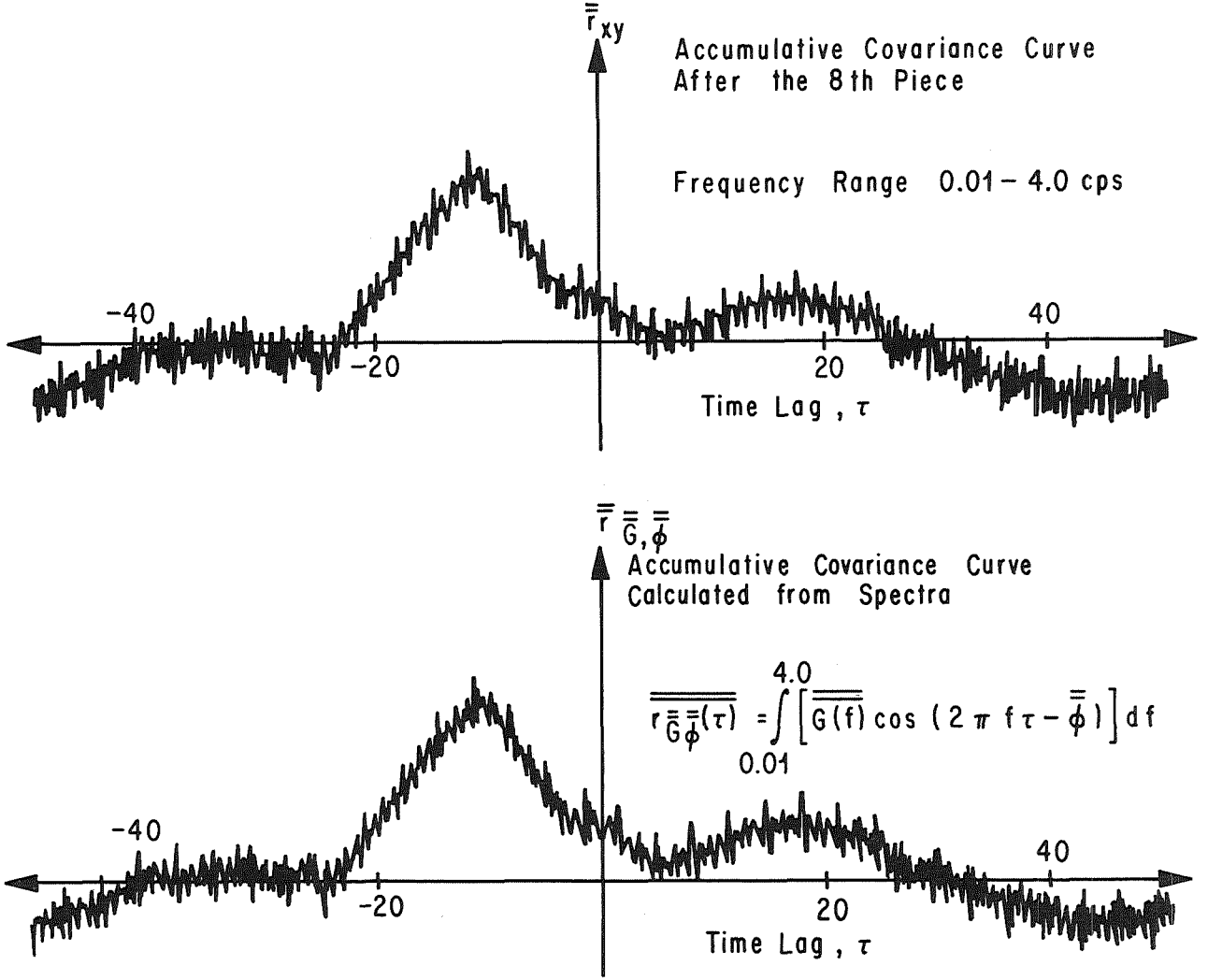

FIGURE VI.2. DIRECT AND DOUBLE-TRANSFORMED ACCUMULATIVE CORRELATION CURVES

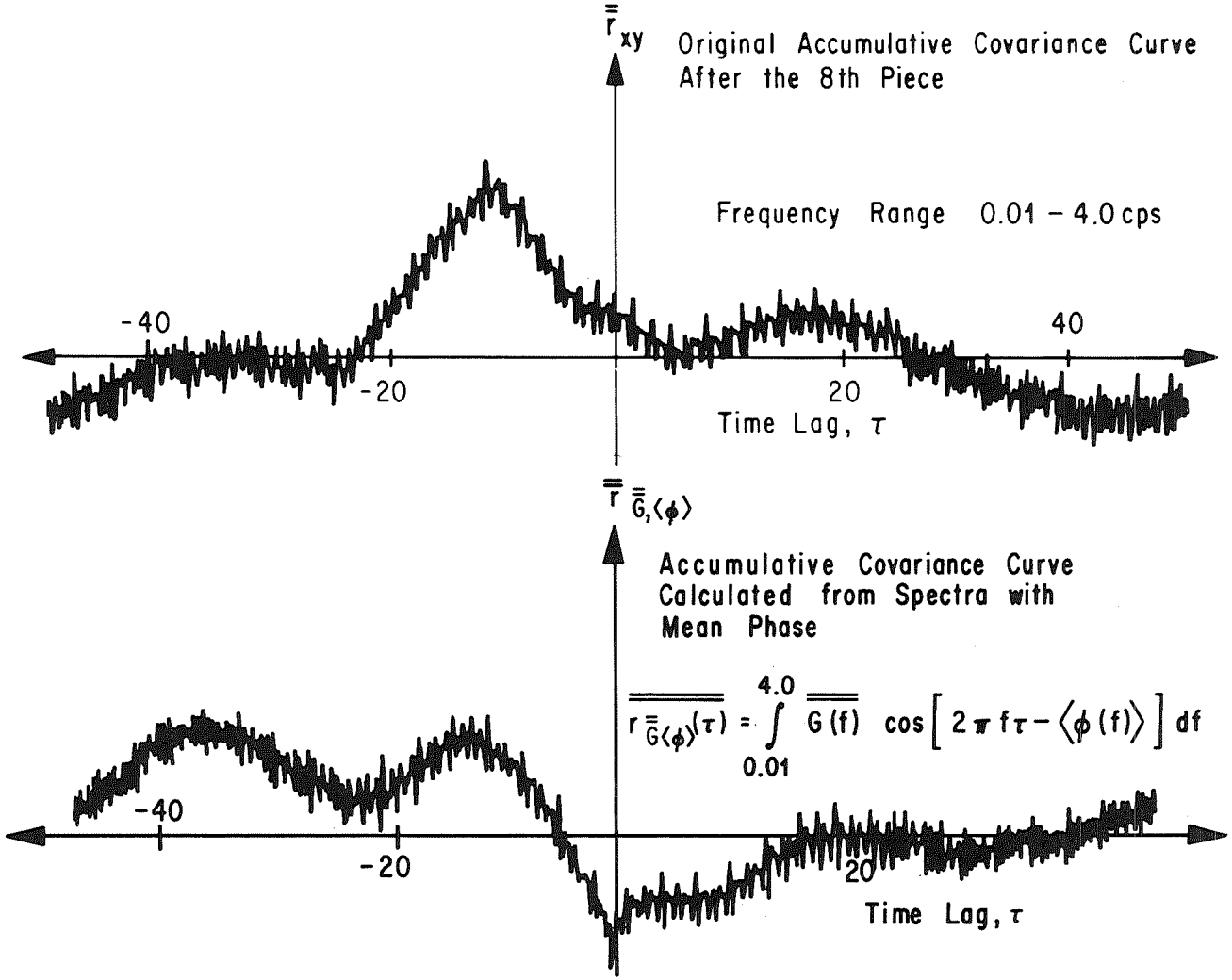

FIGURE VI.3. DIRECT AND DOUBLE-TRANSFORMED ACCUMULATIVE CORRELATION CURVES

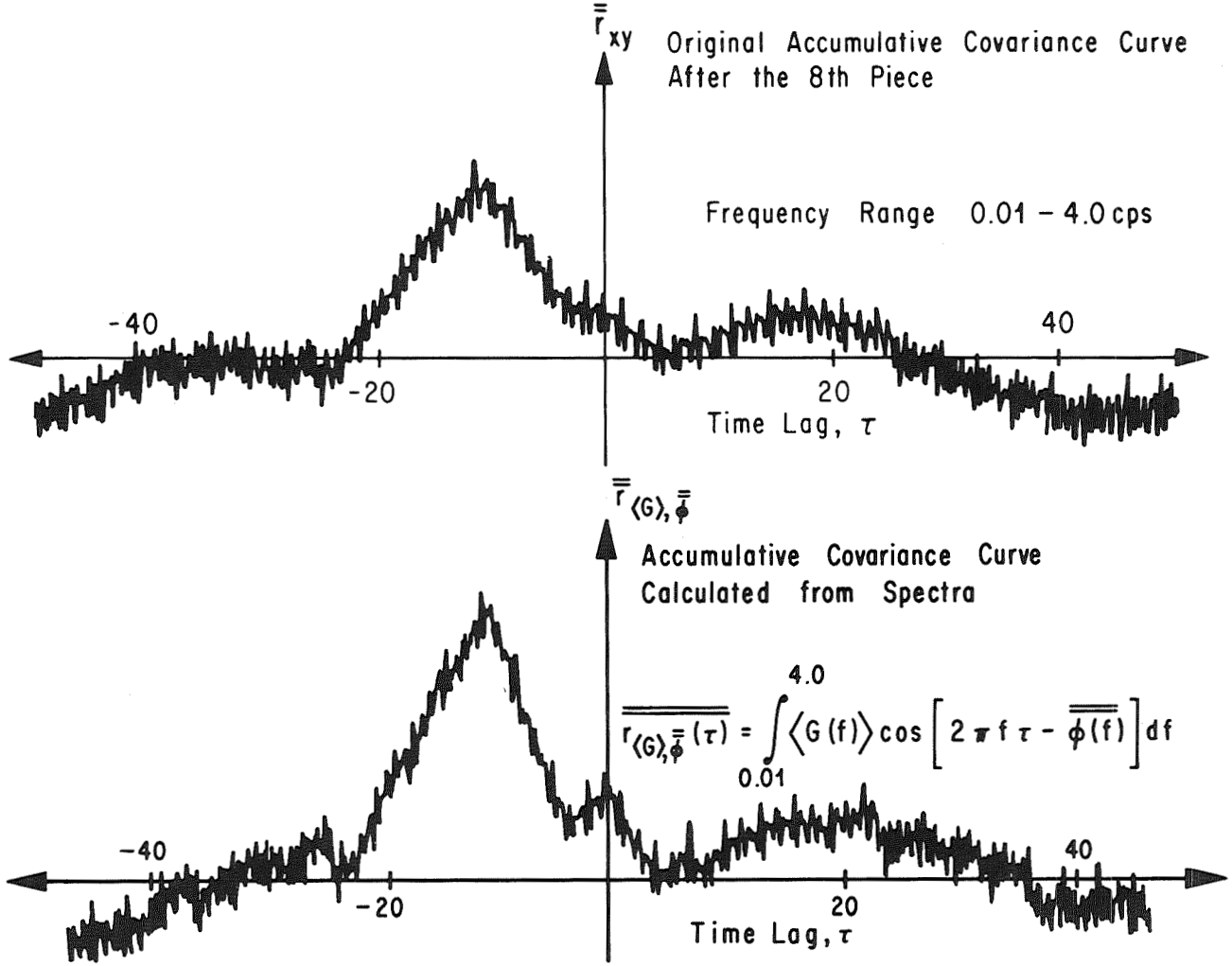

FIGURE VI.4. DIRECT AND DOUBLE-TRANSFORMED ACCUMULATIVE CORRELATION CURVES

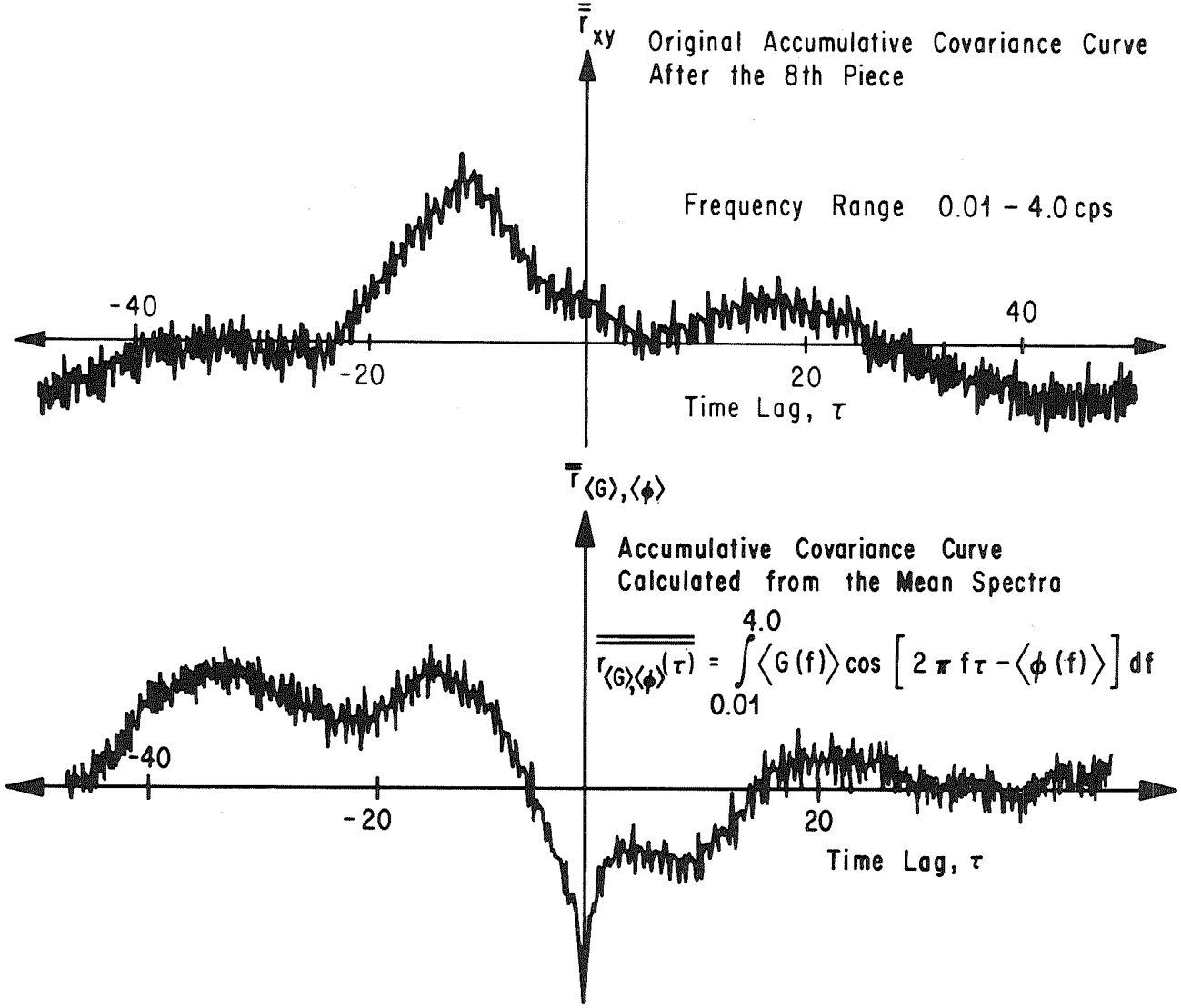

FIGURE VI.5. DIRECT AND DOUBLE-TRANSFORMED ACCUMULATIVE CORRELATION CURVES

REFERENCES

VI-1. Sandborn, V. A. and D. J. Pickelner, "Measurement of Wind Speeds with an Optical Cross Beam System," I.E.E.E. Transactions on Geoscience Electronics, Vol. GE7, Oct. 1969, pp. 244-249.

VI-2. Krause, F. R., V. E. Derr, N. L. Abshire and R. G. Struck, "Remote Probing of Wind and Turbulence through Cross Correlation of Passive Signals," 6th International Symp. on Remote Sensing of Environment, Univ. of Michigan, Oct. 16, 1969.

VI-3. Bendat, J. S. and A. G. Piersol, "Measurement and Analysis of Random Data," John Wiley and Sons, New York, N. Y., 1966.

CHAPTER VII

CORRELATION CURVES OF RETROACTIVELY FILTERED DATA

by

J. Briscoe Stephens and John M. Locklin
NASA - Marshall Space Flight Center, Alabama

SUMMARY

A concept for retroactively filtering a correlation curve is discussed and the results given. Normally, the data are filtered before being correlated with the net result that, if the limits you have set for your high and low pass filters are not suitable, the data must be completely reprocessed. Since the data must be either digitized or processed through a digital filter and then recorrelated, the time lost is considerable. Besides, when the data have been reprocessed, there is no assurance that the filters are still correctly set. Further, this process tends to make filtering of data in near-real-time wind measurements of limited value.

This chapter demonstrates the use of retroactive filtering to produce quickly filtered correlation curves from unfiltered data. This is done by Fourier transforming the correlation curves into the spectra, choosing the frequency range of interest (omitting any instrument noise frequencies), and then Fourier-transforming the spectra back into the time domain.

NOMENCLATURE

INDEPENDENT VARIABLES

Symbol	Definition
t	total observation time
T	total integration time

Symbol	Definition
ΔT	length of time for each piece -- the whole data record is subdivided into pieces for data processing
i	piece number
m	total number of pieces of data integrated over ($m = T/\Delta T$)
f	frequency
τ	time lag between the two signals
τ_m	maximum time lag

DEPENDENT VARIABLES

$x(t)$	signal time history for a sensor
$y(t-\tau)$	delayed time history for a second sensor
$r_i(\tau)$	covariance of the ith piece of data at time lag τ
$\overline{r_i(\tau)}$	accumulative covariance average over the first ith piece of data
$\overline{\overline{r(\tau)}}$	accumulative covariance average over the entire integration time
$\Delta r(\tau)$	is the statistical error of the covariance
$C(f)$	co-spectra (real part)
$Q(f)$	quad-spectra (imaginary part)
$G(f)$	gain, $G^2 = C^2 + Q^2$
$<G(f)>$	mean gain over m pieces of data
$\overline{\overline{G(f)}}$	accumulative gain over m pieces of data
$<\Delta G(f)>$	mean statistical error of the gain
$\overline{\overline{\Delta G(f)}}$	accumulative statistical error of the gain

$r_{G,\phi}$ — the Fourier transpose of the spectra to the correlation curve will have the subscripts of those spectra components used

$r_{yx}(\tau) = r_{xy}(-\tau)$ — this is the cross-covariance (subscript xy indicates positive time lags and yx indicates negative time lags

OPERATORS

$( )$ — statistic

$\overline{( )}_i = \frac{1}{\Delta T} \int_{(i-1)\Delta T}^{i\Delta T} ( ) \, dt$ — piecewise mean (note: when average done over real time or time lag, the symbol $< >$ is used

$\langle ( )_k \rangle = \frac{1}{k} \sum_{i=1}^{k} ( )_i$ — accumulative mean where k is the kth piece of data (when average over pieces)

$\overline{\overline{( )}} = \langle \overline{( )}_{k=m} \rangle$ — total accumulative mean

$\langle ( )_k \rangle^2 = \frac{1}{k-1} \sum_{i=1}^{k} (( )_i - \overline{( )}_k)^2$ — statistical error

$\langle ( ) \rangle = F \{ \langle ( ) \rangle \}$ — the symbols used in the time domain will be transferred into the frequency domain showing the origin of the terms

VII.1 FORMULATION

The concept of retroactive filtering is straightforward. The correlation curve is Fourier-transformed into the frequency domain so that the unwanted frequencies can be removed. Once these frequencies are removed, the spectra are then Fourier-transposed back into the time domain so that the correlation curve no longer contains the undesired frequency components that the original curve had.

The original covariance curve is obtained by

$$\overline{\overline{r_{xy}(\tau)}} = \frac{1}{N} \int_{o}^{T} [x(t) - \langle x \rangle][y(t-\tau) - \langle y \rangle]\, dt. \tag{1}$$

This curve is then Fourier-transposed into the frequency domain by considering the co-spectra $\overline{\overline{C(f)}}$ and quad-spectra $\overline{\overline{Q(f)}}$ individually:

$$\overline{\overline{C(f)}} = \int_{o}^{\tau_m} [\overline{\overline{r_{xy}(\tau)}} + \overline{\overline{r_{yx}(\tau)}}] \cos 2\pi f\tau\, d\tau, \tag{2}$$

and

$$\overline{\overline{Q(f)}} = \int_{o}^{\tau_m} [\overline{\overline{r_{xy}(\tau)}} - \overline{\overline{r_{yx}(\tau)}}] \sin 2\pi f\tau\, d\tau. \tag{3}$$

It follows that the modulus of the gain $\overline{\overline{G(f)}}$ is

$$\overline{\overline{G(f)}} = \sqrt{\overline{\overline{C(f)}}^2 + \overline{\overline{Q(f)}}^2}\ , \tag{4}$$

and the phase angle is

$$\overline{\overline{\phi(f)}} = \arctan \frac{\overline{\overline{Q(f)}}}{\overline{\overline{C(f)}}}\ . \tag{5}$$

The calculations are performed by the computer program given in Appendix I.

The transpose of the spectrum back into the time domain is given by

$$\underset{\overline{\overline{G}}\ \overline{\overline{\phi}}}{r}(\tau) = \int_{f_{min}}^{f_{max}} \overline{\overline{G(f)}} \cos [2\pi f\tau + \overline{\overline{\phi(f)}}]\, df. \tag{6}$$

The frequencies integrated over in equation (6) set the reactive filter. For example, if the reactive filter is used to set a band pass, only those frequencies within the desired band pass are transposed back into the time domain; i.e., f_{min} and f_{max} are set at the upper and lower limits of the band pass. This means basically that the correlation curve arrived at by this practice contains only those frequencies within a given band pass. A second form of filtering is sometimes desired: notch filtering, which is used to remove a very narrow band pass from the data. With the reactive filter, a narrow band pass is removed by not integrating over these frequencies.

The next section will examine how the concept of retroactive filtering works in practice. This can be performed using the computer program given in Appendix II.

VII-2. RESULTS

The general procedure of retroactive filtering on a correlation curve is summarized from data with a broad band pass (0.01 to 4.0 cps).

The first case to be considered is the use of retroactive filtering to set the band pass. The original correlation curve contains frequencies up to 4.0 cps. As can be seen in figure VII.1a, there is a great deal of noise on this curve. The noise frequencies are estimated to be between 1.0 and 2.0 cps. Figure VII.1b shows what happens when the upper frequency is reduced from 4.0 cps to 2.0 cps. The net result is that the correlation curve is almost unchanged, implying that the region from 2.0 to 4.0 cps had little effect on the curve. (This curve will be used as the basis for the notch filtering.)

When the upper frequency limit was set to 1.0 cps, the curve in figure VII.1c resulted. One can observe how well the retroactive filtering has removed the noise on the curve.

A second example of limiting the band pass of the correlation curve by reactive filtering is shown in figure VII.2. The top correlation curve has an upper frequency limit of 4.0 cps, and when the upper limit is reduced to 1.0 cps, the bottom correlation curve resulted. It is of interest to note how, in this case, reactive filtering actually improved the large peak in the correlation curve.

A second type of filtering commonly used is notch filtering. When the data are digitized, certain frequencies are introduced in this process -- if the signal level is low -- that cannot be eliminated by analog filtering. Retroactive filtering is a means of eliminating this noise.

In the first case (Figure VII.1) the noise was eliminated by the "brute force" method of limiting the upper frequency to just below the digitization noise. The disadvantage with this approach is that the information from frequencies greater than 1.0 cps is lost. Thus, ideally we would like just to notch-filter the digitization noise. The top curve in Figure VII.3 was notch-filtered in the three digitization noise frequencies; i.e., those three frequencies were removed. The bottom curve resulted. By increasing the bandwidth of these notch filters from 0.01 cps to 0.03 cps, the digitization noise can be completely removed.

VII-3. CONCLUSIONS

Retroactive filtering has smoothed the correlation curve. The primary advantages to retroactive filtering are that it can be done on small computers without reprocessing the data and it saves turn-around time. Retroactive filtering is ideal for studies in the regions of the spectrum which contribute to transit time measurements.

The principal disadvantage to reactive filtering is that harmonics of the noise will still remain in the results unless they are also removed, although in practice the harmonic effect can never be completely eliminated. In spite of this disadvantage, it is still believed that retroactive filtering is of great value in correlation data analysis and can be used in link 3 of the MULTCOR program to make cross-beam analysis faster and more effective.

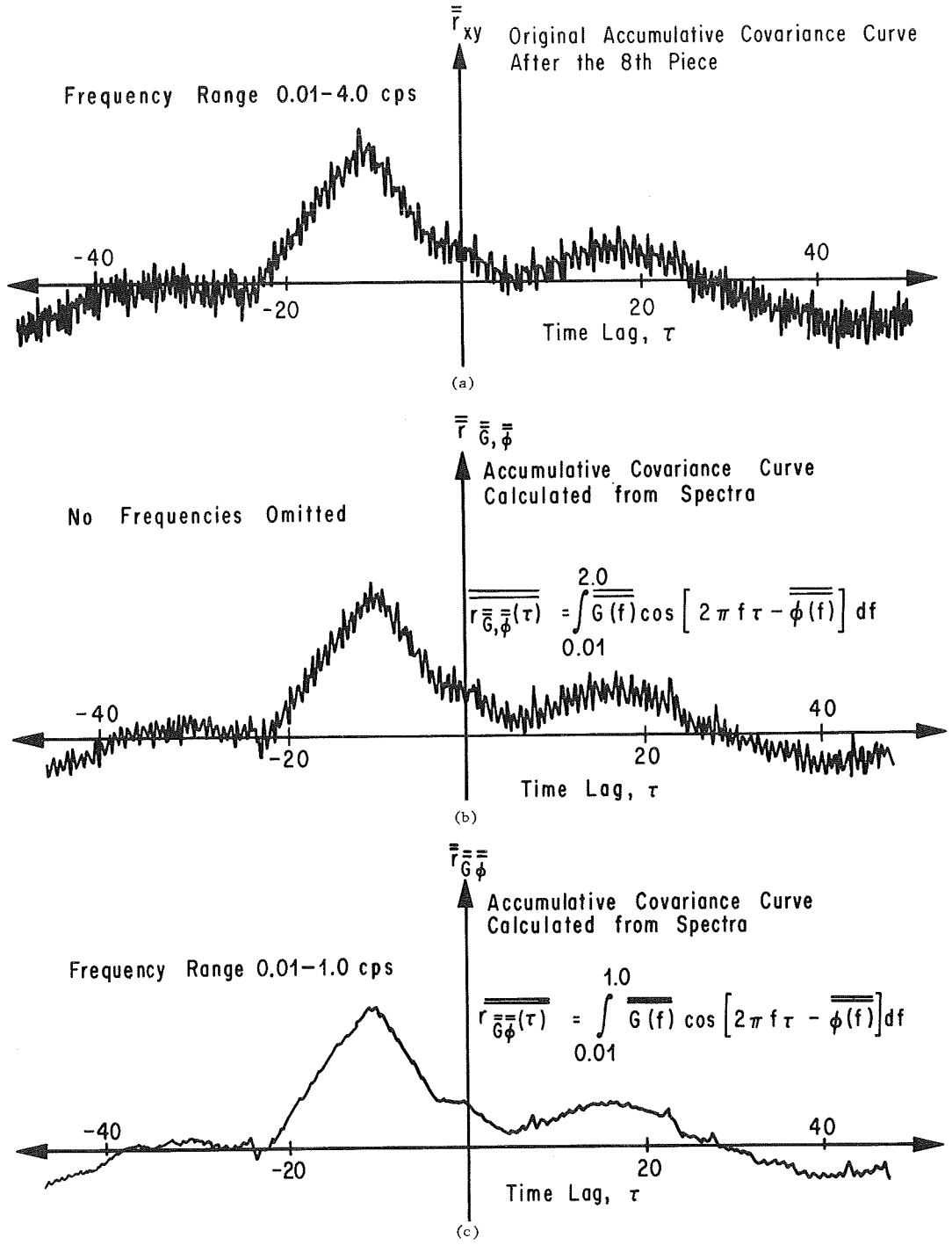

FIGURE VII.1. DIRECT AND DOUBLE-TRANSFORMED ACCUMULATIVE CORRELATION CURVES

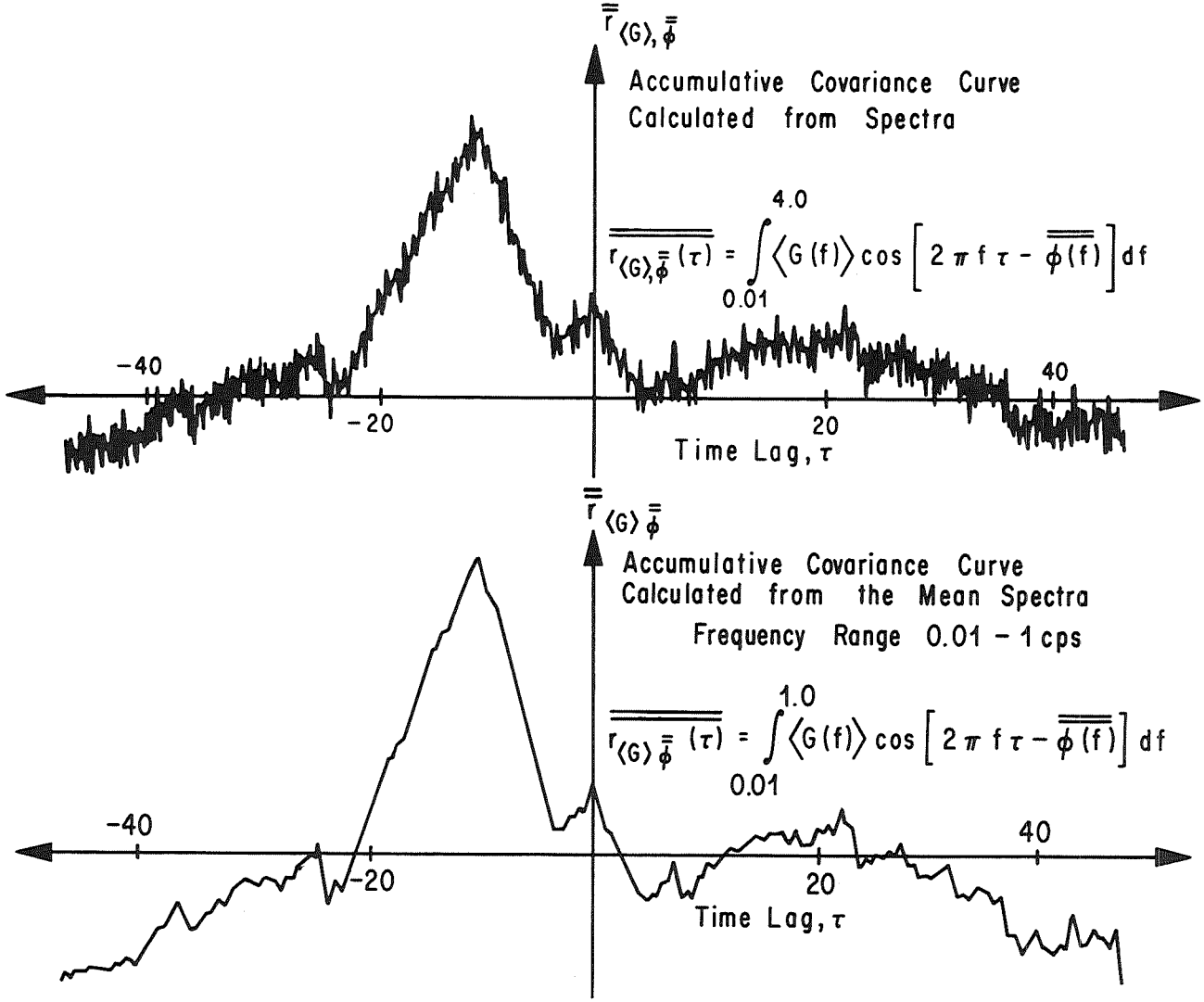

FIGURE VII.2. DIRECT AND DOUBLE-TRANSFORMED ACCUMULATIVE CORRELATION CURVES

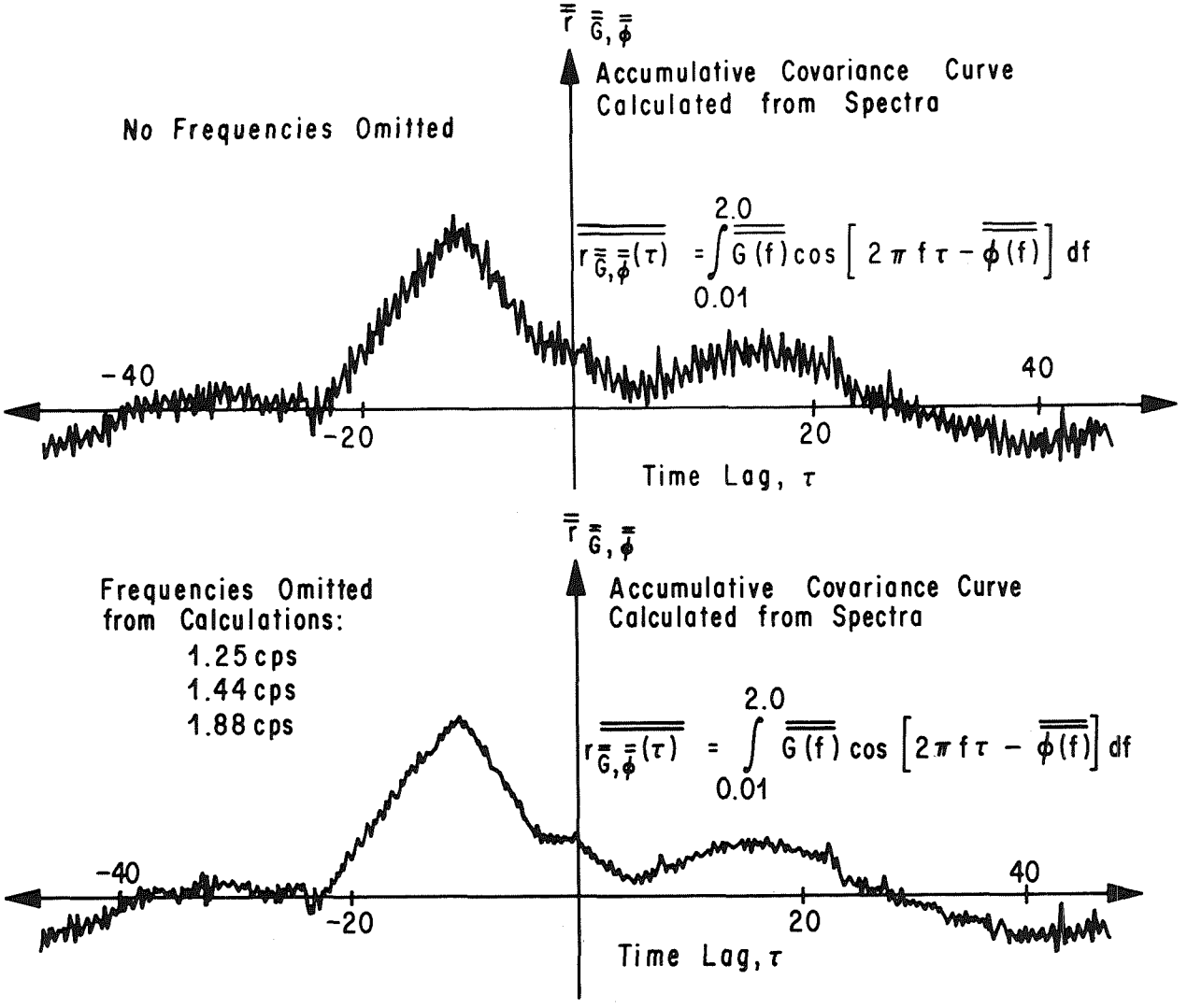

FIGURE VII.3. DIRECT AND DOUBLE-TRANSFORMED ACCUMULATIVE CORRELATION CURVES

CHAPTER VIII

THE RELIABILITY COEFFICIENT FOR CROSS-COVARIANCE

by

J. Briscoe Stephens and Benjamin C. Hablutzel
NASA - Marshall Space Flight Center, Alabama

SUMMARY

The concept for the reliability coefficient of a covariance curve has been developed to improve the previous methods for identifying a peak through confidence levels which employ an arbitrarily chosen probability.

The technique described in this Chapter differs from the technique traditionally used for peak identification in that, rather than setting an arbitrary probability, the probability is now determined as a function of the statistical error and the covariance coefficient. For lack of a better term, this function has been defined as the reliability coefficient.

The physical significance and the reliability coefficient are discussed in terms of a stationary model. Results from the application of the reliability concept to actual atmospheric cross-beam data are discussed.

NOMENCLATURE

INDEPENDENT VARIABLES

Symbol	Definition
t	total observation time
T	total integration time
$\triangle T$	length of time for each piece -- the whole data record is subdivided into pieces for data processing.

Symbol	Definition
i	piece number
m	total number of pieces of data integrated over ($m = T/\Delta T$)
f	frequency
τ	time lag between the two signals
τ_m	maximum time lag

DEPENDENT VARIABLES

$x(t)$	signal time history for the sensor
$y(t-\tau)$	delay time history for the second sensor
$\overline{r_i(\tau)}$	covariance coefficient of the ith piece of data at time lag τ
$\overline{\overline{r(\tau)}}$	accumulative covariance average over the entire integration time
$\Delta r(\tau)$	statistical error of the covariance
$P(t_p, m, \tau)$	reliability for a time delay

OPERATORS

$( )$	statistic
$\overline{( )}_i = \frac{1}{\Delta T} \int_{(i-1)\Delta T}^{i\Delta T} ( ) \, dt$	piecewise mean (Note: when average done over real time or lag, the symbol $< >$ is used.)
$<( )_k> = \frac{1}{k} \sum ( )_i$	accumulative mean where k is the kth piece of data (when averaged over pieces)
$\overline{\overline{( )}} = <\overline{( )}_{k=m}>$	total accumulative mean

Symbol	Definition
$\langle ( )_k \rangle^2 = \frac{1}{k-1} \sum_{i=1}^{k} (( )_i - \overline{( )_k})^2$	statistical error.

VIII-1. INTRODUCTION

The concept of a reliability coefficient for the evaluation of cross-covariance curves obtained from atmospheric cross-beam measurements is developed in this chapter. The reliability concept is a new way of viewing the traditional peak identification procedure, which uses an arbitrary probability level based on test results. The procedure described here requires that the maximum positive peak in the covariance curve (the mean covariance) be greater than the statistical error. When this stipulation is fulfilled, the time lag corresponding to this peak is defined as the transit time. This is the lapsed time used by the turbulence eddy in traversing the distance between the beams.

When an arbitrary probability level is used, validity of the correlation curves is obtained as a binary response and not as a relative measurement. Comparison of the statistical error at different time lags does not determine which time lag is more statistically significant. This fact means that the current approach does not afford a systematic means to compare different parts of the same correlation curve. Furthermore, the variability of the experimental parameters from test to test prohibits the use of marginal correlation results since the use of an arbitrary probability level requires an extra safety factor to account for all test conditions.

The reliability coefficient being proposed here affords a relative evaluation of the reliability of the correlation curve based on both the sample population and the statistical error. This relative evaluation results in the possible elimination of the limitations of the arbitrary probability levels when the reliability coefficient is used as the key criterion for evaluating the consistency of the correlation results. The same information can be obtained directly from the reliability probability used with arbitrary probability levels.

It is hoped that this approach can account for piecewise variations in both the transit time and the amplitude of the peak. It should be recognized that this is merely a proposed approach and not a solution to these problems.

This chapter assumes that the reader is familiar with both the correlation technique (Jayroe and Su [VIII-1]) and the atmospheric cross-beam program (Stephens, Sandborn, and Montgomery [VIII-2]).

VIII-2. THEORETICAL DEVELOPMENT

The statistical error of the covariance can be interpreted physically, as follows, rather than mathematically.

The accumulative covariance is defined as

$$\overline{\overline{r(\tau)}} = \frac{1}{N} \int_0^T [x(t) - \bar{\bar{x}}][y(t-\tau) - \bar{\bar{y}}]\, dt, \tag{1}$$

where x and y are the instantaneous fluctuations of the signal, $\bar{\bar{x}}$ and $\bar{\bar{y}}$ are the accumulative mean values, T is the total integration time, t is the real time measurement from the start of the record, and τ is the time delay.

The statistical error $\overline{\overline{\Delta r(\tau)}}$ for the covariance is

$$\overline{\overline{\Delta r(\tau)}} = \left\{ \frac{1}{(m-1)} \sum_{i=1}^{m} [\overline{r_i(\tau)} - \overline{\overline{r(\tau)}}_m]^2 \right\}^{1/2}, \tag{2}$$

where m is the number of pieces of data used, $\overline{r_i(\tau)}$ is the ith covariance occurring at the time delay τ, and $\overline{\overline{r(\tau)}}$ is the resulting accumulative covariance for the mth piece of data.

When using the statistical error for providing a confidence limit, it is required that

$$\overline{\overline{r(\tau)}} > \overline{\overline{\Delta r(\tau)}} \cdot t_{p=80\%} \tag{3}$$

for the covariance coefficient to be significant. This Student's "t" of 80%, $t_{p=80\%}$, implies a probability level of 80 percent. There are three

categories into one of which a covariance coefficient can fall by the scheme set forth by this last restriction. The covariance coefficient at a time lag can be less than, greater than, or equal to the statistical error.

When the statistical error is greater than the covariance coefficient, i.e.,

$$\overline{\overline{r(\tau_a)}} < \overline{\overline{\Delta r(\tau_a)}} \cdot t_{p=80}, \tag{4}$$

then we say that this is not an acceptable measurement. However, a measurement is statistically significant, i.e.,

$$\overline{\overline{r(\tau_b)}} > \overline{\overline{\Delta r(\tau_b)}} \cdot t_{p=80}, \tag{5}$$

if the average $\overline{\overline{(\ )}}$ exceeds its own standard error $\overline{\overline{\Delta(\ )}}$.

The third category is the one where the statistical error is equal to the covariance coefficient:

$$\overline{\overline{r(\tau_c)}} = \overline{\overline{\Delta r(\tau_c)}} \cdot t_{p=80}. \tag{6}$$

This relationship implies that there exists an 80 percent probability that the sample and the expected value of the covariance have the same sign.

Thus, when the covariance coefficient of a positive covariance sample equals the statistical error, then we have a relation for the probability of having a positive correlation coefficient. This relation is

$$\overline{\overline{r(\tau)}} = \overline{\overline{\Delta r(\tau)}} \cdot t_p, \tag{7}$$

where the probability level, p, is the unknown. However, this unknown is related to the known confidence factor

$$t_p = \frac{\overline{\overline{r(\tau)}}}{\overline{\overline{\Delta r(\tau)}}} \tag{8}$$

by the Student's "t" distribution.

The probability level required to satisfy the Student"s "t" relationship given in equation (8) is

$$P(m;\tau) = \frac{2 \cdot \Gamma(m/2)}{\sqrt{\pi(m-1)} \cdot \Gamma(\frac{m-1}{2})} \int_{x=0}^{x=t_p} [1 + \frac{x^2}{(m-1)}]^{-\frac{m}{2}} dx. \qquad (9)$$

The result for $P(t_p,m,\tau)$ will be defined as the "reliability coefficient." Although the reliability probability was developed for the cross-covariance, it is equally applicable to piecewise derivations of any other statistics. The Student's "t" distribution was used because the samples under consideration are normally small ($m < 30$). For larger piece numbers, the normal distribution might be used, i.e., the reliability coefficient becomes independent of the number of pieces used.

VIII-3. APPLICATION OF THE RELIABILITY TO THE STATIONARY COVARIANCE CURVE

The variation of the reliability coefficient with time lag can be used to afford a more meaningful peak identification technique because:

(1) The reliability curve provides a systematic procedure to establish the relative reliability of different portions of the same covariance curve.

(2) The reliability curve can be used for estimating the noise level tolerance.

(3) The reliability coefficient accurately accounts for the uncertainty associated with small sample size by employing the Student's "t" distribution.

Before discussing the properties of the reliability coefficient, we must first review additional characteristics of both the covariance and standard error.

The limitation in computer storage prohibits the integration of the covariance (equation (1)) over the entire record at one time. Therefore, the record is subdivided into m pieces at length ΔT such that

$$T = m \cdot \Delta T. \qquad (10)$$

For each piece, a piecewise covariance coefficient $\overline{r(\tau)_i}$, where i is the piece number, is obtained. Then the accumulative covariance coefficient $\overline{\overline{r(\tau)_m}}$ for the entire record is

$$\overline{\overline{r(\tau)_m}} = \overline{\langle r(\tau) \rangle_m} = \frac{1}{m} \sum_{i=1}^{m} \overline{r(\tau)_i}. \tag{11}$$

Thus, the statistical error $\overline{\Delta r(\tau)}$ defined in equation (1) is the effective measure of how the piecewise covariance $\overline{r(\tau)_i}$ varies about the accumulative covariance $\overline{\overline{r(\tau)_m}}$. The primary physical requirement of the correlation technique is that the phenomenon being measured is recurring. Thus, the consistency of certain piecewise covariance coefficients is the necessary property (implied by the requirements of the correlation technique) that enables us to retrieve temporal information. The reliability is nothing more than an estimate of this consistency.

To expand on the significance and application of this requirement of consistency, let us consider the following argument. This argument will be restricted to stationary data obtained from the convection of a frozen pattern at a constant speed such that the eddies traverse the transit distance between the two beams in a transit time, τ_s. The piecewise covariance coefficient at the time delay τ_s should be

$$0 < \overline{r(\tau_s)_i} < 1, \tag{12}$$

and will be referred to as "the covariance due to the signal." The remaining covariance coefficients, $\overline{r'(\tau_s)_i}$ (the prime indicates all time delays other than when $\tau = \tau_s$), can have values between

$$-1 < \overline{r'(\tau_s)_i} < 1, \tag{13}$$

and will be referred to as "the covariance due to the noise." (For ease of discussion, the signal component is defined as a spike in the covariance curve. This does not restrict the effect of this discussion.)

For random stationary data, the signal component of the accumulative covariance curve has the following property:

$$0 < \lim_{m \to \infty} \overline{\overline{r(\tau_s)}} = \text{constant} \leq 1, \tag{14}$$

while the noise component has the property that

$$\lim_{m \to \infty} \overline{\overline{r'(\tau_s)}} \simeq 0. \tag{15}$$

This property has the resultant implication that the peak in the covariance curve due to the signal remains at approximately the same time lag from piece to piece, but a peak in the piecewise covariance due to noise will be moving from piece to piece. Previous peak identification efforts thus assumed that the peak corresponding to the convection speed in the accumulative covariance curve can be differential from a peak of equal magnitude due to noise by using the statistical error of the covariance, since the statistical error of the signal peak is less than the statistical error due to the noise peak. A more sophisticated approach is required in practice because of finite integration times and because of the varying magnitudes of the peaks in the covariance curve.

The reliability concept affords an approach which should circumvent these problems. To understand the behavior of the reliability coefficient, let us consider the following (see eqs. (7) and (8)): A large reliability coefficient at a time delay means that the covariance coefficient has the same sign from piece to piece; whereas, a small reliability coefficient means that the covariance coefficient at that time delay is oscillating from piece to piece. These oscillations are the characteristics of noise and it is thus apparent that the signal should have a higher reliability than the noise, once a sufficient sample of the population has been obtained. Thus, the reliability curve affords a method that, along with the covariance curve, can permit the signal to be distinguished from the noise in the curve before the noise has been completely suppressed.

The above discussion can be extended to set a noise tolerance by using a knowledge of the beam geometry and the wind direction. With this knowledge, one can determine whether the transit time should be a positive or negative time lag. The signal half-plane will be defined as the half-plane of the covariance curve in which the transit time must exist. The other half-plane is the noise half-plane, since any peak existing in this half-plane will be assumed to be due to noise. The maximum reliability coefficient which exists in the noise half-plane is then a measure of the minimum acceptable confidence level, and will thus give the noise tolerance.

This approach obviously has some shortcomings, the major one being a periodic signal. For a periodic signal, the noise half-plane will have a reliability equal to the sum of the noise and the signal. Thus, in this case, a more complex formula will have to be used to obtain the noise level. An example of such a formula is to subtract the known signal reliability coefficient from the maximum reliability coefficient existing in the noise half-plane. The result is the noise reliability level. These problems should not exist with a broadband process, but it is always necessary to know the kind of process that is being measured. The above concepts are thus incomplete and should be taken as a basis for a new systematic approach to peak identification, not as a finished identification criterion.

To summarize the application of the reliability coefficient for setting the noise tolerance, let us consider the following two applications. First, for zero beam separation (Figure VIII.1), the procedure for the interpretation is as follows. The signal is what occurs around zero time delay. All other peaks then must be noise peaks. If the noise reliability coefficient is less (see peak (a)) than the signal reliability coefficient, then the covariance curve can be meaningfully evaluated; but if the noise reliability coefficient is greater (see peak (b)) than the signal reliability coefficient, then it does not seem to be meaningful to accept these results. (The case of a periodic signal has been omitted.)

The second application is to the measurement of a wind speed (Figure VIII.2). In this case, the signal range of time lags is set by the range of possible wind speeds during the period of observation. Once this is established, the same argument that was used in the case of a zero beam separation applies here. If the reliability coefficient of the signal is not greater than the reliability coefficient of the noise, then the results are questionable.

The reliability affords one final feature that can be useful for setting the integration times. When the reliability of the signal peak does not increase (or if it decreases) with additional integration time,

and if the probability of noise does not decrease, then additional integration time will afford no improvement in the covariance curve. The advantage of this over the accumulative error currently used is that it provides closer control. That is, the accumulative error monitors only the overall variation, while the reliability can be used to monitor specific peaks and to determine how the integration time affects these peaks.

VIII-4. APPLICATION OF THE PROBABILITY TO ACTUAL ATMOSPHERIC DATA

In section VIII-3 the discussion was limited to stationary data, because at best this approach leaves a certain amount to conjecture. When dealing with nonstationary data, the amount of conjecture increases; therefore, the power of these concepts will be empirically demonstrated.

The first case shown in Figure VIII.3 is a model example of the use of this probability concept. The peak in the covariance curve at -10 seconds compares favorably with the wind speed. The signal peak of the reliability coefficient is about 99 percent, while the maximum noise peak is only 73 percent. The fact that the reliability coefficient of the signal is greater than the reliability coefficient of the noise indicates that the signal peak is significant, a fact already obvious from the statistical error. This is the only wind measurement evaluated that had a 99 percent reliability coefficient for the signal. We have found by independent experiments of other statistical techniques that this is our most well-behaved run.

The second case of a wind measurement, shown in Figure VIII.4, demonstrates the use of the "noise" half-plane. Winds compare only at negative lags. The peak at -15 seconds corresponds to the wind speed, but the peaks at -25 seconds is also statistically significant, according to the statistical error. Our concept holds that the noise peak at 50 seconds has a reliability coefficient of 71.6 percent. This eliminates the peak in the signal plane at -25 seconds, since it has a reliability coefficient of only 70.2 percent. We are left with the signal peak of a 81.6 percent probability, which is what we desired.

The third example is a zero beam separation (Figure VIII.5). According to the statistical error, we should reject the results shown in Figure VIII.5, even though they are the desired ones, because they are not statistically significant according to the statistical error. When the reliability coefficient is applied, it is found that it peaks at zero time delay (out to ± 75 seconds). Thus, the reliability coefficient identifies the peak at zero as meaningful. However, this

identification also indicates that the probability for the identified peak to be positive is only 21 percent. Our confidence in the "accepted" result is thus still low.

VIII-5. CONCLUSIONS

At this time, only a preliminary conclusion is possible since a great deal more work is needed with the reliability coefficient before a conclusion can be drawn. At the time this concept was tested, the concepts discussed in section VIII-3 seemed to be valid for all of the cross-beam data available at that time. Furthermore, this concept seems to increase our ability to evaluate the covariance curve, and seems to work for both stationary and nonstationary data. Tests suggest that it also may be useful in evaluating derivatives and spectra. More work is planned with the latter.

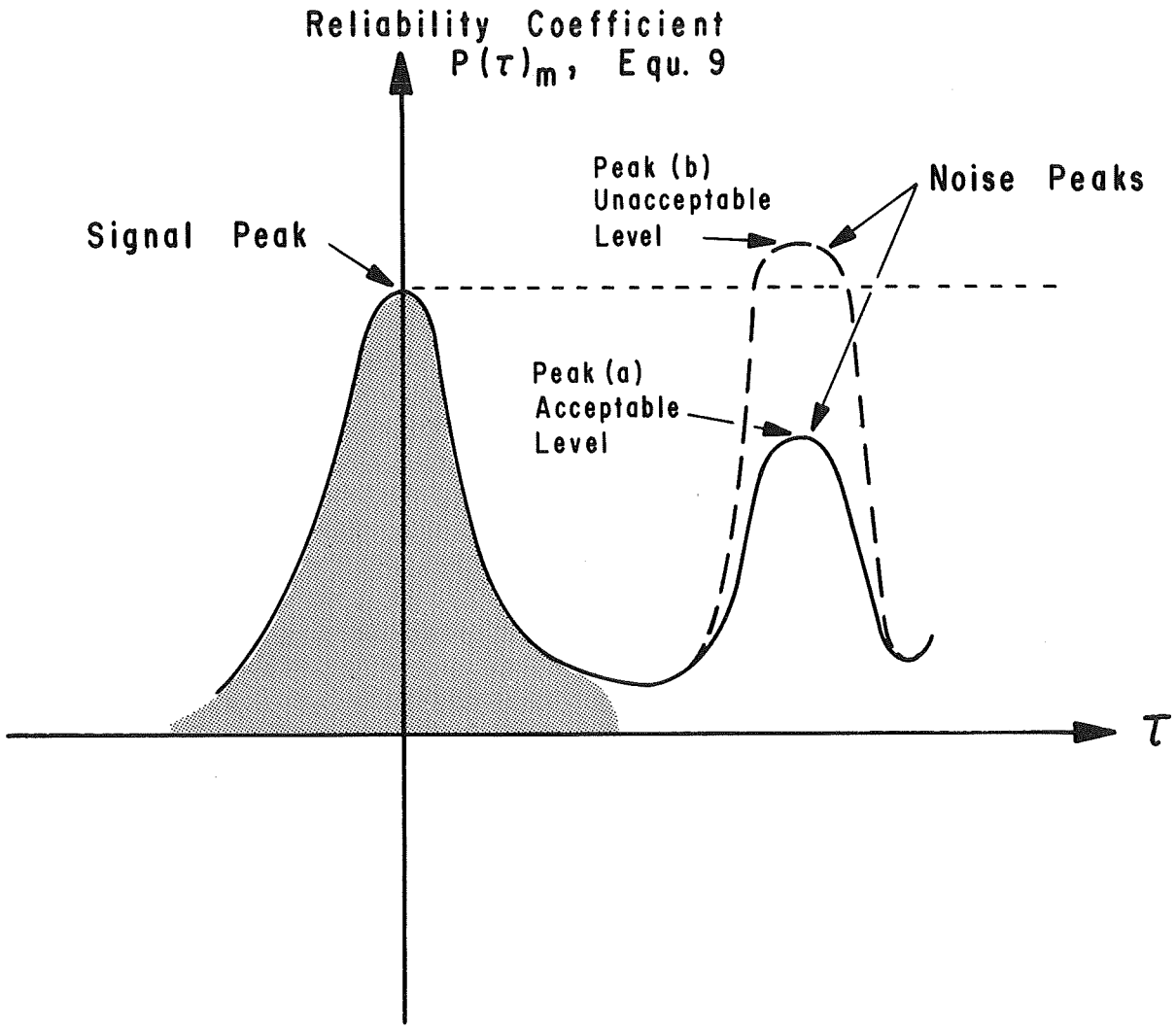

FIGURE VIII.1. MODEL RELIABILITY CURVE
FOR ZERO BEAM SEPARATION

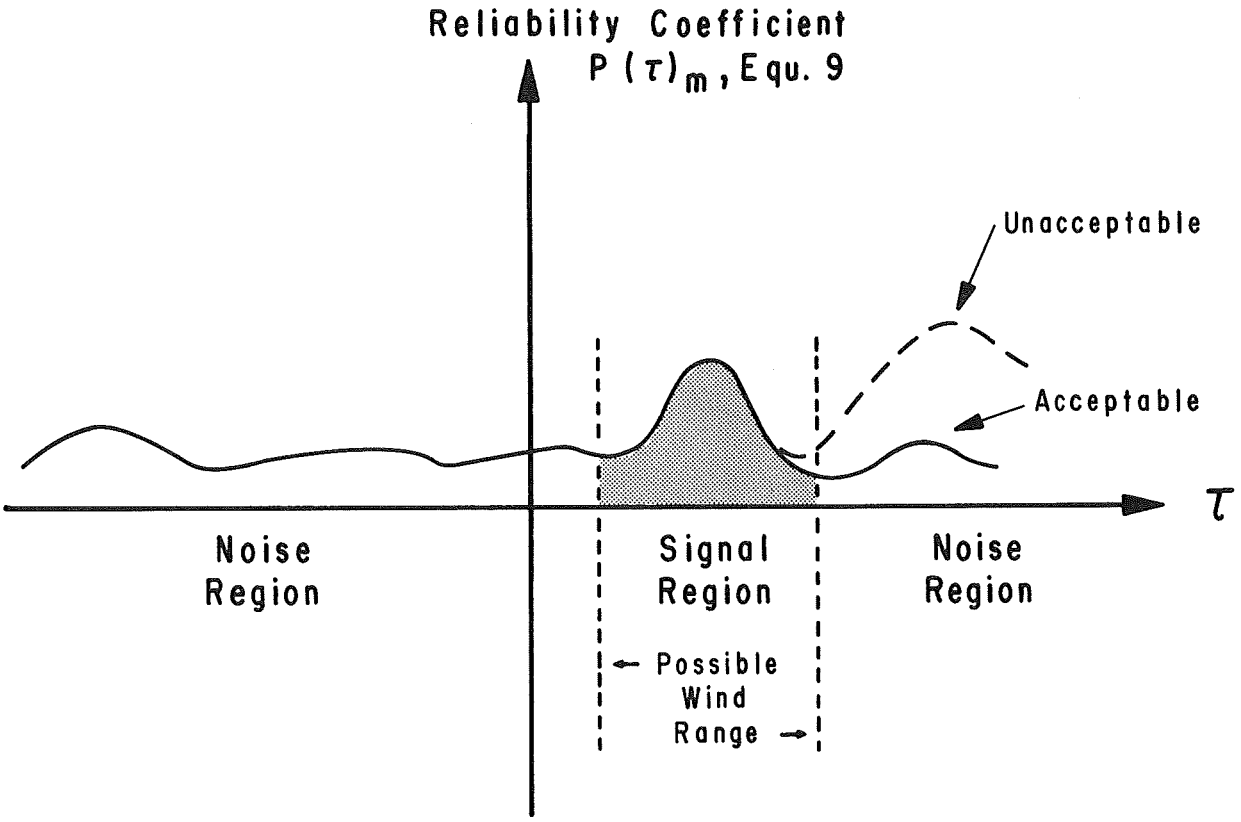

FIGURE VIII.2. MODEL RELIABILITY FOR A BEAM SEPARATION

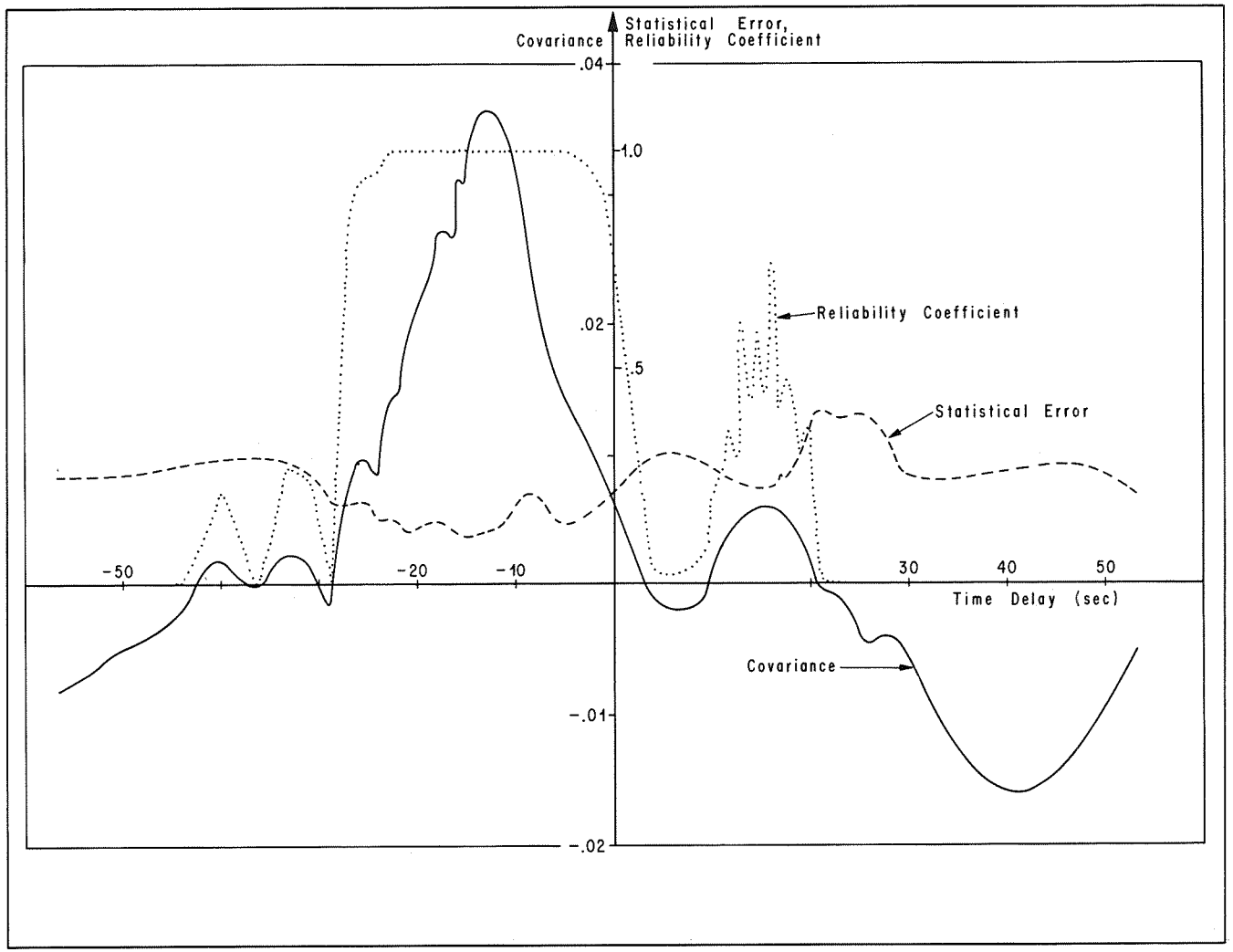

FIGURE VIII.3. ACTUAL BEAM SEPARATION

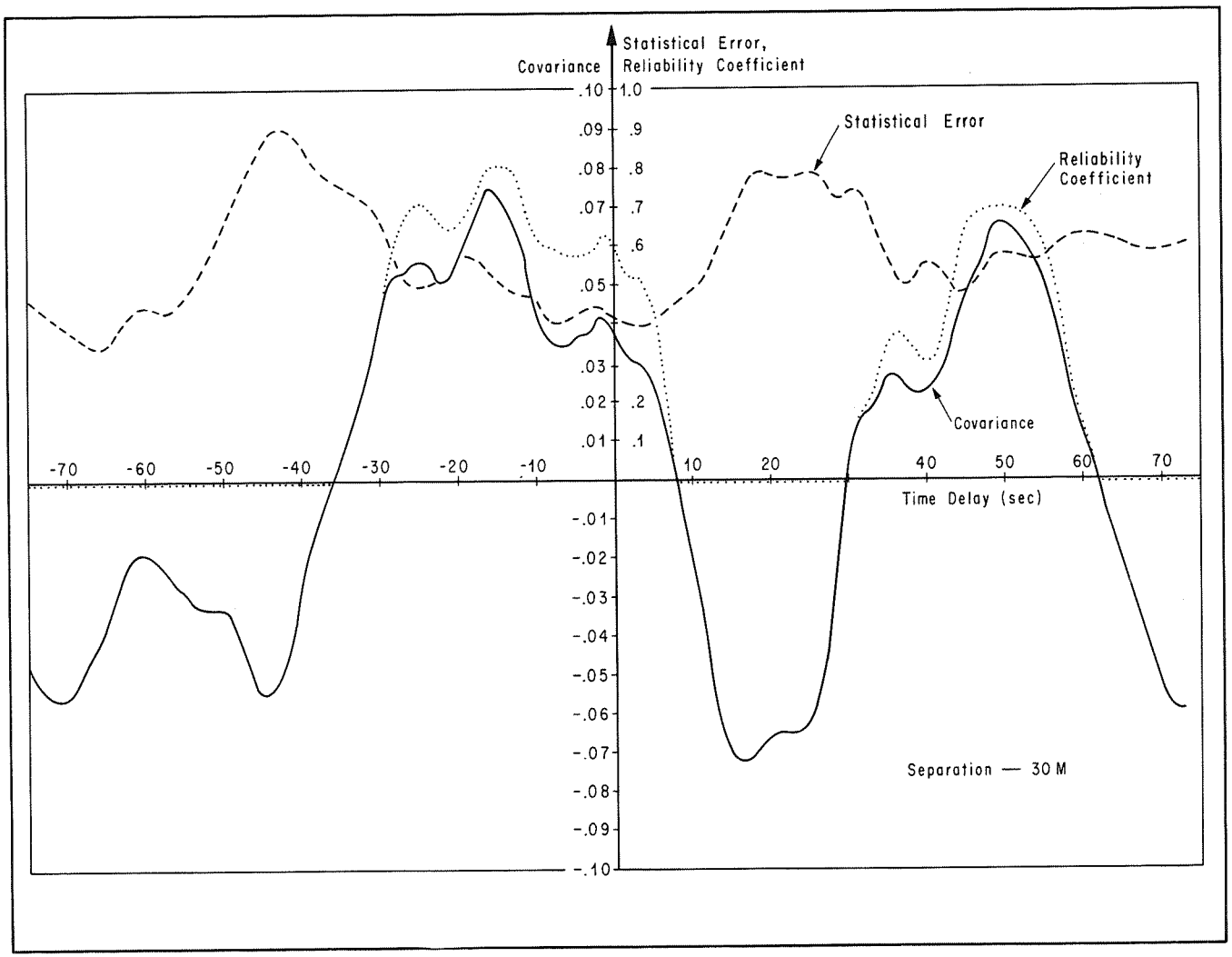

FIGURE VIII.4. ACTUAL BEAM SEPARATION

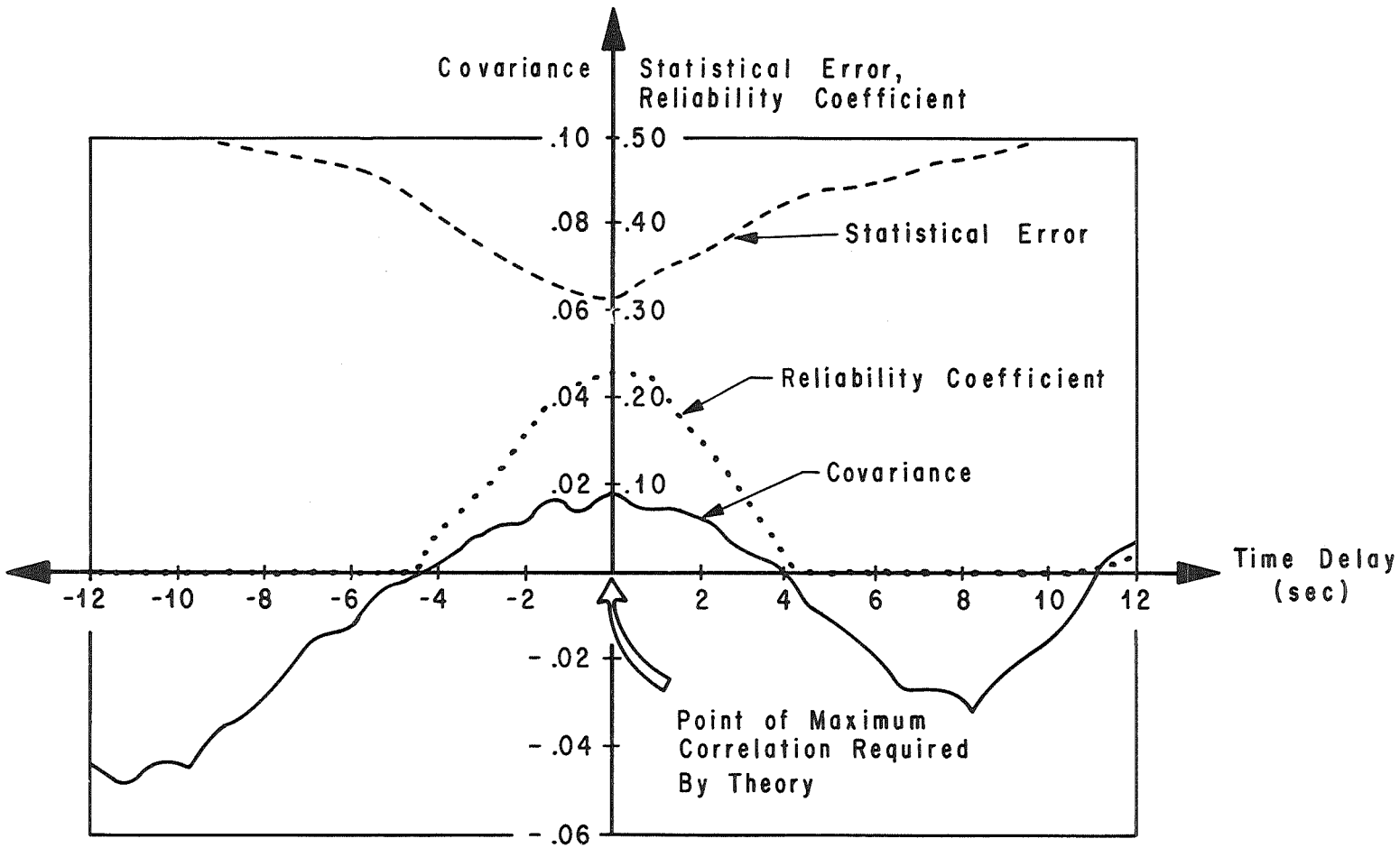

FIGURE VIII.5. ACTUAL ZERO BEAM SEPARATION

REFERENCES

VIII-1. Jayroe, R. R. and M. Y. Su, "Optimum Averaging Times of Meteorological Data with Time-Dependent Means," NASA TM X-53782, October 15, 1968, pp. 103-116.

VIII-2. "Remote Wind Detection with the Cross-Beam Method at Tower Heights," NASA TM X-53782.

APPENDIX I

SPECTRA PROGRAM

This program is designed to calculate the cross-beam power spectral density function from the covariance function by using the Fourier transform which converts from a time domain to a frequency domain.

This program was modified from the current spectral program used in CORFUN in the following ways:

(1) It has the ability to shift the major peak to zero.

(2) It is capable of using Parzen's weighting factor to pre-whiten the covariance function.

(3) It has the option to add zero correlations to increased time lag range which provides for a finer frequency resolution ($1(2^* \tau_{max}) = \triangle f$).

(4) It can provide calculations from covariance coefficients taken directly from the output of the CORFUN program, either from piecewise data or from the accumulative averages of these pieces.

Table 1 defines the input parameters, maximum run time, and available computers at MSFC. Table 2 shows the loading procedure for accumulative data, and Table 3 shows the loading procedure for piecewise data. Table 4 shows all of the output parameters for this program.

TABLE 1

COMPUTER:	SDS 930 - LIMITED STORAGE CAPABILITY	CDC 3200
RUN TIME/PIECE:	10 MINUTES	6 MINUTES

DEFINITIONS OF INPUT DATA:

INPUT CARD (1)

RUN	RUN NUMBER
PHOTO 1	PHOTOMETER IDENTIFICATION
PHOTO 2	PHOTOMETER IDENTIFICATION

INPUT CARD (2)

DELT	TIME LAG BETWEEN POINTS
NLAGS	NUMBER OF POSITIVE TIME LAG POINTS
LSCALE	IF EQUAL TO 1, MULTIPLIES EACH CORRELATION POINT BY RSCALE; IF EQUAL TO 0, THIS PART IS OMITTED.
RSCALE	A SCALE FACTOR WHICH SCALES THE VALUES OF THE CORRELATION POINTS; USUALLY SET EQUAL TO 1.
LPARZN	IF EQUAL TO 1, CALLS PARZEN SUBROUTINE, IF EQUAL TO ZERO, IT IS OMITTED.

TABLE 1 - con't

INPUT CARD (2)	LLAGS	ENABLES PROGRAMMER TO ADD ADDITIONAL TIME DELAYS TO PROVIDE FOR A FINER FREQUENCY RESOLUTION.
	TAUSHF	VALUE WHICH THE PEAK IS TO BE SHIFTED. USED ONLY WITH PARZENS. NORMALLY NOT USED IN OUR WORK. USUALLY SET EQUAL TO 0.
	LYPE	IF EQUAL TO 1, READS ACCUMULATIVE DATA; IF EQUAL TO 0, READS PEICEWISE DATA.
INPUT DATA (3)	TLAGS	REAL ARRAY CONTAINING TIME LAGS.
	RXY	ARRAY OF POSITIVE CORRELATION COEFFIEIENTS.
INPUT CARD (4)	NTEST	IF EQUAL TO -1 IT READS ANOTHER SET OF ACCUMULATIVE DATA AND CALCULATE SPECTRA. IF EQUAL TO 0 TAKES ANOTHER SET OF PIECEWISE DATA. IF EQUAL TO +1, TERMINATES.

TABLE 2

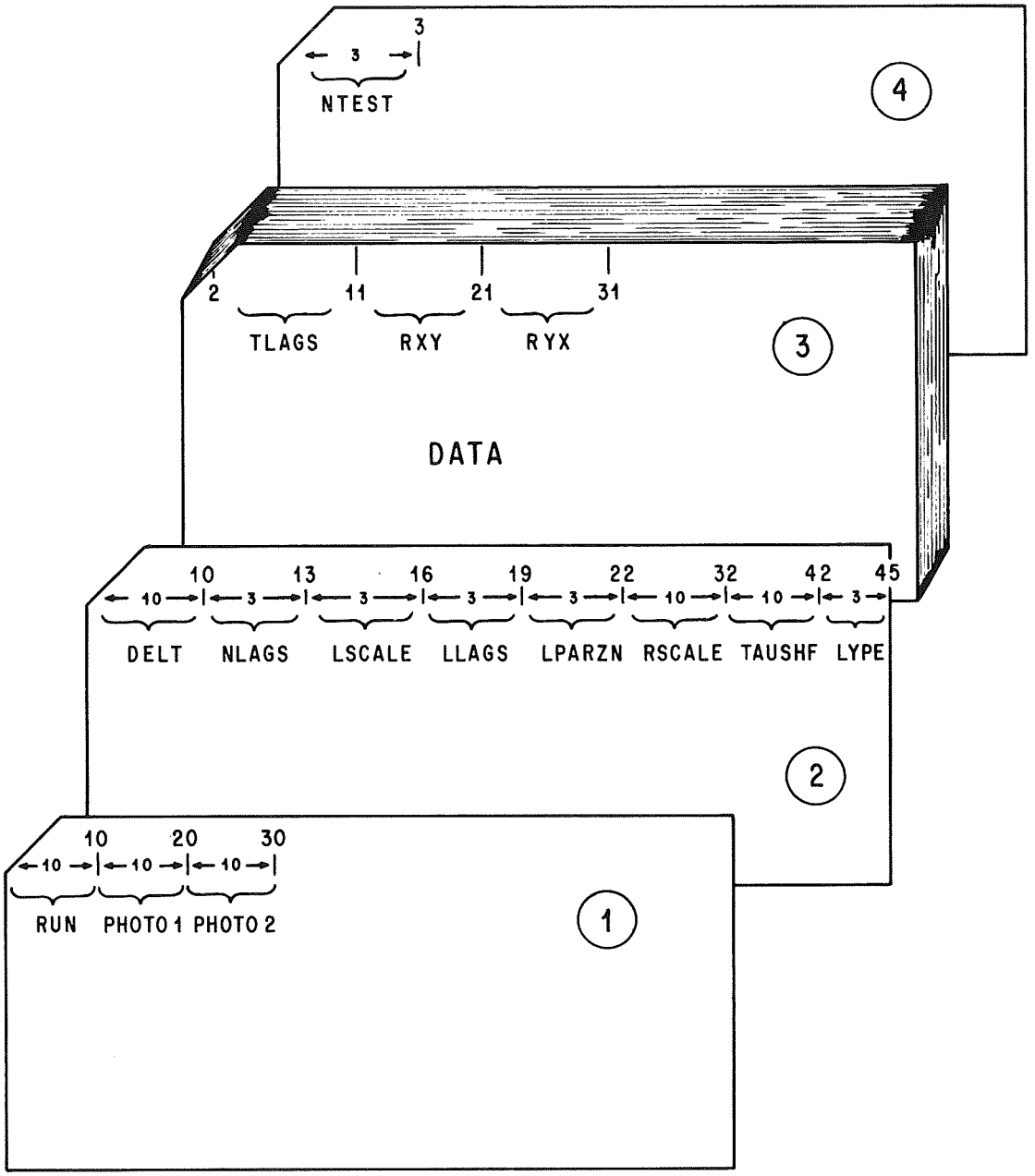

OUTLINE FOR ACCUMULATIVE DATA

TABLE 3

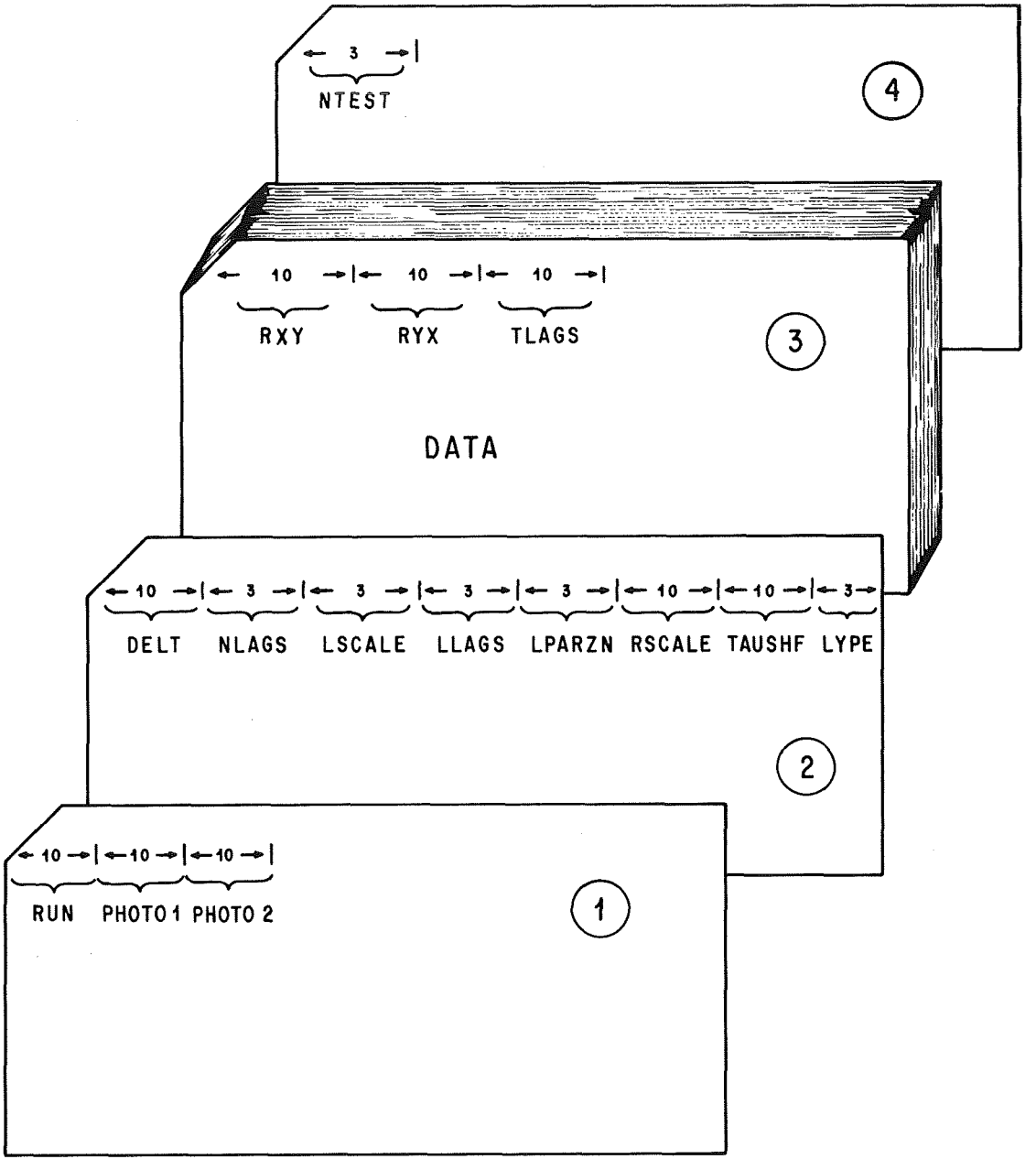

OUTLINE FOR PIECEWISE DATA

TABLE 4

PRINTED:

(TLAGS)	(RXY)	(RYX)	
xxx.xxxxx	xxx.xxxxx	xxx.xxxxx	THIS IS FOR CHECKING THE ORIGINAL INPUT DATA
⋮	⋮	⋮	
xxx.xxxxx	xxx.xxxxx	xxx.xxxxx	
(PARZEN)	(RXY + RYX)	(RXY − RYX)	
xx.xxxxxx	xx.xxxxxx	xx.xxxxxx	THIS OUTPUT PERMITS CHECKING OF CALCULATION
⋮	⋮	⋮	
xx.xxxxxx	xx.xxxxxx	xx.xxxxxx	

FREQUENCY (CPS)	COSPECTRA	QUADSPECTRA	GAIN	CROSS PSD	PHASE (DEG)	LOG FREQ.	LOG GAIN	LOG CROSS PSD
xxx.xxxxxx	xxx.xxxxxx	xxx.xxxxxx	xxx.xxxxxx	xxx.xxxxxx	xxx.xxxxxx	xxx.xxxxxx	xxx.xxxxxx	xxx.xxxxxx
⋮	⋮	⋮	⋮	⋮	⋮	⋮	⋮	⋮
xxx.xxxxxx	xxx.xxxxxx	xxx.xxxxxx	xxx.xxxxxx	xxx.xxxxxx	xxx.xxxxxx	xxx.xxxxxx	xxx.xxxxxx	xxx.xxxxxx

END OF PRINTED OUTPUT

PUNCHED ON EACH CARD:

FREQUENCY (CPS)	COSPECTRA	QUADSPECTRA	GAIN	CROSS PSD	PHASE (RADIANS)	LOG FREQ.	LOG GAIN	LOG CROSS PSD
xx.xxxxx	xx.xxxxxx	xx.xxxxx	xx.xxxxx	xx.xxxxx	xx.xxxxx	xx.xxxxx	xx.xxxxx	xx.xxxxx

OUTPUTS FOR SPECTRA PROGRAM

```
C      SPECT COMPUTES THE CROSS SPECTRAL DENSITY FUNCTION
       EQUIVALENCE (RYX,RMI)
       EQUIVALENCE (RXY,RPL)
       DIMENSION RXY(406),RYX(406),TLAGS(406),RPL(406),RMI(406),C(406),
      6Q(406)
       READ 101, RUN,PHOTO1,PHOTO2
  101  FORMAT (3F10.0)
       READ 3,DELT,NLAGS,LSCALE,LLAGS,LPARZN,RSCALE,TAUSHF,LYPE
    3  FORMAT (F10.0,4I3,F10.0,F10.0,I3)
C      AS THE FOURIER TRANSFORM OF THE CORRELATION
C      COEFFICIENTS. WHERE---
C
C
C      **INPUT**
C      NLAGS = THE NUMBER OF CORRELATION LAG POINTS, INTEGER.
C      DELT = THE SAMPLING INTERVAL(DELTA TIME), REAL.
C      TLAGS = A REAL ARRAY CONTAINING THE TIME LAGS.
       IF(LYPE) 38,39,38
   38  CONTINUE
 4007  CONTINUE
       DO 1 I=1,NLAGS
       READ 2, TLAGS(I),RXY(I)
    2  FORMAT (1X,2F10.0)
       TLAGS(I)=ABSF(TLAGS(I))
    1  CONTINUE
       DO 13 I=1,NLAGS
       READ 14, RYX(I)
   14  FORMAT (11X,F10.0)
   13  CONTINUE
       GO TO 55
   39  CONTINUE
       DO 37 I=1,NLAGS
       READ 46, RXY(I),RYX(I),TLAGS(I)
   46  FORMAT (1X,F10.4,2F10.6)
   37  CONTINUE
C      RXY = REAL ARRAY IF POSITIVE CORRELATION COEFFICIENTS.
C      RYX = REAL ARRAY IF NEGATIVE CORRELATION COEFFICIENTS.
C
C      **OUTPUT**
C      RPL = A REAL ARRAY CONTAINING THE EVEN PART(+) OF THE
C            CROSS CORRELATION FUNCTION.
C      RMI = A REAL ARRAY CONTAINING THE ODD PART (-) OF THE FUNCTION
C      C = REAL ARRAY CONTAINING CO-SPECTRA,
C      Q = REAL ARRAY CONTAINING QUAD-SPECTRA, WHERE--
C      G(K) = C(K)-J*Q(K)
C
   55  CONTINUE
       IF(LLAGS-NLAGS) 36,36,35
   35  L=NLAGS+1
       DO 32 I=L,LLAGS
       RXY(I)=0.0
       RYX(I)=0.0
       IF (LSCALE) 61,62,61
   62  TLAGS(I)=I*DELT
       GO TO 32
```

```
 61 TLAGS(I)=I
 32 CONTINUE
    NLAGS=LLAGS
 36 CONTINUE
    PRINT 102, RUN,PHOTO1,PHOTO2
102 FORMAT(1X,4HRUN=F10.6,12HPHOTOMETER1=F10.6,12HPHOTOMETER2=F10.6)
    PRINT 22,NLAGS,DELT
 22 FORMAT(1X,6HNLAGS=I5,5X,5HDELT=F10.5)
    PRINT 100
100 FORMAT(1X,10HTIME  LAGS,4X,3HRXY,7X,3HRYX)
    PI=3.14159
    DT = DELT
    M = NLAGS
    R IS THE USUAL VARIABLE OF SUMMATION WHICH NORMALLY RUNS R=0,1,...
    ....,M--WHERE M IS THE NUMBER OF LAGS, FOR CORFUN, TAUMIN IS NOT
    NECESSARILY ZERO SO THAT THE RATIO R/M RUNS FROM RMIN TO 1.0
    RMIN=TLAGS(1)/TLAGS(M)

    RMAX = 1.0
    UV = M-1
    RDEL = (RMAX-RMIN)/UV

    COMPUTE R+ AND R-  BOTH WEIGHED BY LAG FUNCTION
    R = RMIN
    IF (TAUSHF) 400,400,401
401 CONTINUE
    MM=TAUSHF/DELT+1.0
    NLAGS=NLAGS-MM+1
    M=NLAGS
    DO 407 I=1,NLAGS
    N=I-1
    MK=N+MM
    RYX(MK)=RYX(I)
407 CONTINUE
    DO 409 I=2,M
    J=I-1
    J=J-MM
    IF (J+1) 402,403,404
402 J=ABSF(J)
    RYX(J)=RXY(I)
    GO TO 409
403 RXY(1)=RXY(MM)
    RYX(1)=RXY(MM)
    GO TO 409
404 J=J+2
    RXY(J)=RXY(I)
409 CONTINUE
    KK=0
    NN=NLAGS-MM
    KK=KK+NLAGS
    DO 411 I=1,MM
    NN=NN+1
    RXY(NN)=RXY(KK)
    KK=KK+1
411 CONTINUE
```

```
  400 CONTINUE
      DO 11 I=1,NLAGS
      IF(LSCALE) 51,52,51
   51 RXY(I)=RXY(I)*RSCALE
      RYX(I)=RYX(I)*RSCALE
   52 CONTINUE
      PRINT 30, TLAGS(I),RXY(I),RYX(I)
   30 FORMAT (1X,3F10.5)
   11 CONTINUE
      DO 5 I=1,M
C     COMPUTE PARZEN LAG WEIGHING FUNCTION
      IF(LPARZN) 40,40,41
   40 D=1.0
      GO TO 42
   41 CALL PARZEN (R,D)
   42 CONTINUE
      D = D/2.
      UV = RXY(I)
      T=UV+RYX(I)
      S=UV-RYX(I)
      RPL(I) = D*T
      RMI(I) = D*S
      PRINT 6, D,T,S
    6 FORMAT (3X,3F15.8)
      R = R+RDEL
    5 CONTINUE
C     COMPUTE VARIOUS CONSTANTS FOR TRANSFORM
      TWODT = 2.*DT
      FORDT = DT*4.
      TWOPI = 2.*PI
      R = RMIN
      N = M-1
      DO 20 I=1,M
      UV = R*PI
      CARG = UV
      CSUM = 0.
      QSUM = 0.
      DO 10 J=2,N
      ARG = CARG
      IF(ARG-TWOPI) 7,7,12
   12 CONTINUE
      IM = ARG/TWOPI
      FIM = IM
      ARG = CARG-FIM*TWOPI
    7 CONTINUE
      CSUM = CSUM+RPL(J)*COSF(ARG)
      QSUM = QSUM+RMI(J)*SINF(ARG)
      CARG = CARG+UV
   10 CONTINUE
      Q(I) = FORDT*QSUM
      C(I)=TWODT*(RPL(1)+((-1)**(I+1)*RPL(M)))+FORDT*CSUM
      R=R+RDEL
   20 CONTINUE
      UV=NLAGS
      IF(LSCALE) 8,9,8
```

```
    8 TLAGS(M)=TLAGS(M)*DELT
      TLAGS(1)=TLAGS(1)*DELT
    9 CONTINUE
      TMLAGU=TLAGS(M)
      TMLAGL=TLAGS(1)
      FMAX=.5*UV/(TMLAGU-TMLAGL)
      FMIN=0.
      FDEL=(FMAX-FMIN)/UV
      PRINT 103
  103 FORMAT (5X,9HFREQUENCY,3X,9HCOSPECTRA,1X,11HQUADSPECTRA,6X,4HGAIN,
     14X,10HCROSS  PSD,3X,5HPHASE,4X,9HLOG  FREQ,5X,9HLOG  GAIN,3X,
     113HLOG CROSS PSD)
      DO 3010 I=1,NLAGS
      GAIN=SQRTF(C(I)*C(I) + Q(I)*Q(I))
      IF (C(I))3015,3012,3015
 3015 CONTINUE
      PHASE=Q(I)/C(I)
      PHASE=ATANF(PHASE)
      GO TO 3013
 3012 PHASE=1.5708
 3013 CONTINUE
      IF (C(I)) 3333,3334,3334
 3333 PHASE=PHASE+3.14159
 3334 IF (PHASE) 3335,3336,3336
 3335 PHASE=PHASE+6.28318
 3336 CONTINUE
      PHA=57.29582*PHASE
      CPSD=GAIN*FMIN
      IF(FMIN) 1001,1001,1002
 1002 CONTINUE
      CLOG=ALOG(CPSD)*0.4343
      FLOG=ALOG(FMIN)*0.4343
 1001 CONTINUE
      GLOG=ALOG(GAIN)*0.4343
      PRINT 21,FMIN,C(I),Q(I),GAIN,CPSD,PHA,FLOG,GLOG,CLOG
   21 FORMAT (1X,9F12.6)
      C(I)=C(I)/10
      Q(I)=Q(I)/10
      FLOG=FLOG/10
      GLOG=GLOG/10
      CLOG=CLOG/10
   23 FORMAT (1X,9F8.5)
      PUNCH 23,FMIN,C(I),Q(I),GAIN,CPSD,PHASE,FLOG,GLOG,CLOG
      FMIN=FMIN+FDEL
 3010 CONTINUE
      READ 56, NTEST
   56 FORMAT (I3)
      IF (NTEST) 4007,39,4006
 4006 CONTINUE
      STOP
      END

      SUBROUTINE PARZEN(R,D)
      RC = R
      Q = 1.-RC
```

```
      IF(RC-.5)10,10,20
10    D = 1.-(6.*RC*RC*Q)
      RETURN
20    D = 2.*Q*Q*Q
      RETURN
      END
```

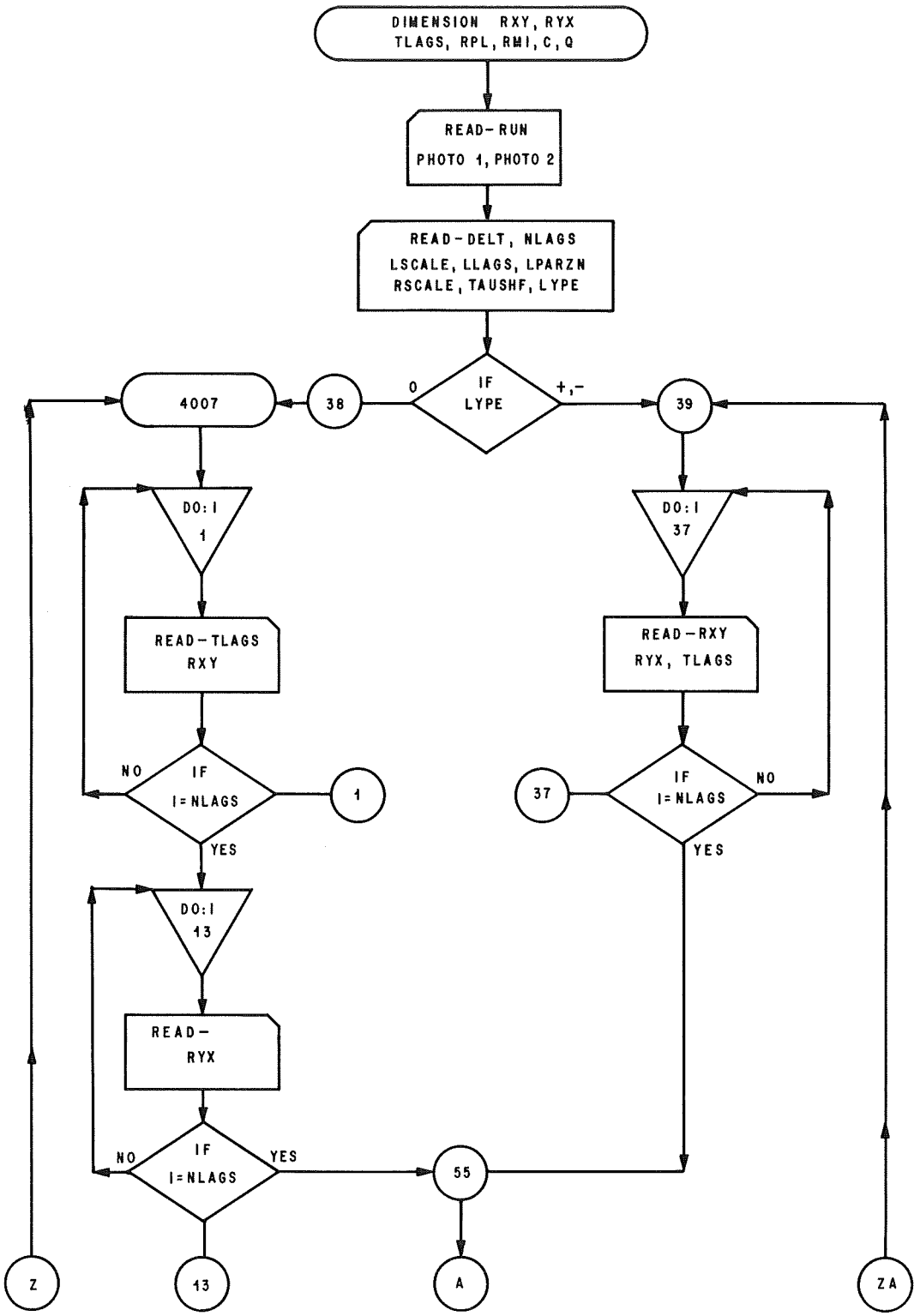
DIMENSION RXY, RYX
TLAGS, RPL, RMI, C, Q
READ-RUN
PHOTO 1, PHOTO 2
READ-DELT, NLAGS
LSCALE, LLAGS, LPARZN
RSCALE, TAUSHF, LYPE
IF
LYPE
0
+,-
38
39
4007
DO: I
1
READ-TLAGS
RXY
IF
I=NLAGS
NO
YES
1
DO: I
13
READ-
RYX
IF
I=NLAGS
NO
YES
13
DO: I
37
READ-RXY
RYX, TLAGS
IF
I=NLAGS
NO
YES
37
55
Z
A
ZA

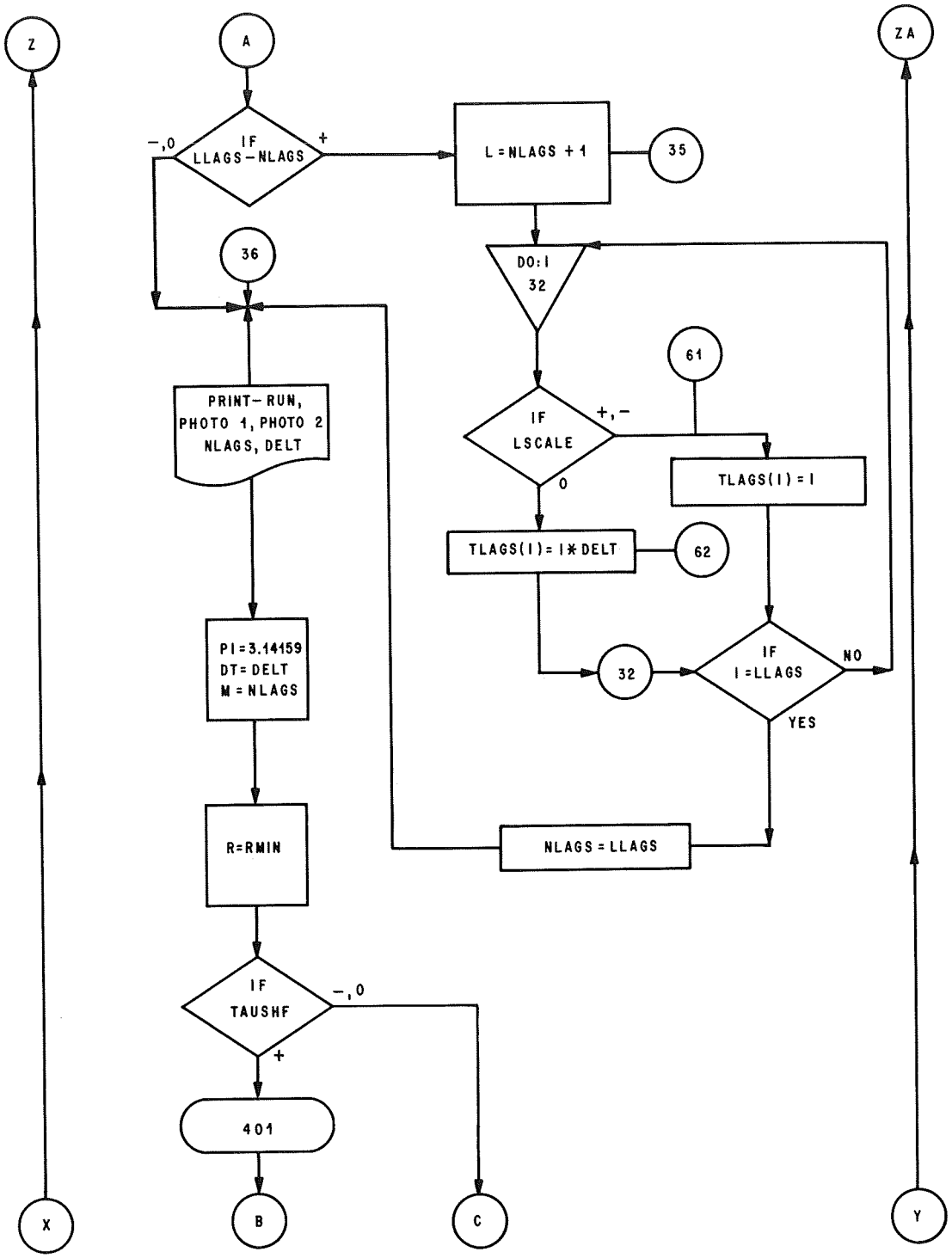
Z
A
ZA
IF
LLAGS – NLAGS
–,0
+
L = NLAGS + 1
35
36
DO: I
32
61
IF
LSCALE
+,–
0
TLAGS(I) = I
TLAGS(I) = I * DELT
62
PRINT– RUN,
PHOTO 1, PHOTO 2
NLAGS, DELT
PI = 3.14159
DT = DELT
M = NLAGS
32
IF
I = LLAGS
NO
YES
R=RMIN
NLAGS = LLAGS
IF
TAUSHF
–,0
+
401
X
B
C
Y

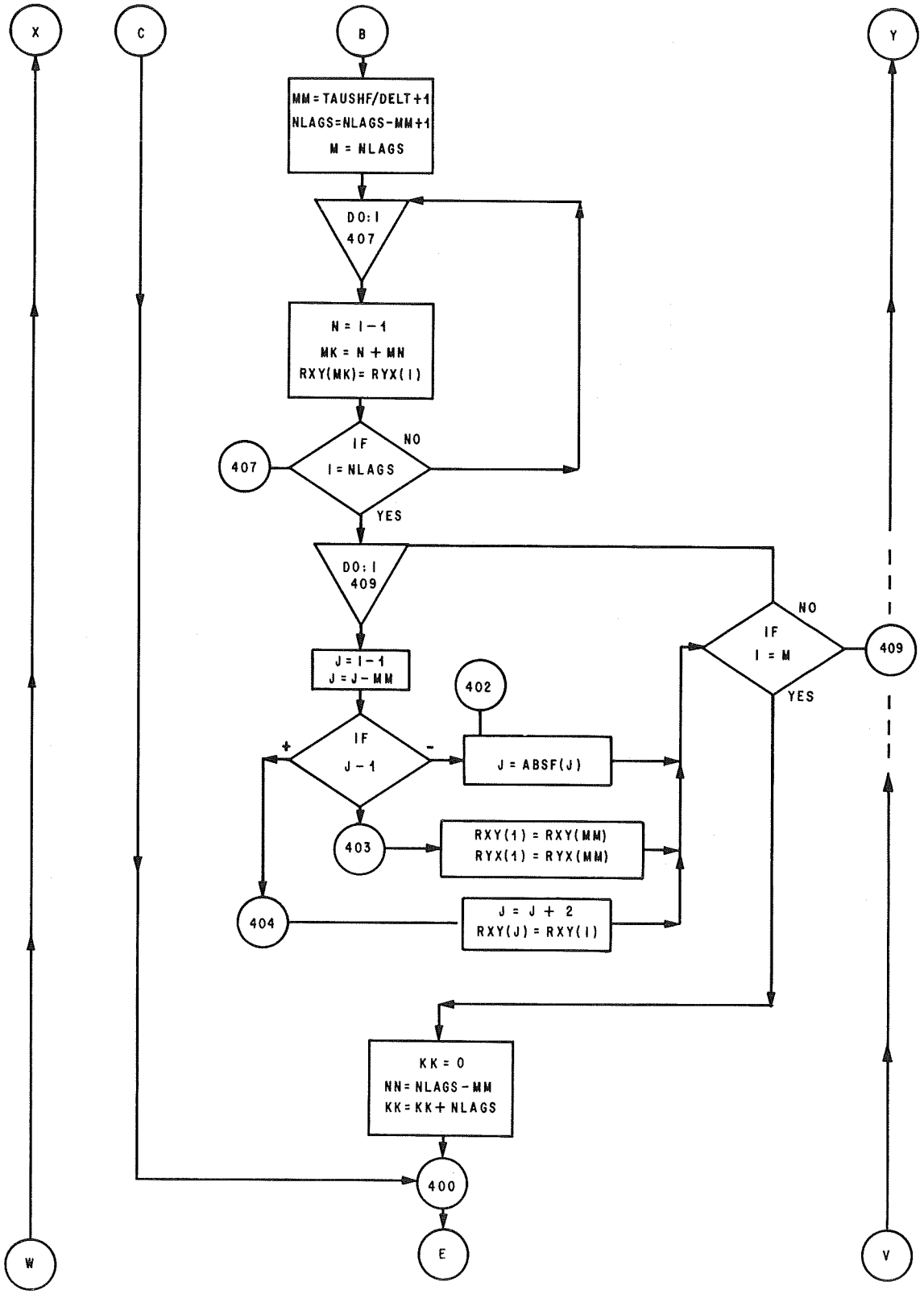
X
C
B
Y
MM = TAUSHF/DELT + 1
NLAGS = NLAGS - MM + 1
M = NLAGS
DO: I
407
N = I - 1
MK = N + MN
RXY(MK) = RYX(I)
IF
I = NLAGS
NO
YES
407
DO: I
409
J = I - 1
J = J - MM
IF
J - 1
+
-
402
J = ABSF(J)
403
RXY(1) = RXY(MM)
RYX(1) = RYX(MM)
404
J = J + 2
RXY(J) = RXY(I)
IF
I = M
NO
YES
409
KK = 0
NN = NLAGS - MM
KK = KK + NLAGS
400
E
W
V

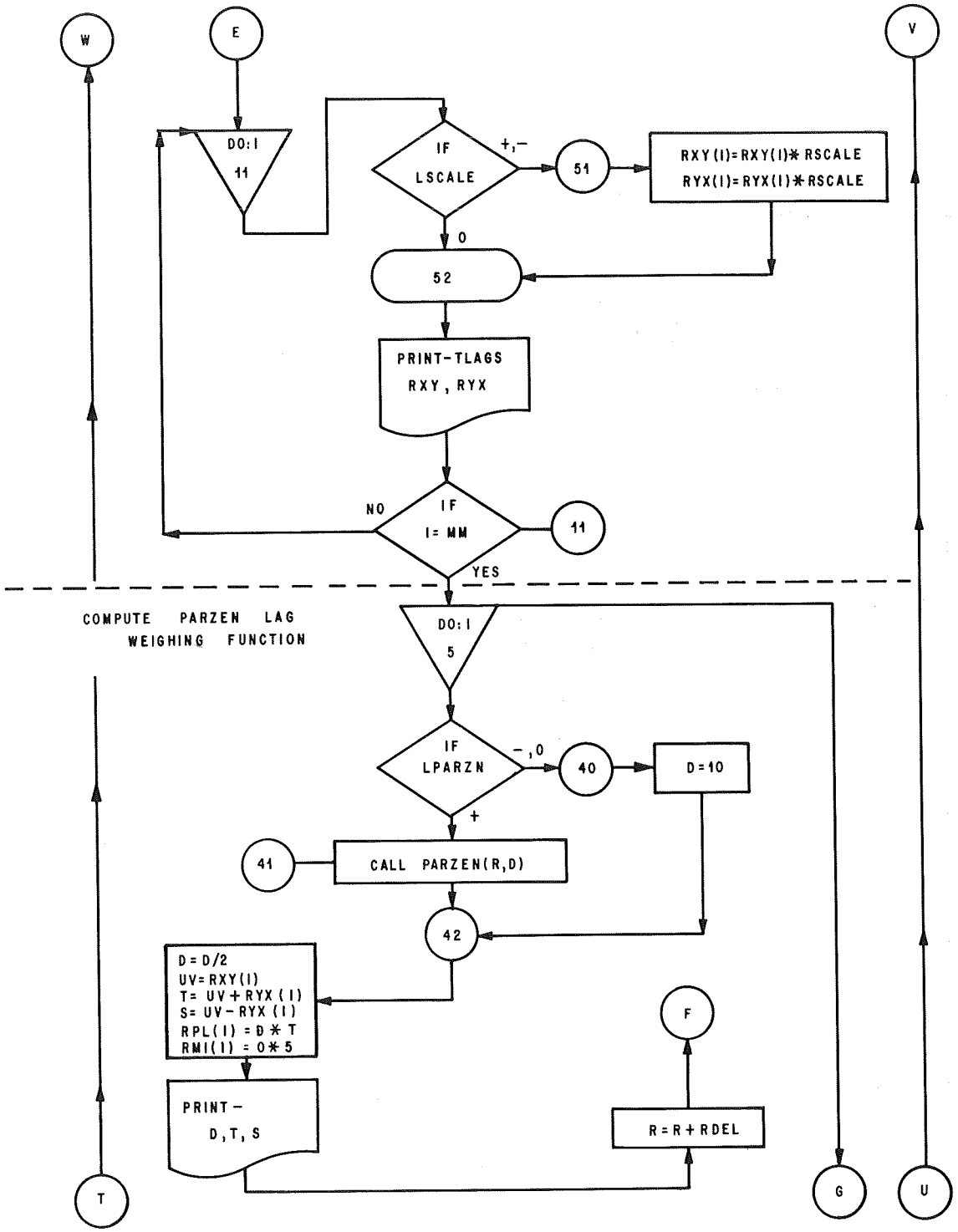
W
E
V
DO: I
11
IF
LSCALE
+,−
51
RXY(I)=RXY(I)* RSCALE
RYX(I)=RYX(I)*RSCALE
0
52
PRINT-TLAGS
RXY, RYX
NO
IF
I= MM
11
YES
COMPUTE PARZEN LAG
WEIGHING FUNCTION
DO: I
5
IF
LPARZN
−,0
40
D=10
+
41
CALL PARZEN(R,D)
42
D=D/2
UV=RXY(I)
T= UV+RYX(I)
S= UV−RYX(I)
RPL(I) = D * T
RMI(I) = 0*5
PRINT−
D, T, S
F
R=R+RDEL
T
G
U

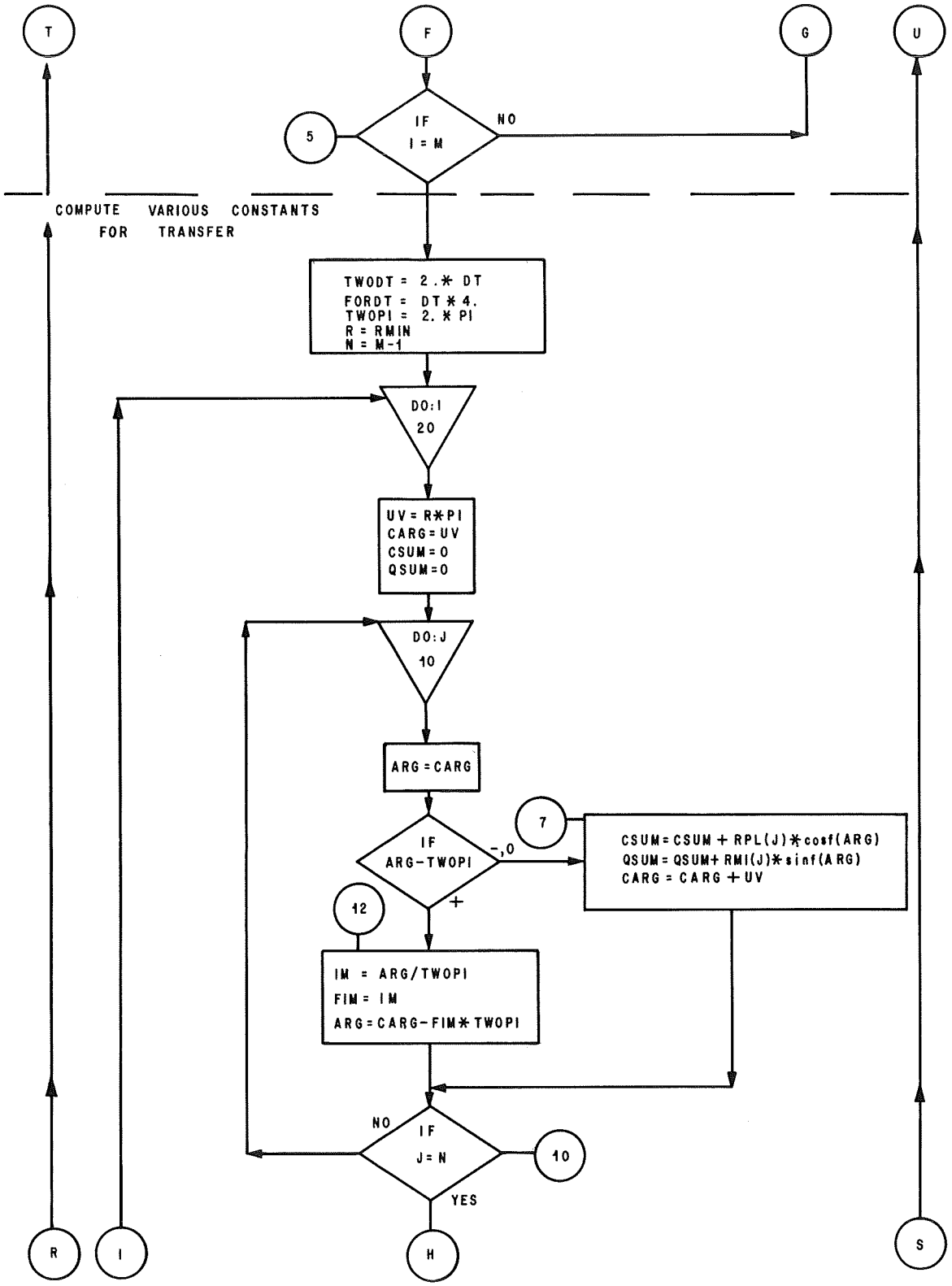
T
F
G
U
5
IF
I = M
NO
COMPUTE VARIOUS CONSTANTS
FOR TRANSFER
TWODT = 2.* DT
FORDT = DT * 4.
TWOPI = 2. * PI
R = RMIN
N = M-1
DO:I
20
UV = R*PI
CARG = UV
CSUM = 0
QSUM = 0
DO:J
10
ARG = CARG
7
IF
ARG-TWOPI
-,0
+
CSUM = CSUM + RPL(J)*cosf(ARG)
QSUM = QSUM + RMI(J)*sinf(ARG)
CARG = CARG + UV
12
IM = ARG/TWOPI
FIM = IM
ARG = CARG-FIM*TWOPI
NO
IF
J = N
10
YES
R
I
H
S

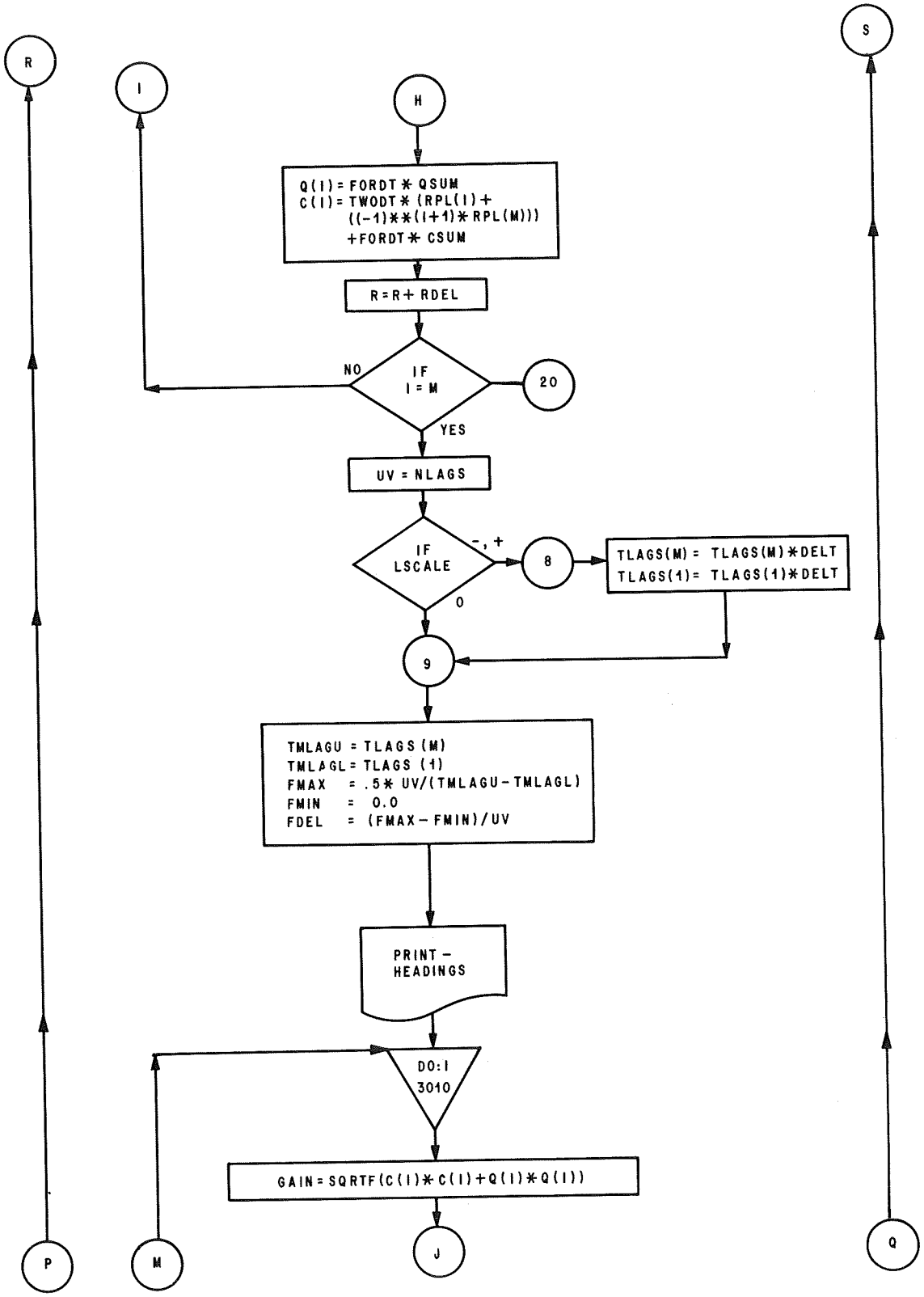
R
I
H
S
Q(I) = FORDT * QSUM
C(I) = TWODT * (RPL(I) +
((-1)**(I+1) * RPL(M)))
+FORDT * CSUM
R = R + RDEL
NO
IF
I = M
20
YES
UV = NLAGS
IF
LSCALE
-, +
8
TLAGS(M) = TLAGS(M) * DELT
TLAGS(1) = TLAGS(1) * DELT
0
9
TMLAGU = TLAGS(M)
TMLAGL = TLAGS(1)
FMAX = .5 * UV/(TMLAGU - TMLAGL)
FMIN = 0.0
FDEL = (FMAX - FMIN)/UV
PRINT -
HEADINGS
DO: I
3010
GAIN = SQRTF(C(I) * C(I) + Q(I) * Q(I))
P
M
J
Q

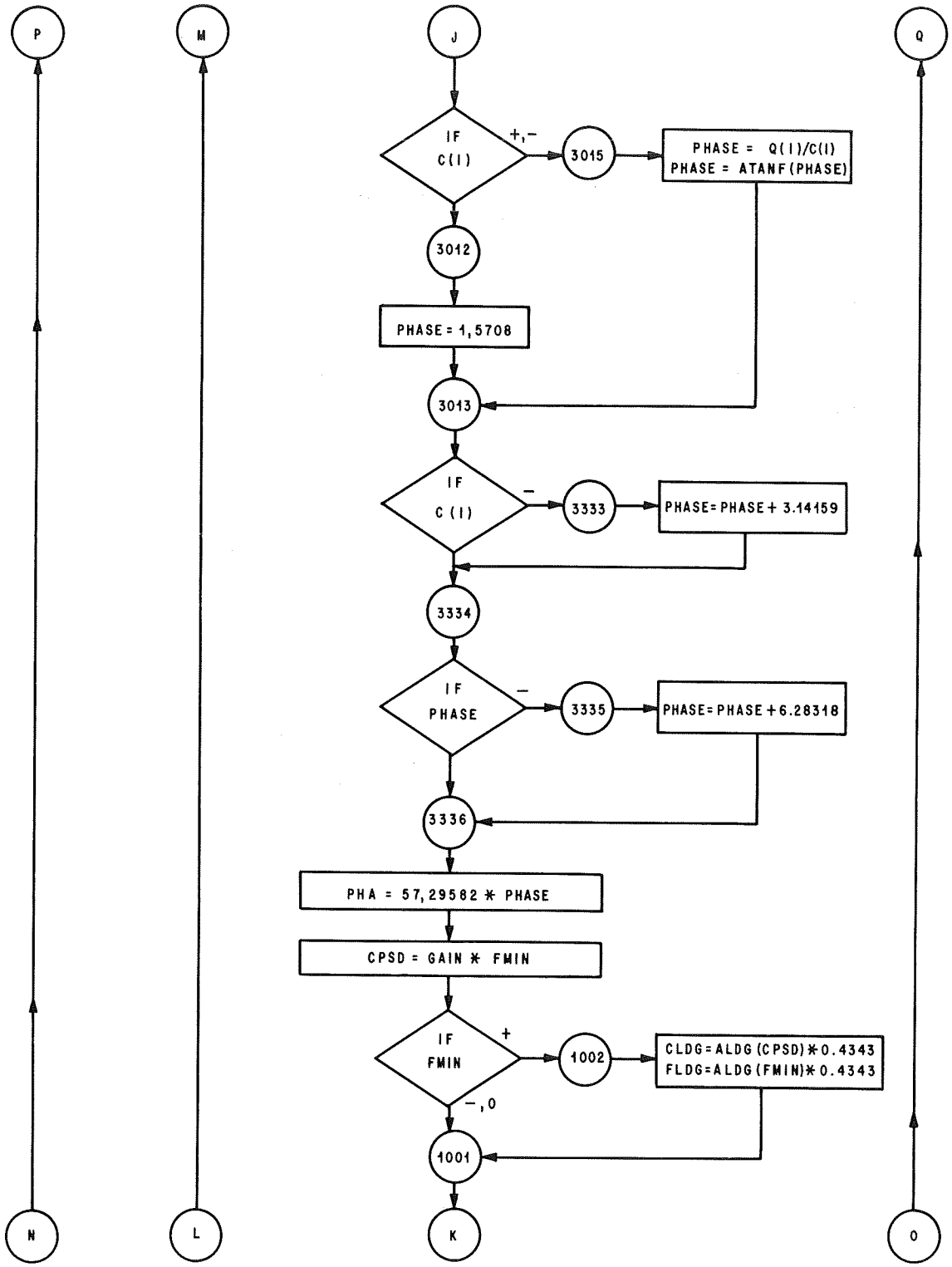
P
M
J
Q
IF
C(I)
+,-
3015
PHASE = Q(I)/C(I)
PHASE = ATANF(PHASE)
3012
PHASE = 1,5708
3013
IF
C(I)
-
3333
PHASE=PHASE+3.14159
3334
IF
PHASE
-
3335
PHASE=PHASE+6.28318
3336
PHA = 57,29582 * PHASE
CPSD = GAIN * FMIN
IF
FMIN
+
1002
CLDG=ALDG(CPSD)*0.4343
FLDG=ALDG(FMIN)*0.4343
-,0
1001
N
L
K
O

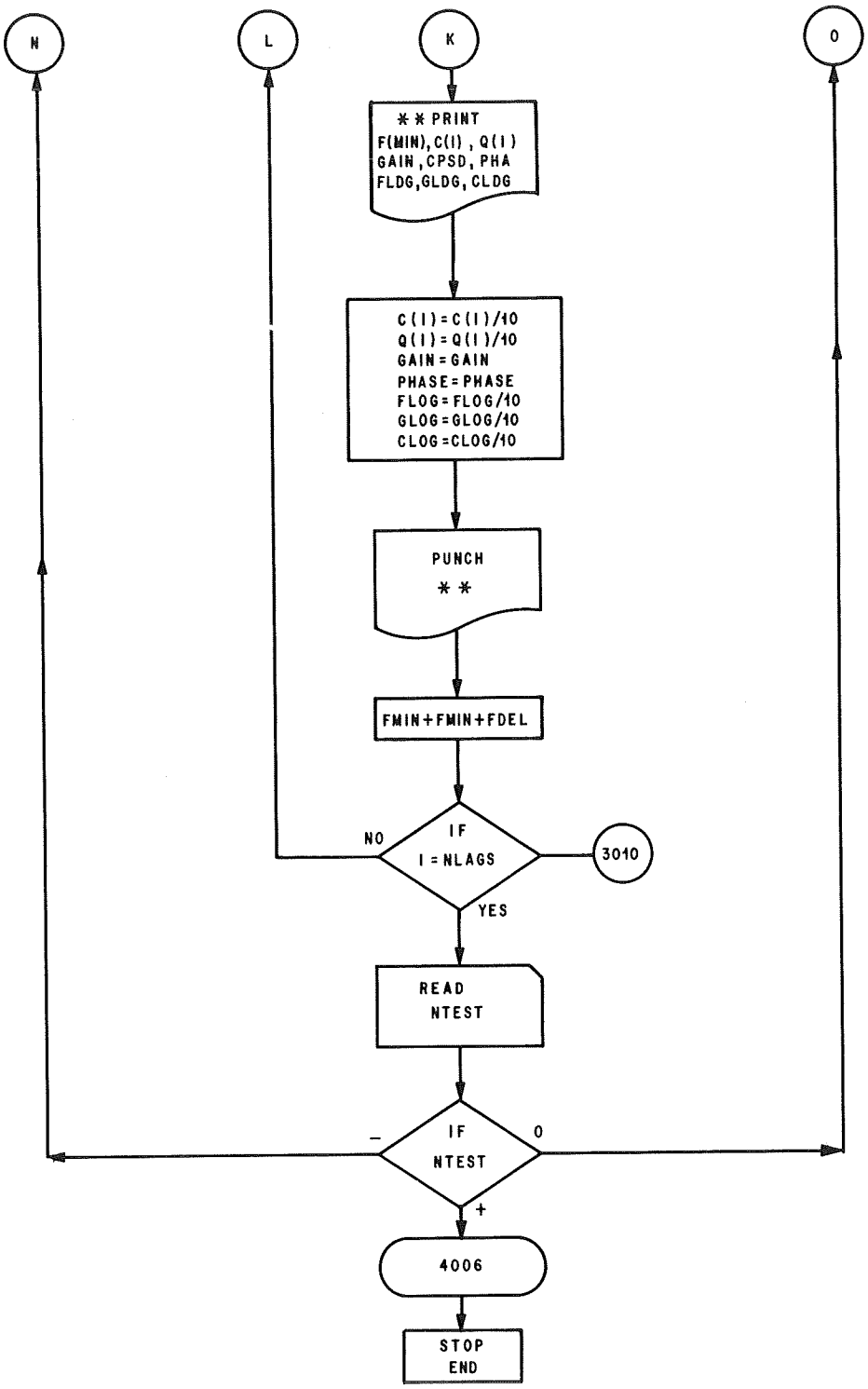
N
L
K
O
** PRINT
F(MIN), C(I), Q(I)
GAIN, CPSD, PHA
FLDG, GLDG, CLDG
C(I) = C(I)/10
Q(I) = Q(I)/10
GAIN = GAIN
PHASE = PHASE
FLOG = FLOG/10
GLOG = GLOG/10
CLOG = CLOG/10
PUNCH
* *
FMIN + FMIN + FDEL
IF
I = NLAGS
NO
3010
YES
READ
NTEST
IF
NTEST
–
0
+
4006
STOP
END

SUBROUTINE PARZEN (R, D)

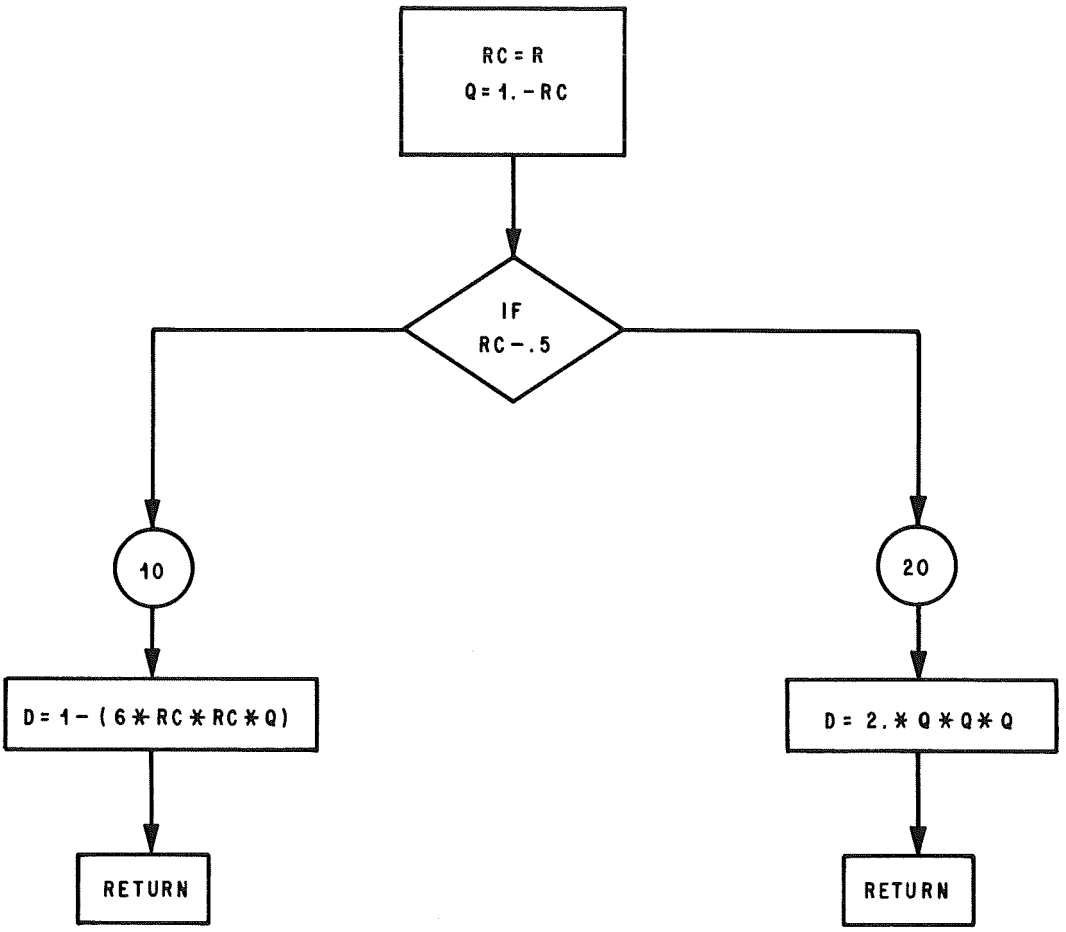

APPENDIX II

PROGRAM FOR FOURIER TRANSPOSE

This program is designed to calculate the covariance function from the spectra. This is done by using a Fourier transpose of the gain and phase to convert from a frequency domain to a time domain.

One property of this program is that all or any group of frequencies (from 0.01 - 4.0 cps) can be either omitted or used in calculating the covariance curve. The inputs must include the beginning frequency and the ending frequency along with any certain frequencies to be omitted from the calculations.

Table 5 shows available computers, maximum run time, and a definition of input terms. Also shown are the output parameters for both printed and punched outputs. Table 6 shows a loading procedure for data along with the input parameters.

TABLE 5

COMPUTER:	SDS 930	CDC 3200
RUN TIME:	DEPENDENT ON THE FREQUENCY RANGE DESIRED--FROM 0.01-4.0 cps MAX. TIME IS 25 MINUTES. TIME IS DECREASED BY USING CDC 3200.	

DEFINITIONS OF INPUT DATA:

INPUT CARD (1)	NLAGS	NUMBER OF TIME LAG POINTS WHICH YOU INTEND TO CALCULATE.
	DELTAU	TIME LAG BETWEEN POINTS.
	BFREQ	FREQUENCY AT WHICH CALCULATIONS ARE TO BEGIN.
	EFREQ	FREQUENCY AT WHICH CALCULATIONS SHOULD BE STOPPED.
INPUT CARDS (2)	SKIP	FREQUENCY THAT IS TO BE OMITTED FROM CALCULATIONS.
	M	IF EQUAL TO 0, IT MEANS TO READ ANOTHER SKIP VALUE; IF EQUAL TO 1, THEN ALL SKIP VALUES HAVE BEEN READ IN AND THE SKIP LOOP IS TERMINATED.

TABLE 5 - con't

INPUT DATA (3)

FREQ
GAIN
PHASE

THIS DATA IS THE DIRECT OUTPUT FROM THE PROGRAM IN APPENDIX I.

OUTPUTS

PRINTED:

NLAGS	DELTAU	BFREQ	EFREQ
XXXX	X.XXXX	XX.XXXX	XX.XXXX

(LSKIP)	SKIP FREQ
XX	X.XXXXXX
⋮	⋮
XX	X.XXXXXX

TABLE 5 — OUTPUTS con't

FREQUENCY LESS THAN BFREQ.

FREQUENCY	GAIN	PHASE
xxxx.xxxxxx	xxxx.xxxxxx	xxxx.xxxxxx
⋮	⋮	⋮
xxxx.xxxxxx	xxxx.xxxxxx	xxxx.xxxxxx

FREQUENCY	GAIN	PHASE
xxxx.xxxxxx	xxxx.xxxxxx	xxxx.xxxxxx
⋮	⋮	⋮
xxxx.xxxxxx	xxxx.xxxxxx	xxxx.xxxxxx

TAU	RXY	-TAU	RYX
xxxx.xxxxxx	xxxx.xxxxxx	xxxx.xxxxxx	xxxx.xxxxxx
⋮	⋮	⋮	⋮
xxxx.xxxxxx	xxxx.xxxxxx	xxxx.xxxxxx	xxxx.xxxxxx

TABLE 5 — OUTPUTS con't

PUNCHED OUTPUTS

PUNCHED FOR SPECIAL PLOTTING PURPOSES

TAU	I2	RXY	I3	-TAU	I4	RYX
XX.XXXX ⋮ XX.XXXX	INTEGER EITHER -1 FOR NEGATIVE NUMBER, OR 0 FOR POSITIVE NUMBER	XX.XXXX ⋮ XX.XXXX	SAME AS I2	XX.XXXX ⋮ XX.XXXX	SAME AS I2	XX.XXXX ⋮ XX.XXXX

TABLE 6

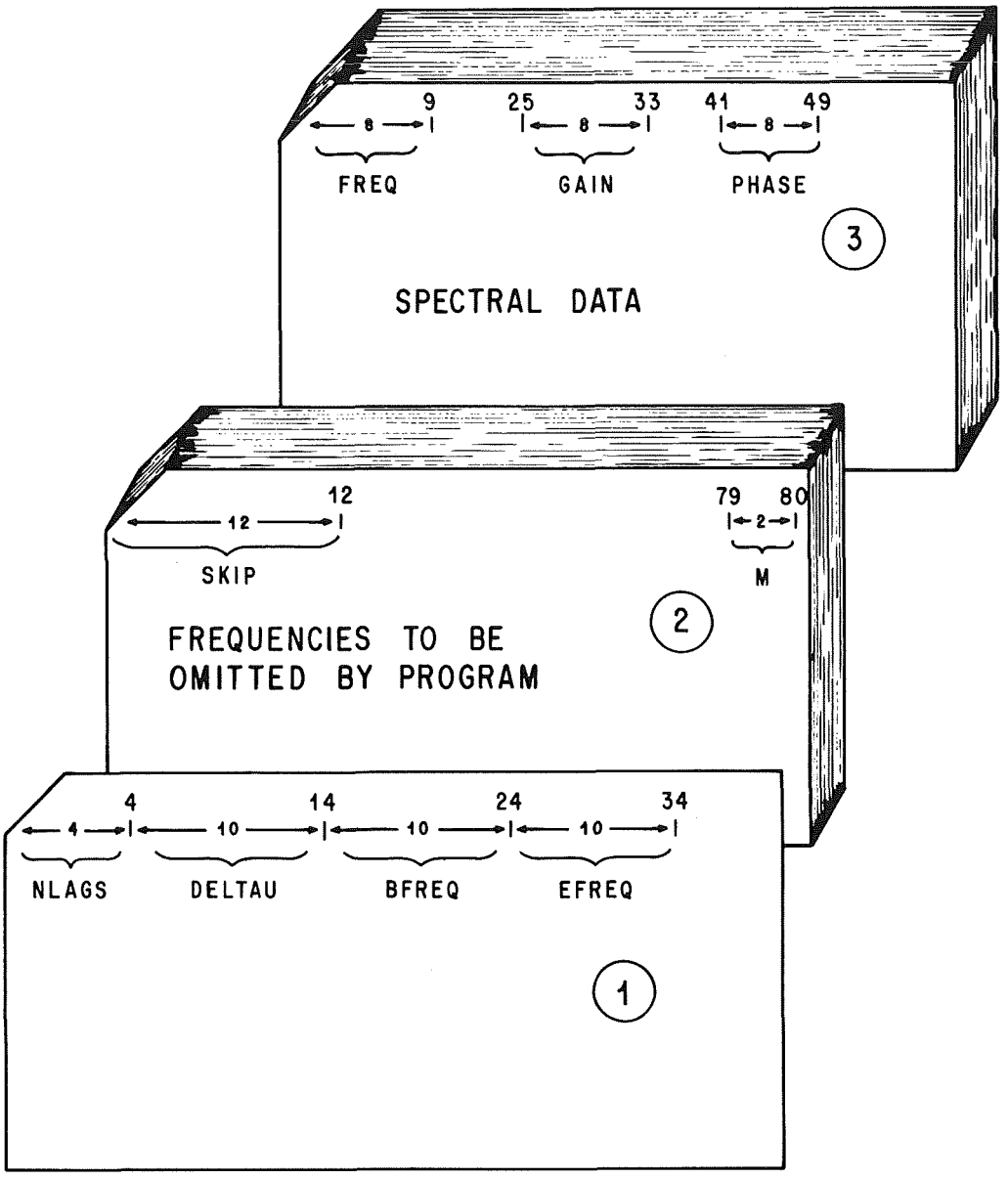
9
25
33
41
49
8
8
8
FREQ
GAIN
PHASE
3
SPECTRAL DATA
12
79
80
12
2
SKIP
M
2
FREQUENCIES TO BE
OMITTED BY PROGRAM
4
14
24
34
4
10
10
10
NLAGS
DELTAU
BFREQ
EFREQ
1

FOURIER TRANSPOSE PROGRAM

```
      DIMENSION C1(402),C2(402),SKIP(50)


      THIS PROGRAM WILL TAKE THE FINAL SPECTRA AND SUPPOSSEDLY COMPUTE
      THE CORRELATION CURVE FROM THE SPECTRA


      READ 1, NLAGS,DELTAU,BFREQ,EFREQ
    1 FORMAT (I4,3F10.0)
      PRINT 31
   31 FORMAT (4X,5HNLAGS,5X,6HDELTAU,5X,5HBFREQ,5X,5HEFREQ)
      PRINT 32, NLAGS,DELTAU,BFREQ,EFREQ
   32 FORMAT(4X,F5.3,5X,F6.4,5X,F5.3,5X,F5.3,///)
      LSKIP=0
      PRINT 33
   33 FORMAT (7X,10HSKIP FREQ.)
      DO 2 L=1,50
      LSKIP=LSKIP+1
      READ 3, SKIP(L),M
    3 FORMAT (F12.0,66X,I2)
      PRINT 30, LSKIP,SKIP(L)
   30 FORMAT (I2,5X,F8.6)
      IF (M) 4,2,4
    2 CONTINUE
    4 CONTINUE
      DO 5 I=1,NLAGS
      C1(I)=0.0
      C2(I)=0.0
    5 CONTINUE
      PRINT 34
   34 FORMAT (///,1X,21H FREQ LESS THAN BFREQ)
      DO 12 J=1,NLAGS
      READ 6, FREQ, GAIN, PHASE
    6 FORMAT (1X,F8.0,16X,F8.0,8X,F8.0)
      PRINT 26, FREQ,GAIN,PHASE
   26 FORMAT (1X,3F15.6)
      IF (FREQ-BFREQ) 12,7,12
   12 CONTINUE
    7 CONTINUE
      PRINT 35
   35 FORMAT (///,57X,4HFREQ,11X,4HGAIN,9X,5HPHASE)
      DO 11 K=1,NLAGS
      READ 6, FREQ, GAIN, PHASE
      PRINT 27, FREQ,GAIN,PHASE
   27 FORMAT (50X,3F15.6)
      IF (FREQ-EFREQ) 8,13,8
    8 CONTINUE
      DO 9 L=1,LSKIP
      IF (FREQ-SKIP(L)) 9,111,9
  111 PRINT 28, FREQ,GAIN,PHASE
   28 FORMAT (1X,25HFREQ GAIN_PHASE__LEFT OUT,3F15.6)
      GO TO 11
    9 CONTINUE
      TAU=0.0
```

```
      TAUN=-TAU
      DO 10 I=1,NLAGS
      RP=(2.*3.14159*FREQ*TAU)
      RM=(2.*3.14159*FREQ*TAUN)
      A=RP-PHASE
      B=RM-PHASE
      CP=GAIN*COS(A)
      CN=GAIN*COS(B)
      C1(I)=C1(I)+CP
      C2(I)=C2(I)+CN
      TAU=TAU+DELTAU
      TAUN=-TAU
   10 CONTINUE
   11 CONTINUE
   13 TAU=0.0
      TAUN=-TAU
      PRINT 41
   41 FORMAT (14X,3HTAU,14X,3HRXY,13X,4H-TAU,14X,3HRYX)
      DO 24 I=1,NLAGS
      PRINT 40, TAU,C1(I),TAUN,C2(I)
   40 FORMAT (5X,4F15.6)
      IF (C1(I)) 14,15,15
   14 C1(I)=C1(I)*(-1.)
      I2=-1
      GO TO 16
   15 I2=0
   16 IF (TAUN) 17,18,18
   17 TAUN=TAUN*(-1.)
      I3=-1
      GO TO 19
   18 I3=0
   19 IF (C2(I)) 20,21,21
   20 C2(I)=C2(I)*(-1)
      I4=-1
      GO TO 22
   21 I4=0
   22 PUNCH 23, TAU,I2,C1(I),I3,TAUN,I4,C2(I)
   23 FORMAT (5X,F10.6,3(4X,I2,F10.6))
      TAU=TAU+DELTAU
      TAUN=-TAU
   24 CONTINUE
      STOP
      END
```

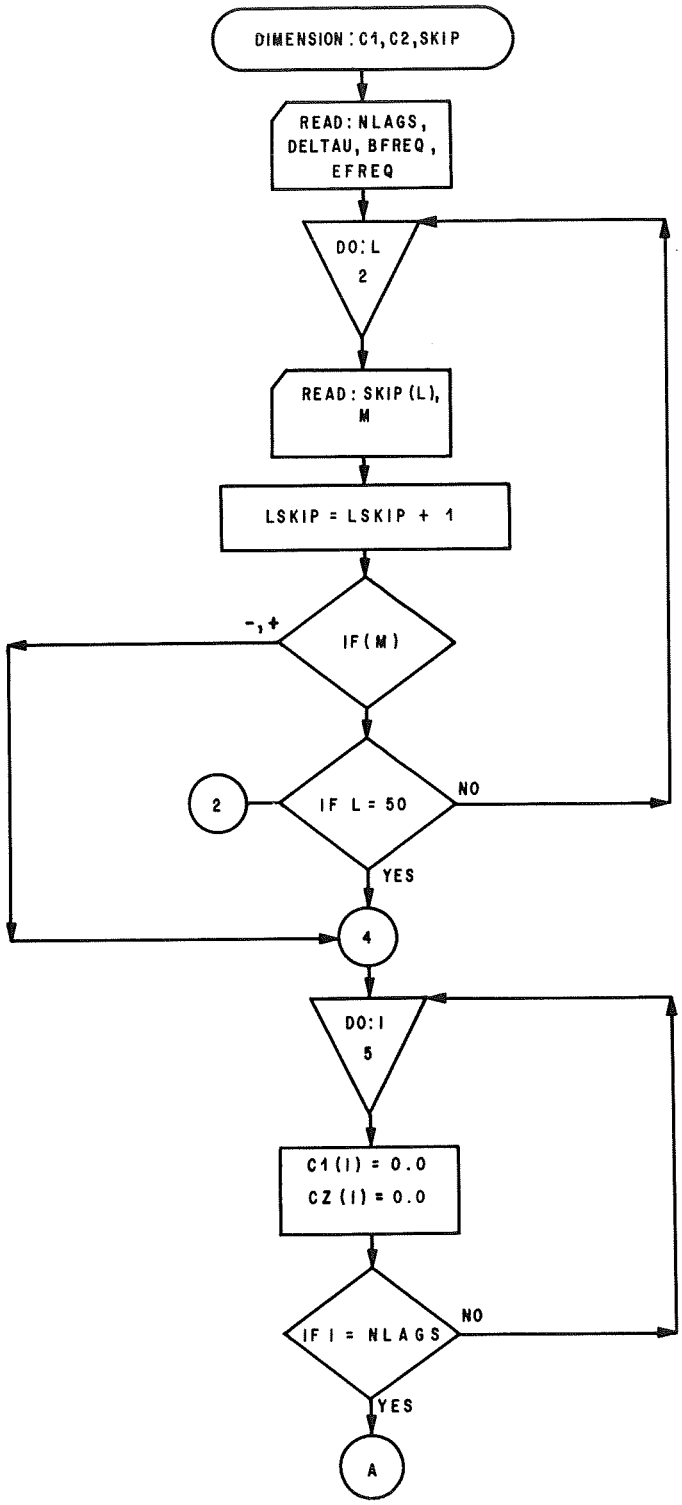
DIMENSION : C1, C2, SKIP
READ : NLAGS, DELTAU, BFREQ, EFREQ
DO : L 2
READ : SKIP (L), M
LSKIP = LSKIP + 1
IF (M)
-, +
2
IF L = 50
NO
YES
4
DO : I 5
C1 (I) = 0.0
CZ (I) = 0.0
IF I = NLAGS
NO
YES
A

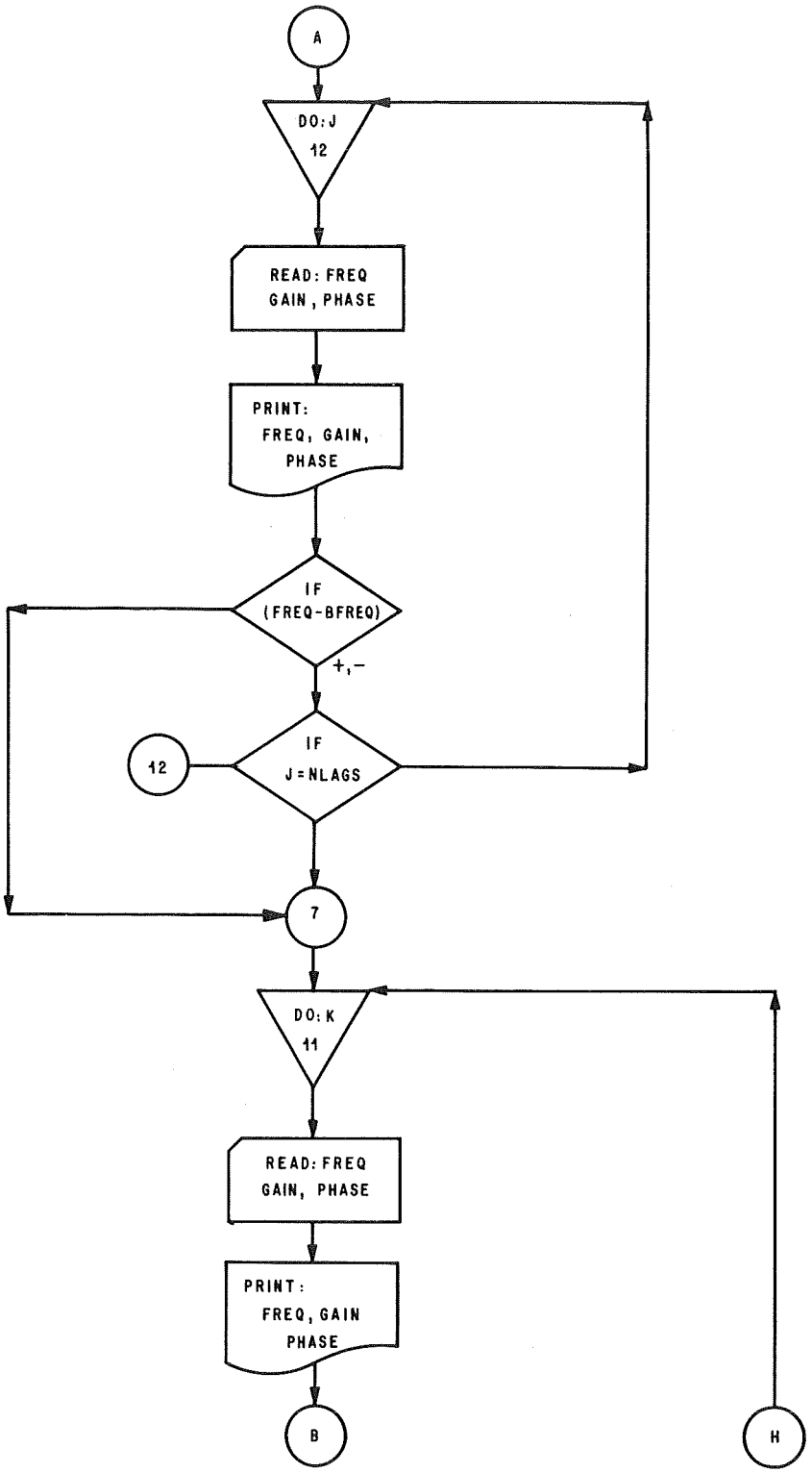
A
DO: J
12
READ: FREQ
GAIN , PHASE
PRINT:
FREQ, GAIN,
PHASE
IF
(FREQ-BFREQ)
+,-
12
IF
J = NLAGS
7
DO: K
11
READ: FREQ
GAIN, PHASE
PRINT:
FREQ, GAIN
PHASE
B
H

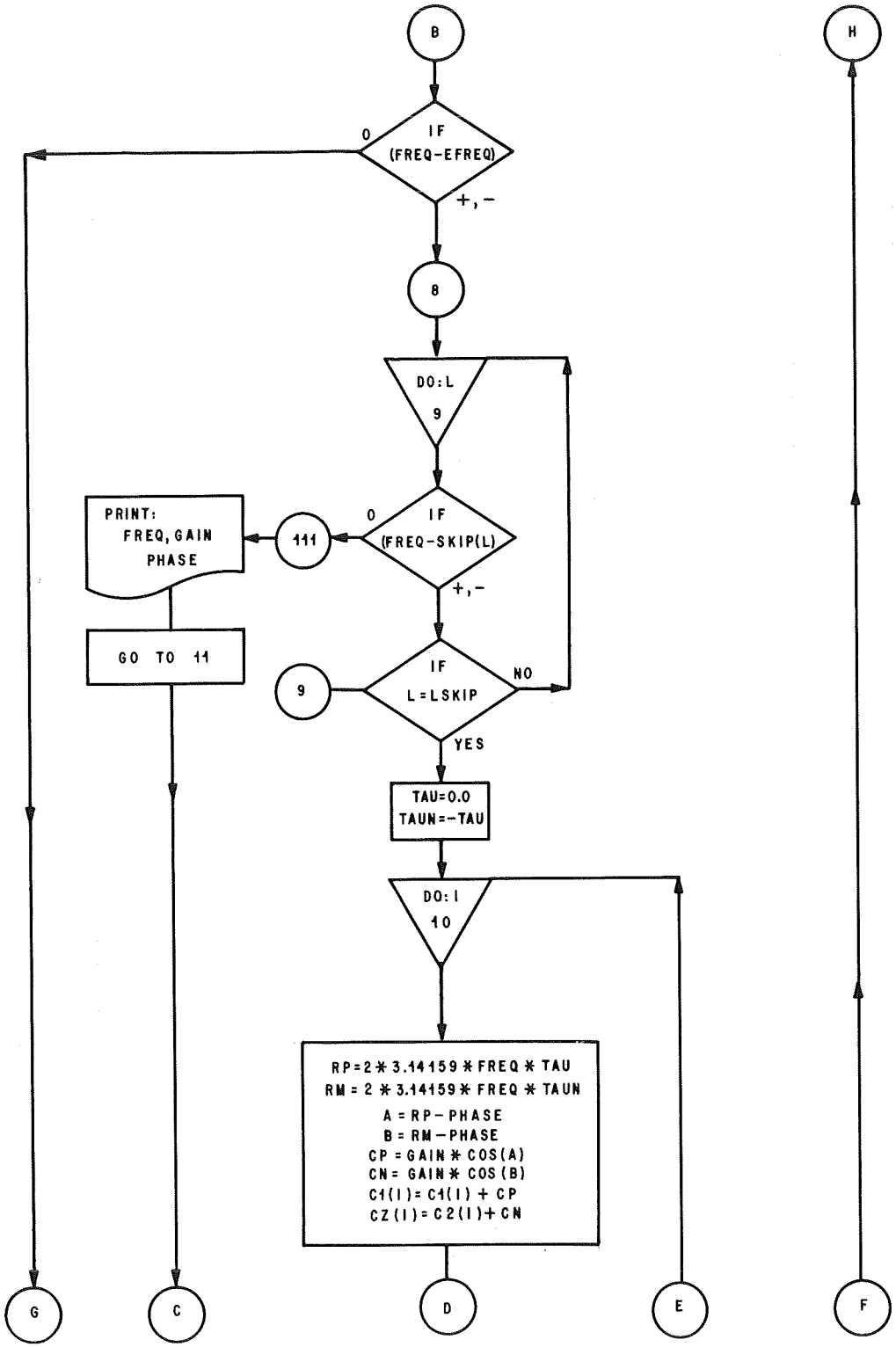
B
H
0
IF
(FREQ-EFREQ)
+,-
8
DO:L
9
PRINT:
FREQ, GAIN
PHASE
111
0
IF
(FREQ-SKIP(L)
+,-
GO TO 11
9
IF
L=LSKIP
NO
YES
TAU=0.0
TAUN=-TAU
DO:I
10
RP=2*3.14159*FREQ*TAU
RM=2*3.14159*FREQ*TAUN
A=RP-PHASE
B=RM-PHASE
CP=GAIN*COS(A)
CN=GAIN*COS(B)
C1(I)=C1(I)+CP
C2(I)=C2(I)+CN
G
C
D
E
F

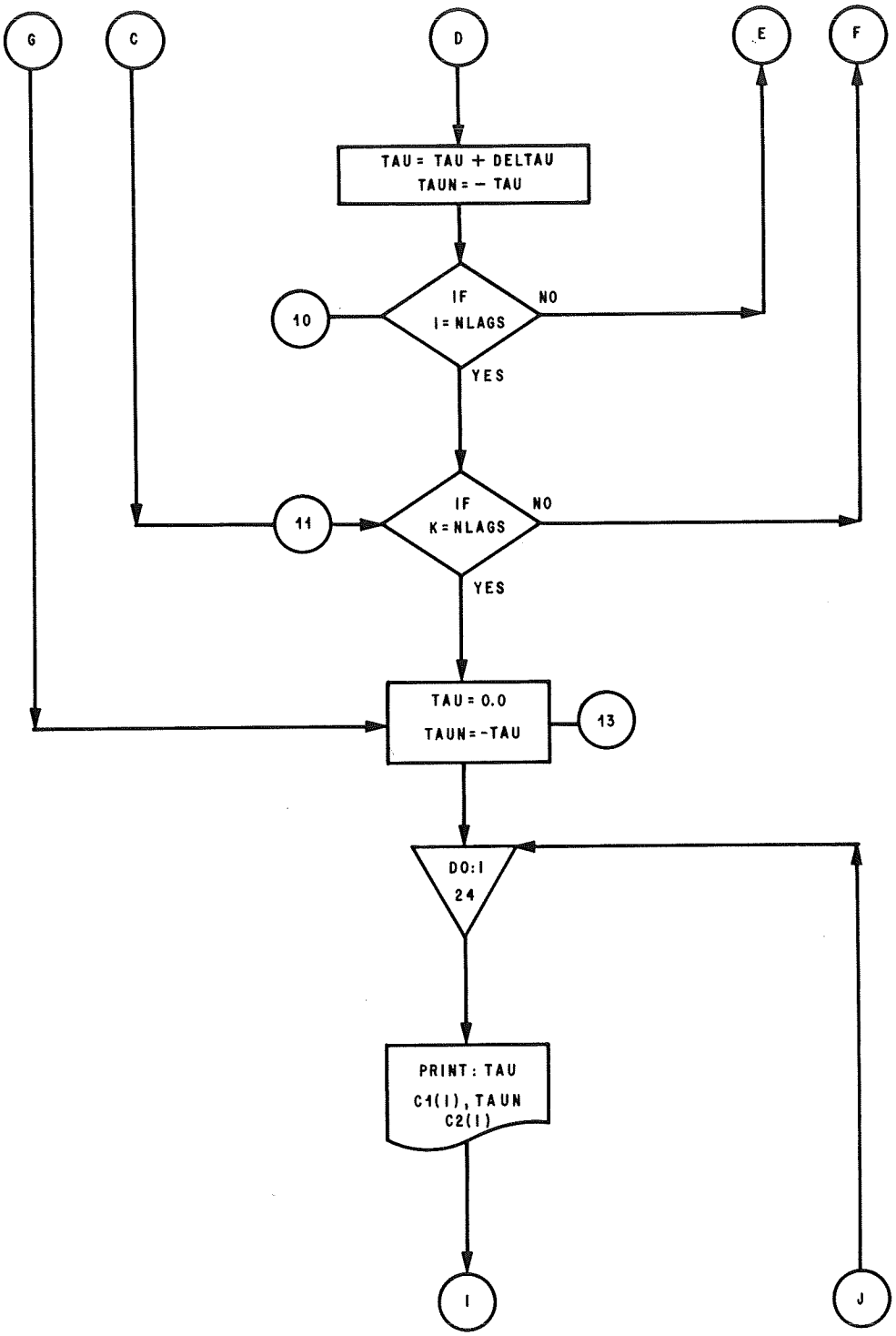
G
C
D
E
F
TAU = TAU + DELTAU
TAUN = – TAU
10
IF
I = NLAGS
NO
YES
11
IF
K = NLAGS
NO
YES
TAU = 0.0
TAUN = -TAU
13
DO: I
24
PRINT: TAU
C1(I), TAUN
C2(I)
I
J

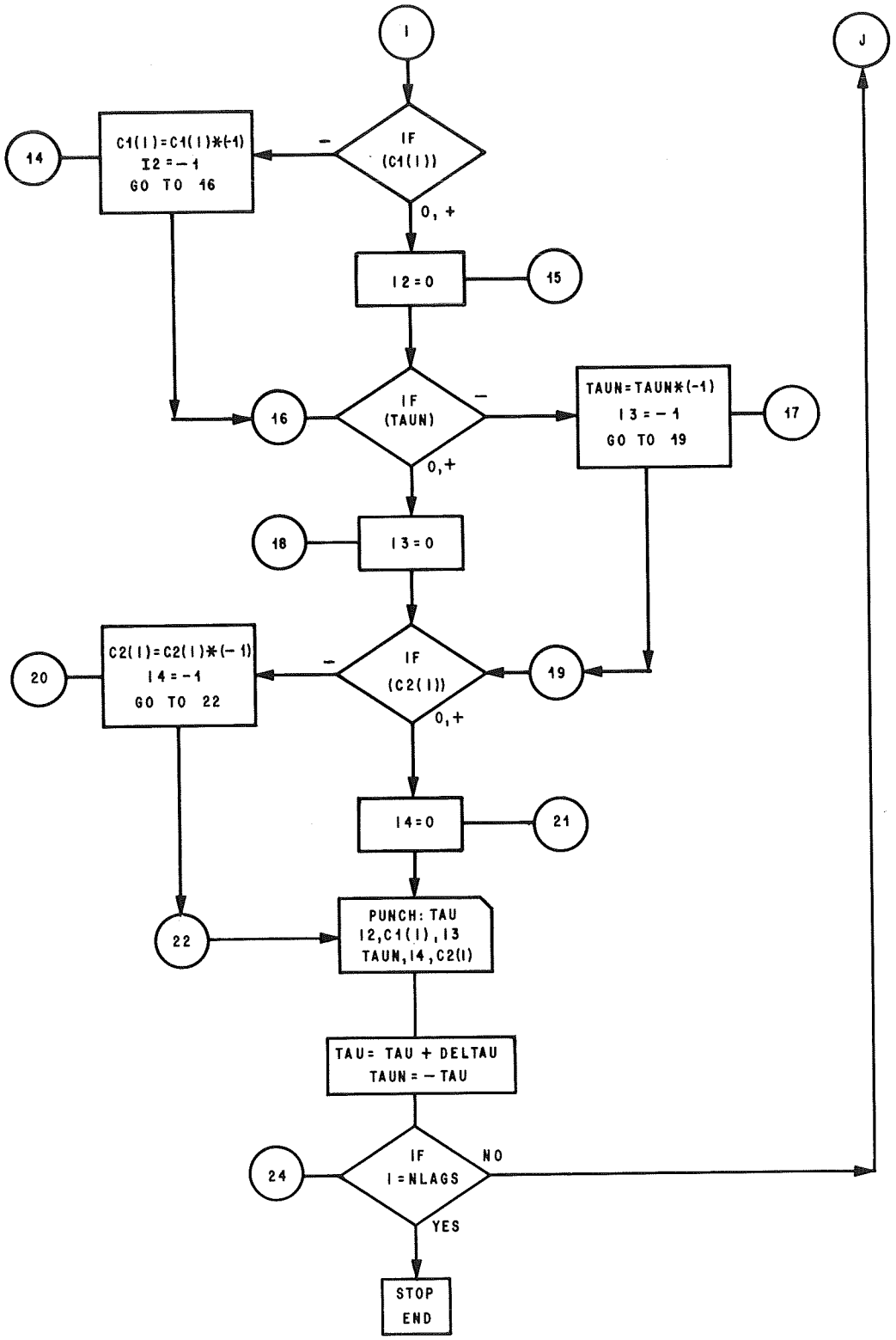
I
J
IF
(C1(I))
-
0, +
C1(I)=C1(I)*(-1)
I2 = -1
GO TO 16
14
I2=0
15
IF
(TAUN)
16
-
0,+
TAUN=TAUN*(-1)
I3 = -1
GO TO 19
17
I3=0
18
IF
(C2(I))
19
-
0,+
C2(I)=C2(I)*(-1)
I4 = -1
GO TO 22
20
I4=0
21
PUNCH: TAU
I2,C1(I),I3
TAUN,I4,C2(I)
22
TAU= TAU + DELTAU
TAUN = - TAU
IF
I = NLAGS
24
NO
YES
STOP
END

APPENDIX III

PROGRAM FOR ACCUMULATIVE STANDARD DEVIATION

This program is designed to calculate the standard deviation of piecewise spectral data using the accumulative last piece of data as the mean. Other calculations include a standard error calculation for each piece of data, and a student's t-distribution of the spectral data.

While the program itself is not complex, it has been included so that anyone wishing to use it will not have to write it.

```
C       STD COMPUTED FROM PIECEWISE SPECTRA CALCULATIONS BY USING FINAL
C        ACCUMULATIVE SPECTRA
C        ************************************        ********************
C        ************************************        ********************
        DIMENSION G(402),C0(402),Q(402),STDG(402),STDC(402),STDQ(402)
        READ 1, N,MAX,DELFRQ
      1 FORMAT (1X,I3,2X,I3,3X,F4.0)
        DO 20  I=1,MAX
        READ 10, C0(I),Q(I),G(I)
     10 FORMAT (9X,3F8.5)
        STDC(I)=0.0
        STDQ(I)=0.0
        STDG(I)=0.0
     20 CONTINUE
        Y=MAX-1
        FREQ=0.0
        PRINT 43
     43 FORMAT (5X,10H     SC     ,4X,10H     SQ     ,4X,10H     SG     )
        DO 50 J=1,N
        SC=0.0
        SQ=0.0
        SG=0.0
        DO 30  I=1,MAX
        READ 40, COSP,QUAD,GAIN
     40 FORMAT (9X,3F8.5)
        STDC(I)=(COSP-C0(I))**2+STDC(I)
        STDQ(I)=(QUAD-Q(I))**2+STDQ(I)
        STDG(I)=(GAIN-G(I))**2+STDG(I)
        SC=SC+(COSP-C0(I))**2
        SQ=SQ+(QUAD-Q(I))**2
        SG=SG+(GAIN-G(I))**2
     30 CONTINUE
        SC=SQRTF(SC/Y)
        SQ=SQRTF(SQ/Y)
        SG=SQRTF(SG/Y)
        PRINT 41, SC,SQ,SG
        PUNCH 41, SC,SQ,SG
     41 FORMAT (1X,3(4X,F10.6))
     50 CONTINUE
        PRINT 110
    110 FORMAT (5X,7H FREQ ,4X,7H  C0  ,4X,7H  TC  ,4X,7H STDC ,4X,
       17H    Q  ,4X,7H  TQ  ,4X,7H STDQ ,4X,7H    G  ,4X,7H   TG
       24X,7H STDG )
        DO 60  I=1,MAX
        X=N
        STDC(I)=SQRTF(STDC(I)/(X))
        STDQ(I)=SQRTF(STDQ(I)/(X))
        STDG(I)=SQRTF(STDG(I)/(X))
        TC=C0(I)/STDC(I)
        TQ=Q(I)/STDQ(I)
        TG=G(I)/STDG(I)
        PRINT 111, FREQ,C0(I),TC,STDC(I),Q(I),TQ,STDQ(I),G(I),TG,STDG(I)
    111 FORMAT (1X,10(4X,F7.4))
```

```
      PUNCH 112, FREQ,CO[I],TC,STDC[I],Q[I],TQ,STDQ[I],G[I],TG,STDG[I]
  112 FORMAT (1X,F4.2,9F8.4)
      FREQ=FREQ+DELFRQ
   60 CONTINUE
      STOP
      END
```

APPENDIX IV

PROGRAM FOR MEAN STANDARD DEVIATION

This program is designed to calculate the standard deviation of piecewise spectral data by using mean values calculated in the program. Also included is a standard error calculation for each piece of data , and a student's t-distribution of the mean values to its standard deviation.

This program is included as a time-saving device for those who wish to use it. It is essentially the same program that is included in Appendix III.

```
C      STD COMPUTED FROM PIECEWISE SPECTRA CALCULATIONS USING MEAN
C        VALUES CALCULATED IN THIS PROGRAM
C      ***************************************************************
C      ***************************************************************
       DIMENSION G[402],C0[402],Q[402],STDG[402],STDC[402],STDQ[402]
       READ 1, N,MAX,DELERQ
     1 FORMAT [1X,I3,2X,I3,3X,F4.0]
       DO 33 I=1,MAX
       STDC[I]=0.0
       STDQ[I]=0.0
       STDG[I]=0.0
       C0[I]=0.0
       Q[I]=0.0
       G[I]=0.0
    33 CONTINUE
       Z=N
       FREQ=0.0
       PRINT 43
    43 FORMAT [5X,10H    SC    ,4X,10H    SQ    ,4X,10H    SG    ]
       DO 50 J=1,N
       SC=0.0
       SQ=0.0
       SG=0.0
       DO 30  I=1,MAX
       READ 40, COSP,QUAD,GAIN
    40 FORMAT [9X,3F8.5]
       C0[I]=C0[I]+COSP
       Q[I]=Q[I]+QUAD
       G[I]=G[I]+GAIN
       STDC[I]=STDC[I]+COSP**2
       STDQ[I]=STDQ[I]+QUAD**2
       STDG[I]=STDG[I]+GAIN**2
       SC=SC+[COSP-[C0[I]/Z]]**2
       SQ=SQ+[QUAD-[Q[I]/Z]]**2
       SG=SG+[GAIN-[G[I]/Z]]**2
    30 CONTINUE
       Y=[MAX-1]
       SC=SQRTF[SC/Y]
       SQ=SQRTF[SQ/Y]
       SG=SQRTF[SG/Y]
       PRINT 41, SC,SQ,SG
       PUNCH 41, SC,SQ,SG
    41 FORMAT [1X,3[4X,F10.6]]
    50 CONTINUE
       PRINT 110
   110 FORMAT [5X,7H  FREQ ,4X,7H  XC   ,4X,7H  TC   ,4X,7H  STDC ,4X,
      17H   XQ  ,4X,7H  TQ   ,4X,7H  STDQ ,4X,7H   XG  ,4X,7H   TG
     24X,7H  STDG ]
       DO 60  I=1,MAX
       STDC[I]=SQRTF[[STDC[I]/Z]-[C0[I]/Z]**2]
       STDQ[I]=SQRTF[[STDQ[I]/Z]-[Q[I]/Z]**2]
       STDG[I]=SQRTF[[STDG[I]/Z]-[G[I]/Z]**2]
       XC=C0[I]/Z
```

```
      XQ=Q(I)/Z
      XG=G(I)/Z
      TC=(CO(I)/Z)/STDC(I)
      TQ=(Q(I)/Z)/STDQ(I)
      TG=(G(I)/Z)/STDG(I)
      PRINT 111, FREQ,XC,TC,STDC(I),XQ,TQ,STDQ(I),XG,TG,STDG(I)
  111 FORMAT (1X,10(4X,F7.4))
      PUNCH 112, FREQ,XC,TC,STDC(I),XQ,TQ,STDQ(I),XG,TG,STDG(I)
  112 FORMAT (1X,F4.2,9F8.4)
      FREQ=FREQ+DELFRQ
   60 CONTINUE
      STOP
      END
```

APPENDIX V

COMPUTER USAGE

This section of the paper is included to inform others of the procedure for operating the small computers at MSFC (the GE-205, SDS-930, and CDC-3200).

The GE-205, located in building 4732, is operated by two Northrop employees. Anyone wishing to use this computer must give his program to one of the operators, who will then run it for him. Those who wish to use the computer themselves must obtain special permission from Mr. John Heaman.

There are three SDS-930 computers available for our use. These computers, located in buildings 4200, 4202, and 4610, are self-operated. There are special control cards which must be placed at the front and back of the user's program (see Table 7). Table 8 gives the operation procedures for these computers. A copy of these instructions is usually found on the computer console.

The CDC-3200 computer is located on the ground floor of building 4200. It is operated by CDC personnel only. NASA has only three hours of priority each day: 0800-0900, 1200-1300, and 1500-1600. NASA contractors have priority for the remaining time. To use this computer, you must have a job number and submit a job card with each run. This computer, like the SDS-930, has certain control cards which are placed before and after the program (see Table 9).

Data for for the program are stacked the same way for all three computers, directly behind the last control card. On the 3200 computer a card with a seven - eight punch in the first and second columns should be placed behind the data. This is just in case the computer has not correctly been told when to STOP.

TABLE 7

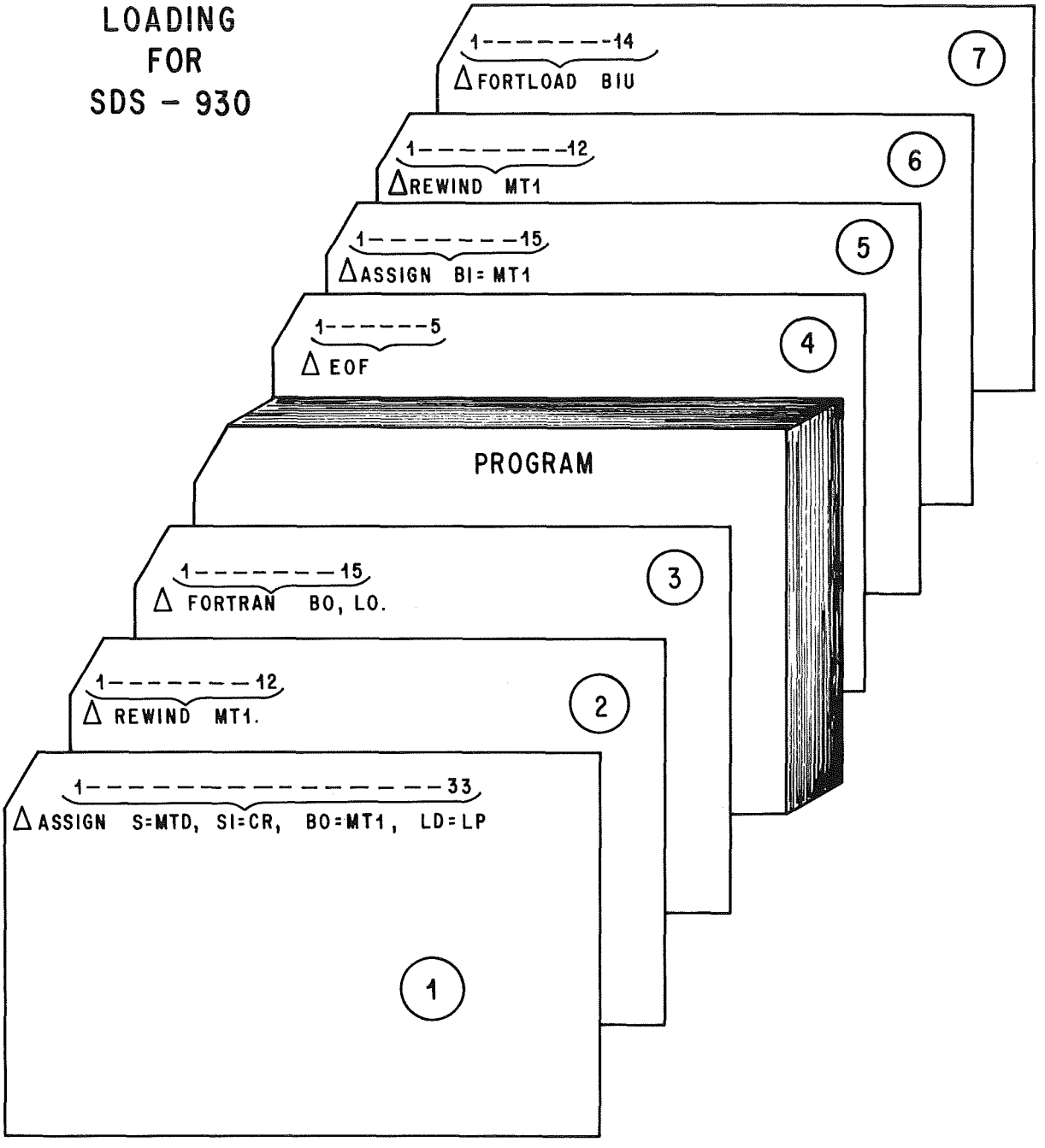
LOADING
FOR
SDS - 930
1-------14
ΔFORTLOAD BIU
7
1--------12
ΔREWIND MT1
6
1--------15
ΔASSIGN BI=MT1
5
1------5
Δ EOF
4
PROGRAM
1--------15
Δ FORTRAN BO, LO.
3
1--------12
Δ REWIND MT1.
2
1----------33
ΔASSIGN S=MTD, SI=CR, BO=MT1, LD=LP
1

TABLE 8

```
          * * * SDS COMPUTER OPERATING INSTRUCTIONS * * *
THIS GUIDE TO MACHINE OPERATIONS APPLIES TO THE TYPICAL JOB WHICH
CONSISTS OF
        (A) COMPILE A FORTRAN SYMBOLIC DECK
        (B) LOAD AND EXECUTE THE PROGRAM
OTHER TYPES OF COMPUTER RUNS MAY REQUIRE MODIFIED PROCEDURES.
 I. LOG IN.
II. CHECK MACHINE SET UP, NORMAL SET UP IS AS FOLLOWS
        (A) SYSTEM TAPE ON UNIT WITH 'UNIT SELECT' ON ZERO, 'DENSITY
            SELECT' ON 200, UNIT IN 'AUTOMATIC', 'READY LIGHT' ON.
        (B) SCRATCH TAPE ON UNIT WITH 'UNIT SELECT' ON ONE, 'DENSITY
            SELECT' ON 200, UNIT IN 'AUTOMATIC', 'READY LIGHT' ON.
        (C) THE LETTER 'C' SHOULD BE DISPLAYED IN THE COMPUTER CONSOLE
            'REGISTER' WINDOW.
        (D) CONSOLE 'RUN-IDLE-STEP' SWITCH SHOULD BE IN 'IDLE' POSITION.
        (E) PRINTER SHOULD HAVE 'READY' LIGHT ON.
III.INITIALIZE MACHINE FOR YOUR RUN
    A. LONG METHOD
        1. CHECK SYSTEM TAPE 'LOAD POINT' LIGHT, IF LIGHT IS NOT ON
           PROCEED AS FOLLOWS
            (A) PRESS 'START' BUTTON ON COMPUTER CONSOLE.
            (B) PRESS THE SMALL BUTTONS ON THE COMPUTER CONSOLE
                NUMBERED 7,11,12,20.
            (C) PRESS 'RUN-IDLE-STEP' SWITCH TO 'STEP' AND BACK TO
                'IDLE', WAIT FOR SYSTEM TAPE 'LOAD POINT' LIGHT
        2. PRESS 'START' BUTTON ON COMPUTER CONSOLE.
        3. PRESS BOTH 'MEMORY CLEAR' BUTTONS SIMULTANEOUSLY.
        4. PRESS 'START' BUTTON AGAIN.
        5. MOVE 'RUN-IDLE-STEP' SWITCH TO 'RUN'.
        6. PRESS 'FILL-MAG TAPE' SWITCH DOWN (THIS SWITCH IS ON LEFT
           SIDE OF CONSOLE).
        7. PUT YOUR DECK IN CARD READER AND PRESS CARD READER 'READY'
           BUTTON.
        8. WHEN 'INPUT' LIGHT ON RIGHT SIDE OF THE TELETYPE KEYBOARD
           COMES ON TYPE IN
                        ΔC=CR.
           THEN PRESS 'RETURN' BUTTON ON TELETYPE KEYBOARD.
        9. THIS MESSAGE TELLS THE SYSTEM CONTROL PROGRAM THAT CONTROL
           MESSAGES ARE ON CARDS IN THE CARD READER. YOUR JOB
           PROCESSING WILL NOW START.
    B. SHORT METHOD
       THIS METHOD WORKS MOST OF THE TIME BUT WILL SOMETIMES FAIL DUE
       TO THE WAY THE PRECEEDING JOB WAS TERMINATED. IF THIS METHOD
       FAILS TRY THE LONG METHOD.
        1. PRESS 'START' BUTTON ON COMPUTER CONSOLE.
        2. PUT 'RUN-IDLE-STEP' SWITCH TO 'STEP' AND THEN TO 'RUN'.
        3. PUT YOUR DECK IN CARD READER AND PRESS CARD READER 'READY'
           BUTTON.
        4. IF THE PROCESSING OF YOUR JOB DOES NOT START PUT 'RUN-IDLE-
           STEP' SWITCH TO 'IDLE' AND TRY LONG METHOD.
IV. AT END OF YOUR JOB PUT 'RUN-IDLE-STEP' SWITCH TO 'IDLE' POSITION.
 V. LOG OFF AND CLEAN UP YOUR CARDS, PAPER, ETC.
```

TABLE 9

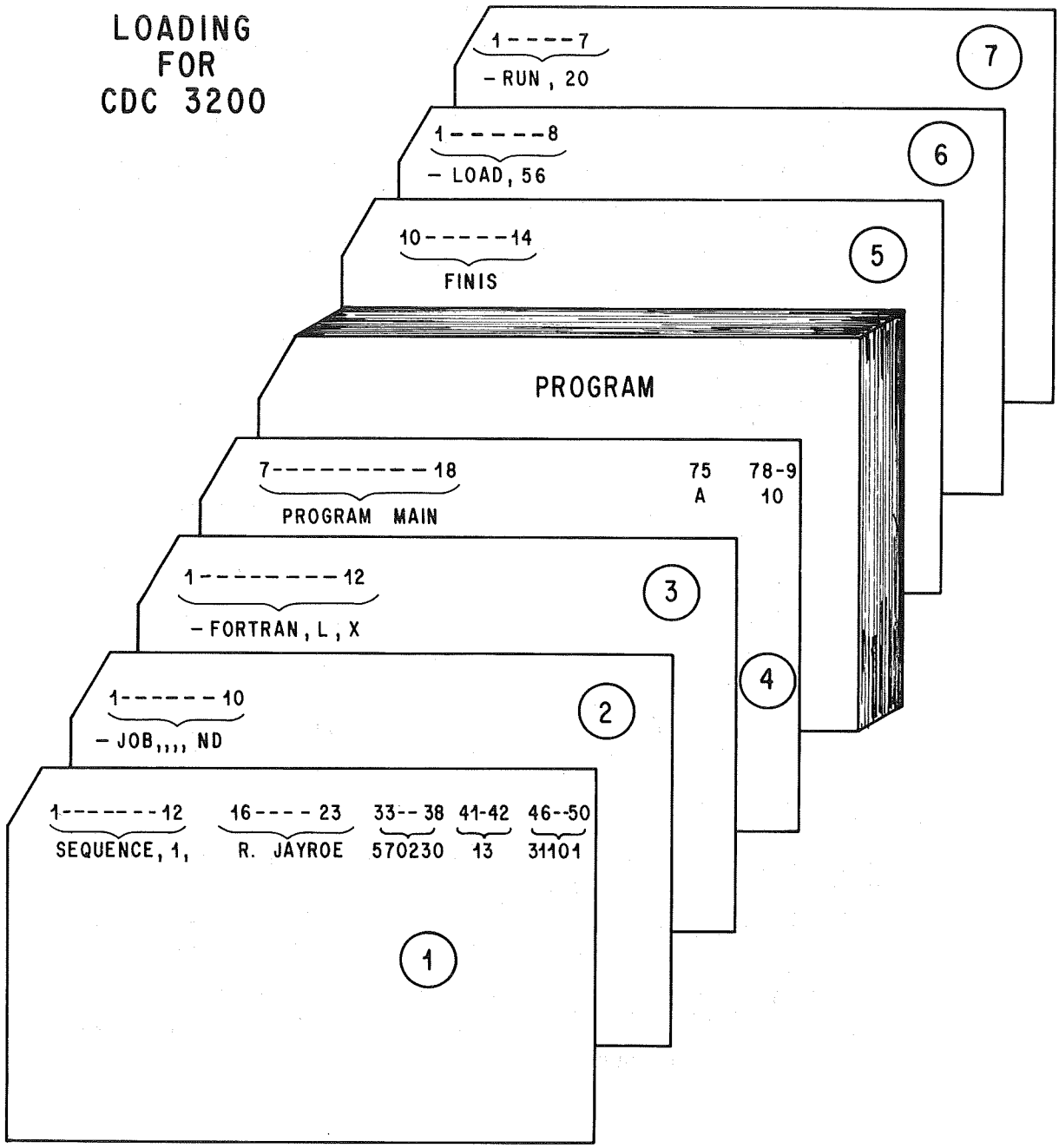
LOADING
FOR
CDC 3200
1----7
- RUN , 20
7
1------8
- LOAD, 56
6
10-----14
FINIS
5
PROGRAM
7---------18
PROGRAM MAIN
75
A
78-9
10
1---------12
- FORTRAN , L , X
3
4
1------10
- JOB,,,, ND
2
1--------12
SEQUENCE, 1,
16----23
R. JAYROE
33--38
570230
41-42
13
46--50
31101
1

APPROVAL NASA TM X-64505

RESEARCH ON ELECTROMAGNETIC CORRELATION TECHNIQUES

edited by Fritz R. Krause

The information in this report has been reviewed for security classification. Review of any information concerning Department of Defense or Atomic Energy Commission programs has been made by the MSFC Security Classification Officer. This report, in its entirety, has been determined to be unclassified.

This document has also been reviewed and approved for technical accuracy.

W. K. Dahm
Chief, Aerophysics Division

E. D. Geissler
Director, Aero-Astrodynamics Laboratory

MSFC—RSA, Ala

DISTRIBUTION

DIR
DEP-T
A&TS-PAT
PM-PR-M, Mr. Goldston
A&TS-MS-H
A&TS-MS-IP
A&TS-MS-IL (8)
A&TS-TU, Mr. Wiggins (6)
A&TS-PAT, Mr. Wofford
AD-S, Dr. Stuhlinger
PM-DIR
PM-AA, Mr. Belew

PD
Dr. Lucas
Mr. Craft
Mr. Brooksbank
Mr. Thomae

AST-U
Col. Mohlere

S&E-DIR
Mr. Weidner
Mr. Cook
Mr. Weaver
Mr. Richards

S&E-R
Dr. Johnson
Mr. Attaya
Mr. Miles
Mr. Hopper
Mr. Lake
Mr. Chase
Mr. Coons

S&E-COMP
Mr. Hopper
Mr. Jones
Mr. Cochran
Dr. Hoelzer
Dr. Kerner

S&E-CSE
Mr. Fredrick

S&E-SSL
Mr. Heller
Dr. Sieber
Mr. Snoddy
Mr. Shelton

S&E-ASTN-PTD
Mr. Hopson

S&E-AERO
Dr. Geissler
Mr. Horn
Mr. Bean
Mr. Dahm
Mr. W. Vaughan
Mr. Butler
Mr. Baker
Mr. Lovingood
Mr. Felix
Mr. Reed
Mr. Lindberg
Mr. Turner
Mr. Kaufman
Dr. F. Krause (25)
Mr. Holderer
Mr. Heaman
Mr. Huffaker
Mr. Ellner (25)
Mr. Forney
Mr. Kadrmas
Mr. Pickelner
Mr. I. Jones
Mr. Johnston
Mr. Funk
Dr. Heybey
Mr. Cummings
Mr. Murphree
Mr. Jandebeur
Mr. Few
Mr. Brewer
Mr. Bush

S&E-AERO (Cont'd)
Mr. Neighbors
Mr. Carter
Mr. Wilhold
Mr. Jayroe
Mr. Burkett
Dr. deVries
Mr. Swenson
Mr. Camp
Mr. Thomison
Mr. Walker
Mr. Borcherding
Mr. Cliff
Mr. Stephens
Mr. Powell
Mr. Humphries
Mr. J. Smith
Mr. Locklin
Mr. Brecht
Mr. Dalton
Mr. Campbell
Mr. Graham
Mr. Hablutzel

RSIC

Sci. & Tech. Info. Facility (25)
P. O. Box 33
College Park, Md. 20740
Attn: NASA Rep. (S-AK/RKT)

NASA-Langley Research Center
Langley Field
Hampton, Va. 23365
Attn: Tech. Library (2)

NASA-Goddard Space Flight Center
Greenbelt, Md. 20771
Attn: Tech. Library (2)

NASA-Ames Research Center
Moffett Field
Mountain View, Calif. 94035
Attn: Tech. Library (2)

NASA-Lewis Research Center
21000 Brookpark Rd.
Cleveland, Ohio 44135
Attn: Tech. Library (2)

Jet Propulsion Lab.
Calif. Inst. of Tech.
4800 Oak Grove Dr.
Pasadena, Calif. 91103
Attn: Tech. Library (2)

NASA-JFK Space Center
Kennedy Space Center, Fla. 32899
Attn: Tech. Library (2)

IITRI
10 W. 35th St.
Chicago, Ill. 60616
Attn: Dr. Damkevala
Mr. Goldfinch
Dr. Wilson
Col. Ferrell
Mr. Phillips
Mr. Weigandt

Northrop-EMD
Technology Drive
Huntsville, Ala. 35805
Attn: Mr. Grady
Mr. Hand
Mr. Tidmore
Dr. Su
Mr. Barnett
Mr. Miller
Mr. Pooley
Mr. Cikanek
Mr. Townsend

ESSA - Wave Propagation Lab.
National Burea of Standards Bldg.
Boulder, Colorado 80302
Attn: Dr. Beam
Dr. Derr
Mr. Sweezy
Mr. McGavin
Mr. Abshire

Colorado State University
Ft. Collins, Colorado 80521
Attn: Prof. Sandborn
Dr. Marshner
Dr. Sadeh
Dr. Huff
Prof. Reiter
Dr. Simon
Dr. Baldwin

University of Oklahoma
Department of Physics
Norman, Okla. 73069
Attn: Dr. Canfield
Dr. Fowler
Dr. Day
Mr. Lysobey

Alabama A&M
Huntsville, Ala.
Attn: Dr. Foster
Mr. C. Foster

FAA, NO-10
800 Independence Ave. S. W.
Washington, D. C. 20590
Attn: Dr. K. Powers
Dr. J. Powers

NASA Headquarters
Attn: Dr. vonBraun
Mr. Foster
RF, Mr. Ginter
SM, Mr. Badgley
SFM, Mr. Spreen
SF, Mr. Tepper
REI, Mr. Vacca
RVI, Mr. DeMerritt
MA, Mr. Reiffel
RV-2, Mr. Rosche
RVA, Mr. Underwood
MTG, Mr. Livingston
SA, Mr. Spriggs
SRB, Mr. Koutsandreas
SRB, Mr. Centers

NASA Hdqs. (Cont'd)
Attn: SRF, Dr. Summers
SG, Lt. Col. Lehman
RAO, Mr. McGowan
SAB, Mr. George
REI, Dr. Menzel
RV-2, Mr. Michel
RAA, Mr. Parkinson
RAP, Mr. Rekos
RRF, Mr. S hwartz
RD-A, Mr. Harper
RR, Dr. Kurzweg
MTG, Mr. Peil
RV-1, Mr. Cerreta